More Than Just Skin Deep: Peptoid Applications in Dermatology

by,

Danielle Marie Nalband

A dissertation submitted in partial fulfillment

of the requirements for the degree of

Doctor of Philosophy

Department of Chemistry

New York University

January, 2018

_____

Kent Kirshenbaum

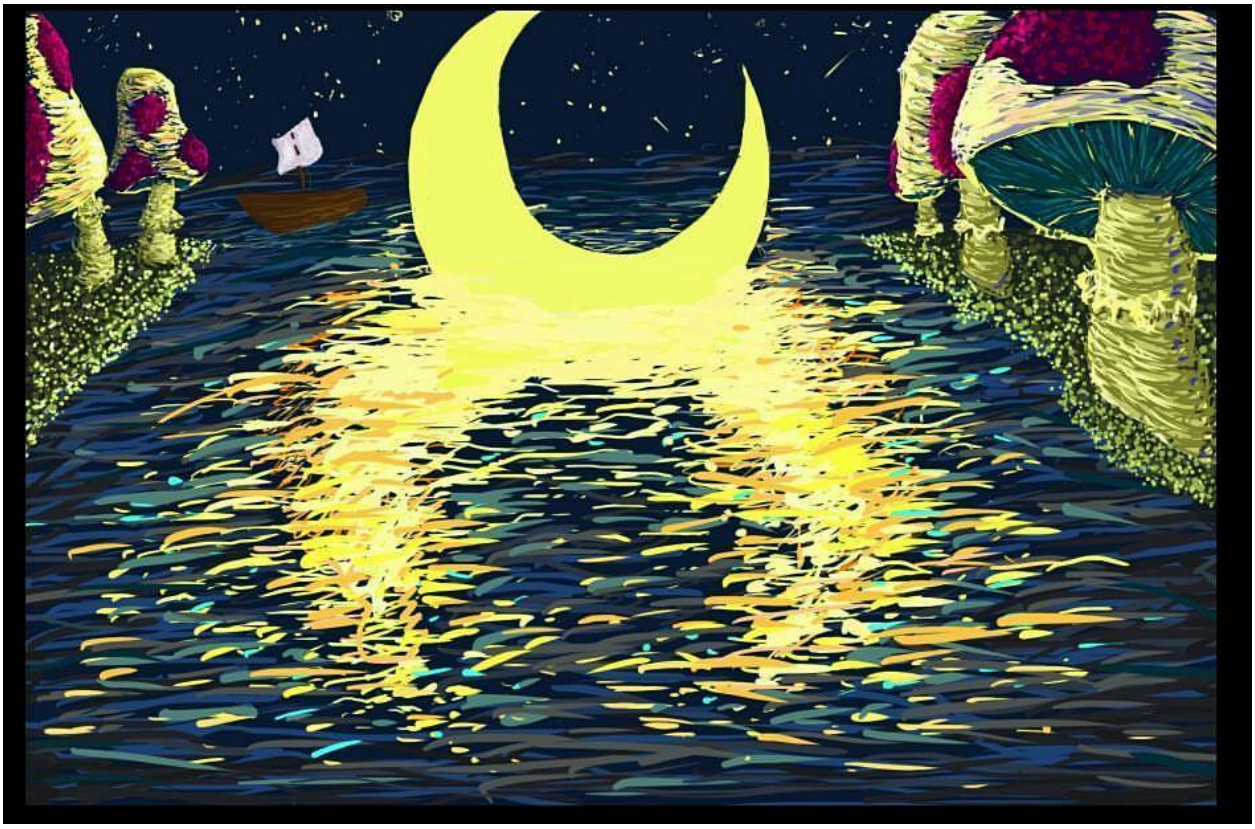

Danielle Marie Nalband. *The Truth About Magic II.* 2017. Digital.

“Why do we have to listen to our hearts?" the boy asked.

"Because, wherever your heart is, that is where you will find your treasure.”

-Paolo Coehlo, The Alchemist

“Astrology”

It's so clear tonight, and calm,
that if I stepped outside,
and raised my head, I imagine
I could see the silver

chest hairs of Orion,
the hummingbird tattoo upon
the outside of his thigh.
And further back, the unfathomable

dark, which makes it possible for him
to draw his bow,
and gives him room to choose
a target for the night.

So I remember the luxury of what
I've had the poor taste in the past
to call, sometimes, our loneliness,
which is the absence of others

who have left us stranded here,
with only oxygen to breathe
and nothing more than time
to breathe it in.

And I honor, for a moment, the million
things forgotten, the things
which have so graciously
forgotten me--the bulging

saddlebags of history, the myriad, self-cancelling
blunders and eurekas
of fathers and mothers
of fathers and mothers and fathers--

who have handed down something
of tremendous importance
by handing down nothing
but plenty of quiet and dark.

And in the fields of sky above our houses,
these well-lit
hieroglyphics, open to
our own interpretation.

-Tony Hoagland, Sweet Ruin

Dedication

This work is dedicated in sincere appreciation and deep gratitude to the Soul of the World, to every unseen force in the universe that conspired to help me realize this dream. Thank you, from the bottom of my heart.

Acknowledgments

I would like to take the opportunity to formally acknowledge all of those who have made it possible for me to follow my wildest and weirdest interests and aspirations. First, and most importantly, I would like to thank my Ph.D. advisor, Prof. Kent Kirshenbaum for welcoming me into the program and into his lab, for seeing something special in me and going above and beyond to make sure that I left NYU as Dr. Nalband. He always encouraged and supported me to follow my own unique path to this degree and has been the best mentor I could have ever dreamed of having the privilege to work with. To my other committee members: Prof. Daniela Buccella, Prof. Lara Mahal, Prof. Bart Kahr, and Dr. Ryan Branski; thank you seeing this journey through to the end with me and for all of your guidance and expertise to mold me into a scientist worthy of a Ph.D. Dr. Branski, thank you personally for participating in our very rewarding collaboration, and I look forward to future scientific endeavors with you and your lab.

Instrumental to my chemistry and teaching training as well as and my Ph.D. trajectory was my undergraduate advisor at Hampshire College, Prof. Rayane Moreira; thank you for showing me just what I am capable of and never accepting anything less than my best. I would also like to acknowledge Murray Goodman and Melinda Burbank, my mentors from beyond the veil, thank you for paving the way for my education, research, and contributions to the field. For all of their countless help, patience, and expertise, I owe many, many thanks Dr. Chin Lin and Ronald McLurkin; you helped turn my experiments into meaningful scientific works.

I would like to pay an outstanding debt of gratitude and thanks to Mallika Tatikola, my assistant on the lipitoid and collagen projects. During our time together, she grew to

be one of my best friends; her energy and enthusiasm infectious, always with a smile on her face, willing to do anything to help out and support. She kept me focused, motivated, and sustained my faith in myself and in my dreams. You really are a treasure of a human being in every facet of the phrase.

To the rest of the Kirshenbaum lab, my classmates, and my friends from my 'other life', especially: Dr. Paul Levine, Dr. Timothy Craven, James Eastwood, Daniel Heindel, Dr. Christopher Vaiana, Sara Kupermic, Rita Brandt-Meyer, Lauren Galloway, Sofia Markusfeld, Luke Chiaruttini, Jon Gernhart, and Shea Stadium as a collective entity; thank you for all of the friendship, support, guidance, help, and laughter on and off the clock with science and beyond. Your creativity, honesty, and courageous self expression inspire me to be the best, most authentic version of myself. You saw me for who I truly am and loved and accepted that person. I feel as though I have found my place and a home in NYC with you all, and this wouldn't have been possible without you.

I would like to recognize Sonia Rivera, my dear friend who became a mentor to me in ways that I could never have known I wanted or needed in the past two years. I will always cherish our time spent together and all of our adventures. Your presence in my life has significantly shaped me into who I am, but I think you already know that.

Finally, I would like to thank my family and my dog Coco, my best little buddy, for catching me the many times I've fallen, setting me straight, and for sticking right by my side through thick and thin. I know it wasn't easy, and I cannot even begin to express the gratitude I have for everything you've done and sacrificed to put me where I am today. I love you, and I hope I have made you proud.

Abstract

Wound healing is a complex biological process that prevents infection, minimizes scarring, and restores strength and function of injured tissue. With an aging population, and a rise in age-related pathologies, innovative solutions to wound healing are sought that include new materials for wound dressings and for delivery of drugs that promote the wound healing process. Biopolymers are employed extensively for wound healing applications, yet native biomolecules can fall short in some critical requirements for the design and implementation of novel materials to address the repair and regeneration of tissue. Peptoids, *N*-substituted glycine oligomers, are a class of sequence-specific peptidomimetic foldamers constituted from repeating tertiary amide linkages that exhibit enhanced proteolytic stability, cell permeability, and biocompatibility. Peptoids are synthesized according to a robust and simple solid phase synthesis protocol, and due to their modular nature, can be tailored to suit a variety of biomedical research objectives, including new materials applications. The contents of this thesis describe peptoids utilized in three different contexts to address distinct aspects of wound healing. Herein I explore the implementation of a peptoid macrocycle to template reversible triple helix formation of collagen-like peptides; a peptoid-based transfection reagent to attenuate scar tissue formation via oligonucleotide therapeutics, and a rapid X-ray fluorescence analytical technique to screen libraries of peptoids for metal binding interactions, enabling discovery of peptide mimics that can be exploited to deliver therapeutic metal ions for dermatological applications.

Table of Contents

Dedication……v

Acknowledgments……vi

Abstract……viii

List of Figures……xi

List of Tables……xv

List of Appendices……xvi

Authorship……xviii

Chapter 1: Biopolymers for Wound Healing

Introduction……2

Summary and Outlook……23

References……24

Chapter 2: Peptoid-Based Tethers as Effective Triple Helix Templates for Collagen Mimetic Peptides

Abstract……38

Introduction……38

Results and Discussion……54

Summary and Outlook……66

Experimental Procedures……69

References……..…78

Chapter 3: siRNA Transfection with Lipitoids for Scar Tissue Inhibition

Abstract……86

Introduction……..…87

Results and Discussion……96

Summary and Outlook……..…..104

Experimental Procedures……...…106

References……112

Chapter 4: Rapid Identification of Nickel-Binding Peptoid Oligomers by On-Resin X-ray Fluorescence Screening

Abstract……117

Introduction……...117

Results and Discussion……..…133

Summary and Outlook……...151

Experimental Procedures……...153

References……161

Appendices……168

List of Figures

Figure 1. Stages of Normal Wound Healing.....5

Figure 2. Structural Hierarchy of Collagen Fibers.....10

Figure 3. Models of Hartgerink's CLP Constructs 12

Figure 4. Common Covalent Scaffolds for CLP Triple Helix Templation....14

Figure 5. Polypeptides vs. Peptoids 20

Figure 6. Micro-Array Based HTS of a Peptoid Library.....21

Figure 7. CD Analysis of Solution Phase Peptoid-Metal Binding.....22

Figure 8. Collagen-Like Peptide Models.....39

Figure 9. Structural Hierarchy of Collagen Fibers 40

Figure 10. Amide Bond Isomerization and Ring Pucker in L-Proline 42

Figure 11. Stereoelectronic Effects of Substituted Prolines.....43

Figure 12. Structural Comparison of Native Glycine vs. Aza-Glycine.....44

Figure 13. Hartgerink's de Novo Designed ABC CLP Triple Helix.....45

Figure 14. Common Covalent Scaffolds for CLP Triple Helix Templation..47

Figure 15. Comparison of Previous Work Templating CLPs into a Triple Helix with KTA, to the Current Work, Utilizing a Peptoid Scaffold.....51

Figure 16. Peptoid Scaffolds Used to Template CLPs into a Triple Helix...52

Figure 17. Crystal Structure of a Hexameric Peptoid Macrocycle.....53

Figure 18. Synthetic Scheme of Peptoid Scaffolds and Scaffold-CLP Constructs 55

Figure 19. CD Analysis of Free and Templated CLPs.....58

Figure 20. CD Analysis of Templated CLPs with 4M Urea 60

Figure 21. Melting and Refolding Experiments of Free and Templated CLPs.....61-62

Figure 22. Energy-Minimized Structure of **CLP_3-Mac.** 64

Figure 23. Energy-Minimized Structure of **CLP_3-Mac.** 65

Figure 24. Stereoview Overlaying **Mac** and the X-Ray Crystal Structure ..65

Figure 25. Overlay of the Peptoid Macrocycle Crystal Structure and the Energy-Minimized Structure of **CLP_3Mac.**.....66

Figure 26. siRNA Therapy.....88

Figure 27. Relationship Between TGF-β Signaling and SMADs 91

Figure 28. Lipofection with Cationic Lipids 92

Figure 29. Structure of the **Lipitoid** Oligomer 93

Figure 30. Solid Phase Synthesis of **Lipitoid**.....97

Figure 31. Comparison of Crude **Lipitoid** Purity 98

Figure 32. Cell Viability Assays Across Different Cell Lines 99

Figure 33. Percentage of Smad3 Expression after siRNA Transfection...101

Figure 34. Expression of Smad3 mRNA after Lipitoid Injection 103

Figure 35. Polypeptide Backbone and the 20 Canonical Amino Acids..118

Figure 36. Cartoon Depiction of a Zinc Finger Protein ……...120

Figure 37. Circular Dichroism Monitors Peptoid-Metal Binding ……....124

Figure 38. X-ray Crystallography of Peptoid-Metal Association..……...125

Figure 39. ICP-MS Analysis of Chromium Sequestration by Peptoids….126

Figure 40. Colorimetric Screening for Cr-Peptoid Binding .....……...128

Figure 41. Illustration of the Principles of X-ray Fluorescence Analysis...130

Figure 42. Schematic Representation of XRF Analysis ……..131

Figure 43. OBOC Peptoid Library Screen for Metal Binding with MXRF..133

Figure 44. Design of the OBOC Metal Binding Peptoid Library…..……...135

Figure 45. Chemical Structures of Peptoid Hit Compounds……..138

Figure 46. Results from the X-ray Fluorescence Metal-Binding Screen...139

Figure 47. Microscope Images of Peptoid Resin Beads in a Colorimetric Metal Binding Assay……..……141

Figure 48. Nickel Depletion Assay at 24 μM ……...143

Figure 49. Nickel Depletion Assay at 222 μM ……..……....144

Figure 50. Representative MXRF Analysis of Peptoid Library Members..146

Figure 51. Representative MXRF Analysis of Peptoid Library Members..147

Figure 52. Representative MXRF Analysis of Peptoid Library Members..149

Figure 53. Smad3 Expression as a Function of Transfection ……....170

Figure 54. Smad3 Expression as a function of Continuous Transfection.172

Figure 55. Smad3 Expression as a Function of Transfection……...174

Figure 56. Lipitoid Variations……..……..…...186

Figure 57. Crude HPLC Analytical Spectra of **Lipitoid** Variants.....188-189

Figure 58. Purifed Analytical HPLC Traces of **Lipitoids 5-7** ……..……...190

Figure 59. Snapshot of a Standard XRF Spectrum..……..……...196

Figure 60. Depiction of the Full 35-Member Peptoid Library ……197-199

Figure 61. RP-HPLC trace of crude **PentA** ……..……...201

Figure 62. Additional MXRF data **PentA**, **NonaB**, **ConC**, **ConTG**…202-203

Figure 63. Uv/vis Plot Titrating Ni^{2+} into 108 uM **89A** ……..……...205

Figure 64. Uv/vis Plot Titrating Ni^{2+} into 48 uM **101A** ……..…...206

Figure 65. Job Plot Analysis Titrating Ni^{2+} into **101A** ……..……...207

Figure 66. Uv/vis Plot Titrating Ni^{2+} into **101A** in 4:1 Methanol:Water 208

Figure 67. Job Plot Analysis Titrating Ni^{2+} into **101A** in a Dram Vial ..…..209

Figure 68. Analysis of Precipitate Isolated in Ni^{2+} Binding Experiments...211

Figure 69. ^{1}H NMR Analysis of **101A** Before and After Ni^{2+}……...213

Figure 70. Uv/vis Plot Titrating Ni^{2+} into 1 mM **89A** ……..……...214

Figure 71. Bonneau Laboratory-Designed Cyclic Peptoid Hexamer……...216

Figure 72. Analysis of Cyclic Peptoid Hexamer ……...217

Figure 73. Analysis of Cyclic Hexamer Titrated with 1 eq. Cu^{2+}……...219

List of Tables

Table 1.Summary of Commercial Collagen-Based Dressings……...9

Table 2. Zuckermann's **Lipitoid** Variations from 1998……..…..184

Table 3. Second Generation **Lipitoid** Identities……..186

List of Appendices

Appendix 1: A Novel Transfection Modality for in vivo siRNA Delivery to Vocal Fold Fibroblasts

Introduction……...169

Results and Discussion……..170

Summary……...178

Experimental Procedures……...179

References……181

Appendix 2: Design, Synthesis, and Purification of Next Generation Lipitoid Variations

Introduction……...183

Results and Discussion……..185

Experimental Procedures……...191

References……194

Appendix 3: Additional Data and Experiments from Metal Binding Studies in Chapter 4: Rapid Identification of Nickel-binding Peptoid Oligomers by On-Resin X-ray Fluorescence Screening

Validation of Library Synthesis……..200

Solution Phase Binding Experiments……..204

Designing Cyclic Metal Binding Peptoids for Cu^{2+} Complexation…215

References……220

Authorship

The text of Chapter 1 contains material that was originally published as: Kraja, I., Bing, R., Hiwatashi, N., Rousseau, B., Nalband, D., Kirshenbaum, K. and Branski, R. C. (2016), The Laryngoscope, December 20, 2016, 1-7. Hiwatashi N, Kraja I, Benedict PA, Dion GR, Bing R, Rousseau B, Amin MR, Nalband DM, Kirshenbaum K, & Branski RC (accepted; in press). The Laryngoscope*;* Nalband, D. M., Warner, B. P., Zahler, N. H. and Kirshenbaum, K. (2014), Biopolymers,102: 407–415 Danielle Nalband wrote and contributed significantly to the preparations of the manuscript, the design of the experiments, and the synthesis and purification of the lipitoids in the lipitoid papers; and wrote the manuscript, conducted all of the experiments, and is the primary author of: Nalband, D. M., Warner, B. P., Zahler, N. H. and Kirshenbaum, K. (2014), Biopolymers,102: 407–415.

The text of Chapter 2 contains material that is being prepared for submission as: Nalband, D.M.; Eastwood, J.R.; Tatikola, M.; and Kirshenbaum, K. (2018). “Peptoid-Based Tethers as Effective Triple Helix Templates for Collagen Mimetic Peptides”. Danielle Nalband wrote the manuscript, conducted the bulk of the experiments, and is the primary author.

The text of Chapter 3 contains material originally published as: Kraja, I., Bing, R., Hiwatashi, N., Rousseau, B., Nalband, D., Kirshenbaum, K. and Branski, R. C. (2016), The Laryngoscope, December 20, 2016, 1-7. Hiwatashi N, Kraja I, Benedict PA, Dion

GR, Bing R, Rousseau B, Amin MR, Nalband DM, Kirshenbaum K, & Branski RC (accepted; in press). The Laryngoscope. Danielle Nalband wrote and contributed significantly to the preparations of the manuscript, the design of the experiments, and the synthesis and purification of the lipitoids.

The text of Chapter 4 contains material originally published as: Nalband, D. M., Warner, B. P., Zahler, N. H. and Kirshenbaum, K. (2014), Biopolymers,102: 407–415. Danielle Nalband wrote the manuscript, conducted all of the experiments, and is the primary author.

The text of Appendix I contains material originally published as: Kraja, I., Bing, R., Hiwatashi, N., Rousseau, B., Nalband, D., Kirshenbaum, K. and Branski, R. C. (2016), The Laryngoscope, December 20, 2016, 1-7. Danielle Nalband wrote and contributed significantly to the preparations of the manuscript.

Chapter 1

Introduction:

Biomimetic Polymers for Wound Healing

The use of biopolymers to promote wound closure and healing has been in practice for millennia, dating back to traditional African medicine, which applies crude plants and herbs, animal fats and muscles, and honey to injured areas for their antibacterial and anti-inflammatory properties.[1] The earliest written account of this dates back to a papyrus text from 1580 B.C., describing how ancient Egyptians dressed wounds with linen and fresh meat. However, it was not until the birth of modern surgery that biodegradable sutures, termed 'catgut', were developed from collagen fibers of sheep intestine; this experimentation marked the use of biopolymers as materials in modern wound healing tools.[2]

Biological-based wound dressings remain an attractive option because biopolymers exhibit an extraordinary diversity of structural and functional attributes, endowing these macromolecules with attractive qualities for biomedical applications, including dressings and materials used to modulate the wound healing process.[3,4] Therefore, they can assist in one or more of the stages in wound healing[5] and meet many, and in some cases, all of the criteria for an ideal wound dressing.[6] In addition, they can be formulated into a diverse set of constructs, such as hydrogels, films, wafers, sheets, foams, and sponges, specialized to the needs of each wound.[6,7] By virtue of their self-assembly, materials properties, and biocompatibility, peptide based biopolymers in particular are a promising resource for discovery of treatment modalities in wound care and maintenance.[3]

Now, equipped with the insight from decades of peptidomimetic research, scientists have begun to experiment with novel peptide-like scaffolds which may be

capable of accessing structures to invoke additional functions not immediately available to natural biopolymeric systems.[8] This research is advancing on the heels of recent reports comparing the effectiveness of different dressings for treating wounds. Certain types of wounds exhibit improved responses for treatment by specific dressings.[9] Thus, our quest for novel and innovative materials for wound healing solutions continues, especially for those that can deliver bioactive substances which directly influence the chemical and cellular environment at the wound site and trigger the body's natural wound healing responses.[10] Such designs could potentially improve wound treatment in complicated and slow-healing injuries, reduce scar tissue formation, and interact synergistically with the body's mechanisms for effective wound treatment.

The contents of this thesis explore research that supports three different modalities of wound treatment using a family of peptidomimetic oligomers called peptoids. Chapter 2 describes templating short sequences of synthetic collagen into a triple helix formation from a peptoid macrocycle. Further development into this area of study seeks to construct large, abiotic assemblies of synthetic collagen materials to be used for wound dressings and other wound healing applications. Chapter 3 discusses scar tissue inhibition and strategies to attenuate fibrotic outcomes at wound lesion sites through siRNA silencing therapy, using a peptoid-based transfection reagent. Finally, Chapter 4 reviews the application of micro X-ray fluorescence to screen libraries of resin-bound peptoids for metal binding interactions. These "metallopeptoids" will contribute to the discovery of new delivery vehicles for therapeutic metal species which can be formulated into cosmetic preparations. The introduction provides an overview of

the biological intricacies of wound healing and the current challenges with wound care in order to give the reader the proper framework and motivation for this thesis.

The Biology of Wound Healing and the Social and Economic Burden of Wound Care

Wound healing is the process of tissue repair manifest by a concerted and complex series of biological and molecular events in the body subsequent to injuries that compromise the structure and/or function of an organ.[11] Once a tissue suffers damage, the process of healing can be broken down into four stages which serve to mend the damage and restore the strength and capabilities of the tissue, though most of the events do not occur at discrete timepoints. (**Figure 1**) The four stages of wound healing include haemostasis, inflammation, proliferation, and remodeling, and typically proceed over the course of days to weeks. The final stage can take years, however, depending on the condition of the patient, severity and complexity of wound, and other environmental considerations.[12] Briefly, haemostasis is the process by which blood vessels constrict and coagulation of platelets and fibrin ensues to form a clot. Attracted by growth factors and other chemokines, neutrophils and macrophages infiltrate the wound site, initiating inflammation in which debris is removed, compromised tissue is broken down, and more growth factors are released to recruit fibroblasts.[13] During proliferation, fibroblasts aggregate in the wound bed and deposit a dense mat of collagen that, in contrast to healthy collagen in the body, is highly disorganized and can give the healed skin a raised and textured appearance, commonly known as a scar.[12] The final stage of wound healing, remodeling, works to regain the structure and intricate

morphology of other collagen fibers seen in the body, breaking down the scar tissue and restoring most, but not all, of the strength and function to the newly healed tissue.[14]

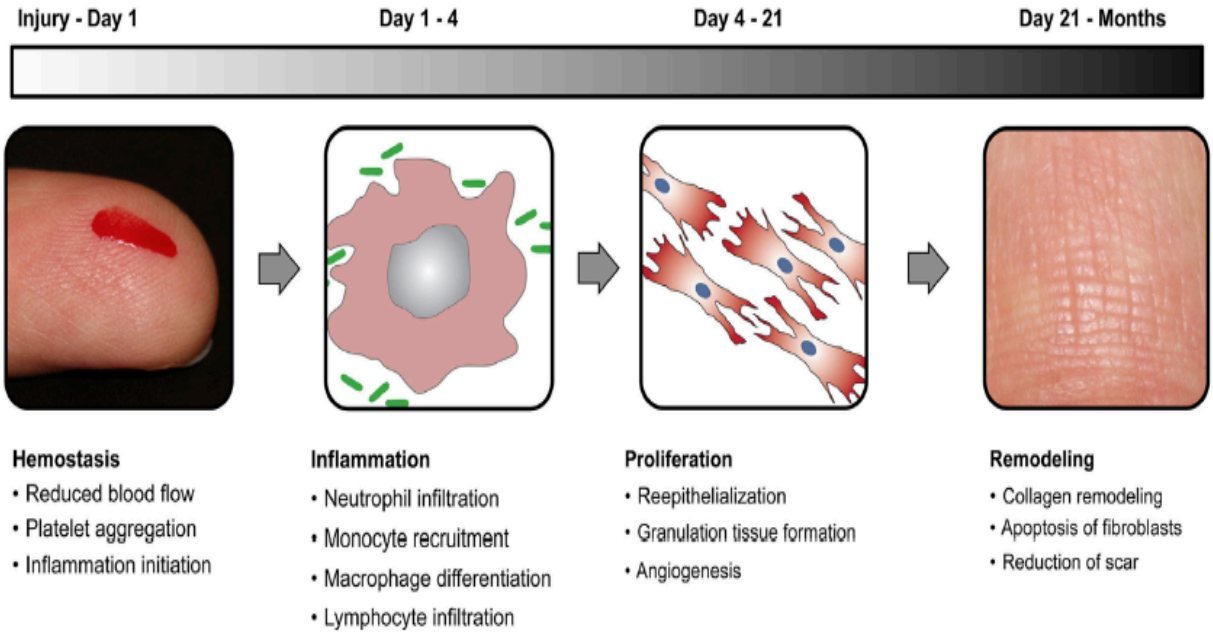

Figure 1. Stages of Normal Wound Healing. (Subhamoy, D. S. and Baker, A.B., 2016)[15]

However, not all wound healing proceeds without complications, as these processes can be altered by infection, poor circulation, the size and depth of the wound, and other pre-existing medical conditions such as diabetes, obesity, heart disease, or simply old age. Wounds that fail to continue through the stages of normal wound healing in an orderly and timely manner, usually within 30 days (with the exception of the remodeling phase), are considered to be chronic wounds.[12] In the US alone, chronic wounds affect 6.5 million patients annually, and about $25 billion dollars are spent on

the maintenance and treatment of chronic wounds. This expenditure is expected to increase due to an aging population and, therefore, more age-related pathologies that interfere with the healing normal trajectory.[14] The majority of all amputations originate from ulcers which cannot heal, and about 70% of all lower limb amputations are associated with diabetic ulcers.[15] However, the reported mortality rate associated with sustaining a diabetic ulcer, between 40% and 70% within five years, presents a bleak outcome for these patients, who then experience added mental health trials after suffering the loss of a limb including social and physical isolation, depression, and family hardship.[16]

While an obvious solution to healing chronic injuries is to deposit enough collagen and build up granulation tissue to enable wound closure, the healing process must be regarded and treated as a delicate equilibrium. Conversely, an overactive healing course leads to severe scarring and fibrotic outcomes.[12] These types of scars are typically either classified as hypertrophic, such as observed in cases of extreme burns, or keloidic scarring, which can ensue from non-traumatic injury.[11,16]

Scarring can result from excessive deposition of collagen and a failure to remodel the extracellular matrix properly, causing a loss of tissue strength and/or function. Scarring can be aesthetically unappealing and contribute to mental health and diminished self esteem. The repair process typically regains only 80% of the injured area's former strength, compromising its function.[11] This is of particular interest and relevance when studying scarring diseases, such as pulmonary or liver fibrosis. Considering the scar tissue formed from myocardial infarction contributes to congestive heart failure and causes close to 100,000 mortalities annually in the United States,

aberrant scarring and healing developments carry grave consequences in determining the survival outcomes of aging populations.[17]

Traditional Wound Healing Solutions

Promoting wound closure while also preventing the formation of excessive scar tissue is critical, and one approach to this challenge is through the use of precisely designed dressings.[5] In order to be classified as an effective dressing, the following criteria must be met: establish a moist environment over the wound area while absorbing exudates, prevent bacterial infection, be immuno-compatible, allow gas exchange, protect the wound bed, and adhere to the wound site but enable removal easily and painlessly.[1,5,18,19] Ideally, the wound dressing would also be biodegradable in a time frame consistent with the healing rate and be transparent so that the healing progress can be monitored and the regimen tailored without changing the dressing, thus encouraging patient compliance without disturbing the wound healing process.[20]

Traditional dressings typically are fashioned from cotton, gauze, wool, and various other synthetic materials. Dry and absorbent in nature, they primarily serve to absorb exudates and protect the wound, but have their shortcomings as they may require frequent changes, may fail to provide a moist healing environment, tend to adhere to the wound bed as healing progresses, and are permeable to bacteria.[1,18] Due to their propensity to harbor bacterial colonies, these dressings are applied simultaneously with prophylactic antibiotics.[10] While these preparations remain heavily utilized, during the last few decades progress has been made toward improving the traditional dressing by using preparations containing biological and synthetic polymers

that maintain the hydration of the wound site while still absorbing exudates and offering additional benefits that vary depending on the formulation. [1,5,18-22]

Collagen and the Application of Biopolymers in Wound Healing Materials

Common biopolymers used for wound healing today include alginates, chitin/chitosan, self assembling peptides, hyaluronic acid, silk, and cellulose,[3,6,23-25] but perhaps the most widely utilized biological polymer to induce wound closure and healing is collagen. Collagen is considered to be highly optimal for a wound dressing obtained from a native biopolymer construct. Collagen-derived materials are biocompatible, are non-toxic to cells (accompanied by non-toxicity of the degradation products), and are thoroughly characterized regarding their physical, structural, chemical, and biological attributes.[26] Numerous commercial wound-healing applications for collagen exist and are summarized in **Table 1.** Its broad utility is primarily due to its outstanding gel forming characteristics, which supply a moist healing environment at the site of injury and present a large surface area of uniform composition with tunable viscosities that are dependent on the level of crosslinking.[27] While collagen-based hydrogels are most noted for their applications in cosmetic surgery by virtue of their swelling capabilities, they also represent ideal materials for injection into injured sites and for drug delivery purposes. [18,26,28-44] In addition to hydrogels, collagens have been formed into several other types of commercial matrices, such as sheets, specialized for differing types of wounds and healing environments.[2,6,14, 39,41,46]

Collagen-derived sheets are impermeable to bacteria, modulate the levels of fluid around the wound bed, facilitate the migration of fibroblasts and microvascular endothelial cells by providing a matrix for aggregation, and aid in minimizing scar tissue

formation. Considering their physical properties, the sheets are supple, elastic, and demonstrate a high resistance to tearing, all of which are proven to be valuable characteristics for dressing materials.[31]

Collagen form	Name	Manufacturer	Description
Collagen composite dressing	Promogran®	Systagenix	Collagen-oxidized regenerated cellulose
	Fibracol®	Systagenix	Collagen-alginate wound dressing
	Biobrane®	Smith & Nephew	Artificial skin substitute composed of nylon mesh, silicone, and porcine skin collagen
Collagen fiber	Helitene®	Integra LifeSciences	Microfibrillar, absorbable hemostatic agent
	Instat®	Ethicon	Microfibrillar collagen hemostat
	Avitene®	Davol	Microfibrillar hemostat
Collagen powder	Medifil®	BioCore (Kollagen)	Spherically particles of native bovine collagen
Collagen sponge	Helistat®	Integra LifeSciences	Absorbable hemostatic sponge
	ActiFoam®	MedChem	Hemostatic sponge
	SkinTemp®	BioCore (Kollagen)	Native collagen in the nonhydrolyzed form

Table 1. Summary of commercial collagen-based dressings. (Aramwit, P. 2016)[3]

The physicochemical attributes and qualities of collagen fibers themselves will be reviewed and discussed in detail within the thesis (**See Chapter 2**). Briefly, collagen fibrils are polypeptide-based supramolecular structures consisting of a right-handed triple helix comprising three polyproline type II (PPII) helices, termed alpha chains, which are wrapped around each other via hydrogen bonding to form an extended structure through covalent crosslinking and non-covalent interactions. Each individual collagen strand is stabilized in a left-handed PPII helical formation mainly by hydrogen

bonding and stereoelectronic effects.[2,47-49] These fibrils, termed 'tropocollagen', are crosslinked and then interdigitate and aggregate with neighboring fibrils; the resulting structure is comparable to a coiled microfiber assembling to form a braided nanometer-scale rope.[32] (**Figure 2**) Consequently, the collagen triple helical fiber is endowed with outstanding mechanical, thermal, and tensile strength, and flexibility; it's apparent why it is the most abundant structural protein in the human body.[31,48]

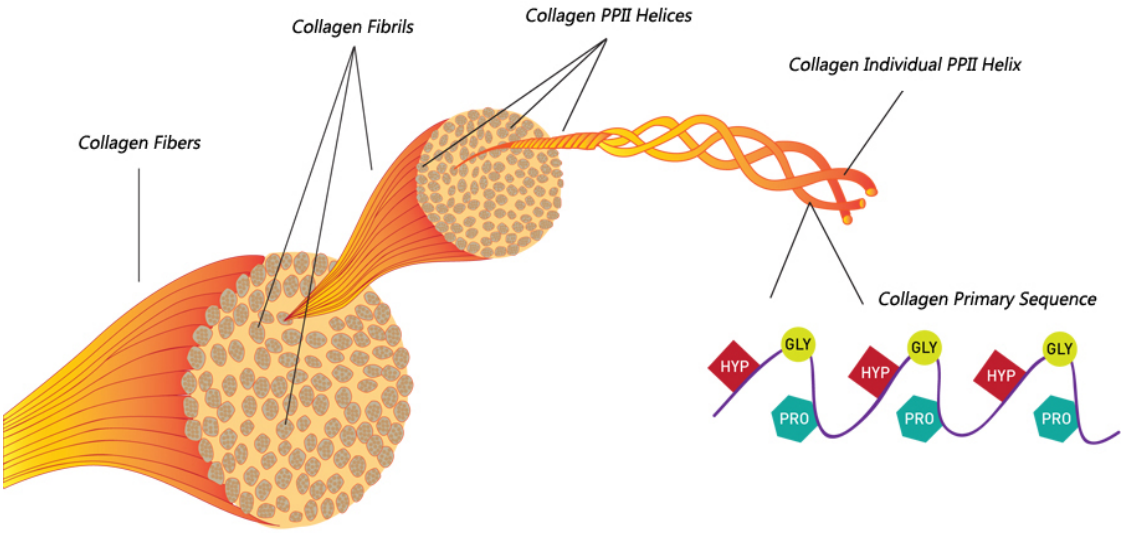

Figure 2. Structural hierarchy of collagen fibers (image taken from : http://bayareapelleve.com/pelleve/collagen/)[50]

The self-assembly properties of collagen have garnered significant interest for the development of new biomimetic materials with superior properties.[51,52] Due to the challenges associated with long and complex native collagen, ongoing studies are developing both covalent and non-covalent interactions to preorganize collagen-like peptides (CLPs) to investigate their biological functions. [52-62] CLPs are shorter

sequences that simulate native collagenous materials. Their synthesis is generally rapid and cost-effective.[53,58] The structure, stability, and self-assembly of these constructs have been explored since the late 1960s, using both covalent and non-covalent strategies to impart greater physical stability and encourage fibril formation.[57]

The simplest approach utilizes the endogenous properties originating from the individual amino acids of the alpha chains. In addition, incorporation of non-natural amino acids can further tune the biopolymer properties - inclusion of functionalized prolines can influence stereoelectronic effects,[59-61] while azaglycines exploit additional hydrogen bonding interactions.[62-64] Ionizable side chain pairs, such as lysine and aspartate or glutamate, form interchain salt bridges between dissimilar collagen strands with high thermal stabilities, as designed de novo by the Hartgerink laboratory.[65,66] They were also among the first to experiment with the application of electrostatic interactions to self assemble CLP hydrogels exhibiting viscoelastic properties, storage and loss moduli, comparable to native collagens despite the CLPs being approximately 30 times shorter in length.[65] **(Figure 3)**.

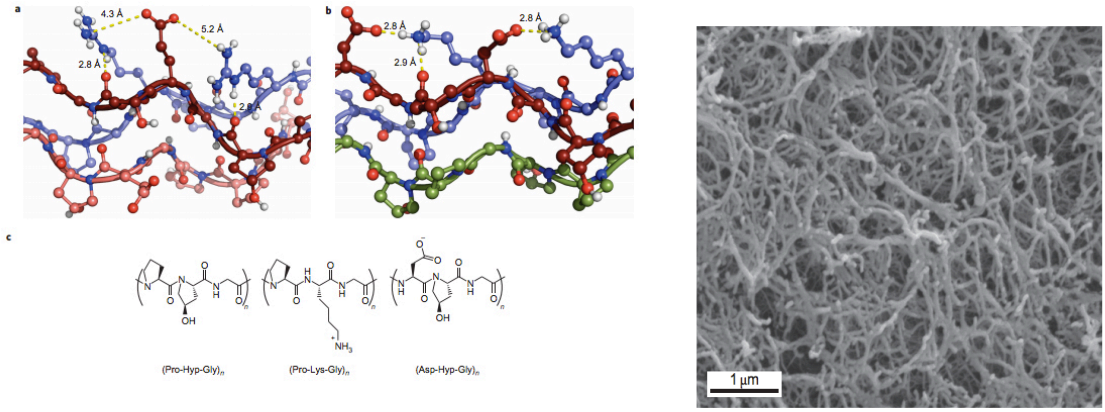

Figure 3 Left: Models of Hartgerink's first self assembling collagen related peptide constructs, stabilized by electrostatic interactions between charged pairs Arg-Glu in (a) and Lys-Asp (b). Amino acid triplet repeats incorporated into the collagen-like self assembling peptides (c).Right: SEM images showing hydrogel formation. (Hartgerink, J.D. *et. al,* 2011).[65]

Covalent stabilization can also be an effective means to assemble and secure the triple helix. A common covalent strategy is tethering CLPs from a molecular scaffold at either the N or the C terminus in order to promote triple helix formation. [57, 58, 67-86] Tethering not only liberates triple helix formation from a concentration dependent organization, but also engenders greater conformational stability for the resulting constructs at shorter chain lengths, further simplifying the synthesis and subsequent analysis of synthetic collagen triple helices.[58,70,71] (**Figure 4**) Early work from the Heidemann and Fields labs employed simple lysine dimers and tricarboxylic acid

templates to encourage triple helix formation,[72-76] while the Goodman lab assessed other modest trifunctional scaffolds including tris(2-aminoethyl)amine (TREN) and tris(hydroxymethyl)aminomethane (TRIS) assisted by the coordination of Fe^{3+}.[78,79,83,84] Recent reports describe disulfide and oxime bridges as additional functional covalent tethers. [80-82]

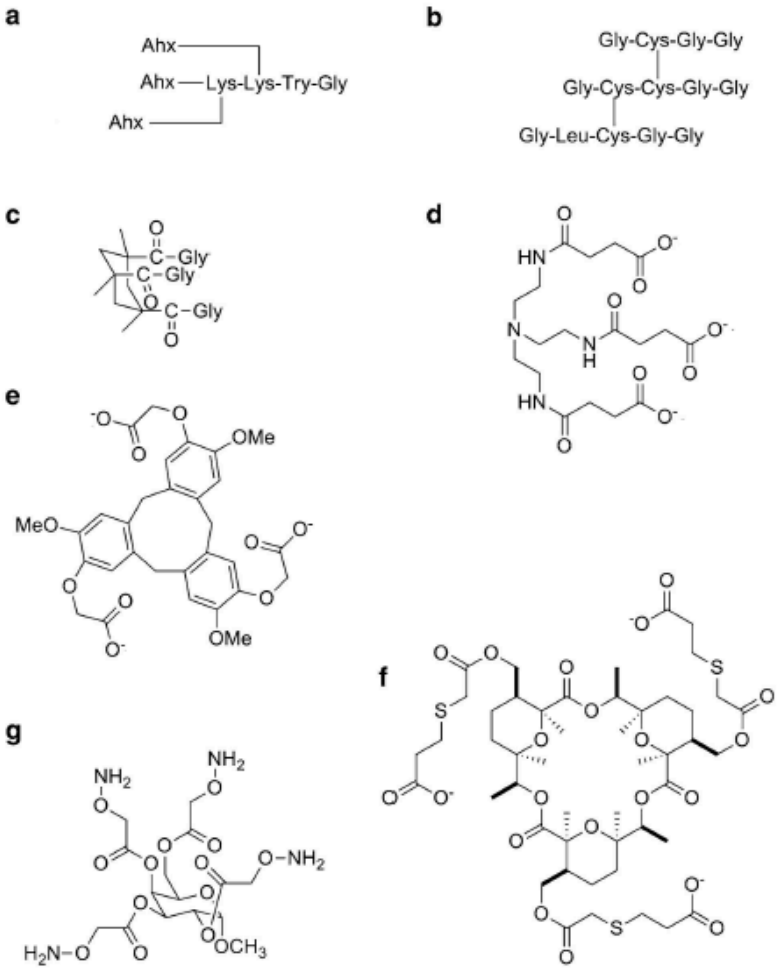

Figure 4 Common covalent scaffolds for templating triple helix formation of CLP. Dilysine branch functionalized with 6-aminohexanoic acid (Ahx) handle for CLP attachment (a); cysteine knot (b), *cis*,*cis*-1,3,5-trimethylcyclohexane-1,3,5-tricarboxylic acid (KTA) (c), tris(2-aminoethyl)amine (TREN) (d), cyclotriveratrylene (CTV) (e), macrocyclic hydropyran oligotide (f), methyl 2,3,4,6-tetra-O-Aoa-α-D-Gal*p* (g). (Bhowmick, M and Fields. G.B., 2014).[51]

Templating CLPs from a cyclic scaffold was pioneered by the Goodman lab in the 1990's. For example, tethering CLPs to one face of a rigid cyclohexane ring (Kemp's

Triacid) by virtue of three axially oriented reactive groups afforded not only the shortest CLP triple helix at room temperature, but also a thermal stability similar to that of native tropocollagen.[69] More recently, the Raines lab has elaborated this approach, using a hydropyran oligotide macrocycle with three foci for CLP attachment oriented on one face of the macrocycle, forming an equilateral triangle and improving stability.[58]

Metal-mediated triple helix formation has also been achieved by metal-chelating groups, as in bipyridine and other systems with high electron density, coupled to the peptide oligomer which take advantage of electron-poor metal centers and initiate complex and stable arrangements of collagen like peptide into triple helices.[85-87] Functional wound healing materials, such as bio-based hydrogels have also benefitted from the addition of metal ions to control assembly, and have enriched these materials with additional wound healing benefits. Metal binding centers incorporated into CLPs encapsulating growth factor payloads induced gelation upon Ni^{2+} coordination and have been exploited to enhance cell proliferation and affect cell morphology in a time-controlled manner.[88]

Despite the extensive practice and research of incorporating native oligopeptide systems for wound healing and drug delivery, a few inherent challenges are posed with this choice of biopolymer. Collagen is a large and structurally intricate protein, and its synthesis in the lab or expression by bacteria is arduous, time consuming, and subject to contamination.[88-92] Contamination is also a concern when sourcing from biological origins,[3,91,93] While proteolytic degradation may be advantageous in some cases, the rate and extent of degradation of the dressing must be carefully controlled.[95] In addition, the study of collagen is often difficult not only due to its large size and repeating

structure, but also because of its insolubility.[94,95] Solubilizing this rigid and stable structural protein often results in a loss of the complex hierarchical assembly that researchers wish to investigate. Further derivatization of shorter collagen-like sequences or replacement of large native collagen scaffolds with bio-inspired polymers could impart these peptide-based scaffolds with enhanced physical, chemical, mechanical, and medically applicable features.

The Role of Therapeutic Metal Ions in Cosmecuetical Agents

Metal ions play an underappreciated role in the wound healing processes. Zn^{2+} is long established as a known antimicrobial metal species, but the transition metal is also an essential cofactor in cellular and wound repair and shown to improve wound healing outcomes when applied topically.[96-100] Nanoparticulate silver ions have a heavily documented history as non-toxic antibacterial agents,[101] and have recently found their use contained in bioploymer dressings.[102]

Since the 1970's metal-peptide complexes, most notably the copper chelated tri-peptide sequence, Cu-GHK, have garnered a niche following and gained stature in the cosmetics community in anti-aging and skin conditioning treatments.[103] Its outstanding performance in clinical trials when included as a performance ingredient in various cosmetic products to treat photo damage, pigmentation, and diminished skin elasticity and thickness, mirror its natural biological function. [104-106] During the onset of injury, this sequence is proteolytically cleaved at the site of damage, which then directs cellular regulatory molecules towards healing damaged tissues.[104]

Practical challenges associated with the discovery of these metal-binding peptide complexes impede the creation and implementation of such materials into commercial practice. The prediction of these sequences to bind metals can be difficult, and the design, creation, and evaluation of every possible sequence is arduous, time consuming, and expensive.[107] Over the past several decades, research has been conducted into creating combinatorial libraries of resin-bound peptides and polymers to evaluate their metal binding capabilities in a high-throughput manner.[107,108] These strategies are often colorimetric in nature, only provide a qualitative binding event, and are only optimized to screen one metal at a time.[109,110] With this technical challenge and obvious need to generate better methods for rapidly detecting metal binding events, we are also offered an outstanding opportunity to discover new oligomers capable of binding a plethora of different metal species, as automated high throughput screening has the capacity to evaluate large compound libraries in excess of 100,000 members per day.[111]

Attenuating Gene Expression and Scar Tissue Formation through siRNA Silencing Therapy

In addition to collagen-based dressings and metal-meditated strategies, exploration of other modalities for wound treatments has been pursued through genetic therapies. For example, implementation of siRNA-mediated gene silencing currently represents an active area of research that holds promise for use in commercial biomedical applications.[112-116] The rationale behind such approaches takes aim at attenuating scar tissue formation, preventing excessive collagen deposition at the site of injury by altering gene expression. The focus of much of this research is, in particular,

the silencing of the gene SMAD3, which has recently been implicated as a major regulator of fibrotic outcomes.[117-122] Its activation by TGF-β leads to translocation of the complex to the nucleus where it upregulates genes that transcribe many collagen and extracellular matrix proteins.[123] During *in vivo* testing, SMAD3 null mice were resistant to radiation-induced cutaneous injury and experienced accelerated healing durations in delayed wound healing models, indicating successful suppression of a key mediator in phenotypic pathologies and returning the tissue to a more healthy condition.[124-127]

Several research groups,[117,122,126,127] including the Branski laboratory, have devoted efforts to silencing SMAD3 and discovering functional/physiological outcomes. However, intracellular delivery of SMAD3-silencing oligonucleotides is not trivial. siRNA therapy is most appropriate for treatment areas that are accessible for localized delivery, as systemic administration of siRNA has demonstrated unintended off-target effects.[115,128] In order to be most effectively transfected into the cell, siRNAs require a delivery vehicle which will protect the nucleic acid cargo from hydrolytic cleavage and facilitate passage through the cell membrane into the desired area of interest since the oligonucleotide's high molecular weight and anionic charge impedes cellular uptake.[129-131] Many options of varying compositions are used, from virus capsids, to polycationic lipids, and carbohydrate based systems.[131-138] Intriguingly, only a subset of clinical trials incorporate a delivery method, creating not only a medically, but also a financially inefficient therapeutic modality.[114] Currently, the most popular and commercially available transfection reagent is Lipofectamine®, a polycationic lipid complex. Unfortunately, Lipofectamine is not suitable or approved for *in vivo* use, an obvious hurdle towards the discovery of meaningful biomedical solutions.[114] In addition to

cytotoxicity, other hurdles that plague such delivery systems include cell, oligonucleotide, and tissue specificity.[138] There exists a need for a delivery reagent that is potent enough to effectively transfect a variety of oligonucleotide therapeutics to different cell and tissue types with limited cytotoxicity.

Addressing the Pitfalls of Biomaterials with Bio-inspired Materials

This dissertation describes how a family of peptidomimetic oligomers termed "peptoids" may address the challenges posed by natural biopolymers as wound dressing preparations and biomedically and cosmetically relevant materials. N-substituted glycine peptoid oligomers are an important class of sequence-specific biomimetic foldamers that exhibit a range of structural and functional attributes, some reminiscent and others distinct from natural peptides.[139] Peptoids can be readily assembled via a robust solid phase synthesis protocol to incorporate a wide variety of side chain functional groups.[140] Relative to peptides, peptoids contain tertiary amide linkages, establishing proteolytic stability, broader solvent compatibility, and enhanced cell permeability.[141-145] (**Figure 5, Left**) Although peptoids lack inherent chirality and hydrogen bonding capacity in the amide backbone, structure-inducing side-chains and covalent constraints can be incorporated to provide stable, well defined peptoid oligomers. [144] (**Figure 5, Right**)

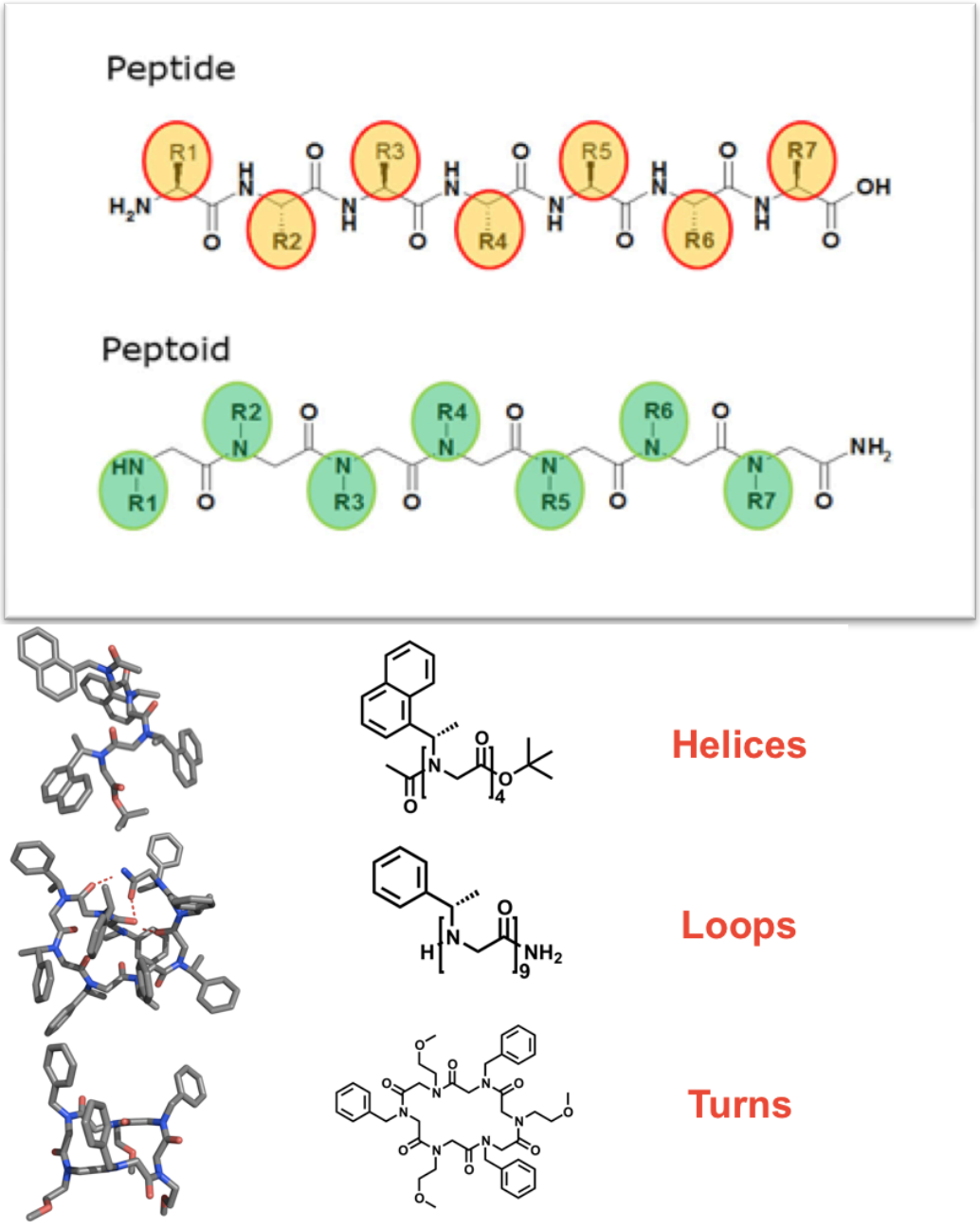

Figure 5. Side by side comparison of a natural polypeptide versus a peptoid. Note the lack of inherent backbone chirality and hydrogen bond donor groups on the peptoid chains (top). Experimentally determined structures of several stable peptoid architectures mimicking natural protein secondary structures (bottom). (Yoo, B., 2008).[146]

The incorporation of chemical diversity within peptoid oligomers has been investigated to focus on biomedical and materials objectives.[144-153] For example, multivalent peptoid conjugates displaying steroid hormone ligands targeting the androgen receptor, indicated for prostate cancer, have shown significant activity in vitro and are currently being tested in vivo.[146] In addition, cyclic antimicrobial peptoids have demonstrated the ability to compromise the cell membranes of antibiotic-resistant pathogenic bacteria.[147] Pertinent to wound healing, peptoid compound combinatorial libraries have been evaluated using high throughput micro-array based screening techniques to identify antagonists of fibroblast growth receptors, which are implicated in angiogenesis, embryonic development, cell proliferation, and cell differentiation.[154] (**Figure 6)** Four linear peptoid sequences were identified as hit compounds from the high throughput screen, and one hit was determined to be a particularly potent activator of two FGFR signaling pathways in a dose and time dependent manner.

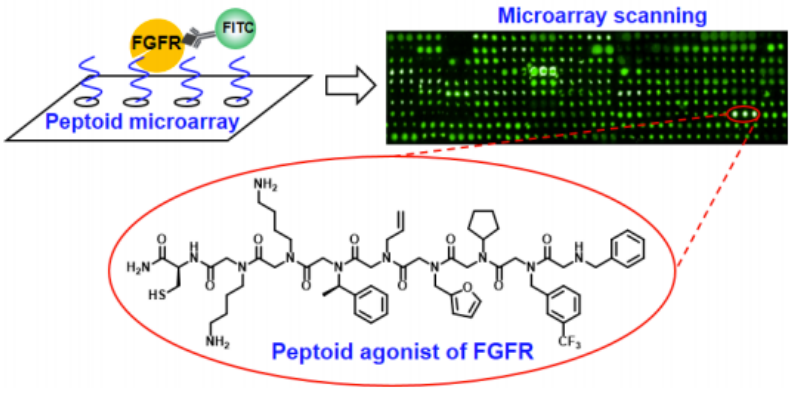

Figure 6. Micro-array based high throughput screening of a library of peptoid nonamers for antagonist activity of FGFR. (Qi, X., 2016).[154]

Additional functional attributes may be attained through the coordination of metallic species to the oligomer framework, as in the case with peptides.[155-164] Previous reports have determined that peptoid secondary structure can be modulated upon metal binding.[158,159,160] In 2009, Maayan and colleagues reported an increase in helical character of two peptoid polyproline I helices once bound to divalent Cu or Co.[161] (**Figure 7**)

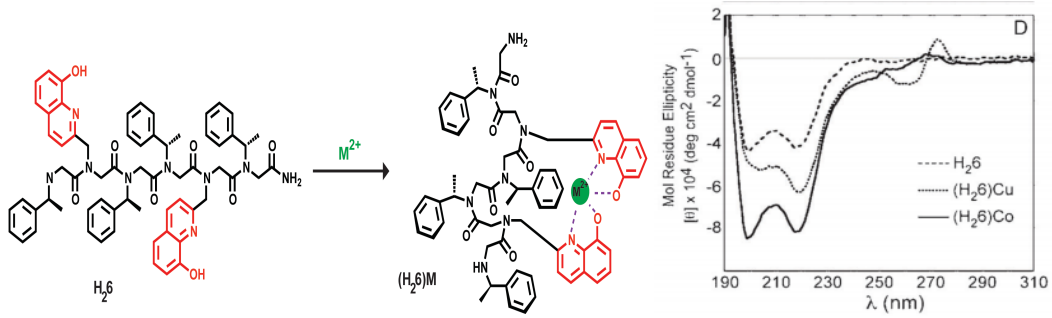

Figure 7. CD analysis of solution phase peptoid-metal binding to Cu and Co. Peptoid hexamer **$H_2$6** bearing quinoline-type binding ligands and nature of their binding structure upon exposure to Cu or Co (Left). CD spectrum demonstrating enhanced PPI helicity upon metal binding (Right).(Maayan, G., 2009)[161]

Zuckermann also explored the formation of peptoid helix bundles through coordination of Zn^{2+} to imidazole and thiol sidechains.[159] Additionally, peptoids displaying sulfhydryl functional groups can be used to selectively deplete chromium (VI) from solution, showing promise for peptoids as anti-oxidant and waste water remediation agents.[109]

1.2 Summary and Outlook

Through continued experimentation and discovery of novel bio-based molecules, progress can be made toward improved wound closure, re-epithelialization, scar tissue inhibition, and perhaps even tissue regeneration in acute and chronic wound states. In our quest to conceive novel bio-inspired materials, we are currently only limited by our own creativity, as nature has provided us with ample resources to combine, mimic, and template into such creations that modulate and improve wound-healing outcomes. With an aging population and increase in age-related pathologies, the pursuit of knowledge and invention of molecular solutions to our current challenges in wound healing becomes all the more urgent. The late Susan Lindquist, member of the Whitehead Institute and Professor of Biology at MIT, captured this sentiment concerning the future of molecular pioneering best: “About 10,000 years ago, [humans] began to domesticate plants and animals. Now it’s time to domesticate molecules.”[164] With our sights set on molecular mastery, we have two key objectives: the domestication of wild molecules, and the cultivation of their tempered, synthetic mimics.

1.3 References

1. Boateng, J.S.; Matthews, K.H.; Stevens, H.N.E.; Eccleston, G.M. *Journal of Pharmaceutical Sciences*. **2008,** *97*, 2892-2923.
2. Chattopadhyay, S. and Raines, R.T. *Biopolymers*. **2014,** *101*, 821-833.
3. (a) Aramwit, P*. Wound Healing Biomaterials*, Woodhead Publishing: Cambridge, 2016; pp 3-38. (b) Das, S. and Baker, A.B. *Front. Bioeng. Biotechnol.* **2016**. *4,* 1-20.
4. Rahimnejad,M. Soroosh Derakhshanfar, S.; Zhong, W. *Burns & Trauma*. **2017**, *5*, 1-9.
5. Deng, J.J.; Li, P.Y.; Cheng, H. *"Advances of Smart Materials for Wound Healing" Smart Materials for Tissue Engineering: Applications;* Wang, Q.; Ed.; Royal Society of Chemistry: Cambridge, 2017; pp. 258-289.
6. Agrawal, P.; Soni, S.; Mittal, G.; Bhatnagar, A. *The International Journal of Lower Extremity Wounds*. **2014**, *13*, 180–190.
7. Han, S.K. *Innovations and Advances in Wound Healing*. Springer-Verlag:Berlin Heidelberg, 2015.
8. (a) Gellman, S.H. *Acc. Chem. Res*. **1998**, *31*, 173–180. (b) Goodman, C.M.; Choi, S.; Shandler, S.; DeGrado, W.F. *Nat. Chem. Biol*. **2007**, *5*, 252–262. (c) Sood, A.; Granick, S.M.; Tomaselli, N.L. *Advances in Wound Care*. **2014**. *3,* 511-529. (d) DeGrado, W. F. *Chem. Rev.* **2001**, *101*, 3025.
9. (a) Piraino, F. and Selimović, S. *BioMed Research International*. **2015**, 1-10. (b) Andreu, V.; Mendoza. G.; Arruebo, M.; Irusta, S. *Materials*. **2015**, *8*, 5154-5193;
10. Geoffrey, C.; Gurtner, G.C.; Werner, S.; Barrandon, Y.; Longake, M.T. *Nature*. **2008**, *453*, 314-321.

11. Velnar, T.; Bailey, T.; Smrkolj, V. The Journal of International Medical Research. **2009**, *37*, 1528 – 1542.
12. Beanes, S.R.; Dang, C.; Soo, C.; Ting, K. *Expert Reviews in Molecular Medicine*. **2003,** *5*.
13. Budovsky, A.; Yarmolinsky, L.; Ben-Shabat, S. *Wound Rep. Reg*. **2015**, *23*, 171–183.
14. Subhamoy, D. S. and Baker, A.B. *Frontiers in Bioengineering and Biotechnology*. **2016**, *4*.
15. Järbrink, K.; Ni, G.; Sönnergren, H.; Schmidtchen, A.; Pang, C.; Bajpai, R.; Car, J. *Systematic Reviews*. **2017**, *6*.
16. Chalmers, R. L. *International Wound Journal*. **2011**, *8*, 218-223.
17. Conway, B. *Wall Street BioBeat*. **2010**, *30*(21).
18. Singh, O.; Gupta, S.S.; Soni, M.; Moses, S.; Shukla, S.; Mathur, R.K. *Journal of Cutaneous and Aesthetic Surgery*. **2011**, *4*, 12-16.
19. Demir Sezer, A. and Cevher, E. *Biopolymers as Wound Healing Materials: Challenges and New Strategies, Biomaterials Applications for Nanomedicine;* Prof. Pignatello, R. Ed.; InTech: [Online] **2011**; Available from: http://www.intechopen.com/books/biomaterials-applications-fornanomedicine/biopolymers-as-wound-healing-materials-challenges-and-new-strategies
20. Ulery, B.D.; Nair, L.S.; Laurencin, C.T. *J. Polym. Sci. B. Polym. Phys.* **2011**, *49*, 832–864.

21. Methods in Molecular Biology. In *Wound Regeneration and Repair: Methods and Protocols.* Gourdie, R.G. and Myers, T.A.; Eds.; Humana Press. Springer Science+Business Media :New York, 2013, Vol. 1037.
22. *Wound Healing and Skin Physiology*. Altmeyer, P.; Hoffmann, K.; el Gammal, S.; Hutchinson, J.; Eds.; Springer-Verlag: Berlin Heidelberg, 1995.
23. Gil, E.S.; Panilaitis, B.; Bellas, E.; Kaplan, D.L. *Adv. Healthcare Mater.* **2013**, *2*, 206–217.
24. Ong, S.-Y.; Wu, J.; Moochhala, S.M.; Tan, M.H.; Lu, J. *Biomaterials*. **2008**, *29*, 4323–4332.
25. Kumar, T.R.S; Bai, M.V.; Krishnan, L.K. *Biologicals*. **2004**, *32*, 49–55.
26. Ruszczak, Z. *Adv. Drug Deliv. Rev.* **2003**, *55*, 1595-1611.
27. Wallace, D. G.; Rhee, W.; Reihanian, H.; Ksander, G.; Lee, R.; Braun, W. B.; Weiss, B. A.; Pharriss, B. B. *J. Biomed. Mater. Res*. **1989**, *23*, 931–945.
28. Slavin, J.; Nash, J. R.; Kingsnorth, A. N. *Br. J. Surg*. **1992**, *79*, 69–72.
29. Chattopadhyay, S. and Raines, R.T. *Biopolymers*, **2014**, *101*, 821-833.
30. Lazovic, G.; Colic, M.; Grubor, M.; Jovanovic, M. *Annals of Burns and Fire Disasters*, **2005**, *18*, 151-156.
31. Gottlieb, D.; Morin, S.A.; Jin, S.; Raines, R.T. *Journal of Materials Chemistry*, **2008**,*18*.
32. Luo, T. and Kiick, K.L. *Bioconjugate Chem*. **2017**, *28*, 816−827.
33. Marchand, R.; Woerly, S.; Bertrand, L.; Valdes, N. *Brain. Res. Bull.* **1993**, *30,* 415–422.
34. Urello, M. A.; Kiick, K. L.; Sullivan, M. O. *J. Mater. Chem. B*. **2014**, *2,* 8174−8185.

35. Urello, M. A.; Kiick, K. L.; Sullivan, M. O. *Bioengineering and Translational Medicine. **2016**, 1*, 207−219.

36. Miclau, T.; Edin, M.L.; Lester, F.E.; Lindsey, R.W.; Dahners, L.E. J. Orthop. Trauma. **1995**, *9*, 401–406.

37. Ruszczak, Z. and Friess, W. *Advanced Drug Delivery Reviews*, **2003**, *55*, 1679–1698.

38. Singh, M.P.; Stefko, J.; Lumpkin, J.A.; Rosenblatt, J. *Pharmaceutical Research*. **1995**, *12*, 1205-1210.

39. LeBourlais, C.; Acar, L.; Zia, H.; Sado, P.A.; Needham, T.; Leverge, R. *Prog. Retin. Eye Res.***1998,** *17*, 33 – 58.

40. Aquavella, J.V. ; Ruffini, J.J.; LaCascio, J.A. *J. Cataract Refract. Surg*. **1988**,*14* 492 – 495.

41. Knaepler, H. *International Journal of Surgery*, **2012**, *10*, S15-S20.

42. Gopinatha, D.; Ahmeda, M.R.; Gomathia, K.; Chitraa, K.; Sehgalb, P.K.; Jayakumar, R. *Biomaterials*, **2004**, *25*, 1911–1917.

43. Yannas, I. V. *Angew. Chem. Int. Ed*. **1990**, *29*, 20–35.

44. Stompro, B. E.; Hansbrough, J. F.; Boyce, S. T. J. Surg. Res. **1989**, *46*, 413–421.

45. Wendy A. Petka, W.A.; Harden, J.L.; McGrath, K.P.; Wirtz, D.; Tirrell, D.A. *Science*.**1998**, *281*, 389-392.

46. (a) Wachol-Drewek, Z.; Pfeiffer, M.; Scholl, E. *Biomaterials*. **1996,** *17*, 1733–1738. (b) Marks, M. G.; Doillon, C.; Silvert, F. H. *J. Biomed. Mater. Res.* **1991**, *25,* 683–696. (c) Sung, K. E.; Su, G.; Pehlke, C.; Trier, S. M.; Eliceiri, K. W.; Keely, P. J.; Friedl, A.; Beebe, D. J. *Biomaterials*. **2009**, *30*, 4833– 4841.

47. Brodsky B, Shah NK. (1995). FASEB J., 9:1537–1546.

48. Shoulders, M.D. and Raines, R.T. *Annual Review of Biochemistry*. **2014**, *78*, 929–958.

49. Jenkins, C.L. and Raines, R.T. *Nat. Prod. Rep*. **2002**,*19*, 49–59.

50. Image Retrieved from: http://bayareapelleve.com/pelleve/collagen/)

51. Bhowmick, M. and Fields, G. B. *Methods Mol. Biol*.**2013**,*1081*,167–194.

52. Fields, G.B. and Prockop, D.J. *Biopolymers*. **1996**, *40*, 345–357.

53. Koide, T. *Connect. Tissue Res*. **2005**, *46*,131–141.

54. Koide ,T. *Philos. Trans. R. Soc. Lond. B. Biol. Sci*. **2007**, *362*,1281–1291.

55. Brodsky, B.; Thiagarajan, G.; Madhan, B.; Kar, K. *Biopolymers*. **2008**, *89*, 345–353

56. Fields, G.B. *Org. Biomol. Chem*. **2010**, *8,* 1237–1258.

57. Yu, S. M.;Li, Y.; Kim, D. *Soft Matter*, **2011**, *7*, 7927–7938.

58. Horng, J.-C.; Hawk, A. J.; Zhao, Q.; Benedict, E. S.; Burke, S. D.; Raines, R. T. *Org. Lett.* **2006**, *8*, 4735−4738.

59. Hodges, J.A. and Raines, R.T. *J. Am. Chem. Soc*. **2005**, *127*, 15923-15932.

60. Shoulders, M.D.; Hodges, J.A.; Raines, R.T. *J. Am. Chem. Soc.,* **2006**, *128*, 8112–8113.

61. Pandey, A.K.; Naduthambi, D.; Thomas, K.M.; Zandlo, N.J. *J. Am. Chem. Soc.* **2013**, *135*, 4333−4363.

62. Zhang, Y.; Malamakal, R.M.; Chenoweth, D.M. *J. Am. Chem. Soc*., **2015**, *137*, 12422–12425.

63. Kasznel, A.J.; Zhang, Y.; Hai, Y.; David M. Chenoweth, D.M. *J. Am. Chem. Soc.* **2017**, *139*, 9427–9430.

64. O'Leary, L. E. R.; Fallas, J. A.; Bakota, E. L.; Kang, M. K.; Hartgerink, J. D. *Nat. Chem.* **2011**, *3*, 821−828

65. Paramonov, S. E.; Gauba, V.; and Hartgerink, J. D. *Macromolecules*. **2005**, *38,* 7555–7561.

66. Byrne, C.; McEwan, P. A.; Emsley, J.; Fischer, P. M.; Chan, W. C. *Chem. Commun.* **2011**, *47*, 2589−2591.

67. Feng Y, Melacini G, Taulane JP, Goodman M. *J. Am. Chem. Soc.* **1996**,*118*, 10351–10358.

68. Goodman, M.; Bhumralkar, M.; Jefferson, E.A.; Kwak, J.; Locardi, E. *Biopolymers (Peptide Science).* **1998**, *47,* 127–142.

69. Boudko, S. P.; Engel, J.; Bächinger, H. P. *The Journal of Biological Chemistry*. **2008**, *283*, 34345–34351.

70. Mizuno, K.; Boudko, S. P.; Engel, J.; Bächinger, H. P. *Biophysical Journal*. **2010**, *98*, 3004-3014.

71. Greiche, Y.; Heidemann, E. *Biopolymers*. **1979**, *18*, 2359-2361.

72. Roth, W.; Heidemann, E. *Biopolymers*. **1980**, *19*, 1909-1917.

73. Fields, C. G.; Grab, B.; Lauer, J. L.; Fields, G. B. *Anal. Biochem*. **1995**, *231*, 57-64.

74. Grab, B.; Miles, A. J.; Furch, L. T.; Fields, G. B. *J. Biol. Chem***. 1996**, *271*, 12234-12240.

75. Miles, A.; Skubitz, A. P. N.; Furch L. T.; Fields, G. B. *J. Biol. Chem*. **1994***, 269*, 30939-30945.

76. Khew, S. T.; Tong, Y. W. *Biochemistry*. **2008**, *47*, 585−596.

77. Kwak, J.; De Capua, A.; Locardi, E.; Goodman, M. *J. Am. Chem. Soc*. **2002**, *124*, 14085-14091.

78. Cai, W.; Wong, D.; Kinberger, G.A.; Kwok, S.W.; Taulane, J.P.; Goodman, M. *Bioorg. Chem*. **2007**, *35*, 327-337.

79. Boulègue, C.; Musiol, H.J.; Götz, M.G.; Renner, C.; Moroder, L. *Antioxid. Redox. Signal*. **2008**, *10*, 113-125.

80. Tanrikulu, I. C. and Raines, R. T. *J. Am. Chem. Soc*. **2014**. *136*, 13490−13493.

81. Hentzen, N.B.; Smeenk, L.E.J.; Witek, J.; Riniker, S.; Wennemers, H. *J. Am. Chem. Soc*. **2017**, *139,* 12815−12820.

82. Kinberger, G.A.; Cai, W.; Goodman, M. *J. Am. Chem. Soc.* **2002**, *124*, 15162–15163.

83. Rump, E.T.; Rijkers, D.T.; Hilbers, H.W.; de Groot, P.G.; Liskamp, R.M. *Chemistry*. **2002**, *8*, 4613-4621.

84. Cai, W.; Kwok, S.W.; Taulane, J.P.; Goodman, M. *J. Am. Chem. Soc.* **2004**, *126*, 15030–15031.

85. Kinberger, G.A.; Taulane, J.P.; Goodman, M. *Inorg. Chem*. **2006**, *45*, 961–963.

86. Pires, M.M. and Chmielewski, J. *J. Am. Chem. Soc*. **2009**, *131*, 2706–2712.

87. Lemire, J.A.; Harrison, J.J.; Turner, R.J. *Nature Reviews Microbiology*, **2013**, *11,* 371-384.

89. Schneider, A.; Garlick, J.A.; Christophe Egles, C. *PLoS ONE*. **2008**,*1*, e1410.

90. Buechter, D. D. et al. *J. Biol. Chem*. **2003**, *278*, 645–650.

91. Kotch, F.W. and Raines, R. T. *PNAS*, **2006**, *103*, 3028-3033.

92. Paramonov, S. E.; Gauba, V.; Hartgerink, J. D. *Macromolecules*, **2005**, *38*, 7555–7561.

93. Lynn, A. K., Yannas, I. V. and Bonfield, W. *J. Biomed. Mater. Res. B*. **2004**, *71*, 343–354.

94. *Advanced Wound Repair Therapies;* Farrar, D., Ed.; Woodhead Publishing: Philadelphia, 2011.

95. Shoulders, M.D. and Raines, R.T. *Annu. Rev. Biochem*. **2009**, *78*, 929–958.

96. Lansdown, A. B. G. ; Mirastschijski, U.; Stubbs, N.; Scanlon, E.; Gren, M.S. *Wound Repair Regen*. **2007**, *15*, 2-16.

97. Scanlon, E. and Agren, M.S. *Wound Repair Reg*. **2007**, *15,* 2–16.

98. Agren, M.S.; Soderberg, T.A.; Reuterving, C.O.; Hallmans, G.; Tengrup, I. *Eur. J. Surg.* **1991**, *157*, 97–101.

99. Akiyama, H.; Yamasaki, O.; Kanzaki, H.; Tada, J.; Arata, J. *J. Dermatol. Sci.* **1998**, *17*, 67-74.

100. Podbielski, A.; Boeckh, C.; Haller, B.; *J. Endod*. **2000**, *26*, 398–403.

101. Wiegand, C.; Heinze, T.; Hipler, U-C. *Wound Rep. Reg.* **2009**, *17,* 511–521.

102. Kim, J.; Kwon, S.; Ostler, E. *Journal of Biological Engineering*. **2009**, *3*.

103. Pickart, L. and Shagan, S. (2015). New Data from the Cosmeceutical and Tripeptide GHK [publication]. SOFWA-Journal. Retrieved from: [http://skinbiology.com/SOFW2015_CosmeceuticalTriPeptideGHK.pdf .

104. Gorouhi, F. and Maibach, H. I. *International Journal of Cosmetic Science*. **2009**, *31*, 327–345

105. Abdulghani, A.A.; Sherr, A.; Shirin, S.; Solodkina, G.; Tapia, E.; Wolf, B. *et al*. *Dis. Manag. Clin. Outcomes*. **1998**, *1*, 136–141.

106. Finkey, M.B.; Appa, Y.; Bhandarkar, S. *Copper peptide and skin. In: Cosmeceuticals and Active Cosmetics*, 2nd edn.; Elsner, P. and Maibach, H.I., Eds.; Marcel Dekker: New York, NY, 2005, pp. 549–564.

107. Minogue, E.M.; Havrilla, G.J.; Taylor, T.P.; Warner, B.P.; Burrell, A.K. *New J. Chem.* **2006**, *30*, 1145–1148.

108. Szymański, P.; Markowicz, M.; Mikiciuk-Olasik, E. *Int. J. Mol Sci*. **2012**, *13,* 427–452.

109. Knight, A.S.; Zhou, E.Y.; Pelton, J.G.; Francis, M.B. *J. Am. Chem. Soc*. **2013**, *135*, 17488-17493.

110. Francis, M. B.; Finney, N. S.; Jacobsen, E. N. *J. Am. Chem. Soc*. **1996**, *118,* 8983-8984.

111. Michael, S.; Auld, D.; Klumpp, C.; Jadhav, A.; Zheng, W.; Thorne, N.; Austin, C.P.; Inglese, J.; Simeonov. A. *ASSAY and Drug Development Technologies*. **2008**. *6*, 637-657.

112. Whitehead, K.A.; Langer, R.; Anderson, D.G. *Nature reviews Drug discovery.* **2009**, *8*, 129-138.

113. Bobbin, M.L. and Rossi, J. *J. Annu. Rev. Pharmacol. Toxicol*. **2016**, *56*, 103–122.

114. Burnett JC, Rossi JJ. Chem Biol 2012;19:60–71.

115. Burnett JC, Rossi JJ, Tiemann K. Biotechnol J 2011;6:1130–1146.

116. Resnier P, Montier T, Mathieu V, Benoit JP, Passirani C. *Biomaterials.* **2013**, *34*, 6429–6443.

117. Kraja, I.; Bing, R.; Hiwatashi, N.; *et al*. *The Laryngoscope.* **2016.** 1-7

118. Lim, X.; Tateya, I.; Tateya, T.; Munoz-Del-Rio, A.; Bless, D.M. *The Annals of otology, rhinology, and laryngology.* **2006**, *115*, 921-929

119. Leask, A. and Abraham, D.J. *FASEB journal : official publication of the Federation of American Societies for Experimental Biology.* **2004**, 18, 816-827.

120. Border, W.A. and Noble, N.A. *The New England journal of medicine.* **1994**, *331*,1286-1292.

121. Branski, R.C.; Barbieri, S.S.; Weksler, B.B.; *et al. Ann. Otol. Rhinol. Laryngol.* **2009**, *118*, 218-226.

122. Branski, R.C.; Bing, R.; Kraja, I.; Amin, M.R. *The Laryngoscope.* **2016**, *126*,1151-1156.

123. Kubiczkova, L.; Sedlarikova, L.; Hajek, R.; Sevcikova, S. *Journal of Translational Medicine*. **2012**, *10*, 2-24.

124. Flanders, K.C.; Sullivan, C.D.; Fujii, M.; Sowers, A.; Anzano, M.A.; Arabshahi, A.; *et. al. Am. J. Pathol*. **2002**, *160*, 1057.

125. Falanga, V.; Schrayer, D.; Cha, J.; Butmarc, J.; Carson, P.; Roberts, A.B.; Kim, S.-J. *Wound Repair and Regeneration*. **2004**.*12*, 320–326.

126. Layliev, J.; Wilson, S.; Warren, S. M.; Saadeh, P. B. *Advances in Wound Care*. **2012**, *1,* 218–223.

127. Lee, J.W.; Tutela, J.P.; Zoumalan, R.A.; Thanik, V.D.; Nguyen, P.D.;

Varjabedian, L.; Warren, S.M.; Saadeh, P.B. *Arch. Otolaryngol*. **2010**,*136*,714.

128. Sorensen, D.R.; Leirdal, M.; Sioud, M. *J. Mol. Biol*. **2003**,*327*,761–766.

129. Lee, R.C.; Fieinbaum, R.L.; Ambros, V. *Cell*. **1993**,*75*, 843–854.

130. *RNA Interference, Methods in Molecular Biology*, Akaneya, Y.; Min, W.-P.; Ichim, T., Eds.; Springer Science and Business Media: New York, NY, 2010.

131. Aigner, A. J. *Biomed. Biotechnol*. **2006**,*71*,659.

132. Dykxhoorn, D.M.; Lieberman, J. *Cell*. **2006**,*126*, 231-235.

133. Felgner, P.L.; Gadek, T.R.; Holm, M.; *et al*. *Proc. Natl. Acad. Sci. USA*.**1987**, *84,* 741–7417.

134. Andersen, M.O.; Howard, K.A.; Paludan, S.R.; Besenbacher, F.; Kjems, J. *Biomaterials*. **2008**, 506–512.

135. Beh, C.W.; Seow, W.Y.; Wang, Y.; *et al. Biomacromolecules*. **2009**,*10*,41–48.

136. Breunig, M.; Hozsa, C.L.U.; Watanabe, K.; Umeda, I.; Kato, H.; Geopferich, A. *J. Control Release*. **2008**,*130*,57–63.

137. Crombez, L.; Aldrian-Herrada, G.; Konate, K.; *et al. Mol. Ther*. **2009**,*17*,95–103.

138. Green, J.J.; Langer, R.; Anderson, D.G. *Acc. Chem. Res*. **2008**, *41*,749–759.

139. (a) Figliozzi, G.M.; Goldsmith, R.; Ng, S.; Banville, S.C.; Zuckermann, R.N. *Methods Enzymol*. **1996**, *267*, 437-447. (b) Culf, A.S. and Oulette, R.J. *Molecules.* **2010**, *15*, 5282-5335.

140. Huang, M. L.; Benson, M. A.; Shin, S. Y.; Torres, V. J.; Kirshenbaum, K. *Eur JOC*. **2013**, 3560-3566.

141. Levine, P. M.; Imberg, K.; Garabedian, M. J.; Kirshenbaum, K. *J. Am. Chem. Soc*. **2012**, *134*, 6912-6915.

142. Kwon, Y-U. and Kodadek, T. *J. Am. Chem. Soc*. **2007**, *129*, 1508-1509.

143. Miller, S.; Simon, R.; Ng, S.; Zuckermann, R.; Kerr, J.; Moos, W. *Bioorg. Med. Chem. Lett*. **1994**, *4*, 2657-2662.

144. (a) Yoo, B. and Kirshenbaum, K. *Curr. Opin. Chem. Biol*. **2008**, *12*, 714-721. (b) Shin, S.-B.Y., Yoo, B., Todaro, L., Kirshenbaum, K. *J. Am. Chem. Soc.* **2007**, *129,* 3218-3225. (c) Huang, K.; Wu, C.W.; Sanborn, T.J.; Patch, J.A.; Kirshenbaum, K.; Zuckermann, R.N.; Barron, A.E.; Radhakrishnan, I. *J. Am. Chem. Soc.* **2006**, *128*, 1733-1738. (d) Kirshenbaum, K.; Barron, A.E.; Goldsmith, R.A.; Armand, P.; Bradley, E.K.; Truong, K.T.V.; Dill, K.A.; Cohen, F.E.; Zuckermann, R.N. *Proc. Natl. Acad. Sci. USA*. **1998**, *95*, 4303-4308.

145. Chongsiriwatana, N.P.; Patch, J.A.; Czyzewski, A.M.; Dohm, M.T.; Ivankin, A.; Gidalevitz, D.; Zuckermann, R.N.; Barron, A.E. *PNAS.* **2008**, *105*, 2794-2799.

146. Huang, M. L.; Benson, M. A.; Shin, S. Y.; Torres, V. J.; Kirshenbaum, K. *Eur. JOC*, **2013**, 3560-3566.

147. Levine, P. M.; Imberg, K.; Garabedian, M. J.; Kirshenbaum, K. *J. Am. Chem. Soc*. **2012**, *134*, 6912-6915.

148. Turner, J.P.; Lutz-Rechtin, T.; Moore, K.A.; Rogers, L.; Bhave, O.; Moss, M.A.; Servoss, S.L. *ACS Chem. Neurosci*. **2014**, *5*, 552–558.

149. Maayan, G.; Ward, M.; Kirshenbaum, K. *Proc. Natl. Acad. Sci. USA*. **2009**, *106*, 13679-13684.

150. Della Sala, G.; Nardone, B., De Riccardis, F.; Izzo, I. *Org. Biomol. Chem*. **2013**, *11*, 726-731.

151. Statz, A. R.; Meagher, R. J.; Barron, A. E.; Messersmith, P. B. *J. Am. Chem. Soc*. **2005**, *127*, 7972–7973.

152. Huang, M.; Ehre, D.; Jiang, Q.; Hu, C.; Kirshenbaum, K.; Ward. M. *Proc. Natl. Acad. Sci. USA*. **2012**,*109,*19922-19927.

153. Fu, J.; Xia. A.; Qi, X. *Med. Chem. Commun*.v**2016**, *7*, 1183-1189.

154. Sanii, B.; Kudirka, R.; Cho, A.; Venkateswaran, N.; Oliver, G.K.; Olson, A.M.; Tran, H.; Harada, R.M.; Tan, L.; Zuckermann, R.N. *J. Am. Chem. Soc*. **2011**, *133*, 20808-20815.

155. Chen, C.L.; Qi, J.; Zuckermann, R.N.; DeYoreo, J.J. *J. Am. Chem. Soc* .**2011**, *133*, 5214-5217.

156. Kölmel, D.K.; Rudat, B.; Schepers, U.; and Bräse, S. Eur. J. Org. Chem. **2013**, 2761–2765.

157. Izzo I; Ianniello, G.; De Cola, C.; Nardone, B.; Erra, L.; Vaughan, G.; Tedesco, C.; DeRiccardis, F. *Org. Lett*. **2013**, *15*, 598-601.

158. Maayan, G.; Ward, M.; Kirshenbaum, K. *Chem. Commun*. **2009**, 56-58.

159. Lee, B. C.; Chu, T.K.; Dill, K.A.; Zuckermann, R.N. *J. Am. Chem. Soc*. **2008**, *130*, 8847-8855.

160. Pirrung, M. C.; Park, K.; Tumey, L. N. *J. Comb. Chem*. **2002**, *4*, 329-344.

161. Maayan, G. and Lui, L-K. *Biolpolymers*. **2011**, *96*, 697-687.

162. Cola, D. C.; Fiorillo, G.; Meli, A.; Aime, S.; Gianolio, E.; Izzo, I; De Riccardis, F. *Org. Biomol. Chem*. **2014**, *12*, 424-431.

163. Fischer, A. E. O. and Naughton, D. P. *J. Inorg. Biochem*. **2004**, *98*, 343-346

164. Zhang, S. *Nature Biotechnology*. **2003**, *21*, 1171-1178.

Chapter 2

Peptoid-Based Tethers as Effective Triple Helix Templates for Collagen Mimetic Peptides

2.1 ABSTRACT

Collagen is a biocompatible and resilient material characterized by an intricate triple helical architecture that endows this biopolymer with favorable attributes for wound dressing materials. Unfortunately, native collagen cannot recover its structural integrity following thermal denaturation. *N*-substituted glycine oligomers, or peptoids, are versatile architectures assembled by modular synthesis that can be engineered to enhance folding and stability. Here, we take advantage of peptoid oligomers as scaffolds for conjugation and preorganization of three collagen-like peptide chains into a canonical triple helix architecture with improved thermal stability. The triple helical structure was validated by circular dichroism and thermal denaturation studies, establishing both linear and macrocyclic peptoid scaffolds as effective templates for the self-assembly of collagen-like peptides into a robust triple helix assembly. This strategy will facilitate creation of novel biomaterials for wound healing and provides a platform for the generation of novel biomimetic materials with a variety of desirable physiochemical properties.

2.2 Introduction

Collagen, the most abundant structural protein in the human body, is a large and architecturally complex biopolymer responsible mechanical stability of bones and tissue.[1-6] The prototypical collagen polypeptides consist of repetitive Xaa-Yaa-Gly units, with

Xaa and Yaa commonly proline and hydoxyproline, respectively, forming a polyproline type II helix (PPII), termed an alpha chain. The glycine units are tightly packed in the interior of a triple helix formed by three PPII strands, which intertwine with a one amino acid stagger. The assembly is stabilized via intrastrand backbone hydrogen bonding that engenders self-assembly into its right-handed triple helical form, termed tropocollagen.[1] (**Figure 8**) Tropocollagen protein chain lengths can reach about 260 nm, over 1,000 residues in sequence. [6] Currently, there are 29 different types of collagen that have been identified and at least 25 unique PPII chain sequences which are known to form the collagen triple helix, most commonly in a heterotrimeric fashion.[7]

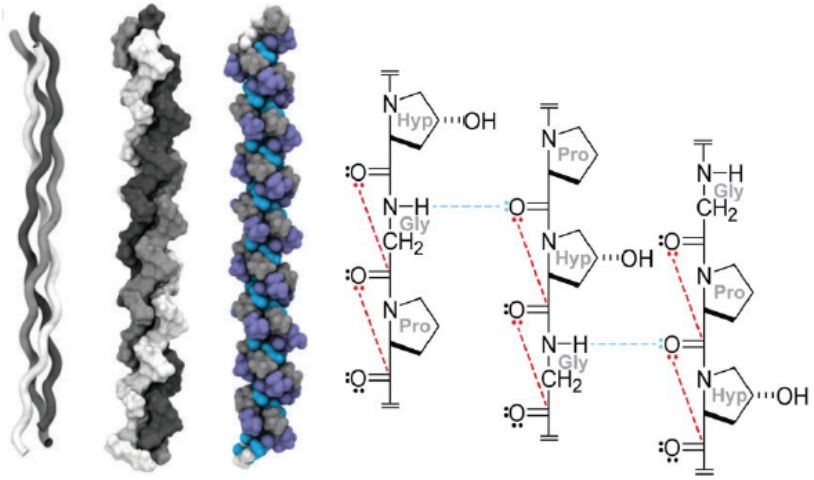

Figure 8. Cartoon, surface, and space filling models of a collagen model peptide (Pro-Hyp-Gly)$_{10}$.(Left).[7] **(**Hartgerink, 2010). **Depiction of** non-covalent means of triple helix stabilization: Blue dashes signify hydrogen bonding interactions, while red dashes denote main chain n-π* interaction. (Right)[2] (Chattopadhyay and Raines 2014)

Collagen fibrils, a collagen-based supramolecular assembly, consist of an

extended tropocollagen structure fashioned through covalent crosslinking and non-covalent interactions.[2,8] Tropocollagens are crosslinked through post-translationally modified lysine residues which then interdigitate and aggregate with neighboring fibrils; the resulting structure is comparable to a coiled microfiber assembling to form a braided nano-scale rope.[4,7] (**Figure 9**) Outstanding mechanical, thermal, and tensile strength, as well as flexibility result from this hyper stable triple helical fiber.[8]

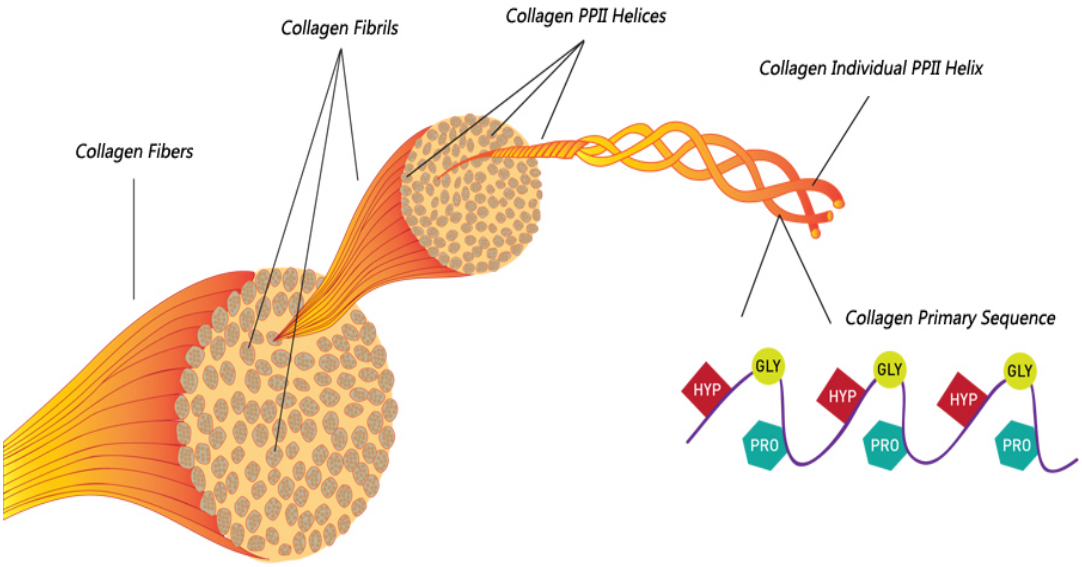

Figure 9. Structural hierarchy of collagen fibers (image taken from : http://bayareapelleve.com/pelleve/collagen/)[9]

Due to collagen's exceptional physical properties and self assembling capability, researchers have been eager to develop new biomimetic materials incorporating these superior traits. However, ongoing studies aim to circumvent some of the challenges associated with long and complex native collagens by utilizing strategies which rely on preorganizing collagen-like peptides (CLPs) to

investigate their structural roles and biological functions via covalent and non-covalent techniques.[7,10-17] Simulating native collagenous materials, CLPs are shorter and simpler sequences that boast synthetic ease and diminished synthetic costs.[17,19] Preliminary work on CLPs began in the late 1960s, exploring the structure, stability and self assembly of these constructs while working towards imparting greater physical stability and encouraging fibril formation.[18]

Simple non-covalent strategies rely on the inherent propensities of the individual amino acids of the alpha chains to construct linkages or, alternatively, the derivatization of such amino acid side chain groups, enhancing their natural electronic, steric, and hydrogen bonding effects. Substitution of hydroxyproline by other 4' functionalized prolines can exert an enhanced stereoelectronic effect,[20,21] and azaglycines offer additional hydrogen bonding contacts between the chains.[22-24] Inclusion of lysine and aspartate or glutamate engage in the formation of interchain salt bridges between different collagen strands, resulting in triple helices with high thermal stabilities upon ionization, as designed de novo by the Hartgerink laboratory.[25]

The Raines and Zondlo laboratories have extensively explored the forces that stabilize the triple helix at the level of each individual PPII chain, citing a stereoelectronic effect.[20,26] The rationale behind this lies in the conformational preferences of the pyrrolidine ring of both the Xaa and Yaa proline, adopting one of two stable conformational puckers at room temperature, C^{γ}-exo or C^{γ}-endo (**Figure 10**).[26]

The functionalization of the ring, such as in the addition of hydroxyl groups, can enhance stability of the triple helix.[27,28]

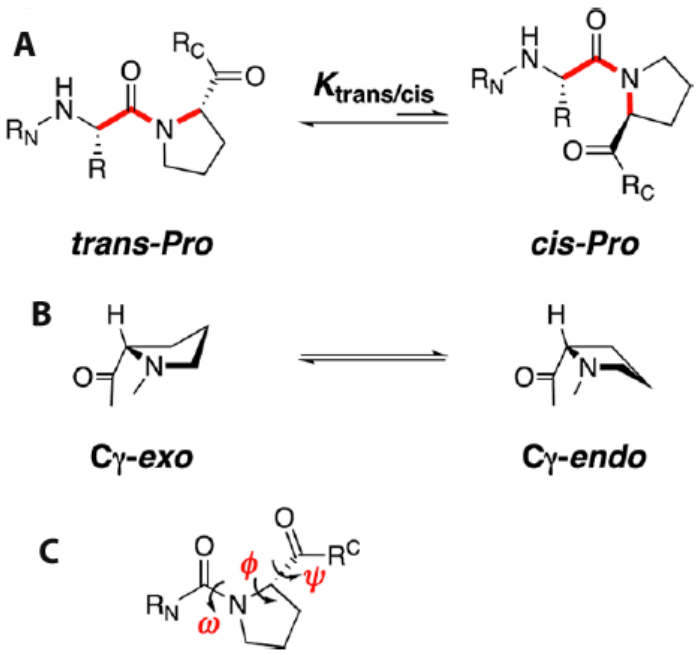

Figure 10. Slow cis-trans isomerization of the proline amide bond (a) the C^{γ} exo and the C^{γ} endo ring puckers of the pyrrolidine ring (b) Main chain torsion angles of proline which are influenced by the ring pucker.[26]

Independent from its behavior in collagen, depending on the stereochemistry of the ring functionalization, the pyrrolidine exhibits a preference to favor one conformer.[28,29] Furthermore, substitution of poor-hydrogen bonding, electron withdrawing substituents, like fluorine, induce preferential ring puckering as well, invoking the gauche effect. [20,30-32] (**Figure 11**). The Wennemers group has contributed to this approach through the use of azide-alkyne cycloaddition (click chemistry) reactions to conjugate other bulky groups, such as entire carbohydrate monomers, to the Yaa proline in the triplet repeat.[33] Their results further establish the stereoelectronic effect as an effective approach for triple helix stabilization.

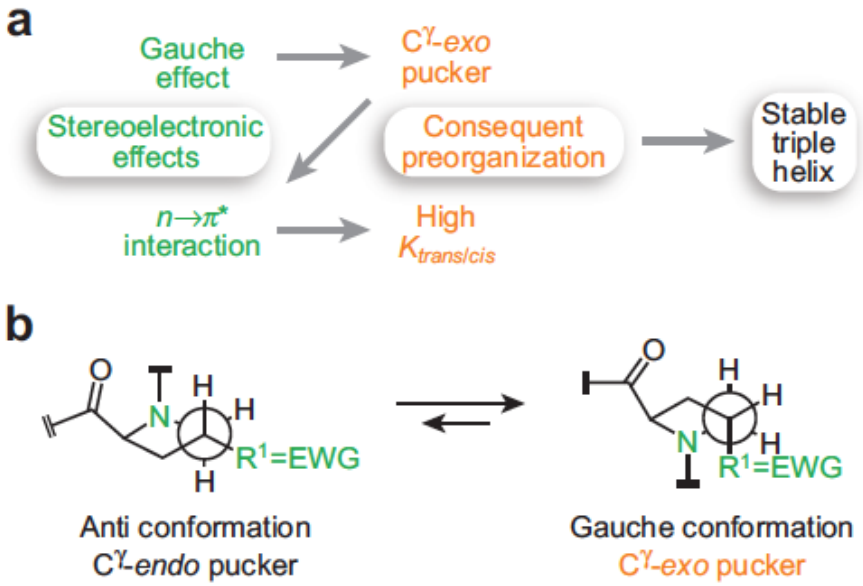

Figure 11. Diagram depicting how stereoelectronic effects on substituted prolines can stabilize the triple helix. Gauche effects and n-π* interactions bias the backbone dihedral angles to PPII conformations, and thereby enhance triple helix formation. (a) Stabilization of the C^{γ}-exo ring pucker via a gauche effect induced by electron withdrawing groups on the 4*R* position of the pyrrolidine ring. (b)[1]

Glycine analogues, as in Chennoweth's azaglycines, incorporated throughout CLPs, induce a hyperstability of triple helices via glycine editing of these biopolymeric chains.[22-24] (**Figure 12**) These mutations minimally disrupt the structure while increasing the interfacial hydrogen bonding contacts. Notably, their contributions to the triple helix increase the T_m to over 50°C with a $(Pro\text{-}Hyp\text{-}azGly)_n$ repeat with n=3, signifying a 8.6°C increase per azaglycine unit.[23]

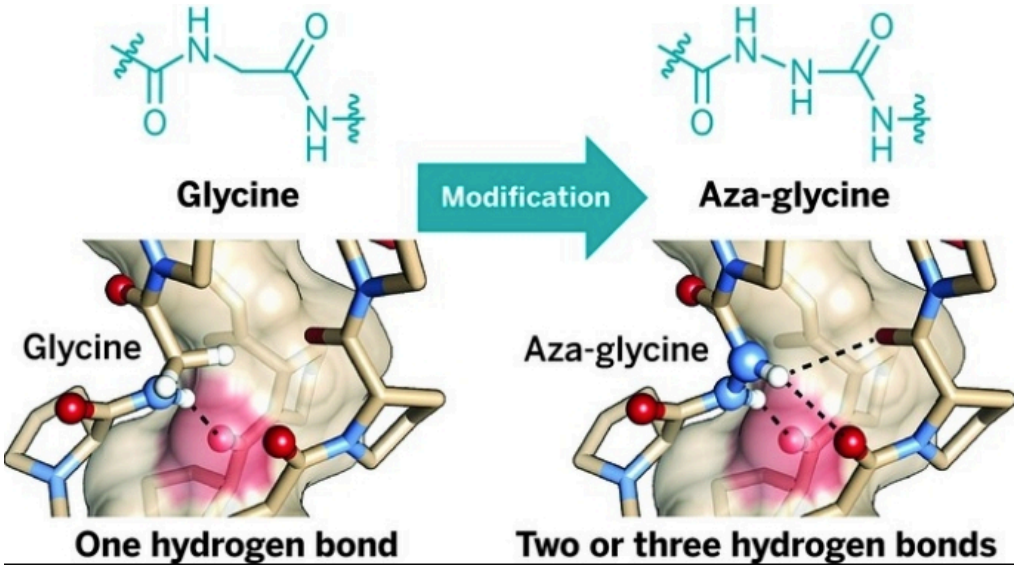

Figure 12. Comparison of native glycine and azaglycine in structure (top) and hydrogen bonding contacts (bottom)[23]

The Hartgerink laboratory has completed some of the most impressive work to date in assembling stable CLP triple helices.[25,34] Reporting in *Nature*, the group employed a sequence-based scoring method to design, de-novo, an ABC type heterotrimeric triple helix which melted at an astounding 58°C.[25] (**Figure 13**) They were also among the first to experiment with the application of electrostatic interactions to self assembling CLP hydrogels which possessed viscoelastic properties, storage and loss moduli, comparable to native collagens.[34] This work comes on the heels of the exhaustive efforts conducted by the Brodsky lab who recognized, among many other facets of collagen research, the importance of charged pairwise interactions within host-guest studies involving CLPs.[35-37]

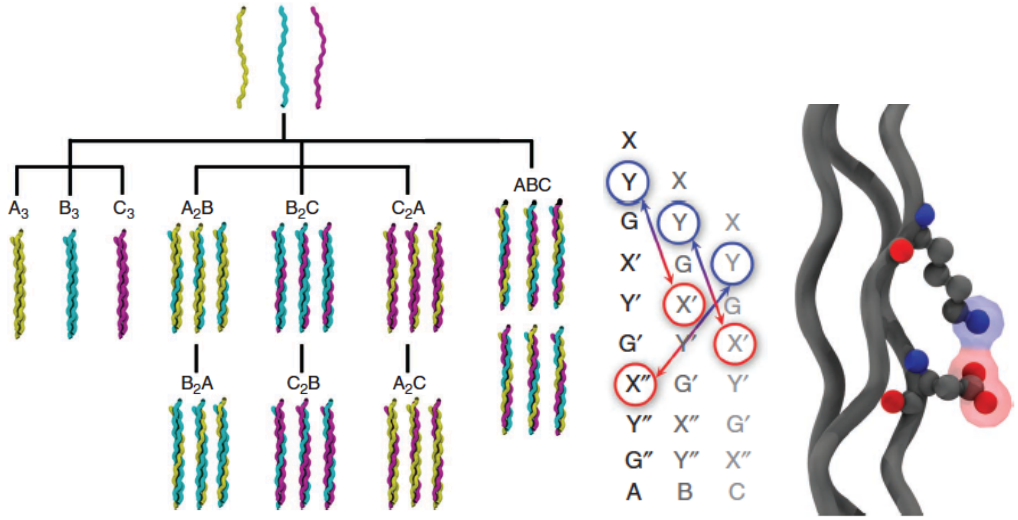

Figure 13. Hartgerink's de novo designed ABC heterotrimeric triple helix. Potential sequence combinations (left). Placement and representation of the axial lysine-aspartic acid salt bridges between the ABC chains (right)[25]

The contributions of metal chelation to the structure and stability of the triple helices have also proved to be important. Coupling metal-chelating groups, such as bipyridine and other systems with high electron density to the peptide oligomer, researchers developed the ability to use electron-poor metal centers to initiate complex and stable arrangements of collagen like peptides into triple helices via metal binding.[38-42] Chiemelewski *et al.* obtained completely reversible macromolecular assemblies of CLPs with a variety of divalent transition metals coordinated to a His_2 cluster at the *C*-terminus while the *N*-terminus was occupied by another metal ion through a nitriloacetic acid moiety in aqueous, ambient conditions.[39] The Nanda group used structural modeling techniques to design CLPs with His_3 binding sites in the chain termini to improve self assembly and stability upon metal chelation. Their assessment of Zn^{2+} and

Cu^{2+} to drive triple helix formation led to the discovery of both homo- and hetero-trimeric collagen-like materials supplemented with increases in metal-induced thermal stability.[42] The addition of metal ions has also assisted the creation of functional wound healing materials, by controlling assembly thereby enriching these materials with additional wound healing benefits. Bio-based hydrogels incorporating metal binding centers into CLPs strands have encapsulated growth factor payloads and exhibit induced gelation upon Ni^{2+} coordination. These loaded gelatinous preparations have been exploited to enhance cell proliferation and affect cell morphology in a time-controlled manner.[43]

In terms of covalent methods to stabilize and encourage triple helix assembly, a common strategy is tethering CLPs from a scaffold at either the N or the C terminus to promote triple helix formation.[19,40,44-62] (**Figure 14**) Tethering not only liberates triple helix formation from a concentration dependent organization, but also engenders greater conformational stability for the resulting constructs at shorter chain lengths, simplifying the synthesis and subsequent analysis of synthetic collagen triple helices.[19,46] Early work from the Heidemann and Fields labs employed simple lysine dimers[49-53] while Tong *et. al.* exploited tricarboxylic acid templates to encourage triple helix formation. Using a $(Ala\text{-}Pro\text{-}Gly)_n$ n=5-15 trimeric repeat templated on a lysine dimer display, triple helix formation was initiated at n=8 and continued to garner stabilization as the chain grew, but unremarkable thermal stability.[54] This work was later improved upon by Fields and co-workers, flanking their native collagen sequences with a wider variety of amino acids and $(Pro\text{-}Hyp\text{-}Gly)_8$ repeats.[62]

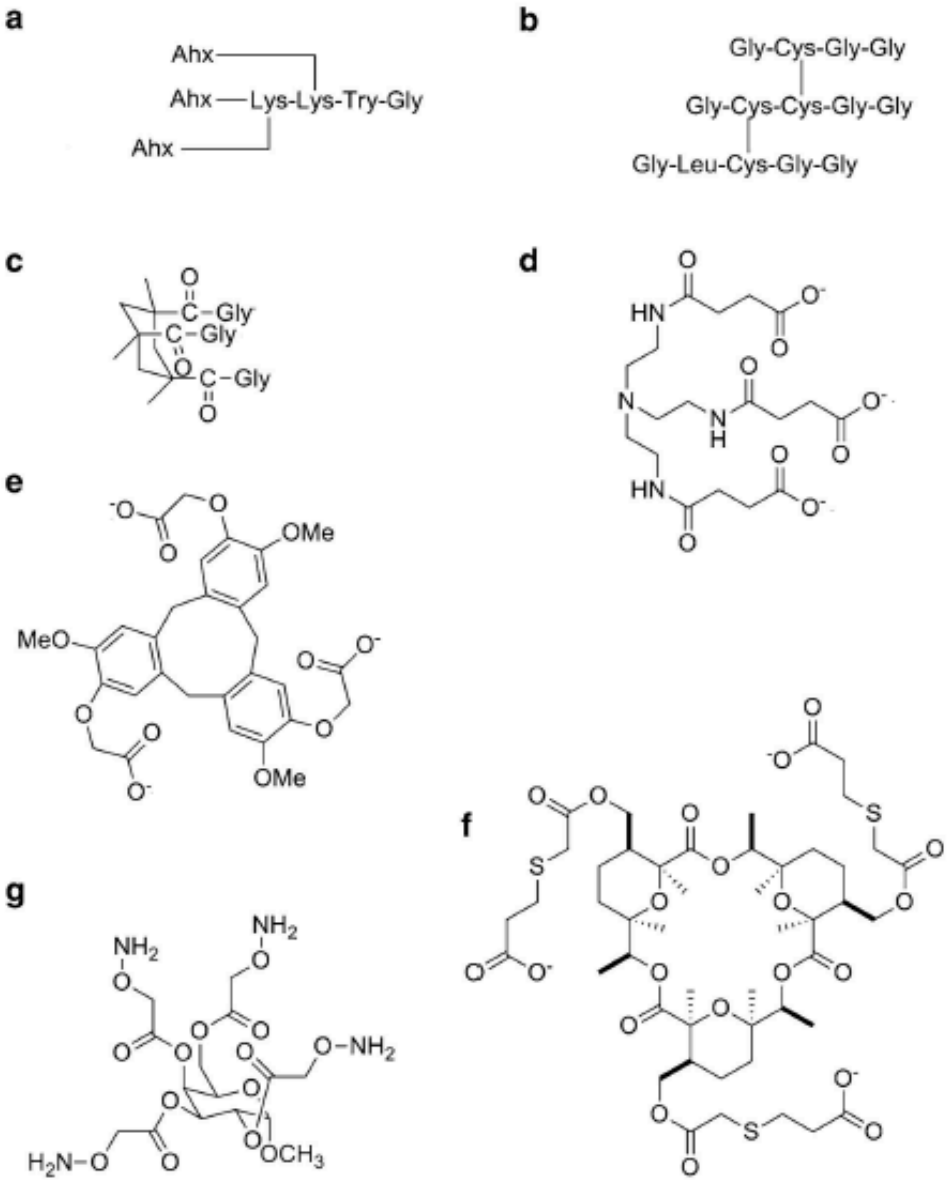

Figure 14. Common covalent scaffolds for templating triple helix formation of CLP. Dilysine branch (a); cysteine knot (b), *cis*,*cis*-1,3,5-trimethylcyclohexane-1,3,5 tricarboxylic acid (KTA) (c), tris(2-aminoethyl)amine (TREN) (d), cyclotriveratrylene (CTV) (e), macrocyclic hydropyran oligotide (f), methyl 2,3,4,6-tetra-O-Aoa-α-D-Gal*p* (g). (Bhowmick, M and Fields. G.B., 2014).[10]

Other simple linear tethers have been evaluated by prominent researchers in the peptide science community, lending support to their effectiveness as molecular scaffolds. The Goodman lab assessed basic and flexible tripodal scaffolds including tris(2-aminoethyl)amine (TREN) and tris(hydroxymethyl)aminomethane (TRIS). The increase in enthalpy led to a modest enhancement in thermal stability of the TREN-templated triple helices,[55] and TRIS-templated helical arrays displayed in a dendrimer-like fashion from a peptide chain exhibited similar melting behavior in water, with greater enhancements upon solvent variation.[56] Within the last 10 years, the use of these two scaffolds continues to be a popular choice, with the Yu lab leading the charge into creating simple but hyperstable ABB heterotrimers.[18]

Covalent cysteine-based and oxime strategies draw inspiration from native collagen's use of disulfide linkages to assemble individual helices into collagen fibrils.[57-59] Employing a cysteine knot tethering strategy, the Morodor laboratory elegantly displays helical arrays from both the N and C termini with both homo and heterotrimeric ABB CLPs with nearly double the thermal stability of their free CLP counterparts.[57] The Raines and Wennemers laboratories harness the power of these covalent constraints by locking the helices throughout the structure.[58,59]

Macrocyclic templating was pioneered by the Goodman group in the late 1990's, tethering CLPs to one face of a rigid cycloxhexane ring by virtue of three axially oriented reactive groups (Kemp's triacid).[45,46] (**Figure 14 c**) Templation from a rigid scaffold minimizes the amount of unfavorable entropy experienced by the CLP chains during triple helix nucleation. Goodman's KTA scaffold strategy afforded not only the shortest CLP triple helix at room temperature, but also a thermal stability similar to that of native

tropocollagen.[46] More recently, the Raines lab has followed this work with a hydropyran oligotide macrocycle utilizing three foci for CLP attachment oriented on one face of the macrocycle, forming an equilateral triangle with improved stability.[19] (**Figure 14 f**) Another noteworthy scaffold, the cone-shaped cyclotriveratrylene (CTV), offers chiral attributes and tunable flexibility in addition to its templating abilities, and its use marks the first incidence of a scaffold successfully stabilizing a native collagen sequence.[61]

With so much already been accomplished using shorter collagen mimics, scientists should now begin to direct their efforts towards the creation of higher order assemblies which will mimic natural collagen. The Raines, Hartgerink, Chiemelewski, Brodsky, and Yu laboratories are notable pioneers in achieving initial success with longer and more intricate multistrand collagen constructs on the order of nanometer- to micron-sized materials.[3,60-71] Many opportunities and room for creative invention within the field of synthetic collagen fibril and fiber formation are now at hand, especially in the way of scaffold derivativization, but many of the scaffolds presented above lack the chemical handles for further development.

Pertinent to wound healing, the union of higher order collagen assemblies and further functionalization of the collagen-like constructs to be more suited for therapeutic applications could be realized in the design of 'smart' dressing materials. The design and implementation of smart dressings has become an active area of research.[72,73] The utility of such materials can be exploited as vehicles for drug delivery, stimuli responsive materials for labeling, imaging, and oxidative protection of wound sites; and enzyme responsive materials which are sensitive to the intrinsic wound healing chemicals of the wound site and can be engineered to degrade in a precise manner, delivering growth

factors and other cytokines.[74-90] A unique, synthetically versatile molecular scaffold that allows the exploration of a vast array of chemical through sequential modification could unify synthetic collagen fibers to biologically active dressings, assisting in the creation of the next generation of wound healing materials.

N-substituted glycine oligomers, termed peptoids, are a class of sequence-specific oligomers that exhibit a range of biomimetic structural and functional attributes.[91,92] Peptoid scaffolds can be readily assembled via a robust solid phase synthesis protocol to incorporate a wide variety of side chain functional groups, and hold potential for therapeutics and in materials science.[93-115] We perceived that we can template triple helix formation using a peptoid scaffold similar to previous efforts. Unlike Kemp's triacid and TREN scaffolds, peptoids provide precise control of multiple reactive chemical functionalities that can be tailored through an efficient, modular synthesis. (**Figure 15)**

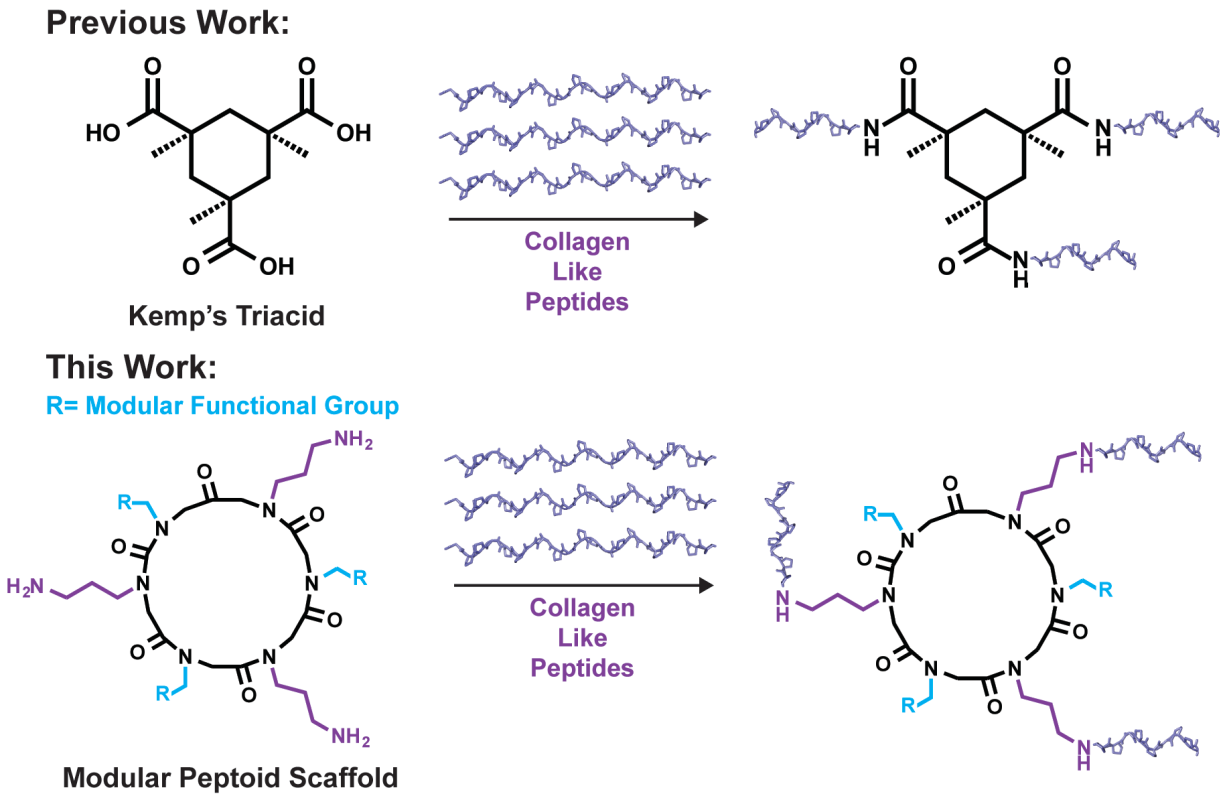

Figure 15. Comparison of previous work with templating collagen like peptides into a triple helix with Kemp's triacid, to the current work, which utilizes a peptoid scaffold. Due to the modular nature of peptoid synthesis, R groups can virtually be any functionality displayed from a primary amine substrate, making peptoids an attractive option for future development and application of templated collagen-like peptides.

Here we demonstrate the implementation of peptoid-based tethers to template triple helix formation of CLPs. Two versatile oligomers, a linear hexamer and its macrocylic analogue, presenting three primary amine groups for coupling to the C-termini of CLPs, were studied. (**Figure 16)**

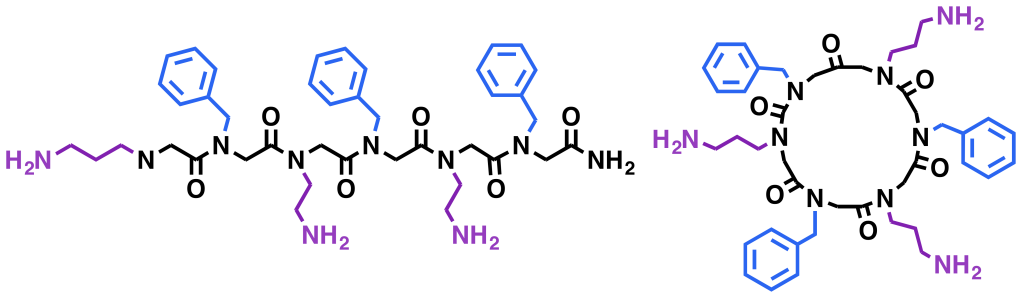

Figure 16. Peptoid scaffolds used in this study to template CLPs into a triple helix. The linear peptoid scaffold, **Lin** (**left**) and corresponding cyclic analogue, **Mac** (**right**).

Our initial hypothesis was that the macrocyclic scaffold was an optimal template for triple helix formation and that the linear scaffold would show a diminished capacity to preorganize the three chains for self-association and therefore exhibit a lower thermal stability. Previous X-ray crystallographic analysis of a hexameric macrocycle has demonstrated the rigid and predictable display of three side chain functionalities on one face of the macrocycle,[92b] (**Figure 17**) rendering this scaffold a particularly attractive platform for CLP tethering and triple helix templation.

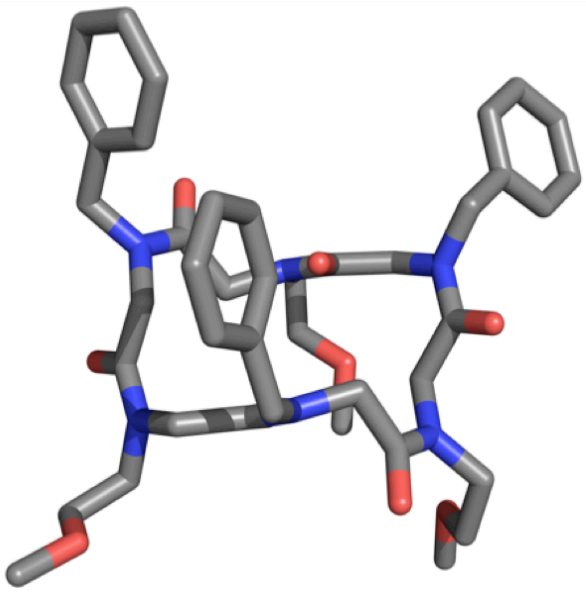

Figure 17. Crystal structure of a hexameric peptoid macrocycle. A trans-cis-cis-trans-cis-cis series of amide backbone geometries create a pattern of side chain positioning on alternating faces of the macrocycle; three benzyl groups point up while three methoxyethyl side chains are oriented down. [92b] (Shin, 2007)

Through CD spectroscopy, thermal denaturation and refolding studies, and molecular dynamics simulations, we report discrete and reversibly forming structures formed from both of the tethered CLPs, which behave differently when exposed to chemical denaturants. The macrocyclic templated CLPs are characterized as well-defined textbook case collagen triple helices and boast similar increases in thermal stability relative to native tropocollagen. Moreover the macrocylic templated triple helix is in excellent agreement with models developed for the construct *in silico*. While the linear construct seems to have an excellent thermal stability and CD profile matching a collagen-like triple helix, its behavior in chemical denaturants remains perplexing, as

described below. We are intrigued by the differences in behavior simply by changing the peptoid scaffold and are excited by the prospects for future exploration and investigation of this discrepancy.

2.3 Results and Discussion

We utilized a CLP composed of seven repeating units (n=7) of the canonical Xaa-Yaa-Gly motif, where proline was included at both the Xaa and Yaa positions to conjugate to a hexameric peptoid macrocycle bearing three reactive primary amine side chains. The CLP was synthesized on 2-chlorotrityl resin, yielding a C-terminal carboxylic acid, according to a modified solid phase synthesis approach.[71b] The predicted T_m of 27°C for $(PPG)_7$ locked in triple helix structure motivated our choice for the length of the peptide.[116] At n=7 the length of the alpha chains is much shorter than that of native tropocollagen, and any possible triple helix that could should also be fairly unstable at room temperature. Therefore, these chains are unlikely to self-associate into the canonical collagen triple helix. This experimental design allows for direct comparison of the thermal stability arising from the CLPs' structure as a result of scaffold-induced templating relative to native tropocollagen.

The two peptoid scaffolds, linear (**Lin**) and macrocyclic (**Mac**) were synthesized on either Rink amide or 2-chlorotrityl resin, respectively, following standard submonomer peptoid synthesis protocols[91] and purified to >95% purity. Boc-protected amine synthons were incorporated for subsequent conjugation to CPLs following acidic cleavage. The patterning of the side chains, alternating benzyl and propyl amine

functionalities, will afford a distinct presentation of each of these groups on opposing faces after cyclization. Following purification of the scaffolds, PyBOP-mediated coupling under anhydrous conditions in dichloromethane for 72 hours afforded **PPG$_3$-Mac** in 15% yield and **PPG$_3$-Lin** in a 7% yield. (**Figure 18**)

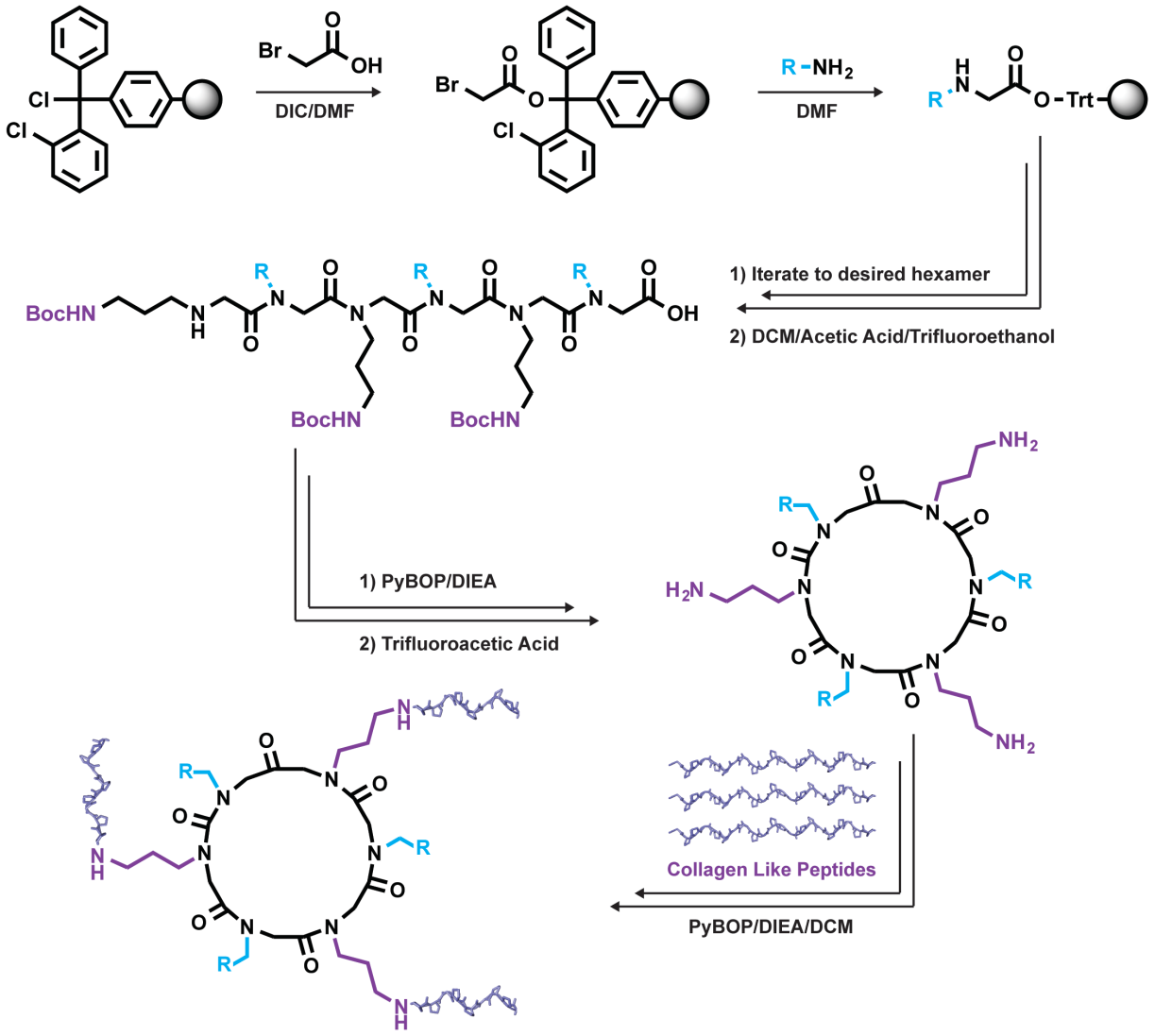

Figure 18. Synthetic scheme of peptoid scaffolds and scaffold-CLP constructs.

It is important to note that the addition of triethylamine (TEA) to the peptoid solution is necessary prior to its introduction into the reaction flask, as primary amines exist as a

TFA salts with reduced nucleophilicity following RP-HPLC purification. Paramount to the success of the reaction was the solvent choice as well. Numerous attempts at synthesis were made using different solvents and solvent combinations, both aqueous and non-aqueous, with and without TEA. Using dimethylformamide (DMF), a general peptide coupling solvent, the peptide experienced aggregation and low solubility, and resulted in diminished yields of tri-substituted scaffold. DCM/DMF combinations were unsuccessful as were attempts in anhydrous DCM when the ambient conditions in the lab were too humid to avoid the introduction of water into the reaction when weighing out the scaffold and peptide. The scaffolds were observed to be very hygroscopic and readily gelled upon exposure to atmosphere, complicating addition to the reaction flask and precise measurements of reagents. Anhydrous DCM with TEA provided the best solubility, highest conversion of peptoid scaffold into tri substituted conjugate, and least amount of visual aggregation when the reactions were conducted during the dry months of the year.

Circular Dichroism Experiments:

In order to evaluate the ability of CLPs to undergo triple helix formation upon templation from a peptoid scaffold, circular dichroism spectroscopy analysis was conducted. Briefly, **CLP_3** (1.05mg/mL or 0.35 mg/mL) **CLP_3-Lin**, and **CLP_3-Mac** (1.2 mg/mL or 0.4 mg/mL) were resuspended in 50 mM acetic acid and far-UV scans were conducted at 4°C from 260-200 nm.[19] When compared to **CLP_3**, both **CLP_3-Lin** and **CLP_3-Mac** displayed the characteristic triple helical signature of native tropocollagen as

evidenced by the positive lobe of ellipticity at 226 nm that arises due to the n-Π* transitions of the α-amino and imino residues of the CLP.[117] (**Figure 19**) The absence of the 226 nm signal from **CLP_3** is indicative that templated assembly is favored, and therefore, we attribute the formation of triple helix only when tethered to the scaffolds to the placement of the chains in close proximity, thereby pre-organizing them to favor self-assembly into the triple helix instead of aggregation through non-specific hydrogen bonding interactions. The precise display of the three CLPs from one face of the macrocycle and the flexibility of the linear scaffold, which enables the ability to fold into a backbone geometry consistent with the triple helix requirements, are responsible for the favorable display of each of the CLP chains. However, the greater signal strength at 226 nm exhibited by the macrocyclic construct is an indication that the **CLP_3-Mac** is superior scaffold for collagen triple helix templation.

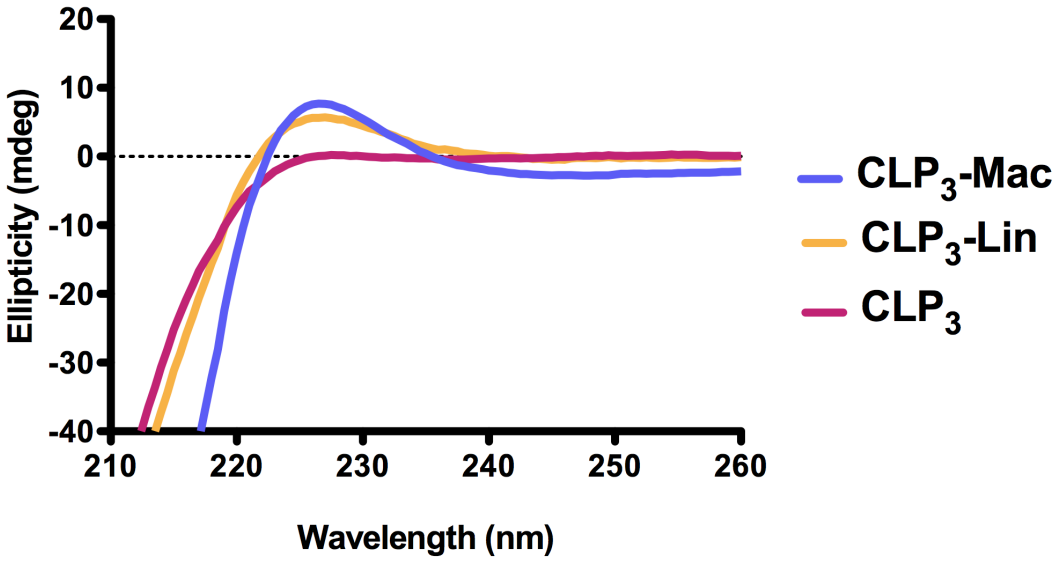

Figure 19. CD analysis of free and templated CLPs. **CLP_3** (1.05 mg/mL or 0.35 mg/mL) **CLP_3-Lin**, and **CLP_3-Mac** (1.2 mg/mL or 0.4 mg/mL) were resuspended in 50 mM acetic acid and far-UV scans were conducted at 4°C from 260-200 nm. Both **CLP_3-Mac** and **CLP_3-Lin** display the triple helical signature of 226 nm, which is absent from the free collagen-like peptides, **CLP_3.**

Chemical Denaturation Experiments:

If **CLP_3-Lin** and **CLP_3-Mac** constitute authentic triple helices as native tropocollagen, then their structure and stability will largely be dependent on hydrogen bonding interactions. Other non-covalent interactions contributing to triple helix stabilization, mainly hydrophobic interactions, can also become compromised in the presence of chaotropic agents. In contrast, a polyproline II helix, which relies on the multiple proline

residues to bias the main chain *phi* and *psi* dihedral angles toward trans-amide isomerization to induce PPII formation, does not have any significant backbone hydrogen bonding. The addition of chaotropic agents should, therefore, only disrupt triple helix self-assembly, and decrease in the CD signature at 226 nm.[118] To test this, 4 M urea was added to **CLP$_3$-Lin** and **CLP$_3$-Mac** (0.4 mg/mL) and far-UV scans were conducted once again. As expected, urea disrupted hydrogen bonding and destabilized the triple helix **of CLP$_3$-Mac** as witnessed by the loss of the signal at 226 nm (**Figure 20**). This indicated that the templated configuration of the CLP chains is significantly influenced by the presence of hydrogen bonds, presumably between the CLPs chains. On the other hand, **CLP$_3$-Lin**, displays a diminished, but not complete, loss of CD signal at 226 nm, suggesting that perhaps the structure formed by **CLP$_3$-Lin** may not be entirely triple helical in character and structure of **CLP$_3$-Lin** is stabilized by some forces other than hydrogen bonding. Other experiments would be necessary to elucidate the cause for such behavior. While we do not yet fully comprehend the resistance to chemical denaturation, we are intrigued by the different sensitivities of the CLP constructs to urea when displayed from different peptoid scaffolds.

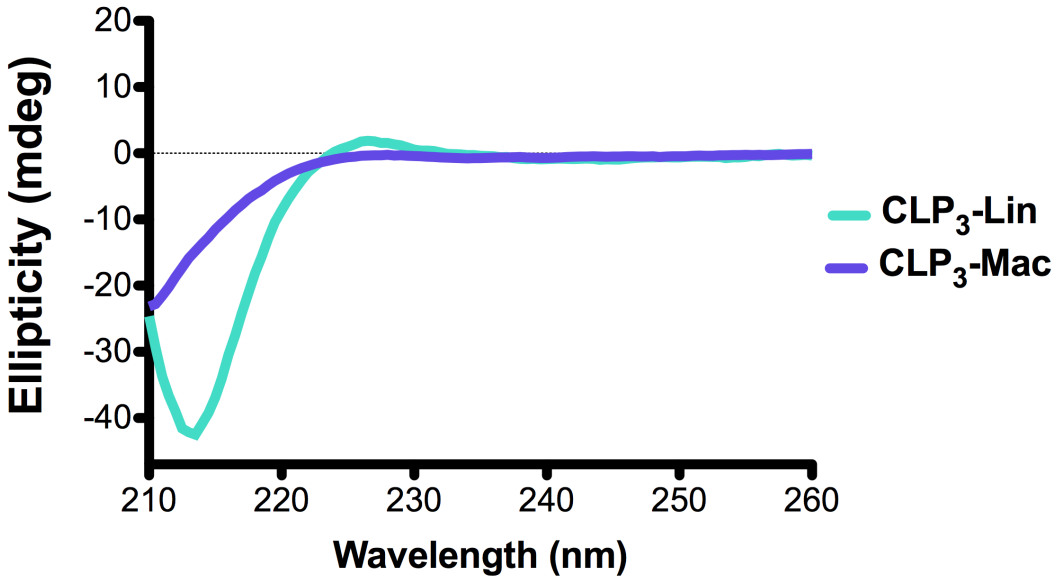

Figure 20. CD analysis of **CLP_3-Lin** and **CLP_3-Mac** in the presence of 4M urea. **CLP_3-Lin** and **CLP_3-Mac** (0.4 mg/mL) were resuspended in 50 mM acetic acid containing 4M urea and far-UV scans were conducted at 4°C from 260-200 nm. While **CLP_3-Mac** experiences a complete loss of triple helical character, **CLP_3-Lin** displays some residual positive ellipticity at 226 nm.

Thermal Denaturation and Refolding Experiments:

Motivated by the recent surge of interest regarding the thermal reversibility of collagen structures in wound dressings,[4,119] the response of all three oligomers to increasing temperatures was monitored by the CD signal at 226 nm. (**Figure 21**) **CLP_3-Lin (Figure 21, top)** and **CLP_3-Mac (Figure 21, middle)** display a sigmoidal melting curve, indicative of a smooth and discrete transition from a folded to an unfolded state with a T_m = 43.6 And 42.2 °C, respectively, which surpassed that of native tropocollagen

when heated to 90 °C. In contrast, **CLP_3** demonstrates only a linear decrease in ellipticity at 226 nm, with T_m < 0 °C. (**Figure 21, bottom**) These data indicate that templation is necessary for **CLP_3** to assemble into a triple helix, as witnessed with both **CLP_3-Lin** and **CLP_3-Mac**, while **CLP_3** was not able to form a stable triple helix.

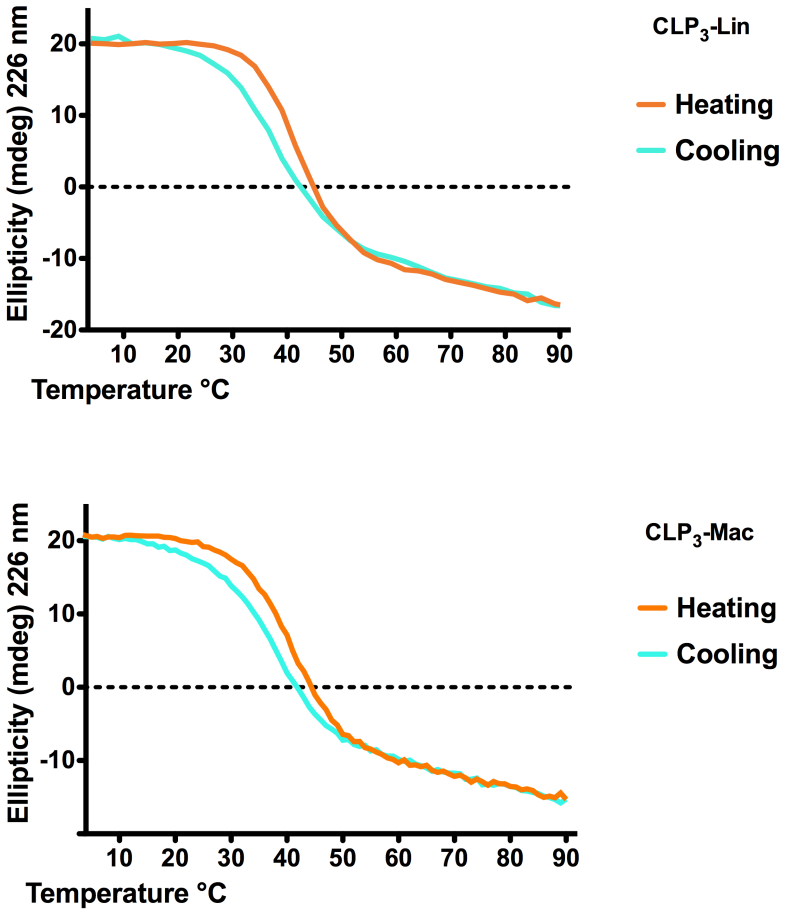

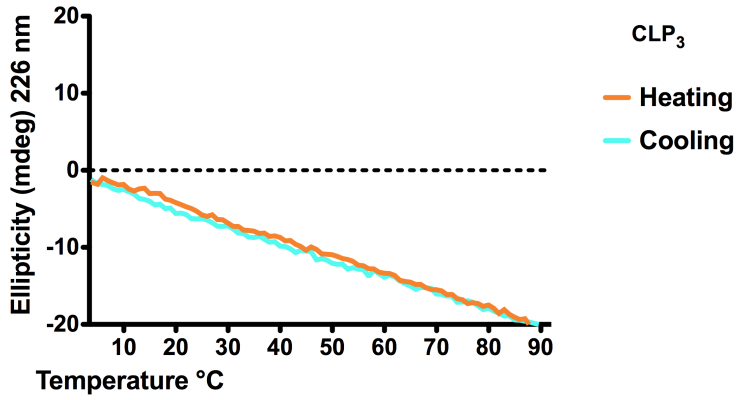

Figure 21. Melting and refolding experiments. **CLP_3-Lin (top)**, **CLP_3-Mac (middle)** (1.2 mg/mL), and **CLP_3 (bottom)** (1.02 mg/mL) were resuspended in 50 mM acetic acid, and the solutions were heated from 4°C to 90°C while monitoring at 226 nm. Following thermal denaturation, the solutions were subsequently cooled back to 4°C at a rate identical to their heating. Both constructs experience a smooth transition from a folded to an unfolded state with approximate melting temperatures of 43°C (**CLP_3-Lin**) or 42°C (**CLP_3-Mac**) and are able to regain their structure upon cooling.

To explore the extent of reversibility in self-assembly, **CLP_3-Lin** and **CLP_3-Mac** were cooled at a rate identical to their heating immediately following thermal denaturation and monitored at 226 nm for a return of positive ellipticity. The cooling curve for both constructs exhibits a full return of the signal at 226 nm, indicative that triple helix formation is reversible if tethered to the peptoid oligomers, and literature precedent supports this behavior exhibited by our templated CLPs.[48] The slight hysteresis observed between the heating and cooling curves implies that templating CLPs in close proximity can overcome some of the negative entropy associated with triple helix formation and reduces the number of misaligned structures.[47,48] In native tropocollagen,

which lacks a covalent constraint to preorganize the chains for favorable self-assembly, considerable hysteresis is present, which can induce registry 'slippage' and not allow helical structure to be recovered.[120]

Molecular Modeling:

To support the structural hypothesis, we turned to molecular mechanics theory, which treats macromolecules as systems of springs and masses. With an appropriate selection of parameters to translate chemical interactions into these newtonian equations, algorithmic minimization of the energy of the system by perturbing the cartesian coordinates of the atoms results in a theoretical equilibrium structure. A model of the macrocyclic templated collagen triple helix was minimized by molecular mechanics. **(Figure 22-25**) (**See Methods and Materials for Details**) Alignment of the crystal structures of the original peptoid macrocycle[72b] and a representative collagen triple helix[121] showed a close alignment (RMSD = 1.28 Å) between terminal C atoms of the peptide chains and β-C atoms of the polar side chains of the peptoid. The minimized structure displayed some minor deviations in the orientation of the aromatic side chains, but virtually no perturbation of the cyclic backbone. Although one of the linking side chains adopts an alternate "rotational isomer" that puts it in alignment with the terminus of the linked peptide, overall the theoretical model requires little disruption from the crystal structures, supporting the design hypothesis that the cyclic scaffold is preorganized into a favorable conformation for templating the collagen triple helix.

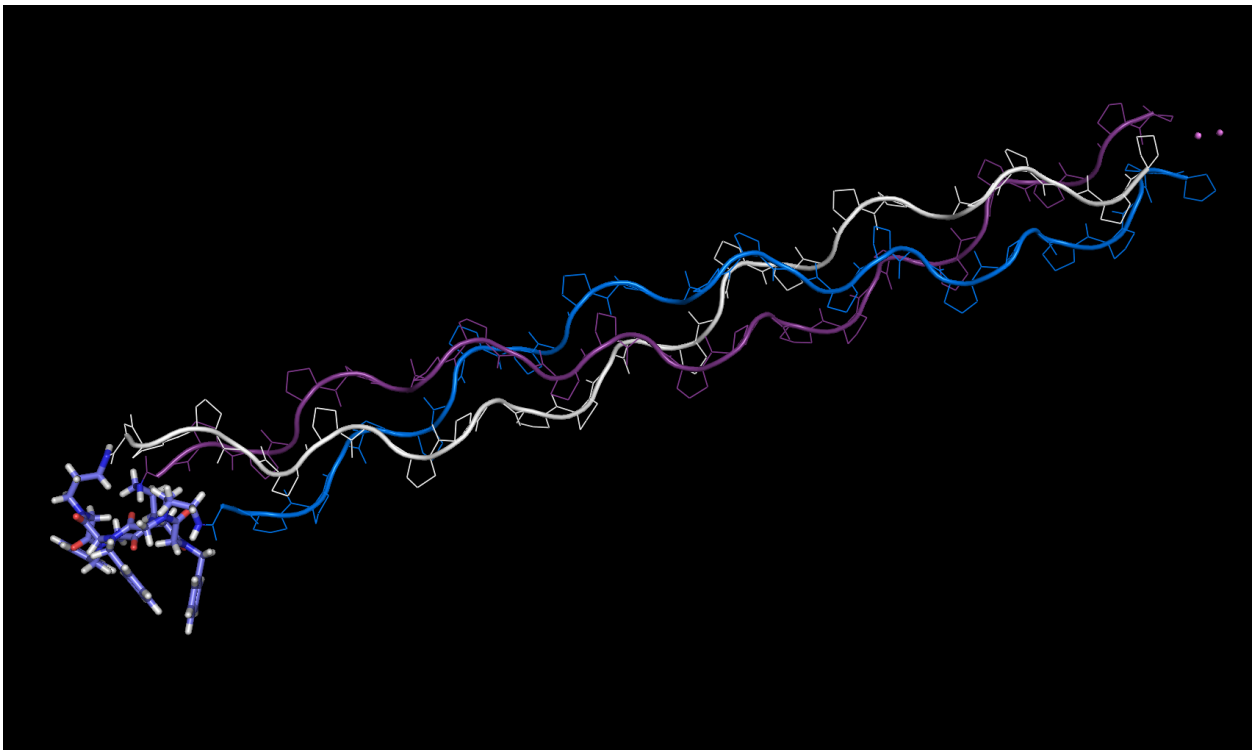

Figure 22. Energy-minimized structure of **CLP_3-Mac. CLP** chains are witnessed in a triple helical presentation.

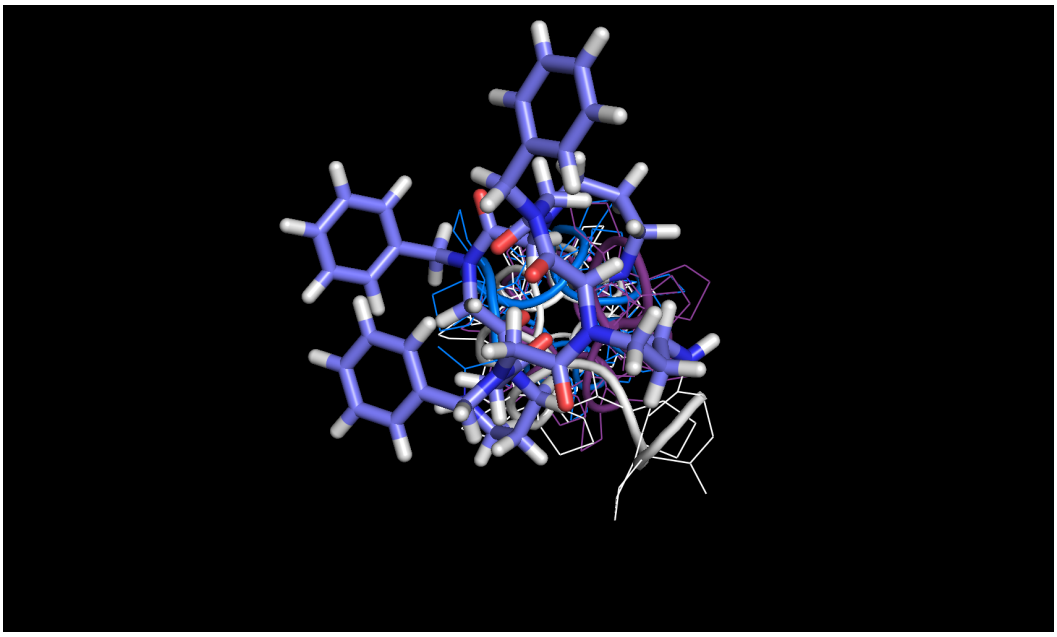

Figure 23. Energy-minimized structure of **CLP$_3$-Mac** showing the view down the center of the helical axis.

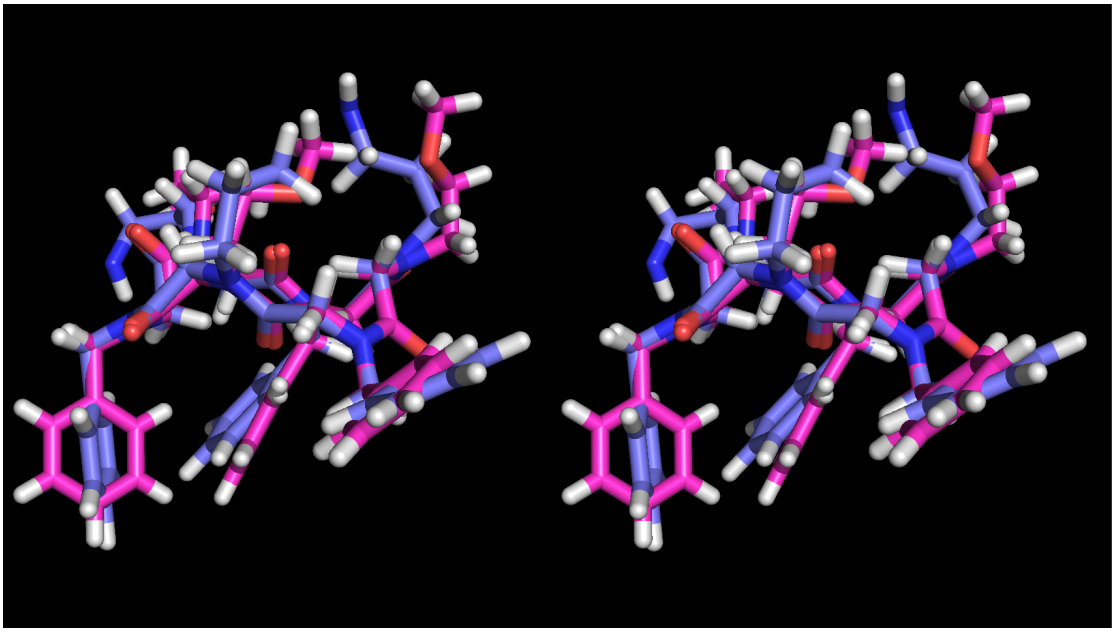

Figure 24. Stereoview of the overlay of the peptoid macrocycle crystal structure (pink) and the minimized structure of **Mac** (purple).

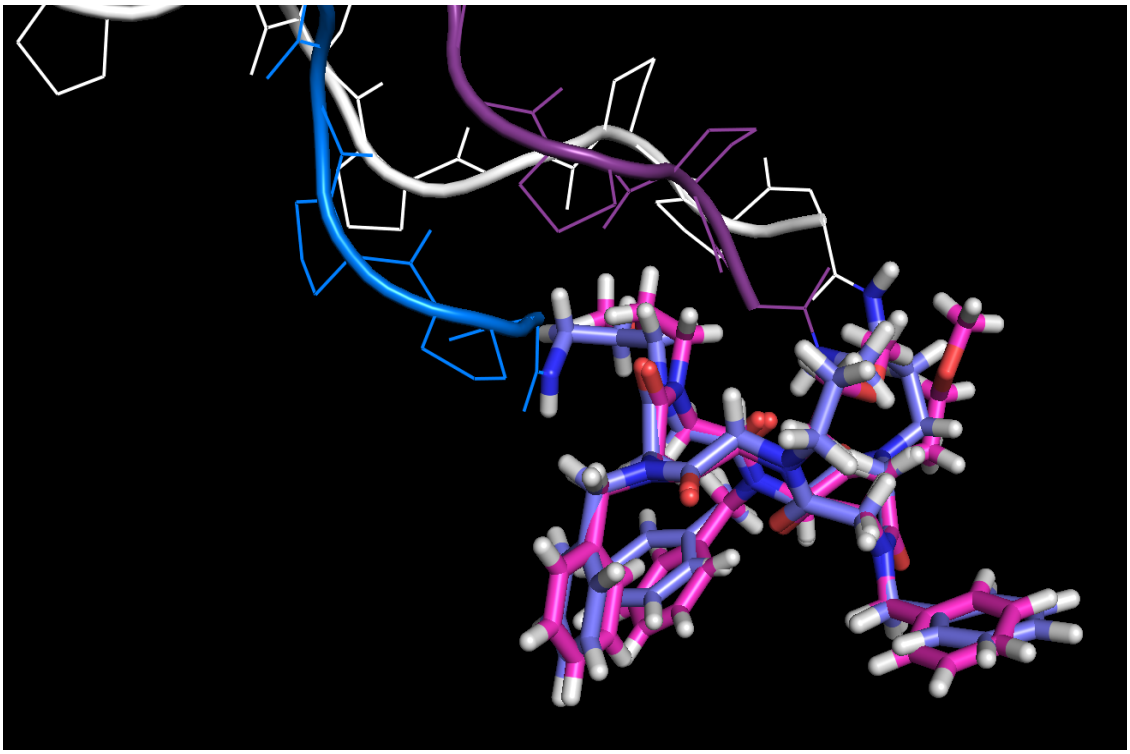

Figure 25. Overlay of the peptoid macrocycle crystal structure (pink) and the energy-minimized structure of **Mac** (purple) with CLPs attached, highlighting the close structural alignment of the two macrocycles even when CLP-functionalized.

2.4 Summary and Outlook

We demonstrate the capability of peptoid macrocycle scaffold to preorganize three collagen-like peptide chains to self-assemble into structures reminiscent of the canonical collagen triple helix with enhanced thermal stability profiles compared to native tropocollagen. The triple helical structure of **CLP$_3$-Mac** was validated by circular dichroism and thermal and chemical denaturation studies, establishing that both linear cyclic peptoids are effective tethers for collagen-like peptides to template triple helix

assembly. Encouragingly, the transition from a folded to an unfolded state was determined to be reversible, indicating that the effect of templating the three CLP chains sustains their preorganization for triple helix formation and supports interest in reversible collagen-based materials.

In the interest of analyzing the ability of different peptoid scaffolds to template triple helix formation, we also synthesized and tested the linear analogue of our cyclic construct, **CLP_3-Lin.** While **CLP_3-Lin** performs comparably to **CLP_3-Mac** in the CD and thermal denaturation studies, there is a deviation from their similarities once exposed to chemical denaturants; **CLP_3-Lin** does not exhibit behavior expected from a triple helical structure. One could hypothesize that if the CLP chains from **CLP_3-Lin** are arranged in a triple helix, that the structure could be held together by additional forces other than hydrogen bonding. Alternatively, perhaps whatever assembly results from **CLP_3-Lin** is not a triple helix at all, and simply misaligned hydrogen bonding contacts between the alpha chains with some residual polyproline II character. We are, however encouraged by the data supporting that the arrangement and presentation of the CLP chains from the tethers illicit different behaviors and sensitivities of the resulting CLP constructs to various physical stresses.

The further application of this tethering strategy will facilitate creation of novel biomaterials for wound healing with unique materials properties. For example, the three available sites on our scaffolds can be functionalized to incorporate handles which deliver biochemically sensitive molecules, including growth factors and other cytokines to assist in wound healing. In addition, peptoid sequences can be crafted to incorporate

different functionalities with the potential to form additional molecular contacts displayed within the peptoid scaffolds, enabling interdigitation of the individual triple helices and synthetic fibril formation. The successes by prominent collagen chemistry laboratories, like Raines, Brodsky, and Hartgerink, have all recently published strategies to achieve longer, multi helix assemblies of synthetic collagen that should serve as the initial blueprint and inspiration for directing our efforts utilizing our peptoid scaffolds.

2.5 Experimental Procedures

Materials:

Synthesis of the peptoid and peptide oligomers was initiated on either Rink Amide resin (Nova Biochem, 100-200 mesh, loading: 0.74 mmol/gram) or 2-Chlorotrityl resin (Nova Biochem, 100-200 mesh, loading: 1.14 mmol/gram). Bromoacetic acid (97%) was supplied by Sigma-Aldrich. Chloroacetic acid (99%), Trifluoroacetic Acid, TFA, (99%), N,N-Dimethylformamide, DMF, (anhydrous and amine free, 99.9%) and N,N' diisopropylcarbodiimide, DIC, (99%) were supplied by Alpha Aesar. benzotriazol-1-yl-oxytripyrrolidinophosphonium hexafluorophosphate, PyBOP, (99%), was supplied by Chem-Impex International, Incorporated. Fmoc-Pro-OH and Fmoc-Gly-OH were obtained from Nova Biochem. Other reagents and solvents were obtained from commercial sources and used without additional purification.

Peptoid Synthesis Submonomers: The introduction of specific peptoid side chain types was achieved through the use of the following primary amines as "submonomer" synthons (see below): Benzylamine (Alfa-Aesar, 99%); N-(tertbutoxycarbonyl)-1,3-diaminopropane (Oakwood Chemical, 99%).

Instrumentation:

Collagen like peptides and Peptoid oligomers were analyzed by reverse-phase HPLC (XBRIDGE BEH300 analytical C_{18} column, Waters, 3.5 μm, 4.6x50 mm) on an Agilent

1260 Infinity LC system. A linear gradient of 5-95% acetonitrile in water (0.1% TFA) over 10 min was used at a flow rate of 700 μL /min. Collagen like peptide samples were pre-heated to 60 ^{o}C and the column heated to 60 ^{o}C for analytical runs. Semi-preparative HPLC was performed on a Waters 2489 instrument using a Phenomenx Jupiter C_{18} column (Phenomenex, 20mm, 100 Angstroms, 21x2500mm). Peaks were eluted with a linear gradient of ACN/water (0.1% TFA) which depended on the sequence composition with a flow rate of 5-10 mL/min. Collagen like peptide samples were pre-heated to 60 ^{o}C and the column heated to 60 ^{o}C for purification Mass spectrometry was performed on an Agilent 1100 series LCMSD VL MS spectrometer or a Bruker Maldi-TOF TOF UltrafleXtreme MS Spectrophotomer using a saturated solution of α-Cyano-4-hydroxycinnamic acid prepared in 70% ACN(aq) with 0.1% TFA. Circular dichroism was conducted on a Jasco J-1500 CD Spectropolarimeter at 4 ^{o}C in a 1 mm path length quartz cuvette.

Preparation of Collagen-like Peptides 2-Chlorotrityl resin: CLPs were synthesized according to a modified solid phase peptide synthesis approach.[91] The resin (300 mg) was swelled for 5 minutes in anhydrous DCM before initiating the synthesis. The resin was incubated with a solution of 20 mg of Fmoc-Gly-OH and DIEA (10eq., 116 μL) in 6 mL anhydrous DCM for 1 hour at room temperature and an agitation rate of 220 rpm. The resin was washed with 3x1 mL anhydrous DCM and 3x 1 mL DMF before resin capping and Fmoc removal with a solution of 20% morpholine in DMF (v/v) (6 mL) for 1 hour at room temperature and an agitation rate of 220 rpm. The resin was washed

again with 6x DMF. Iterative peptide synthesis continued with a solution of Fmoc-Pro-OH (5 eq. relative to Glycine loading), PyBOP (5 eq. relative to Glycine loading), and DIEA (10 eq. relative to Glycine loading) in 1 mL of DMF for 1 hour at room temperature and an agitation rate of 220 rpm. The resin was washed again with 6x DMF. Going forward, Fmoc deprotection was achieved with a 20% piperadine solution in DMF with 1% DBU (v/v) (2 mL) for 30 minutes at room temperature with an agitation rate of 220 rpm x2. This two-step iterative process of amino acid addition and Fmoc deprotection was repeated until the desired chain length and peptide composition was achieved. N-terminal acetylation was achieved with exposure to a 3:2:1 (v:v:v) solution of DMF:DIEA:Acetic Anhydride (6 mL) for 1 hour at room temperature The peptides were cleaved from the resin using a cocktail containing 95% TFA, 2.5% TIPS, and 2.5% water (6 mL) at room temperature for 1 hour. Crude peptides were precipitated in cold t-butyl methyl ether and pelleted using cold ultracentrifugation at 4,000 rpm and 4 ^{o}C. Pellets were suspended in ACN/ H_2O, frozen, and lyophilized. Once dried, crude linear peptoids were stored at 4 ^{o}C until purification.

Purification of Collagen-like Peptides (CLP): CLPs were purified to >95% using a preparatory C_{18} column. CLPs were detected at 220 nm during a linear gradient of 15-45% aqueous ACN with 0.1% TFA over 60 minutes at a flow rate of 5 mL/min. Both samples and column were heated to 60 ^{o}C for at least 15 minutes prior to injection. Fractions were consolidated, frozen, and lyophilized. Once dried, purified CLPs were stored at 4 ^{o}C until use.

Preparation of Peptoid Macrocycle on 2-Chlorotrityl Resin: Peptoid oligomers were synthesized according to a general submonomer approach.[91b] The resin (100 mg, **0.0039 mmol reactive groups**) was swelled for 5 minutes in anhydrous DCM before initiating the synthesis. Bromoacetylation was carried out by incubating the resin with a bromoacetic acid solution in anhydrous DCM (0.65 M, 1 mL) and DIEA (107 μL) for 45 minutes and an agitation rate of 220 rpm. The resin was washed with 3x 1 mL DCM and 3x 1 mL DMF before displacement with the desired primary amine (1M in DMF, 1 mL) for 1 hour and an agitation rate of 220 rpm. The resin was washed with 5x 1mL DMF. This two-step iterative process was repeated until the desired chain length and oligomer composition was achieved. The oligomer was cleaved from the resin with a cocktail of 8:1:1 (DCM:Acetic Acid:TFE) (2 mL) for two hours. Volatile solvents were removed under reduced pressure, and the resulting oil was re-suspended in ACN/H_2O, frozen, and lyophilized. Once dried, crude linear peptoids were stored at 4^oC until cyclization.

Cyclization of Linear Peptoid Scaffold (LinMac): Linear peptoid oliogmers were cyclized according to a modified approach to for head to tail peptoid cyclization.[92] Peptoid scaffolds were dissolved in anhydrous DCM to a concentration of 0.3 M with PyBOP (2.1 eq.) and DIEA (6 eq.). The reaction was put under nitrogen and allowed to stir for 24 hrs. at room temperature. Solvents were evaporated under reduced pressure, the remaining oil resuspended in ACN/H_2O, frozen, and lyophilized. Once dried, crude linear peptoids were stored at 4 ^oC until protecting group removal.

Purification of Protected Cyclic Peptoid Scaffolds (MacPro): Protected cyclic peptoid scaffolds were purified to >95% using a preparatory C_{18} column. Products detected at 220 nm during a linear gradient of 65-95% aqueous ACN with 0.1% TFA over 60 minutes at a flow rate of 10 mL/min. Fractions were consolidated, frozen, and lyophilized. Once dried, purified protected macrocycles were stored at 4°C until deprotection.

Protecting Group Removal of Cyclic Peptoids: Protecting groups were removed with a cocktail of 95% TFA, 2.5% TIPS, and 2.5% water. Protected peptoids were suspended at concentration of 17 mM for 2 hrs. while stirring under inert atmosphere. Volatile solvents were removed under reduced pressure, and the resulting oil was re-suspended in ACN/H_2O, frozen, and lyophilized, and stored at 4 °C until purification.

Purification of Deprotected Cyclic Peptoid Scaffolds (Mac): Cyclic peptoid scaffolds were purified to >95% using a preparatory C_{18} column. Products detected at 220 nm during a linear gradient of 30-65% aqueous ACN with 0.1% TFA over 60 minutes at a flow rate of 10 mL/min. Fractions were consolidated, frozen, and lyophilized. Once dried, purified macrocycles were stored at 4 °C until use.

Preparation of Linear Peptoid Scaffold on Rink Amide Resin: Peptoid oligomers were synthesized according to a general submonomer approach.[91] Rink Amide Resin, 100 mg (0.074 mmol), was swelled in DMF for 30 minutes before initiating the synthesis.

Bromoacetylation was carried out by incubating the resin with a bromoacetic acid solution in DMF (1.2M, 850 μL) and DIC (200 μL) for 20 minutes at room temperature and an agitation rate of 220 rpm. The resin was washed with 4x 1 mL DMF before displacement with the desired primary amine (1M in DMF, 1 mL) for 30 minutes at room temperature and an agitation rate of 220 rpm. This two-step iterative process was repeated until the desired oligomer chain length and monomer sequence composition was achieved. N-terminal acetylation was achieved with exposure to a 3:2:1 (v:v:v) solution of DMF:DIEA:Acetic Anhydride (2 mL) for 1 hour at room temperature. The oligomers were cleaved from the resin using a cocktail containing 95% TFA, 2.5% TIPS, and 2.5% water (4 mL) at room temperature for 2 hours. The solution was removed under reduced pressure, and the crude peptoid was re-suspended in acetonitrile/water, frozen, and lyophilized. Once thoroughly dried, crude peptoids were stored at 4^{o}C until characterization and purification.

Purification of Deprotected Linear Peptoid Scaffold (Lin): Linear peptoid scaffolds were purified to >95% using a preparatory C_{18} column. Products detected at 220 nm during a linear gradient of 20-95% aqueous ACN with 0.1% TFA over 60 minutes at a flow rate of 10 mL/minFractions were consolidated, frozen, and lyophilized. Once dried, purified CLPs were stored at 4 ^{o}C until use.

Conjugation of Collagen-Like Peptides to Peptoid Macrocycle (CLP_3-Mac): To an oven-dried roundbottom flask, 70 mg (0.038 mmol) of **CLP** with 99.8 mg of PyBOP (5 eq., 0.192 mmol) was added. 100 mL Anhydrous DCM was added to the flask with

66.65 μL DIEA (10 eq., 0.383 mmol) and the solution was stirred for 10 minutes under inert atmosphere. 10 mg (0.0127 mmol) of **Mac** was added with 16 μL of TEA (9 eq. relative to **Mac**, 0.115 mmol) with stirring. The reaction was allowed to proceed for 72 hours at room temperature under inert atmosphere. The solvent was evaporated under reduced pressure and the resulting oil suspended in ACN/H_2O, frozen, and lyophilized. Once thoroughly dried, crude **CLP_3-Mac** was stored at 4°C until characterization and purification.

Purification of CLP_3-Mac: **CLP_3-Mac** was purified to >95% using a preparatory C_{18} column. Products detected at 220 nm during a linear gradient of 20-90% aqueous ACN with 0.1% TFA over 60 minutes at a flow rate of 5 mL/min. Fractions were consolidated, frozen, and lyophilized. Once dried, purified CLPs were stored at 4 °C until use.

Circular Dichroism Measurements of CLP_3-Mac, CLP_3-Lin, and CLP_3: Approximately 500 μL solutions of **CLP_3-Mac** and **CLP_3-Lin** (0.4 mg/mL in 50 mM acetic acid) or **CLP_3** (1.2 mg/mL in 50 mM acetic acid) were prepared from lyophilized powders immediately before CD measurements. CD scans were performed at 4°C. Spectra were obtained by scanning the 260 to 190 nm region at a step of 0.5 nm (scan rate=50 nm/min) and a D.I.T. of 4 seconds in a spectrosil quartz cell (Helma, Inc.) (pathlength=1 mm). Raw data were processed for publication using Microsoft Excel and Prism.

Thermal Denaturation and Refolding Measurements of CLP_3-Mac, CLP_3-Lin, and CLP_3: Approximately 500 μL solutions of **CLP_3-Mac** (1.2 mg/mL in 50 mM acetic acid) or **CLP_3** (3.6 mg/mL in 50 mM acetic acid) were prepared from lyophilized powders immediately before thermal denaturation. CD scans were performed monitoring the signal at 226 nm from 4°C to 90°C and a D.I.T. of 4 seconds in a spectrosil quartz cell (Helma, Inc.) (pathlength=1 mm). Scans were performed at a step of 0.2°C (scan rate=5 min/1°C). Refolding experiments were conducted immediately after thermal denaturation with cooling and measurement parameters identical to those used for heating. Raw data were processed for publication using Microsoft Excel and Prism.

Molecular Modeling of CLP_3-Mac:

A model of Mac (amide-capped) was derived from the crystal structure of the original peptoid macrocycle.[92b] by replacing methoxyl groups with formamide. Minimized structures of Npm and Nae monomers, with capping groups on the termini, were used for calculation of partial charges by the semi-empirical AM1-BCC method. These charges were used to apply molecular mechanical parameters to the template molecule by residue using the GAFF force field, which has been shown to reproduce peptoid structures accurately.[122] Collagen peptides were parameterized using the AMBER forcefield ff14SB, and GAFF parameters were used for the amide bond between CLP and Mac. The geometry was minimized in AMBER using the generalized Born implicit solvation model.

2.6 References

1. Shoulders, M.D. and Raines, R.T. *Annual Review of Biochemistry.* **2009**, *78*, 929–958.
2. Chattopadhyay, S. and Raines, R.T. *Biopolymers.* **2014***, 101*, 821-833.
3. Gottlieb, D.; Morin, S.A.; Jin, S.; Raines, R.T. *Journal of Materials Chemistry*. **2008**, *18*, 3865.
4. Luo, T. and Kiick, K.L. Bioconjugate Chem. **2017**, *28*, 816−827.
5. Brodsky, B. *Adv. Protein Chem*. **2005**, *70*, 301-339.
6. Rodwell, V. W. Bender, D.A.; Botham, K.M.; Kennelly, P. J. Weil, P.M. *Proteins: higher orders of structure. In: Harper's Illustrated Biochemistry*; McGraw-Hill Education: New York, 2003, pp 30-39.
7. Fallas, J.A.; O'Leary, L.E.R.; Hartgerink, J.D. *Chem. Soc. Rev*. **2010***, 39,3510-3527.*
8. Bozec, L.; van der Heijden, G.; Horton, M. *Biophysical Journal*. **2007***, 92*, 70–75.
9. Image Retrieved from: http://bayareapelleve.com/pelleve/collagen/**)**
10. Bhowmick, M. and Fields, G. B. *Methods Mol. Biol*. **2013**,*108*,167–194.
11. Brodsky, B. and Shah, N.K. *FASEB J.* **1995**, *9,* 1537–1546.
12. Fields, G.B. and Prockop, D.J. *Biopolymers*. **1996**, *40*,345–357.
13. Jenkins, C.L. and Raines, R.T. *Nat. Prod. Rep*. **2002**, *19*,49–59.
14. Koide, T. *Connect Tissue Res*. **2005**, *46*,131–141.
15. Koide T. *Philos. Trans. R. Soc. Lond. B. Biol. Sci*. **2007**, *362*,1281–1291.
16. Brodsky, B.; Thiagarajan, G.; Madhan, B.; Kar, K. *Biopolymers*. **2008***, 89*,345–353.
17. Fields, G.B. *Org. Biomol. Chem*. **2010**, *8,*1237–1258.
18. Yu, S.M.; Li, Y.; Kim, D. *Soft Matter*. **2011***, 7*, 7927–7938.
19. Horng, J.-C.; Hawk, A. J.; Zhao, Q.; Benedict, E. S.; Burke, S. D.; Raines, R. T. *Org. Lett.* **2006**, *8*, 4735−4738.
20. Hodges, J.A. and Raines, R.T. J*. Am. Chem. Soc*. **2005**, *127*, 15923-15932.

21. Shoulders, M.D.; Hodges, J.A.; Raines, R.T. *J. Am. Chem. Soc.*, **2006**, *128*, 8112–8113.

22. Zhang, Y.; Malamakal, R.M.; Chenoweth, D.M. J. *Am. Chem. Soc.* **2015**, *137*, 12422–12425.

23. Kasznel, A.J.; Zhang, Y.; Hai, Y.; David M. Chenoweth, D.M. J. *Am. Chem. Soc.* **2017**, *139*, 9427–9430.

24. Zhang, Y.; Herling, M.; Chenoweth, D.M. *J. Am. Chem. Soc*. **2016**, *138*, 9751-9754.

25. O'Leary, L. E. R.; Fallas, J. A.; Bakota, E. L.; Kang, M. K.; Hartgerink, J. D. *Nat. Chem*. **2011**, *3*, 821−828.

26. Pandey, A.K.; Naduthambi, D.; Thomas, K.M.; Zandlo, N.J. *J. Am. Chem. Soc.* **2013,** *135*, 4333−4363.

27. Engel, J.; Chen, H. T.; Prockop, D. J.; Klump, H. *Biopolymers*. **1977**, *16*, 601-622.

28. DeRider, M. L.; Wilkens, S. J.; Waddell, M. J.; Bretscher, L. E.; Weinhold, F.; Raines, R. T.; Markley, J. L. *J. Am. Chem. Soc*. **2002**, *124*, 2497-2505.

29. Improta, R.; Benzi, C.; Barone, V. *J. Am. Chem. Soc*. **2001**, *123*, 12568-12577.

30. Mooney, S. D.; Kollman, P. A.; Klein, T. E. *Biopolymers*. **2002**, *64*, 63-71.

31. Briggs, C. R. S.; O'Hagan, D.; Howard, J. A. K.; Yufit, D. S. *J. Fluorine Chem*. **2003**, *119*, 9-13.

32. Taylor, C. M.; Hardre´, R.; Edwards, P. J. B. *J. Org. Chem*. **2005**, *70*, 1306-1315.

33. Erdmann, R.S. and Wennemers, H. *Org. Biomol. Chem*. **2012**,*10*, 1982-1986.

34. Paramonov, S. E.; Gauba, V.; and Hartgerink, J. D. *Macromolecules,* **2005**, *38*, 7555–7561.

35. Venugopal, M.G.; Ramshaw, J.A.; Braswell, E.; Zhu, D.; Brodsky, B. *Biochemistry*. **1994**, *33*,7948–7956.

36. Persikov, A.V.; Ramshaw, J.A.; Kirkpatrick, A.; Brodsky, B. J. *Mol. Biol*. **2002**, *316*, 385–394.

37. Persikov, A.V.; Ramshaw, J.A.; Kirkpatrick, A.; Brodsky, B. *Biochemistry.* **2005**, *44,* 1414-1422.

38. Kinberger, G.A.; Taulane, J.P.; Goodman, M. *Inorg. Chem*. **2006**, *45*, 961–963.

39. Pires, M.M. and Chmielewski, J. J. *Am. Chem. Soc***. 2009,** *131*, 2706-2712

40. Cai, W.; Kwok, S.W.; Taulane, J.P.; Goodman, M. *J. Am. Chem. Soc*. **2004**, *126*, 15030-1.

41. Koide, T.; Yuguchi, M.; Kawakita, M.; Konno, H. *J. Am. Chem. Soc*. **2002**, *124*, 9388-9389.

42. Parmar, A.S.; Xu, F.; Pike, D.H.; Belure, S.V.; Hasan, N.F.; Drzewiecki, K.E.; Shreiber, D.I.; Nanda V. *Biochemistry*. **2015**, *54*, 4987-97.

43. Lemire, J.A.; Harrison, J.J.; Turner, R.J. *Nature Reviews Microbiology*. **2013**, *11*, 371-384.

44. Byrne, C.; McEwan, P. A.; Emsley, J.; Fischer, P. M.; Chan, W. C. *Chem. Commun.* **2011**, *47*, 2589−2591.

45. Feng, Y.; Melacini, G.; Taulane, J.P.; Goodman, M. *J. Am. Chem. Soc*. **1996**, *118*, 10351–10358.

46. Goodman, M.; Bhumralkar, M.; Jefferson, E.A.; Kwak, J.; Locardi, E. *Biopolymers (Peptide Science).* **1998**, *47*, 127–142.

47. Boudko, S. P.; Engel, J.; Bächinger, H. P. *The Journal of Biological Chemistry*. **2008**, *283*, 34345–34351.

48. Mizuno, K.; Boudko, S. P.; Engel, J.; Bächinger, H. P. *Biophysical Journal*. **2010**, *98*, 3004-3014.

49. Greiche, Y.; Heidemann, E. *Biopolymers*. **1979**, *18*, 2359-2361.

50. Roth, W.; Heidemann, E. *Biopolymers*. **1980**, *19*, 1909-1917.

51. Fields, C. G.; Grab, B.; Lauer, J. L.; Fields, G. B. *Anal. Biochem*. **1995**, *231*, 57-64.

52. Grab, B.; Miles, A. J.; Furch, L. T.; Fields, G. B. *J. Biol. Chem*. **1996**, *271*, 12234-12240.

53. Miles, A.; Skubitz, A. P. N.; Furch L. T.; Fields, G. B. *J. Biol. Chem*. **1994**, *269*, 30939-30945.

54. Khew, S. T. and Tong, Y. W. *Biochemistry*. **2008**, *47*, 585−596.

55. Kwak, J.; De Capua, A.; Locardi, E.; Goodman, M. *J. Am. Chem. Soc*. **2002**,*124*, 14085-14091.

56. Cai, W.; Wong, D.; Kinberger, G.A.; Kwok, S.W.; Taulane, J.P.; Goodman, M. *Bioorg. Chem*. **2007**, *35*, 327-337.

57. Boulègue, C.; Musiol, H.J.; Götz, M.G.; Renner, C.; Moroder. L. *Antioxid. Redox. Signal*. **2008**, *10*, 113-125.

58. Tanrikulu, I. C. and Raines, R. T. *J. Am. Chem. Soc*. **2014**,*136,*13490−13493.

59. Hentzen, N.B.; Smeenk, L.E.J.; Witek, J.; Riniker, S.; Wennemers, H. *J. Am. Chem. Soc*. **2017**, *139*, 12815−12820.

60. Kinberger, G.A.; Cai, W.; Goodman, M. *J. Am. Chem. Soc*. **2002**,*124*,15162–15163.

61. Rump, E.T.; Rijkers, D.T.; Hilbers, H.W.; de Groot, P.G.; Liskamp, R.M. *Chemistry*. **2002**, *8*, 461-4621.

62. Fields, G. B. *Organic & Biomolecular Chemistry*. **2010**, *8*, 1237–1258.

63. Tanrikulu, I.C.; Forticaux, A.; Jin, S.;. Raines, R.T. *Nature Chemistry*. **2016**, *8*, 1008–1014.

64. Rele, S.; Song, Y.; Apkarian, R.P.; Qu, Z.; Conticello, V.P.; Chaikof, E.L. *J. Am. Chem, Soc.* **2007**, *129*, 14780-14787

65. Jalan, A. A.; Jochim K.A., and Hatergrink, J.D. *J. Am. Chem. Soc.* **2014**, *136*, 7535–7538

66. Hartgerink, J.D.; Beniash, E.; Stupp, S.I. *Science*. **2001**, *294*, 1684-1688.

67. Kar, K.; Amin, P.; Bryan, M.A.; Persikov, A.V.; Mohs, A.; Wang, Y.H.; Brodsky, B. *J. Biol. Chem***. 2006**, *281*, 33283-33290.

68. Yamazaki, C.M.; Asada, S.; Kitagawa, K.; Koide, T. *Biopolymers*. **2008**, *90*, 816-23.

69. Cejas, M.A.; Kinney, W.A.; Chen, C.; Leo, G.C.; Tounge, B.A.; Vinter, J.G.; Joshi, P.P. Maryanoff B.E. *J. Am. Chem. Soc*. **2007**,*129*,2202-2203.

70. O. D. Krishna and K. L. Kiick, *Biomacromolecules.* **2009**, *10,* 2626.

71. Cejas, M.A.; Kinney, W.A.; Chen, C.; Vinter, J.G.; Almond, H.R.; Balss, K.M.; Maryanoff, C.A.; Schmidt, U.; Breslav, M.; Mahan, A.; Lacy, E.; Maryanoff, B.E. *Proc. Natl. Acad. Sci. U. S. A.* **2008**, *105*, 8513.

72. Deng, J.J.; Li, P.Y.; Cheng, H. *"Advances of Smart Materials for Wound Healing" Smart Materials for Tissue Engineering: Applications;* Wang, Q.; Ed.; Royal Society of Chemistry: Cambridge, 2017; pp. 258-289.

73. Andreu, V.; Mendoza. G.; Arruebo, M.; Irusta, S. *Materials*. **2015**, *8*, 5154-5193;

74. A. Scott, A. Stano, M. Gillard, A. C. Maio-Liu, M. A. Swartz and J. A. Hubbell, *Biomaterials*, **2012**, *33*, 6211.

75. S. T. Reddy, A. Rehor, H. G. Schmoekel, J. A. Hubbell and M. A. Swartz, *J. Controlled Release*. **2006**, *112*, 26.

76. M. K. Gupta, J. R. Martin, T. A. Werfel, T. Shen, J. M. Page and C. L. Duvall, *J. Am. Chem. Soc.* **2014**, *136*, 14896.

77. S. C. Yang, M. Bhide, I. N. Crispe, R. H. Pierce and N. Murthy, *Bioconjugate Chem.* **2008**, *19*, 1164.

78. S. Park, J. Yoon, S. Bae, M. Park, C. Kang, Q. Ke, D. Lee and P. M. Kang, *Biomaterials. **2014***, *35*, 5944.

79. J. Kwon, J. Kim, S. Park, G. Khang, P. M. Kang and D. Lee, *Biomacromolecules*. **2013**, *14*, 1618.

80. S. Y. Lin, K. S. Chen and L. Run-Chu, *Biomaterials*. **2001**, *22*, 2999.

81. C. James, A. L. Johnson and A. T. A. Jenkins, *Chem. Commun*. **2011**, *47*, 12777.

82. B. P. Purcell, D. Lobb, M. B. Charati, S. M. Dorsey, R. J. Wade, K. N. Zellars, H. Doviak, S. Pettaway, C. B. Logdon, J. A. Shuman, P. D. Freels, J. H. Gorman, R. C. Gorman, F. G. Spinale and J. A. Burdick, *Nat. Mater.* **2014**, *13*,

653.

83. J. Gao, W. T. Zheng, J. M. Zhang, D. Guan, Z. M. Yang, D. L. Kong and Q. Zhao, *Chem. Commun*. **2013***, 49*, 9173.

84. S. F. Zhang, J. Ermann, M. D. Succi, A. Zhou, M. J. Hamilton, B. N. Cao, J. R. Korzenik, J. N. Glickman, P. K. Vemula, L. H. Glimcher, G. Traverso, R. Langer and J. M. Karp, *Sci. Transl. Med***. 2015**, *7,* 300ra128.

85. S. Zhu, L. Nih, S. T. Carmichael, Y. Lu and T. Segura, *Adv. Mater*. **2015**, *27*, 3620.

86. 114. J. Alijotas-Reig, M. T. Fernandez-Figueras and L. Puig, *Clin. Rev. Allergy Immunol*. **2013**, *45*, 97.

87. M. Zelzer and R. V. Ulijn, *Chem. Soc. Rev*. **2010**, *39*, 3351.

88. R. J. Williams, R. J. Mart and R. V. Ulijn, *Biopolymers*. **2010**, *94*, 107.

89. J. E. Ghadiali and M. M. Stevens, *Adv. Mater*. **2008**, *20*, 4359.

90. D. Roy, J. N. Cambre and B. S. Sumerlin, *Prog. Polym. Sci*. **2010**, *35*, 278.

91. (a) Figliozzi, G.M.; Goldsmith, R.; Ng, S.; Banville, S.C.; Zuckermann, R.N. Methods Enzymol. **1996**, *267*, 437-447. (b) Culf, A.S. and Oulette, R.J. Molecules. **2010**, *15*, 5282-5335.

92. (a) Yoo, B. and Kirshenbaum, K. *Curr. Opin. Chem. Biol.,* **2008**, *12*, 714-721. (b) Shin, S.-B.Y.; Yoo, B.; Todaro, L.; Kirshenbaum, K. *J. Am. Chem. Soc*. **2007**,*129*, 3218-3225. (c) Huang, K.; Wu, C.W.; Sanborn, T.J.; Patch, J.A.; Kirshenbaum, K.; Zuckermann, R.N.; Barron, A.E.; Radhakrishnan, I. *J. Am. Chem. Soc*., **2006**,*128*, 1733-1738. (d) Kirshenbaum, K.; Barron, A.E.; Goldsmith, R.A.; Armand, P.; Bradley, E.K.; Truong, K.T.V.; Dill, K.A.; Cohen, F.E.; Zuckermann, R.N. *Proc. Natl. Acad. Sci. USA*, **1998**, *95,* 4303-4308.

93. Huang, M. L.; Benson, M. A.; Shin, S. Y.; Torres, V. J.; Kirshenbaum, K. Eur. JOC. **2013**, 3560-3566.

94. Levine, P. M.; Imberg, K.; Garabedian, M. J.; Kirshenbaum, K. *J. Am. Chem. Soc.* **2012**, *134*, 6912-6915.

95. Kwon, Y-U. and Kodadek, T. *J. Am. Chem. Soc.* **2007***, 129*, 1508-1509.

96. Miller, S.; Simon, R.; Ng, S.; Zuckermann, R.; Kerr, J.; Moos, W. *Bioorg. Med. Chem. Lett.* **1994**, *4*, 2657-2662.

97. Chongsiriwatana, N.P.; Patch, J.A.; Czyzewski, A.M.; Dohm, M.T.; Ivankin, A.; Gidalevitz, D.; Zuckermann, R.N.; Barron, A.E. *PNAS*. **2008**,*105*, 2794-2799.

98. Huang, M. L.; Benson, M. A.; Shin, S. Y.; Torres, V. J.; Kirshenbaum, K. Eur. JOC. **2013**, 3560-3566.

99. Levine, P. M.; Imberg, K.; Garabedian, M. J.; Kirshenbaum, K. *J. Am. Chem. Soc* **2012**, *134*, 6912-6915.

100. Turner, J.P.; Lutz-Rechtin, T.; Moore, K.A.; Rogers, L.; Bhave, O.; Moss, M.A.; Servoss, S.L. *ACS Chem. Neurosci*. **2014**, *5*, 552–558.

101. Maayan, G.; Ward, M.; Kirshenbaum, K. *Proc. Natl. Acad. Sci. USA*. **2009**, *106*, 13679-13684.

102. Della Sala, G.; Nardone, B., De Riccardis, F.; Izzo, I. *Org. Biomol. Chem*. **2013**, *11*, 726-731.

103. Statz, A. R.; Meagher, R. J.; Barron, A. E.; Messersmith, P. B. *J. Am. Chem. Soc*. **2005**, *127*, 7972–7973.

104. Huang, M.; Ehre, D.; Jiang, Q.; Hu, C.; Kirshenbaum, K.; Ward. M. *Proc. Nat.l Acad. Sci. USA*. **2012**,*109,*19922-19927.

105. Fu, J.; Xia. A.; Qi, X. *Med. Chem. Commun*.**2016**, *7*, 1183-1189.

106. Sanii, B.; Kudirka, R.; Cho, A.; Venkateswaran, N.; Oliver, G.K.; Olson, A.M.; Tran, H.; Harada, R.M.; Tan, L.; Zuckermann, R.N. *J. Am. Chem. Soc*. **2011**, *133*, 20808-20815.

107. Chen, C.L.; Qi, J.; Zuckermann, R.N.; DeYoreo, J.J. *J. Am. Chem. Soc*. **2011**, *133*, 5214-5217.

108. Kölmel, D.K.; Rudat, B.; Schepers, U.; and Bräse, S. Eur. J. Org. Chem. **2013**, 2761–2765.

109. Izzo I; Ianniello, G.; De Cola, C.; Nardone, B.; Erra, L.; Vaughan, G.; Tedesco, C.; DeRiccardis, F. Org. Lett. **2013**, *15*, 598-601.

110. Maayan, G.; Ward, M.; Kirshenbaum, K. Chem. Commun. **2009**, 56-58.

111. Lee, B. C.; Chu, T.K.; Dill, K.A.; Zuckermann, R.N. *J. Am. Chem. Soc*. **2008**, *130,* 8847-8855.

112. Pirrung, M. C.; Park, K.; Tumey, L. N. *J. Comb. Chem*. **2002**, *4*, 329-344.

113. Maayan, G. and Lui, L-K. *Biolpolymers*. **2011***, 96*, 697-687.

114. Cola, D. C.; Fiorillo, G.; Meli, A.; Aime, S.; Gianolio, E.; Izzo, I; De Riccardis, F. *Org. Biomol. Chem*. **2014**, *12*, 424-431.

115. Fischer, A. E. O. and Naughton, D. P. *J. Inorg. Biochem*. **2004**, *98,* 343-346

116. Ramshaw, J.A. and Brodsky, B. ***J. Biol. Chem.*** **2004***, 280*, 19343-193443.

117. Bhatnagar, R. and Gough, C.A. *Circular Dichroism and the Conformational Analysis of Biomolecules;* Fasman, G.D., Ed.; Springer Science+Business Media: New York,1996, pp 184-199.

118. Lopes, J.L.S.; Miles, A.J.; W, L.; Wallace, B.A. Protein Sci. **2014**, 12, 1765–1772.

119. Liu, Y.; Liu, L.; Chen, M.; Zhang, Q. *Journal of Biomolecular Structure and Dynamics***. 2013**, *31,* 862-873.

120. Engel, J. and Prockop, D.J. *Annu. Rev. Biophys. Biophys. Chem*.**1991**, *20*, 137- 152.

121. Berisio, R.; Vitagliano, L.; Mazzarella, L.; Zagari, A. *Protein Sci*. **2002**, *11*, 262−270.

122. Voelz, V. A.; Dill, K.A.; Chorny, I. *Peptide Science*. **2010**, *96*,639-650.

Chapter 3

siRNA Transfection with Lipitoids for Scar Tissue Inhibition

3.1 Abstract

Lipitoids are cationic peptidomimetic oligomers conjugated to phosopholipid moieties. Lipitoids are known to form nanoparticulate complexes with nucleic acids possessing defined morphology, low cytotoxicity, and broad compatibility across a wide variety of cell types and have proven useful as transfection reagents. The Branski laboratory and others have suggested that Smad3 is a principle mediator of the fibrotic phenotype via its role in transforming growth factor (TGF)-β1 signaling, implicated in vocal fold fibrosis. Alteration of Smad3 expression through short interfering (si) RNA holds therapeutic promise, yet delivery of siRNA remains challenging. We hypothesize that lipitoids can associate with siRNA to enhance stability and cellular uptake and will increase the efficiency of RNA-based therapeutics. Prior to in vivo use, **Lipitoid** cytotoxicity was quantified in vitro compared to commercially available delivery media; **Lipitoid** did not confer additional toxicity. The conditions for binding siRNA to **Lipitoid** for intracellular delivery were then optimized; 20 minute incubation in 1xPBS resulted in maximal Smad3 knockdown in vitro. A rabbit model of vocal fold injury was then employed to evaluate Smad3 knockdown using locally injected **Lipitoid**-complexed siRNA. Smad3 expression was significantly reduced in injured vocal folds at 4 and 24 hours following injection. These results are the first to demonstrate targeted, therapeutic gene knockdown in the vocal folds and the utility of **Lipitoid** for localized delivery of genetic material in vivo. The two reagents suppressed Smad3 mRNA for up to 96 hours; **Lipitoid** performed favorably and comparably. Both compounds yielded 60-80% mRNA

knockdown in rat, rabbit, and human vocal fold fibroblasts. Dose and number of administrations played a significant role in gene suppression. Suppression was more dose-sensitive with **Lipitoid**; with constant siRNA concentration, 50% decrease in gene expression was observed in response to a 5-fold increase in **Lipitoid** concentration. An increased number of administrations also enhanced gene suppression; ~45% decrease between one and four administrations. Neither serum nor media type altered efficiency. **Lipitoid** effectively knocked down Smad3 expression across multiple transfection conditions. The **Lipitoid** /RNA nanoparticle appears to allow enhanced flexibility with regard to transfection conditions and warrants further investigation with the ultimate goal of establishing clinical utility.

3.2 Introduction

siRNA oligonucleotides are a family of small double-stranded RNA molecules between 20-25 base pairs in length that associate with complementary nucleotides within target mRNA species, and temporarily attenuate expression of target genes by triggering sequence-specific degradation of mRNA and diminished translation.[1-3] **(Figure 26)** The gene silencing effects of siRNA can modulate a variety of biochemical pathways and, although transient, the process holds significant therapeutic promise across disease states. Beginning with the discovery of RNA interference in mammals,[4,5] interest has evolved regarding the utility of RNA-based therapeutics.[6-8] siRNA has several ideal characteristics for localized delivery and gene silencing particularly relevant to laryngeal pathologies; it is temporary, genes are targeted directly, and off-

target effects are minimized while high concentrations of siRNA can be maintained at the relevant site.

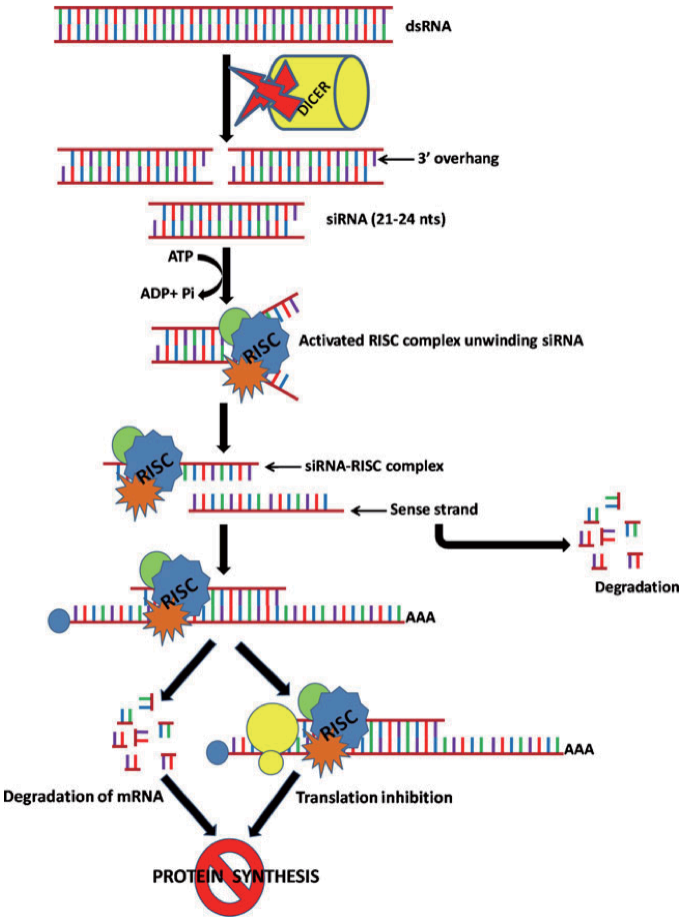

Figure 26. Representation of short interfering RNA therapy. Double stranded RNA is introduced into the cellular environment where it is cleaved by Dicer RNase III, yielding short nucleotide duplexes of RNA about 21 base pairs in length. RISC binding to the siRNA initiates complex formation and unwinds the siRNA duplexes. The sense strand is then degraded while the siRNA-RISC complex then binds to the target complementary mRNA strand where it is either immediately broken down or inhibits translation, also leading to degradation.[9] (Image on left taken from: Jagtap,et. al 2011)

Although administration of siRNA via peripheral circulation has shown promise for systemic diseases, such administration may also induce significant gene silencing in major non-target organs such as the lung, liver, and spleen, resulting in serious morbidity.[1,10] Furthermore, in vivo, systemic administration of Smad3 siRNA is likely associated with profound morbidity. Animals deficient in Smad3 develop osteoarthritis

and humans with Smad3 mutations are at risk for aortic aneurysms and dissections, as well as skeletal abnormalities.[11] Additionally, systemic administration could be limited by rapid degradation of siRNAs by nucleases prior to uptake at the target organ.[12] Confounds of systemic therapy also include the loss of siRNA via urinary output and insufficient penetration into cells in the absence of liposome transfection or electroporation. [13, 14] These factors result in significantly increased costs of systemic siRNA therapy, as exceedingly high concentrations of siRNA are required.[6] Consequently, optimal modalities for direct siRNA treatment and focused delivery are high priorities for treatment of localized disease. Disease states involving defined tissues such as the eye, skin, and certain types of tumors are amenable to localized siRNA treatment. Encouragingly, several current siRNA-based late-stage clinical trials employ localized delivery strategies.[14]

The issue of delivery is particularly germane as a recent review reported that nearly 50% of current, commercially-funded clinical trials employ RNA-based therapeutics administered without any delivery media, and as such, are referred to as "naked" delivery of siRNA[6] which is problematic considering siRNA is vulnerable to rapid hydrolytic cleavage. In addition, siRNA oligonucleotides are resistant to uptake by most cells due to the size of the molecules and their anionic charge.[2,15] However, a carrier molecule can facilitate movement of siRNA through the cell membrane, thereby increasing transfection efficiency and reducing the effective concentration of siRNA required for therapeutic benefit.[14, 16-25] Therefore, the development of novel transfection reagents to enhance the efficacy of siRNA-based therapeutics has the potential to directly impact patient care paradigms.

A working collaboration between our lab and the Branski lab aims to attenutate scar tissue formation in the vocal folds using siRNA therapeutics. Vocal fold (VF) fibrosis is among the most challenging laryngeal abnormalities resulting in significant handicap. In healthy vocal folds, oscillatory symmetry of the pliable epithelium and superficial lamina propria allows for complementary cycle-to-cycle contact and favorable voice quality.[26] Injury and the subsequent fibroblastic response disrupt this delicate architecture via activation and proliferation of profibrotic cells, resulting in disruption of mucosal wave and altered glottic closure.[26-29] Due to the difficulties modulating biochemical processes underlying fibrosis, current therapies for VF scarring primarily target glottic closure.[30] Smad3 is a contributor to Transforming Growth Factor (TGF)-β signaling which is fundamental to aberrant wound healing in the vocal folds and other tissues**.** The Branski Laboratory and others have implicated transforming growth factor (TGF)-β1 as a master regulator of fibroplasia via its interactions with fibroblasts to induce proliferation, migration, adhesion, apoptosis, and extracellular matrix (ECM) metabolism.[22,29-34] These fibroplastic activities are largely mediated via Smad3, a receptor-activated protein. Ligand binding to the receptor phosphorylates Smad3 leading to heterodimerization and nuclear translocation to regulate multiple transcriptional events. (**Figure 27**) The Branski laboratory demonstrated Smad3-dependent regulation of TGF-β1 mediated cellular activities in vocal fold fibroblasts in vitro.[22,29,30] Globally, we hypothesize that Smad3 is an ideal therapeutic target in vivo, as modulating this pathway can likely redirect wound healing toward a more regenerative, less fibrotic phenotype. Given their anatomic location and accessibility, the VFs are an ideal model for local administration of siRNA to ensure precise targeting

of Smad3 with minimal off-target toxicity. This approach has not previously been described in the vocal folds. Recently, our collaboration employed RNA interference (RNAi) via short interfering RNA (siRNA) to alter Smad3 expression in vitro. [22,29,30] .

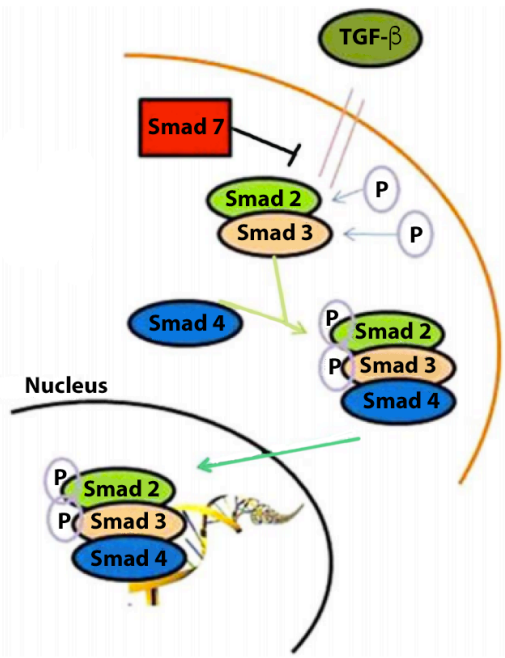

Figure 27. Schematic depicting the relationship between TGF-β signaling and SMADs. TGF-β recruits kinases upon binding to cell surface receptors, which phosphorylate SMAD proteins, resulting in heterodimerzation. Phosphorylated SMADs are subsequently translocated to the nucleus where they regulate transcription of many genes implicated in fibrosis.[29] Image adapted from Branski, Ryan & Bing, Renjie & Kraja, Iv & R Amin, Milan. (2015). The Role of Smad3 in the Fibrotic Phenotype in Human Vocal Fold Fibroblasts. The Laryngoscope. 126. 0.1002/lary.25673.

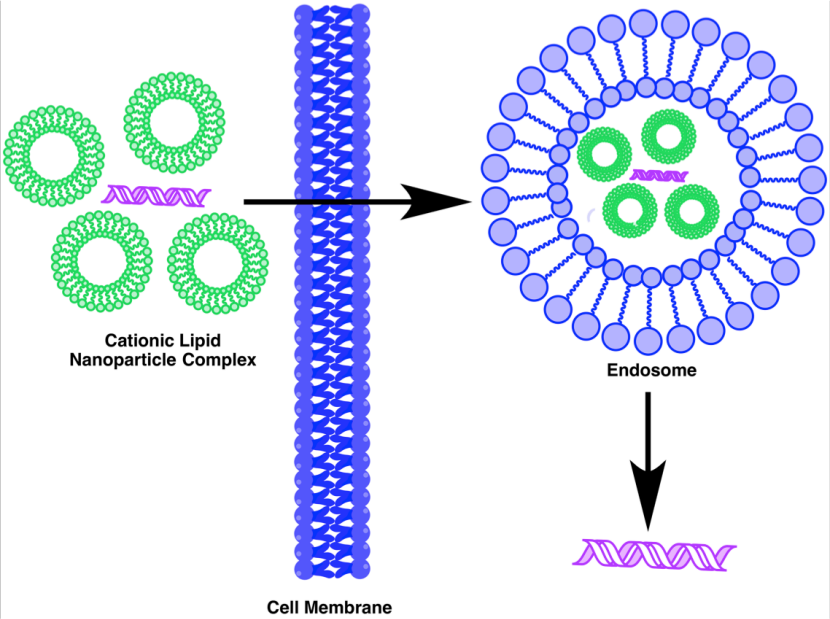

Figure 28. Representation of lipofection with cationic lipids. First a nanoparticulate complex is formed between the nucleic acid (pink) and the cationic lipid (green) by virtue of an electrostatic attraction of the opposing ionic charges of the transfection reagent and negatively charged phosphate backbone of the nucleotide. The lipid segments then facilitate passage through the membrane by formation of an endosome. Once inside the cellular environment, the endosome becomes disrupted, and the genetic material is released into the cytoplasm.

Cationic lipids are attractive delivery molecules for nucleic acids as they undergo electrostatic association with polyanionic siRNA oligonucleotides and facilitate compatibility with the membrane lipid bilayer, enhancing cellular uptake, due to their amphiphilic character.[23-25] This process is similar to lipofection by virtue of a facilitated nucleic acid transport across the hydrophobic cell membrane as part of a nanoparticulate complex. (**Figure 28**) Lipofectamine®, a popular in vitro transfection reagent composed of cationic lipid subunits, similarly delivers siRNA via liposome

formation resulting in lipid compatibility of the sequestered nucleic acids for delivery across the cell membrane.[35,36] Yet, these carrier molecules are limited to a few commercial reagents, which may have limited clinical utility due to cytotoxicity and an undetermined capacity to effectively deliver siRNA in vivo.[6]

To address these issues, our group exploited a class of peptidomimetic oligomers called peptoids. Sequence-specific peptoids displaying cationic side chain groups and conjugated to a phospholipid tail with hydrophobic compatibility are referred to as lipitoids.[37] Lipitoids were initially developed for intracellular plasmid DNA delivery as an alternative to both potentially infectious, yet effective, methods of DNA delivery through viral encapsulation[15,37] along with non-viral DNA delivery vehicles that are typically associated with high cellular toxicity and/or low transfection efficiency.[46, 38-42] Early reports identified a peptoid sequence (subsequently referred to as **Lipitoid**; **Figure 29**) with particularly favorable properties including transfection efficiency, resistance to proteolytic degradation, and limited cytotoxicity. [40-42,46]

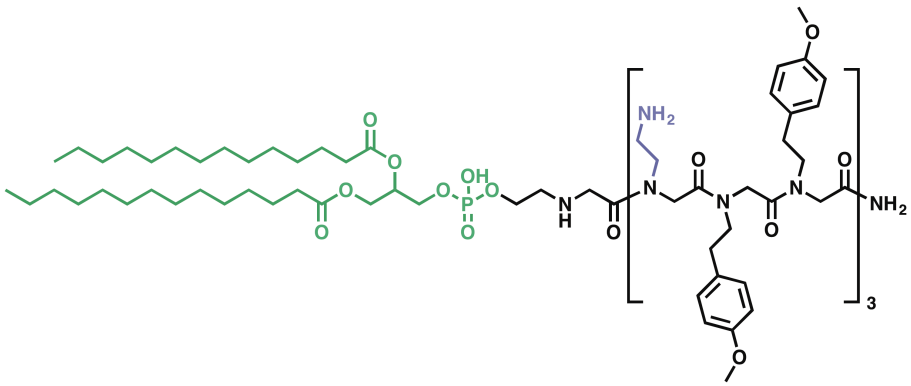

Figure 29. Structure of the **Lipitoid** oliogmer.

Lipitoid features trimeric repeats of cationic and aromatic side chain groups connected to a phosphotidyl moiety presenting mirystic acyl C14 chains, all of which enhance interactions with nucleic acids, facilitate intercellular uptake, and reduce non-

specific cell adhesion. In contrast to Lipofectamine®, Lipitoid appears to avoid formation of a liposome to encapsulate oligonucleotide cargo to provide more effective siRNA delivery.[41] Recently, critical parameters impacting the size and morphology of the siRNA nanometer-scale complexes have been determined for optimal transfection mediated by Lipitoid.[41] **Lipitoid** has been successfully used as a transfection reagent for both plasmid DNA and siRNA, across many types of mammalian cell lines including those that have proven to be refractory to traditional transfection methods.[42]

Ultimately, we seek to effectuate siRNA-based therapies, targeting Smad3 in vivo to alter wound healing in the upper aerodigestive tract. In these studies, we sought to provide pre-clinical data regarding the effectiveness of **Lipitoid** both in vitro and in vivo. Efforts from the Branski laboratory recently described Smad3 as a key biochemical switch underlying the fibrotic phenotype and an ideal target for siRNA-based therapeutics.[29,30]

Cytotoxicity of **Lipitoid**, as well as the optimal conditions for siRNA-lipitoid binding, were established in vitro. The in vivo effects of lipitoid-bound siRNA on Smad3 mRNA expression were then quantified in a rabbit model of vocal fold injury. This is the first reported case of utilizing lipitoids as a transfection reagent for in vivo studies. In addition, a library of 8 other lipitoid variations was generated and tested, in vitro. Ultimately, we seek to identify optimized lipitoid sequences that will lead to physiologically-targeted therapeutics for the millions of patients with voice disorders.

Nanoparticle Delivery of RNA-based Therapeutics to Alter Local Vocal Fold Tissue Response to Injury

The treatment of vocal fold fibrosis remains a substantial problem in clinical laryngology. A promising step towards meeting this challenge is the in vivo modulation of biological pathways underlying the fibrotic phenotype during wound healing. Suppression of Smad3 has been previously shown to reduce fibrotic activities in vitro, [29] and, in vivo, Smad3 deficient mice are resistant to bleomycin-induced pulmonary fibrosis, carbon tetrachloride-induced hepatic fibrosis, and glomerular fibrosis.[43-47] Downregulation of Smad3 expression is thought to blunt the TGF-β1-mediated fibroplastic response in fibroblasts and interrupt TGF-β1 signaling in inflammatory cells within the wound milieu.[48] Smad3 was recently silenced in murine skin using a topical gel, resulting in resistance to radiation-induced cutaneous fibrosis.[49] Cumulatively, therapeutic manipulation of Smad3 likely holds great potential for redirecting wound healing towards a regenerative outcome. In spite of the prevalence of voice disorders and relatively direct access to the vocal folds, the current study is the first to describe manipulation of local gene expression in the vocal folds.

Over 50 ongoing clinical trials utilizing RNA-based therapeutics were identified in a 2012 review,[6] many of which employed “naked” delivery of siRNA. These trials are limited by both the inefficiency of gene silencing and the necessity to administer elevated quantities of the therapeutic agents.[50,51] Motivated by the goal of in vivo siRNA utility to effectuate biologically targeted therapies, our laboratory previously performed a preliminary in vitro investigation regarding a relatively novel lipitoid/siRNA nanoparticle.[22] Data from the current investigation demonstrated limited cytotoxicity of

this nanoparticle in vitro, optimized lipitoid-siRNA binding conditions, and successful knockdown of Smad3 in vivo via lipitoid-complexed siRNA.

3.3 Results and Discussion

In Vitro

Lipitoid Synthesis and Purification. Lipitoid was synthesized on solid support using a modified submonomer synthesis approach. (**Figure 30**) This synthesis protocol entails an iteration of sequential haloacetylation and nucleophilic displacement by various primary amines on solid support. Once the desired peptoid sequence was obtained, bromoacetylated peptoids were exposed to a 0.2 M lipophosphoethanolamine solution prepared in 15% methanol/chlorobenzene. Insoluble in DMF, these highly hydrophobic species necessitated this specialized solvent mixture as previously described in the literature,[37] and were barely soluble at even 0.2 M, five times lower than the normal concentration for primary amine solutions in peptoid synthesis. This displacement was allow to progress for roughly 16 hours at 37°C, yet these authors also cite a lower yield of lipid containing peptoid due to this solvent incompatibility.[51]

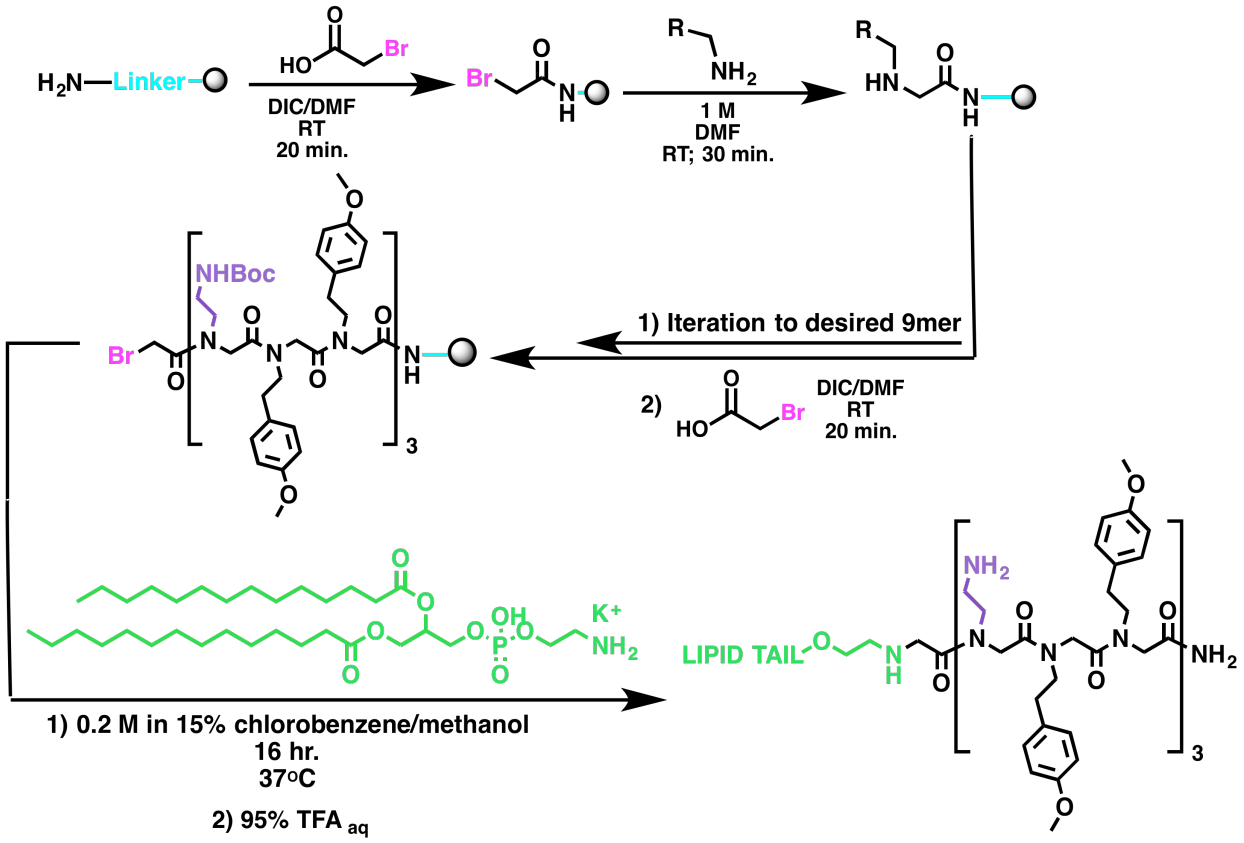

Figure 30. Solid phase synthesis of **Lipitoid.** First sequential haloacylation then displacement of the primary halide with a primary amine synthon creates the poly amide oliogomer, and a final displacement with a lipophosphoethanolamine species will afford the lipidated peptoid product.

We were able to make improvements to the purity of the crude compounds by modifying the phosopholipid addition conditions further. Anecdotal accounts cite the plastic syringe reaction vessel decomposing once exposed to the solvent and temperature conditions during the addition of the lipophosphoethanolamine. Considering this information, we decided to transfer the resin from the syringe to a glass scintillation vial prior to introduction of the lipophosphoethanolamine, and were rewarded with an outstanding level of purity from the crude sample compared to those

prepared in the plastic syringes. (**Figure 31**).

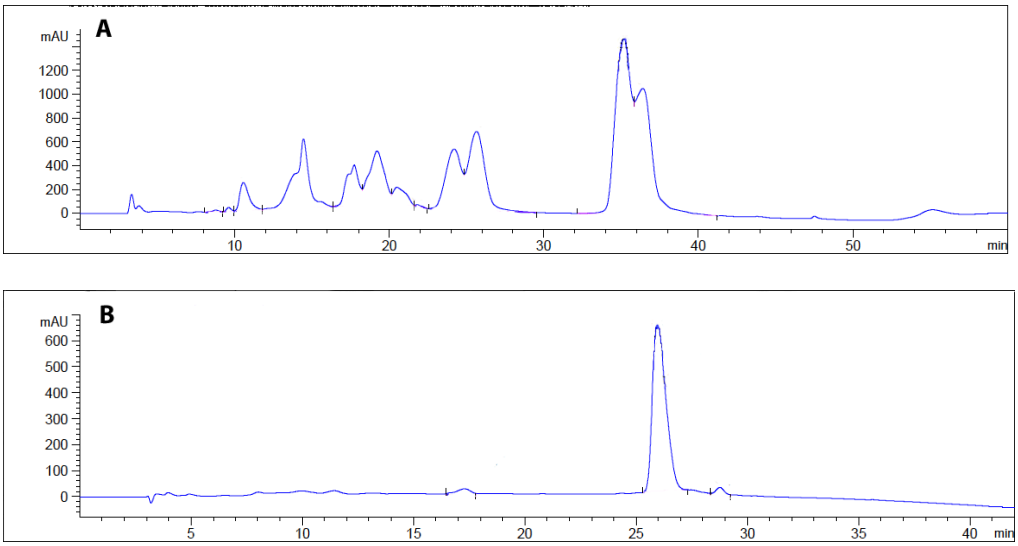

Figure 31. Comparison of crude **Lipitoid** purity when changing the reaction vessel during the lipid addition from plastic syringe (**A**) to glass scintillation vial (**B**). It should be noted that the analytical RP-HPLC analysis could not be performed using the same column in both experiments, therefore retention time of **Lipitoid** changes from 35 minutes (**A**) to 26 minutes (**B**).

Cell Proliferation and Viability. In vitro, lipitoid had no deleterious effect on metabolic activity, in either primary rabbit vocal fold fibroblasts (RVFF) or in immortalized human vocal fold fibroblasts (HVOX) relative to Lipofectamine (Invitrogen), as confirmed via MTS and Dead Live assay. Although both transfection reagents were associated with some toxicity, no statistically significant differences were noted between compounds for either cell type.

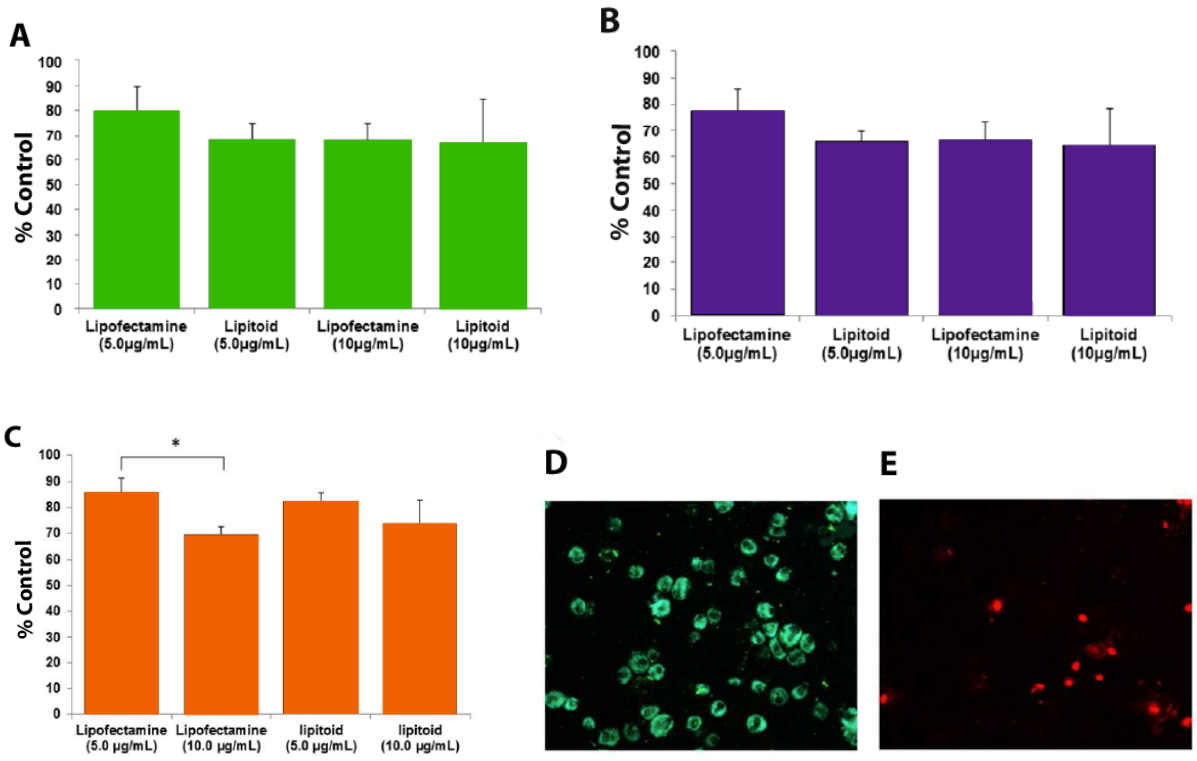

Figure 32. Cell viability as a function of Lipofectamine and lipitoid concentration in human vocal fold fibroblast(A) and rabbit vocal fold fibroblast (B). Results of Dead-Live assay displaying the percentage of live human vocal fold fibroblasts when treated with Lipofectamine and **Lipitoid** relative to control (C); EPI stain of the cells used in the Dead-Live assay. Cells stained/imaged/depicted in green are alive (D); cells stained/imaged/depicted in red are dead (E). All data shown as percent control; *p<0.05.

In human immortalized fibroblasts (**Figure 32 A**) 5mg/µL and 10mg/µL of Lipofectamine (Invitrogen) resulted in cell viability of 80% and 69% relative to the control group, respectively. This dose effect was not present in response to lipitoid; cell viabilities of 69% and 67% were observed at 5mg/µL and 10mg/µL, respectively. In addition, this dose response was not observed in primary RVFFs treated with Lipofectamine (Invitrogen); 78% and 76% at 5mg/µL and 10mg/µL, respectively (**Figure**

32 B).

RVFFs treated with lipitoid also resulted in minimal difference between doses; 66% and 64% at 5mg/μL and 10mg/μL, respectively. To further quantify cytotoxicity in human vocal fold fibroblasts, Dead/Live data were standardized as a percentage of control cell survival (**Figure 32 C-E**). A significant dose response (p=0.0398) as noted with Lipofectamine (Invitrogen); percent alive was 86% and 69% at 5mg/μL and 10mg/μL, respectively. Lipitoid treatment resulted in survival rates of 82% and 74% for 5mg/μL and 10mg/μL, respectively, lacking a significant dose response (p = 0.4430). No significant differences in cell survival were noted between lipitoid and Lipofectamine (Invitrogen) across concentrations.

Transfection Conditions. Relevant to the clinical application of lipitoid, optimal incubation times were sought to ensure desirable nanoparticle formation and morphology, and, by extension, effective gene silencing in vivo. Determination of these variables is critical for the eventual progression to clinical application. Smad3 knockdown as a function of media was quantified using RT-PCR. Relatively brief incubation (e.g., 20 minutes) in PBS yielded significant Smad3 knockdown in vitro.

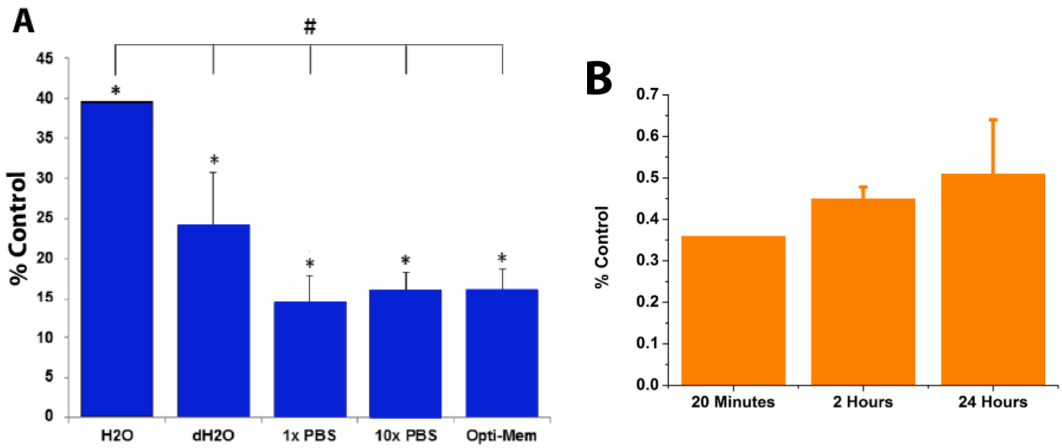

Figure 33. Percentage of Smad3 expression after siRNA transfection with **Lipitoid** as a function of media choice (A) and incubation time (B).*p<0.05 relative to non-transfected control, #p<0.05 relative to H_2O.

Twenty minute incubation in H_2O, deionized H_2O (dH_2O), Opti-MEM, 10x PBS, and 1x PBS yielded RQ values of 0.40, 0.24, 0.16, 0.16, and 0.14, respectively (**Figure 33 A**). Transfection with 1xPBS resulted in the greatest Smad3 knockdown; this difference (as for all of the experimental solutions tested) was significant relative to H_2O ($p<0.0001$ for each). However, differences between 1xPBS and dH_2O, Opti-MEM, and 10x PBS did not reach statistical significance. The influence of siRNA + lipitoid incubation time was then explored. Incubation times of 20 minutes, 2 hours, and 24 hours resulted in RQ values of 0.36, 0.45, and 0.52, respectively, compared to the control sample ($p<0.0001$ for all incubation times compared to control; **Figure 33 B**). However, no significant differences between incubation times were noted ($p=0.1253$ for 20 minutes compared to 24 hours). Thus, these conditions, 20 minute incubation in PBS buffer, were employed in the in vivo component of the current study.

In Vivo Lipitoid-complexed siRNA suppressed Smad3 gene expression after vocal fold injury. An established rabbit model of vocal fold injury was employed to investigate the Smad3 knockdown efficacy of injection of **Lipitoid**-complexed siRNA. We estimated the size of the rabbit vocal folds to be between 1 and 10 g, and therefore, we administered a dose 0.1 mg/kg based on previous in vivo experimentation with siRNA delivery in murine models.[52] 0.05 nmol of Smad3 siRNA was prepared in PBS buffer to a total of 10 μL, and combined with 10 μL of a 42 molar excess of lipitoid solution to a total volume of 20 μL. The large molar excess of lipitoid to siRNA is to ensure a (+/-) charge ratio of 3:1 as directed by previous studies for optimal nanparticle size and morphology during complex formation.[41]siRNA and **Lipitoid** were incubated for 20 minutes and then administered immediately to the animal models.

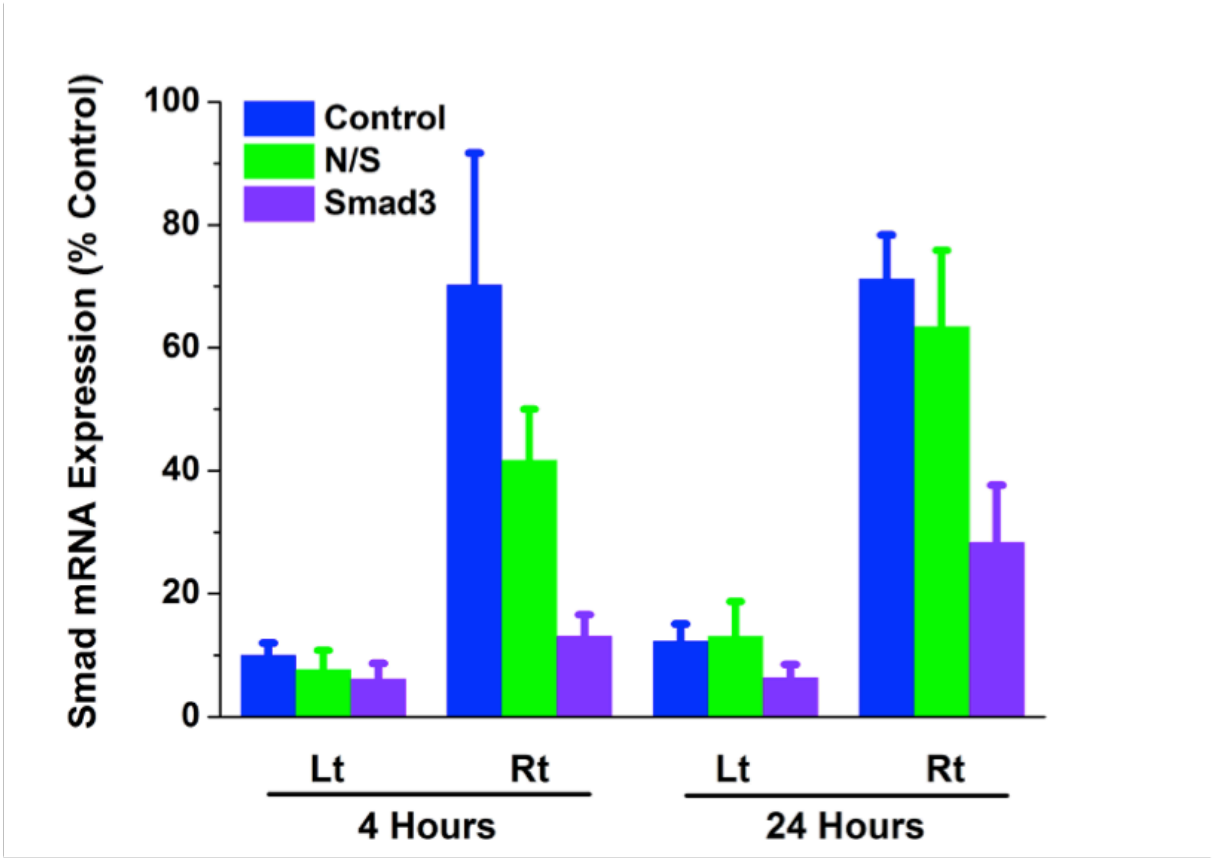

Figure 34. Expression of Smad3 mRNA at 4 and 24 hours after injection of **Lipitoid**-siRNA complex (Smad3) (n=5; p=0.035 at 4 hours and p=0.034 at 24 hours) in the left vocal fold (uninjured, Lt) and the right vocal fold (injured, Rt) compared to the control, and an injection without Smad3 siRNA. Smad3 expression was standardized to GAPDH and presented as fold change relative to control (mean +/-SEM).

Seven days following injury to the vocal folds, animals underwent cricothyroid approach to injection of Smad3 siRNA complexed with lipitoid under endoscopic guidance. This time point was selected because as previous work from the Branski laboratory showed peak Smad3 mRNA expression seven days following vocal fold injury in a similar model.[30,53] As shown in **Figure 34**, Lipitoid-mediated delivery of Smad3 siRNA in a leporine model of vocal fold injury was effective, and expression of

Smad3 mRNA increased significantly in response to injury. Smad3 expression was significantly reduced in injured vocal folds following injection of lipitoid+Smad3 siRNA at both 4 and 24 hours post injection ($p=0.035$ and 0.034, respectively) relative to the control and injection without Smad3 siRNA. Qualitative suppression of Smad3 expression was also observed in the uninjured vocal folds at both time points following lipitoid+Smad3 siRNA injection; this difference was not significant. Although functional outcomes following such genetic manipulation remain to be examined, we hypothesize that suppression of Smad3 using siRNA-lipitoid complex, even for a brief interval, likely holds immense therapeutic potential with minimal toxicity. These preliminary experiments support the therapeutic potential of lipitoid-complexed Smad3 siRNAas a powerful modifier of the wound healing response in the vocal folds.

3.3 Summary and Outlook

The current study is the first successful manipulation of local gene expression in the vocal folds and the first reported incidence of a peptoid-based transfection reagent used for in vivo experimentation, both of which provide foundational data for the further in vivo investigation. Admittedly, the current study is not without limitations. Most notably, the physiologic and functional sequelae of Smad3 suppression following injury were not examined. Optimal dosing, timing, and frequency of siRNA administration were also not explored; these issues are critical to the eventual clinical utility of this treatment modality. Although the current data show that lipitoid has comparable or a modest enhancement of transfection efficacy compared to Lipofectamine, improvements to oligomer can be readily implemented to tailor the nanoparticle complex for compatibility with tissue type, delivery method, and siRNA sequence.[54,55] Efficient modular synthesis of lipitoids as

oligomeric species allows the physicochemical properties of the transfection reagents to be tailored to meet these objectives through the selection of varying side chain chemical groups from the hundreds of commercially available primary amine synthons compatible with peptoid synthesis. Finally, these experiments examined a model of early wound healing, despite established fibrosis of the vocal folds leading to the most morbidity among patients. Nevertheless, the data presented here represent substantial progress towards the development of effective therapeutics to direct wound healing following vocal fold injury toward a less fibrotic, more regenerative outcome.

3.4 Experimental Procedures

Lipitoid Synthesis and Characterization

Materials:

Synthesis of the peptoid and peptide oligomers was initiated on Rink Amide resin (Nova Biochem, 100-200 mesh, loading: 0.74 mmol/gram). Bromoacetic acid (97%) was supplied by Sigma-Aldrich. Trifluoroacetic Acid, TFA, (99%), N,N-Dimethylformamide, DMF, (anhydrous and amine free, 99.9%) and N,N' diisopropylcarbodiimide, DIC, (99%) were supplied by Alpha Aesar. 2-(4-methoxyphenyl)ethylamine and mono-t-BOC ethylenediamine were purchased from Sigma Aldrich. Lipids were purchased from either Avanti Polar Lipids (Avanti Polar Lipids, Inc.) or Sigma Aldrich. Other reagents and solvents were obtained from commercial sources and used without additional purification.

Lipitoid Synthesis. Synthesis of the **Lipitoid** was conducted on solid phase according to previously described procedures according to a modified submonomer synthesis approach[62] and purified via high-performance liquid chromatography. Rink Amide Resin, 100 mg (0.074 mmol), was swelled in DMF for 30 minutes before initiating the synthesis. Bromoacetylation was carried out by incubating the resin with a bromoacetic acid solution in DMF (1.2M, 850 μL) and DIC (200 μL) for 20 minutes at room temperature and an agitation rate of 220 rpm. The resin was washed with 4x 1 mL DMF before displacement with the desired primary amine (1M in DMF) for 30 minutes at room temperature and an agitation rate of 220 rpm. The resin was washed with 5x 1 mL DMF. This two-step iterative process was repeated until the desired oligomer chain length and monomer sequence composition was achieved before the addition of the

lipophosphotidylethylamine. Prior to lipid addition, the peptoid sequence was bromoacetylated once more, and the resin washed and transferred to a glass scintillation vial. A 0.2M solution of dimyristoyl phosphatidyl-ethanolamine was prepared in 15% methanol/chlorobenzene and to it was added 0.95 eq. of 11M KOH. The solution was centrifuged, and the supernatant removed and to the scintillation vial containing the resin. Resins were exposed to the lipid solution for roughly 16 hours while shaking at 37°C. The resins were then washed copiously with 15% methanol/chorobenzene and after with 5 x 1mL DMF and 5 x 1mL DCM. The **Lipitoid** was cleaved from the resin using a cocktail containing 95% TFA, 2.5% TIPS, and 2.5% water (4 mL) at room temperature for 10 minutes. The solution was removed under reduced pressure, and the crude peptoid was re-suspended in acetonitrile/water, frozen, and lyophilized. Once thoroughly dried, crude **Lipitoid** was stored at 4°C until characterization and purification.

Characterization and Purification of **Lipitoid**. Lyophilized powders were suspended in a solution of aqueous acetonitrile then analyzed by MALDI-TOF/TOF and analytical RP-HPLC. **Lipitoid** was purified to >95% using a preparatory C_4 column. HPLC was on a Waters 2489 instrument using a Phenomenx Jupiter C_4 column (Phenomenex, 15 µm, 300 Angstroms, 10x250 mm). **Lipitoid** was detected at 220 nm during a linear gradient of 15-45% aqueous ACN with 0.1% TFA over 60 minutes at a flow rate of 5 mL/min. Fractions were consolidated, frozen, and lyophilized. Once dried, purified **Lipitoid** was stored at 4°C until analysis and in vitro and in vivo testing.

Purity was assessed by reverse-phase HPLC (DeltaPak analytical C_4 column, Waters, 5 µm, 300 Angstroms, 3.9x150 mm) on an Agilent 1260 Infinity LC system. A linear gradient of 20-80% acetonitrile in water (0.1% TFA) over 40 min. was used at a flow

rate of 500 μL /min. Mass spectrometry was performed on an Agilent 1100 series LCMSD VL MS spectrometer or a Bruker Maldi-TOF TOF UltrafleXtreme MS Spectrophotomer using a saturated solution of α-Cyano-4-hydroxycinnamic acid prepared in 70% ACN(aq) with 0.1% TFA

In Vitro

Cell Lines. An immortalized human vocal fold fibroblast cell line (HVOX) developed in our laboratory was employed.[8.1] In addition, primary rabbit vocal fold fibroblasts (RVFF) were provided from the Rousseau Laboratory at the Vanderbilt University School of Medicine.

Cell Proliferation and Viability. HVOX and RVFF were grown in 96-well plates using Dulbecco's Modified Eagle Serum (DMEM; Life Technologies, Carlsbad, CA) with 10% Fetal Bovine Serum (FBS) (Life Technologies) and 1% antibiotic/antimycotic (Life Technologies). Both cell lines were then treated with the experimental concentration of lipitoid or Lipofectamine. (Invitrogen Thermo Fisher Scientific, Waltham. MA) for 24 hours in antibiotic free media. The media was aspirated and the cells were treated with 100μL of complete media and 20μl of CellTiter 96. Aqueous One (Promega, Fitchburg, WI) solution for 2 hours. Absorption was quantified at 490nm.

Dead-Live Assay. HVOX grown to confluence in a six well plate were treated with lipitoid or Lipofectamine. (Invitrogen) in DMEM with 10% FBS for 24 hours. Cells were then harvested and labeled employing the LIVE/DEAD. Cell-Mediated Cytotoxicity Kit (Molecular Probes., Thermo Fisher Scientific, Waltham, MA) following standard protocols. Cell images were analyzed and counted using a Nikon TIRF/Epi-Fluorescent Microscope (Nikon, Tokyo, Japan).

Transfection/Incubation times. HVOX were grown to 80% confluency and 5 μM of siRNA was combined with 1.07mg/mL of lipitoid in 500μL of Opti-MEM (Life Technologies, Carlsbad CA). This solution was incubated at room temperature for 20 minutes, 2 hours, and 24 hours, respectively, for each sample. The solution was then added to cells with 1.5mL DMEM and 10% FBS. After 24 hours, mRNA was extracted and subjected to quantitative polymerase chain reaction.

Transfection/Incubation solutions. HVOX were grown in a 6-well plate until 80% confluency and 5nM of siRNA was combined with 1.07mg/mL of lipitoid in 500mL H_2O, deionized H_2O, 1x Phosphate Buffer Saline (PBS), 10x PBS, or Opti-MEM. This solution was incubated for 20 minutes and added to the cells with 1.5mL DMEM and 10% FBS. After 24 hours, mRNA was extracted and subjected to quantitative polymerase chain reaction.

Quantitative Polymerase Chain Reaction. mRNA was harvested employing the Qiagen RNeasy Kit (Qiagen, Valencia, CA) according to manufacturer's protocols and quantified with the NanoDrop 2000 UV-Vis Spectrometer (Thermo Scientific, Wilmington, DE). The Taqman High-Capacity cDNA Reverse Transcription Kit (Applied Biosystems, Grand Island, NY) was used to perform quantitative reverse transcriptase-polymerase chain reaction (RT-PCR). Gene sequences for Smad3 and glyceraldehyde-3-phosphate dehydrogenase (GAPDH) were obtained in the form of Taqman gene expression assays (Applied Biosystems). Quantitative RTPCR was performed on the Applied Biosystems StepOne Plus Real-Time PCR System following manufacturer's protocols. The ΔΔCt method was used with normalization via GAPDH.

Statistical analysis. All in vitro experiments were performed in triplicate at minimum.

One-way analysis of variance (ANOVA) was employed. If the main effect was significant at $p<0.05$, post hoc comparisons were performed via the Scheff. method using StatView 5.0 (SAS Institute, Berkeley, CA). Data are expressed as mean ± standard error.

In Vivo

Vocal Fold Injury. All procedures were approved the by Institutional Animal Care and Use Committee at the New York University School of Medicine. Thirty adult, 2-3kg New Zealand white rabbits were randomly assigned to 1) no injection (control), 2) lipitoid + nonsense siRNA, and 3) lipitoid + Smad3 siRNA (n=10 in each group). Each group was further categorized according to time of sacrifice: 4 hours and 24 hours after injection (each n=5). All animals received intravenous injection of ketamine (70mg/body) and xylazine (2mg/body) for induction of anesthesia. Inspired isoflurane was added for paralytic maintenance. The animals were placed supine on an operating table and the larynx was visualized via a slotted laryngoscope (Size 1; Karl Storz, Flanders, NJ). Under the guidance of 2.7mm, 0° or 30° telescope (Karl Storz), the vocal folds were injured unilaterally by separating the lamina propria from the thyroarythenoid muscle via insertion of a 22-gauge needle at the lateral portion of right vocal fold, followed by removal of the lamina propria with microscissors and microforceps.

Transfection Solutions. 10μL of 5 μM Smad3 siRNA was complexed with 10 μl of 210 μM **Lipitoid** diluted in deionized water/1x PBS buffer by adding the siRNA to the lipitoid solution and allowed to stand for 20 minutes at room temperature to form nanoparticles of optimal dimension.[46] siRNA **Lipitoid** complexes were formed at an approximate **Lipitoid** to siRNA molar ratio of approximately 42:1, establishing a positive/negative charge ratio of 3:1. Nonsense siRNA solution was prepared similarly,

according to the manufacturer's protocol.

Vocal Fold Injection. Seven days after injury, animals underwent anesthesia and laryngeal visualization as described above. The cricothyroid approach was then employed to inject 20 µl of 0.1mg/kg administered dose of nonsense siRNA or Smad3 siRNA complexed with lipitoid into the subepithelial layer of the scarred right lamina propria using a microinjection system (Hamilton Company, Reno, NV) with a 27-gauge needle. The location of the injection site was confirmed visually via marked distention of the vocal fold mucosa. At 4 or 24 hours following injection, animals were sacrificed and the larynges were harvested and immersed in RNAlater RNA Stabilization Regent (Qiagen Inc., Valencia, CA) and stored at -80^{o}C until analysis.

Quantitative Real-Time Polymerase Chain Reaction. The bilateral vocal folds were dissected under magnification. mRNA extraction, quantification of mRNA, and RT-PCR were performed as previously described. Expression was presented as fold change compared to the left (uninjured) vocal fold in the control cohort. The uninjured, left vocal fold served as an internal control.

Statistical Analyses. Two-way ANOVA followed by the Scheff. post hoc test was employed to investigate differences in gene expression at each time point. When interactions were present between treatment and time point, a one-way factorial ANOVA followed by the Scheff. post hoc test were performed. Statistical significance was defined as $p<0.05$. All data are expressed as means ± standard error.

3.4 References

1. Hamilton, A. and Baulcombe, D. *Science*. **1999**, *286*,950–952.
2. Dykxhoorn D.M. and Lieberman, J. *Cell*. **2006**,*126*,231–235.
3. Whitehead, K.A.; Langer, R.; Anderson, D.G. *Nature reviews Drug discovery.* **2009**, *8*,129-138.
4. Elbashir, S.M.; Harborth, J.; Lendeckel, W.; Yalcin, A.; Weber, K.; Tuschl, T. *Nature*. **2001**, *24*, 494–498.
5. McCaffrey, A.P.; Meuse, L.; Pham, T.T.; Conklin, D.S.; Hannon, G.J.; Kay, M.A. *Nature*. **2002**, *4*, 38–39.
6. Burnett, J.C. and Rossi, J.J. *Chem. Biol*. **2012**,*19*,60–71.
7. Burnett, J.C.; Rossi, J.J.; Tiemann, K. *Biotechnol. J.* **2011***,6*,1130–1146.
8. Resnier, P.; Montier, T.; Mathieu, V.; Benoit, J.P.; Passirani, C. *Biomaterials*. **2013,***34*,6429–6443.
9. Jagtap, U.B. Gurav, R.G.; Bapat, V.A. *The Science of Nature*. **2001**, *98*, 473–492.
10. Sorensen, D.R.; Leirdal, M.; Sioud, M. *J. Mol. Biol.* **2003**, *327*,761–766.
11. van de Laar, I.M.; Oldenburg, R.A.; Pals, G.; *et al. Nature genetics.* **2011**, *43*,121- 126.
12. Lee, R.C.; Fieinbaum, R.L.; Ambros, V. *Cell.* **1993**, *75*,843–854.
13. Akaneya, Y. *A new approach for therapeutic use by RNA interference in the brain. In: RNA Interference, Methods in Molecular Biology*. Min, W.-P. and Ichim, T.; Eds. Springer Science and Business Media: New York, NY, 2010.
14. Aigner, A. *J Biomed Biotechnol.* **2006**, *71*,659.
15. Check, E. *Nature.* **2003**, *423*,573–574.

16. Felgner, P.L.; Gadek, T.R.; Holm, M.; *et al. Proc. Natl. Acad. Sci. USA.* **1987**, *84*,7413–7417.

17. Andersen, M.O.; Howard, K.A.; Paludan, S.R.; Besenbacher, F.; Kjems. *Biomaterials.* **2008**,506–512.

18. Beh, C.W.; Seow, W.Y.; Wang, Y.; *et al. Biomacromolecules.* **2009**,*10*,41–48.

19. Breunig, M.; Hozsa, C.; Lungwitz, U.; Watanabe, K.; Umeda, I.; Kato, H.; Geopferich, A. *J. Control Release.* **2008**,*130*,57–63.

20. Crombez, L.; Aldrian-Herrada, G.; Konate, K.; et al. *Mol. Ther.* **2009**,*17*,95–103.

21. Green, J.J.; Langer, R.; Anderson, D.G. *Acc. Chem. Res.* **2008**, *41*,749–759.

22. Kraja, I.; Bing, R.; Hiwatashi, N.; *et al*. *The Laryngoscope.* **2016.** 1-7.

23. Karmali, P.P. and Chaudhuri, A. *Medicinal research reviews.* **2007**, *27*,696-722.

24. Semple, S.C.; Akinc, A.; Chen, J.; *et al. Nature biotechnology.* **2010**, *28*,172-176.

25. Love, K.T.; Mahon, K.P.; Levins, C.G.; et al. *Proc. Natl. Acad. Sci. USA.* **2010**, *107*,1864-1869.

26. Allen, J. *Current opinion in otolaryngology & head and neck surgery.* **2010**,*18*,475-480.

27. Johns, M.M.; Garrett, C.G.; Hwang, J.; Ossoff, R.H.; Courey, M.S. *The Annals of otology, rhinology, and laryngology.* **2004**, *113*,597-601.

28. Martinez Arias, A.; Remacle, M.; Lawson, G.. *European archives of oto-rhino-laryngology.* **2010**, *267*,1409-1414.

29. Branski, R.C.; Bing, R.; Kraja, I.; Amin, M.R. *The Laryngoscope.* **2016**, *126*,1151-1156.

30. Paul, B.C.; Rafii, B.Y.; Gandonu, S.; Bing, R.; Amin, M.R.; Branski, R.C. *The Laryngoscope.* **2014**,*124*,2237–2231.
31. Lim, X.; Tateya, I.; Tateya, T.; Munoz-Del-Rio, A.; Bless, D.M. *The Annals of otology, rhinology, and laryngology.* **2006**, *115*,921-929.
32. Leask, A. and Abraham, D.J. *FASEB journal*. **2004**, *18*,816-827.
33. Border, W.A. and Noble, N.A. *The New England journal of medicine.* **1994**, *331*,1286-1292.
34. Branski, R.C.; Barbieri, S.S.; Weksler, B.B.; *et al. Ann Otol Rhinol Laryngol.* **2009**, *118*,218-226.
35. Akinc, A.; Goldberg, M.; Qin, J.; *et al. Mol. Ther.* **2009**,*17*,872–879.
36. Dalby, B.; Cates, S.; Harris, A.; *et al. Methods.* **2004**, *33*,95–103.
37. Murphy, J.E.; Uno,T.; Hamer, J.D.; Cohen, F.E.; Dwarki, V. Zuckerman, R.N. *Proc. Natl. Acad. Sci. USA*. **1998**,*95*,1517–1522.
38. Hacein-Bey-Abina, S.; Le Deist. F.; Carlier, F.; *et al. N. Engl. J. Med*. **2002**,*346*,1185–1193.
39. Roesler, J.; Brenner, S.; Bukovsky, A.A.; *et al. Blood*. **2002***,100*, 4381–4390.
40. Utku, Y.; Dehan, E.; Ouerfelli, O.; *et al. Molecular BioSystems*. **2006**, *2*,312-317.
41. Konca, Y.U.; Kirshenbaum, K.; Zuckermann, N.R. *Int. J. Nanomedicine.* **2014**,*10*,2271–2285
42. Schiffmacher, A.T. and Keefer, C.L. *In Vitro Cell Dev. Biol. Anim*. **2012**,*48*,403–406.
43. Flanders, K.C. *International journal of experimental pathology*. **2004**, *85*,47-64.
44. Massague, J. and Chen, Y.G. *Genes & development*. **2000**,*14*,627-644.

45. Ozbilgin, M.K. and Inan, S. *Clinical rheumatology*. **2003**, *22,*189-195.

46. Ma, L.J.; Yang, H.; Gaspert, A.; *et al. The American journal of pathology.* **2003**, *163*,1261-1273.

47. Jonsson, J.R.; Clouston, A.D.; Ando, Y.; *et al.Gastroenterology*. **2001**, *121*,148-155.

48. Ashcroft, G.S.; Yang, X.; Glick, A.B.; et al. *Nature cell biology.* **1999**, *1*,260-266.

49. Lee, J.W.; Tutela, J.P.; Zoumalan, R.A.; *et al. Arch. Otolaryngol. Head Neck Surg*. **2010**, *136*,714-719.

50. Bartlett, D.W. and Davis, M.E. *Biotechnology and bioengineering.* **2007**, *97*,909-921.

51. Bartlett, D.W. and Davis, M.E. *Nucleic acids research*. **2006**, *34*,322-333.

52. Whitehead, K.A.; Dorkin, J.A.; Vegas, J.A.; Chang, P.H.;Veiseh, O.; Matthews, J.; Fenton,O.S.; Zhang,Y.; Olejnik,K.T.; Yesilyurt, V.; Chen, D.; Barros,S.; Klebanov,B.; Novobrantseva,T.; Langer1, R.; Anderson, D.G. *Nature*. *Communications*, **2014**, *5*,4177.

53. Hiwatashi N, Benedict P, Dion Get al. Smad3 expression and regulation of fibroplasia in vocal fold injury Submitted.

54. Hollins, A.J.; Omidi, Y.; Benter, I.F.; Akhtar, S. *J. Drug Target*. **2007**, *15*,83-88.

55. Akhtar, S. and Benter, I. *Adv. Drug Deliv. Rev.* **2007**, *59*,164-182.

Chapter 4

Rapid Identification of Metal-Binding Peptoid Oligomers by X-ray Fluorescence Screening

4.1 Abstract

N-substituted glycine peptoid oligomers have recently attracted attention for their metal binding capabilities. Due to their efficient synthesis on solid phase, peptoids are well suited for generation of compound libraries, followed by screening for molecular recognition and other diverse functional attributes. Ideally, peptoids could be simultaneously screened for binding to a number of metal species. Here, we demonstrate the use of bench-top X-ray fluorescence instrumentation to screen rapidly, on solid support, a library of peptoid oligomers incorporating metal-binding moieties. A subset of the peptoid sequences exhibited significant metal binding capabilities, including a peptoid pentamer and a nonamer that were shown to selectively bind nickel. The binding capabilities were validated by colorimetric assay and by depletion of Ni^{2+} ion concentration from solution, establishing bench-top X-ray fluorescence as a rapid, practicable high-throughput screening technique for peptoid oligomers. This protocol will facilitate discovery of metallopeptoids with unique materials properties.

4.2 Introduction

Metallopeptides: Abundance, Importance, Function, and Application

Natural proteins spontaneously undergo extraordinarily complex and precise folding processes to carry out sophisticated biological functions. This folding is dictated partly by hydrogen bonding interactions formed by secondary amide groups in the protein polymer backbone. Chemical and biological activities are typically established by a range of functional groups comprised within the twenty canonical amino acid side

chains **(Figure 35)**. Nevertheless, this set of functional groups is limited, requiring many proteins to incorporate post-translational modifications or prosthetic groups to carry out their functions. It has been estimated that over half of all proteins are metalloproteins, and one-third of all proteins that have been characterized by X-ray crystallography contain a metal species.[1,2]

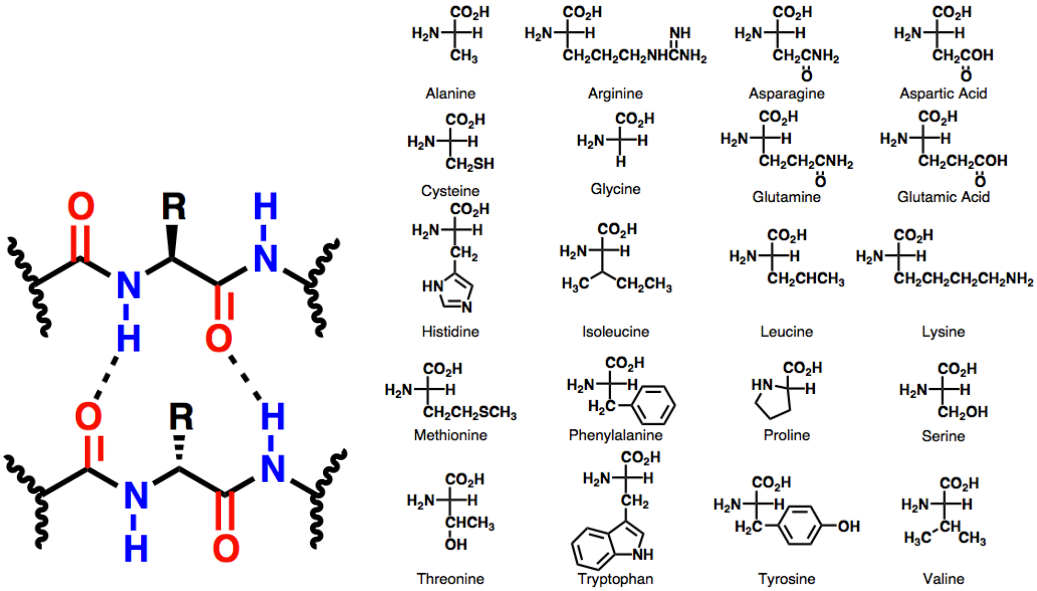

Figure 35. Backbone structure of a natural peptide. Comprised of repeating amide linkages and 20 unique side chain groups at the alpha carbon ("R"), the protein backbone includes both a hydrogen bond donor nitrogen, blue, and a hydrogen bond acceptor carbonyl oxygen, red. (Left). Structures of the 20 proteinogenic amino acid side chain groups. (Right).

Thus, metal species have been proven to be critical to catalytic, regulatory, transportation and storage functions of proteins. Once sequestered or complexed by proteins, metal ions have been associated with the functions of a variety of metalloproteins and enzymes.[3,4] The influence of the metal ion can readily be

appreciated in non-enzymatic metalloproteins. For example, the transcription factor TFIIIA is comprised of a zinc finger motif that stabilizes the protein's secondary structure to enable binding interactions with DNA, activating transcription growth factors and influencing cell generation and maturation. Additionally, when complexed to zinc, the protein is resistant to trypsin digestion **(Figure 36)**.[5,6]

More elaborate architectures and functions can be observed in metallo-enzymes. Metallo-enzyme active sites are often comprised of both endogenous (His, Asp, Ser, etc.) and exogenous (water, nitric oxide, hydroxide, porphyrins etc.) ligands to access solutions to difficult biological transformations.[1] Catalase, a tetramer housing four porphyrin heme groups, catalyzes the degradation of hydrogen peroxide to water and oxygen. It boasts one of the highest known turnover numbers, converting 40 million molecules of hydrogen peroxide per second.[7] Another exemplary metalloenzyme is carboxypeptidase A, utilizing a Zn critical cofactor in its active site. This metalloenzyme catalyzes protein hydrolysis at the C terminus. In the absence of enzyme, the background reaction rate has a half-life of more than seven years under ambient conditions. Once catalyzed in the presence of carboxypeptidase A, the hydrolysis transpires with rate increased by a factor in excess of 10^{11}.[8]

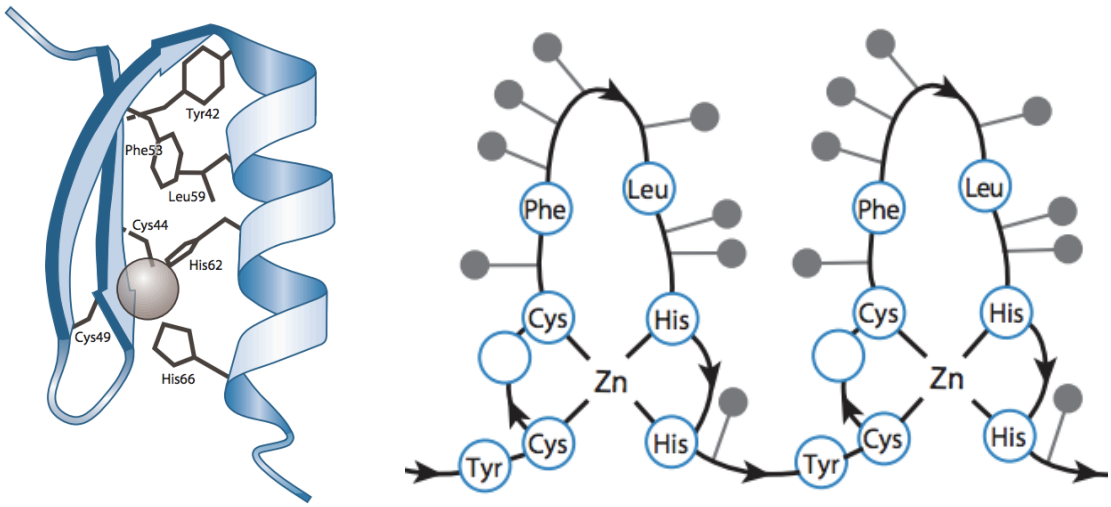

Figure 36. Cartoon depiction of a zinc finger protein showing Cys_2His_2 ligand field (Left). Representation of the folding pattern created by repeating zinc finger units. Gray dots signify amino acids that bind DNA (Right).[7]

Metal complexes have also been shown to critically assist in wound healing and collagen synthesis mechanisms. Divalent zinc participates in the cellular and wound repair processes by acting as an essential cofactor for cellular mitosis, migration, and maturation. Zinc binding proteins, such as metallothionins, which act as sequestration units for zinc, modulate the efficiency of many biomolecular and chemical events during the wound healing process, and upregulation of such metalloproteins to deliver these ions to the wound site often accelerates healing times.[9] Another relevant class of wound-healing biomolecules are matrix metalloproteinases (MMPs), which require a tightly bound zinc in its catalytic domain for function. MMPs are capable of degrading various Extra-Cellular Matrix constituents. During wound healing, MMPs are active in debriding and chemotaxis and also the remodeling stage, breaking down misaligned

and fibrous masses of collagenous scar tissue.[9-11] In addition to collagen degradation, collagen biosynthesis also relies on the chelation of a metal ion. The collagen-crosslinking activity of lysyl oxidase, a copper metalloenzyme, is responsible for the oxidation of lysine from the primary amine to the aldehyde functionality, enabling the creation of a covalent bridge between the fibrils and supporting fiber formation.[12]

An array of chemical tools are now being pursued to craft elaborate synthetic macromolecules incorporating metal ions and to study their functions.[13,14] Relevant to wound healing, metal-assisted collagen-like peptide assemblies can be crafted into hydrogels and other unique architectures for novel dressing materials.[15,16] Bio-based hydrogels have also benefitted from the addition of metal ions to control assembly, and have enriched these materials with additional wound healing benefits.[17,18] Ni^{2+} coordination to metal binding centers incorporated into collagen-like sequences induced gelation of the peptides. Such Collagen-Like Peptides were charged with growth factor payloads and have been exploited to enhance cell proliferation and influence cell morphology in a time-controlled manner.[19]

Additionally, singular metal ions have been demonstrated to improve wound healing outcomes. Endogenous zinc, for example, is a essential cofactor for enzymes critical to the body's natural healing process, and there is an extensive history in the pharmacopeia for zinc as a antimicrobial species.[10,21-24] Formulations containing Zn^{2+} improve wound healing outcomes when applied topically.[20,25] Nanoparticulate silver ions have a heavily documented use as non-toxic antibacterial agents,[25] and recent preparations of bioploymer wound dressings exploit this quality. While the silver ions do not engender dressings with additional structural stability, their presence reduces

microbial infection. Additionally they have been shown to increase antioxidant activity, and elastase, matrix metalloprotease (MMP), and pro-inflammatory cytokine binding affinity relative to dressing preparations containing only native sodium and calcium ions.[26] A 2009 study using cellulose-based dressings incorporating Ag^{+} was effective against C*andida albicans*, *Micrococcus luteu, Pseudomonas putida*, and *Escherichia coli*. Inhibition of all microbial growth above 0.0035 Ag w/v % was reported, a concentration which exhibited no cytotoxicity in human fibroblasts.[27]

Simple peptide complexes, such as the copper chelated tri-peptide sequence Cu-GHK, have been extensively used in the cosmetics community for anti-aging formulations since its discovery and characterization in the 1970's. There are currently more than a dozen companies worldwide with at least 40 products featuring copper-tripeptide complexes as their main performance ingredient.[28] Cu-GHK is cleaved from the damaged tissue by proteolysis at the time of injury, stimulating cellular regulatory compounds, thus healing skin and injured issues.[29] Its proficiency in clinical trials as an active peptide complex in cosmetic preparations of foundations, concealers, and creams, reflect its biological function. Common among all trials using Cu-GHK as a skin conditioning agent to treat photo damage, pigmentation, and general aging appearances, improvements in skin elasticity and clarity within 1-2 weeks of treatment were visible.[30] Consistent treatment over several months resulted in increased skin density and thickness, reduction of fine lines and deeper wrinkles, and evened balanced tone. [30,31] In clinical trials, 70% of subjects exhibited increased procollagen synthesis after one month of topical application.[30] While the justification for research into metal chelating materials exists and lies in the obvious potential to affect both wound healing

outcomes and more cosmetic concerns, the analysis and discovery of these valuable complexes remains challenging and expensive.[32,33]

High Throughput Screening of Peptides and Peptoids

Researchers are now beginning to create synthetic molecules that can mimic protein structure and function, and have developed an array of chemical tools to craft elaborate macromolecules and study their functions. Foldamers, including both synthetic and semi-synthetic oligomers, were initially evaluated as part of a broad effort to understand the fundamental requirements for biopolymer folding and function.[34] However, by extension, the exploration of new folding properties and well-defined structures is leading to novel molecular constructs for applications in materials and biomedical sciences.[34-47]

The precise display of chemical functional groups along the oligomer backbone can influence the crystallization outcome of inorganic species and can also be used to establish selective catalysis.[47] Cyclic peptoids with associated sodium ions were used as a phase transfer catalyst for S_N2 reactions between NaSCN or KSCN with *p*-nitrobenzyl bromide in a methylene chloride/water mixture.[48]

The coordination of metal species to an oligomer framework, as demonstrated with peptides, may confer alternative structures with additional functions. [39-47] It has been established that the secondary structure of peptoids can be induced and modulated upon metal binding.[39-41] Increases in the polyproline I helical character of two peptoid oliogmers once bound to divalent Cu or Co was reported in 2009 by Maayan and colleagues. (**Figure 37**).[40] Maayan's contributions to the study of metallopeptoids

continue to advance the field, discovering new peptide mimics and examining the relationship between such biomimetic oligomers and metal ions and metal nanoparticles.[47b-47e]

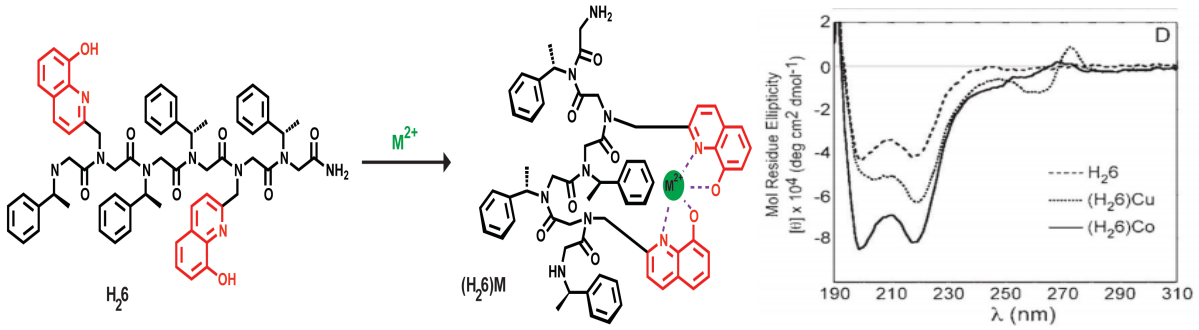

Figure 37. Circular dichroism monitors peptoid-metal binding to Cu and Co in solution. Peptoid hexamer **$H_2$6** bearing quinoline-type binding ligands induce conformational ordering upon complexation with Cu or Co (Left). CD spectra demonstrate enhanced PPI helicity upon metal binding (Right).[40]

Zuckermann also explored the formation of peptoid helix bundles through coordination of Zn^{2+} to imidazole and thiol sidechains.[41] Moreover, work from the Izzo group has been devoted entirely to the construction of cyclic peptoids and metal binding. Notably, they reported an X-ray crystal structure of a supramolecular assembly of

proline-substituted cyclic hexamers assembled through Na^+ coordination. (**Figure 38**).[37]

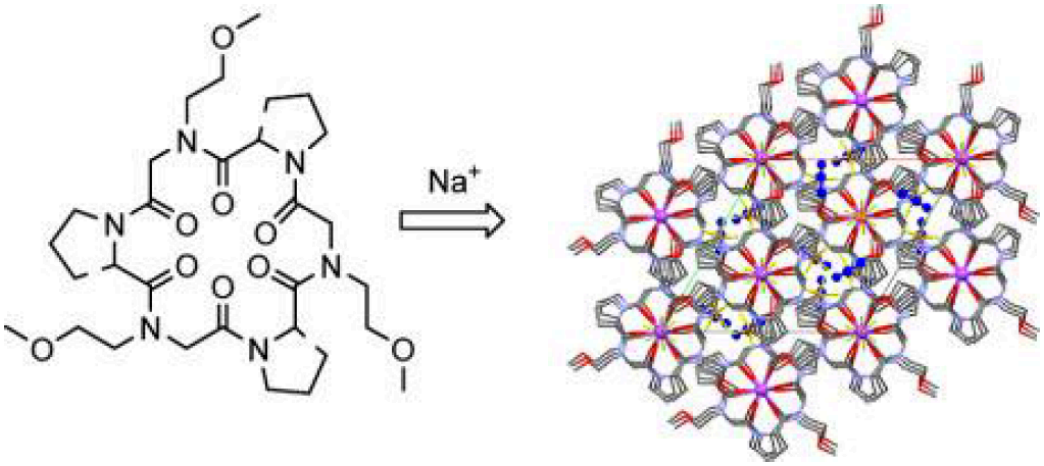

Figure 38. X-ray crystallography of peptoid-metal association**.** X-ray crystal structure of a proline-substituted cyclic hexamer forming a large supramolecular assembly upon exposure to Na^+. Pink spheres represent Na^+, red represents oxygen, and yellow and blue signify the counter ion PF_6^{-1}. [39]

More recently, a conformationally ordered peptoid macrocycle was shown to coordinate Gd^{3+}, establishing favorable magnetic resonance relaxometric properties.[43] Additionally, sulfhydryl-rich peptoids can be applied to address pollution and wastewater concerns through selective depletion of chromium (VI) from environmental aqueous solution. (**Figure 39**).[45] Application of similar screening approaches from the Francis lab have discovered peptoid sequences which can remove toxic uranyl, mecury, and cadmium ions as well.[49]

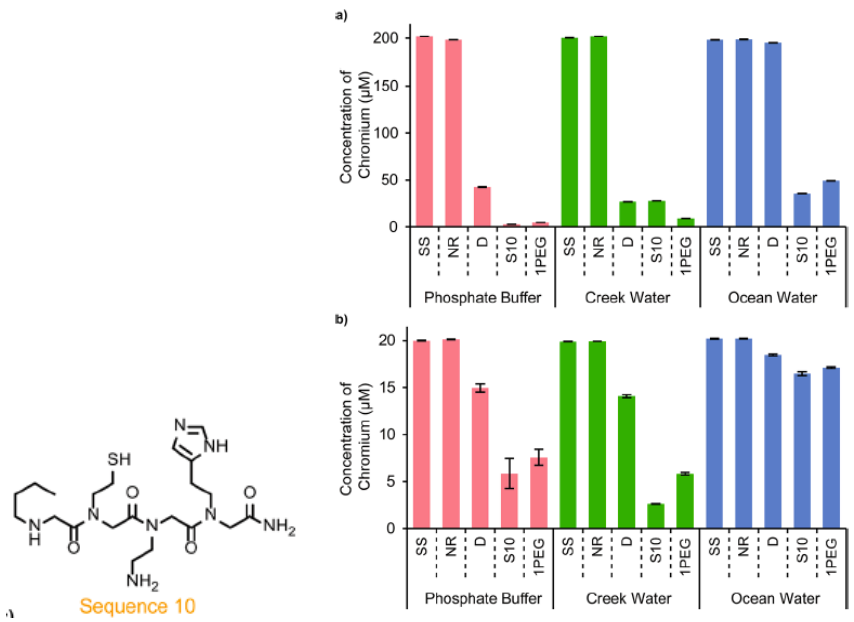

Figure 39. ICP-MS analysis of chromium sequestration by peptoid oligomers. Data from the Francis group demonstrating the ability of resin-bound **Sequence 10** (Left) to deplete aqueous solutions of Cr from a variety of environmental sources (Right). SS indicates the starting solution, NR indicates a solution that was not exposed to any resins or chemical agents, D indicates solution exposure to Dowex ionic exchange resin, S10 indicates solution exposure to **Sequence 10** resin beads, and **1PEG** indicates solution exposure to a PEG-functionalized resin. [45]

Given their simple, modular synthesis, range of chemical diversity that can be appended to the backbone, and stability towards most chemical transformations, peptoids are optimal candidates for high throughput screening. Created initially in the late 1980's to address challenges in small molecule library synthesis for drug discovery, peptoids have excelled in the area of large combinatorial library generation and high throughput screening.[49-52] In 1994, the Zuckermann group reported peptoid trimers that

antagonize protein receptors, which were among the first reports to screen large combinatorial libraries on-resin to identify oligomers targeting proteins of biomedical importance.[47a] Ongoing challenges associated with discovering functional peptoids tend to involve developing reliable screens for desired activity, as the synthesis of peptoid oligomer libraries is generally efficient and reliable.

Following those early efforts from the Zuckermann group, peptoid screening protocols have been elaborated in size and complexity to more advanced biomedical and materials applications.[53] Currently, screening can be conducted on very large peptoid oligomer library populations (with some exceeding 250,000 compounds), and the therapeutic potential of peptoid sequences identified from screening efforts has been verified through both *in vitro* and *in vivo* studies. [50,52,54,55] Notably, the Kodadek group identified peptoids capable of antagonizing the vascular endothelial growth factor receptor 2 (VEGFR2). Using a large combinatorial peptoid library, they utilized a high throughput screening technique based on the binding of fluorescent quantum dot stained cells over-expressing VEGFR2 to a hit peptoid sequence.[54] Additionally, the development of split and pool synthesis techniques for generating diverse one bead one compound (OBOC) libraries, followed by sequence deconvolution of hit compounds by mass spectrometry conducted in the Zuckermann and Kodadek groups has enabled high throughput peptoid screening to become an effective discovery technique.[56-59]

Ideally, we should have the ability to screen for metal-binding interactions with peptoids in the same high throughput manner that we screen peptoids for other functions. Current screening methods for peptoid-metal complexation are designed from the same assays as screening for peptide-metal interactions. Typically, a colorimetric

based assay is run after exposure of the metal to the solid-supported oligomer, and the binding event is witnessed by a color change of the resin.[45,59,60]

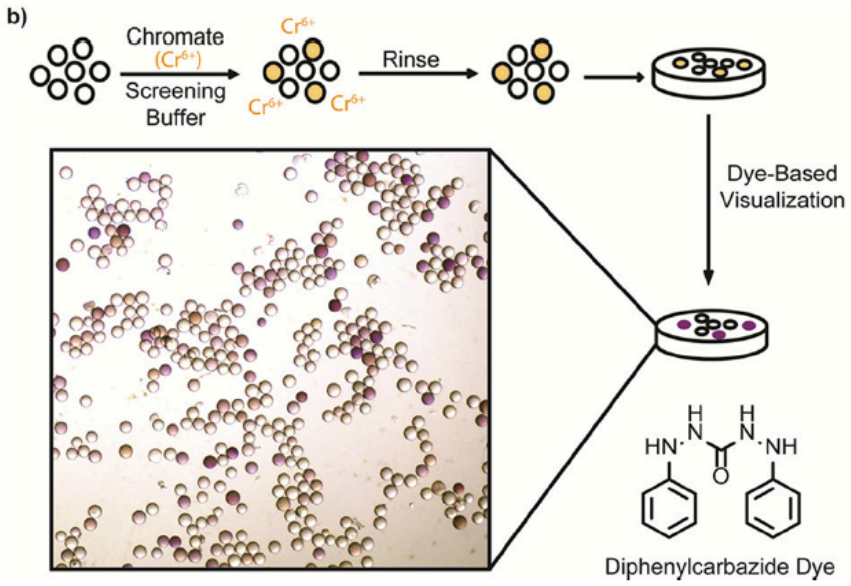

Figure 40. Colorimetric screening for Cr-peptoid binding by Francis group. The resin-supported peptoid library (white circles) was exposed to a solution containing chromium ions. The resin was washed and then exposed to a diphenylcarbazide dye that competitively complexes with chromium causing a change in the resin color. The darkest, most colored beads are then selected as 'hits'.[45]

This approach was popular in the Jacobsen group when identifying Ni- as well as Pt-, Sn-, Pb-, and Cu-binding peptides, and was continued in the Francis group through the screening for heavy metal sequestration by peptoid tetramers.[45,49,59,60] **(Figure 40)** However, these assays are not applicable to all metal species and are usually limited to

the analysis of one metal per screen, impeding the rapid discovery of selective complexation of metal species in the presence of competitors.

Micro X-ray Fluorescence and Screening for Metal Complexation

Recent advances make X-ray fluorescence (XRF) an attractive technology for assaying the ability of peptoids to bind specific metal ions. X-ray fluorescence (XRF) is a versatile technique, commonly used in materials science for quantifying the elemental composition of samples. For XRF, samples are illuminated with an x-ray source with photons sufficiently energetic to eject an electron from a 1*s* or 2*s* orbital.[61] Subsequent electron transitions that fill the resulting vacancy emit photons with energies in the x-ray region of the spectrum (**Figure 41**). The XRF emission lines of each chemical element are distinct and can be quantified simultaneously, allowing unambiguous analysis of complexation or removal of a chemical species from a host within seconds.[61,62]

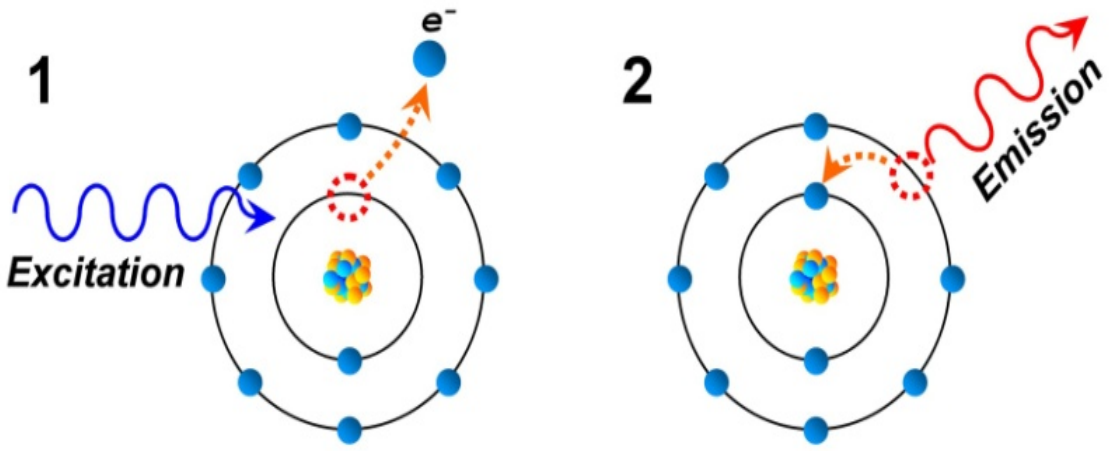

Figure 41. Illustration of the principles of X-ray fluorescence analysis. First, an atomic sample is irradiated by a source with sufficient energy to remove an electron from either the 1*s* or 2*s* orbital (Panel 1). Atoms then undergo electronic transitions to replace the ejected electron, and subsequently release photons characteristic for the element and parent orbital. These distinct emissions allow unambiguous characterization of the sample at an atomic level.[63]

Because XRF electron transitions involve inner electron orbitals, XRF is independent of the chemical form of the elements measured. When quantifying binding events, XRF is simply dependent on the presence and quantity of the atom of interest, and is independent of chemical form (*e.g.*, oxidation state, ligands) or type of binding (*e.g.,* covalent, noncovalent). In addition, XRF eliminates many matrix effects, as complex solutions and background are largely transparent for photons in this energy range. (**See Figure 42 for schematic representation of XRF**). This technique has previously been

successfully implemented for identifying capture of metal ions from a solution of mixed metal species using resin-bound peptides.[64]

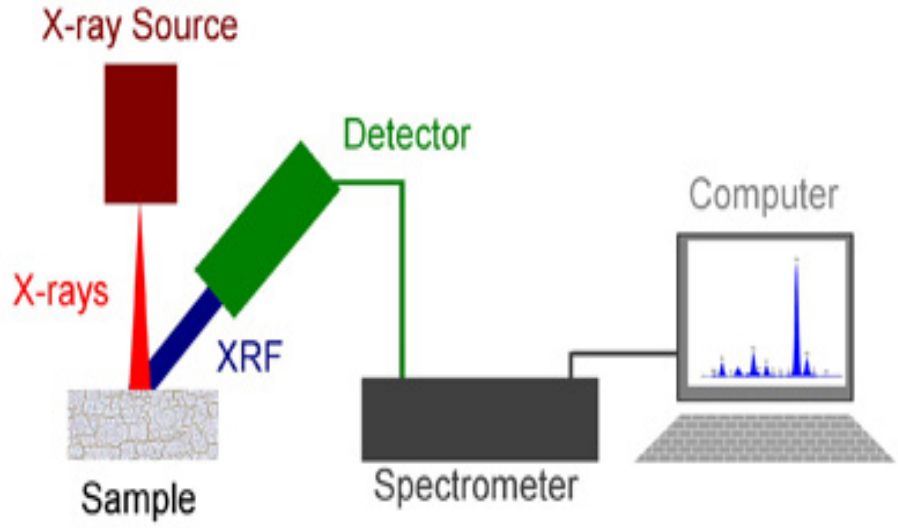

Figure 41. Schematic representation of XRF analysis. First, the sample is irradiated by an x-ray source and that sample emits photon energy. The photon energy is collected in the detector and transformed from an analogue electrical signal to digital information in the spectrophotometer. The raw data is then sent to the computer for processing .[65]

The primary goal of this research is to explore binding interactions between different peptoid oligomer sequences and metal species and to discover efficient methods of detecting these binding events. The advantage of conducting the detection as an on-resin high throughput screen over thousands of potential peptoid binders lies in the significantly reduced time, materials, and effort required to synthesize, purify, and thoroughly analyze sequences for the desired activity. As previously discussed, metal complexation to the peptoid scaffold could permit discovery of previously inaccessible structures and/or functions, especially due to the large measure of chemical diversity

that is available through the side chain functional groups appended during solid phase synthesis.[66] Moreover, because of the tertiary amide linkages, peptoids are highly resistant to proteolysis.[67], and therefore may be more suitable candidates compared to peptides for some biomedical applications.[68,69] Thus, peptoid metal complexes have great potential in the fields of medical and cosmecuetical materials, green chemistry, metal remediation, and catalysis.

Here, we demonstrate the use of a new bench-top XRF high-throughput screening process (XRpro MXRF) for quantifying the metal binding characteristics of peptoid libraries (**Figure 43**). MXRF analysis can be carried out with nanogram-sized samples, and has detection limits between 20 and 100 pmol, enabling analysis of "one-bead one-compound" libraries of oligomers immobilized on solid support for selective metal binding.[61] The analysis is non-destructive and is conducted in seconds per sample, allowing for the screening of large libraries in short overall periods. We employ MXRF to screen a small library of peptoid oligomers on resin for metal binding interactions and identify peptoid sequences that preferentially bind Ni^{2+} from a solution of competing divalent transition metal species.

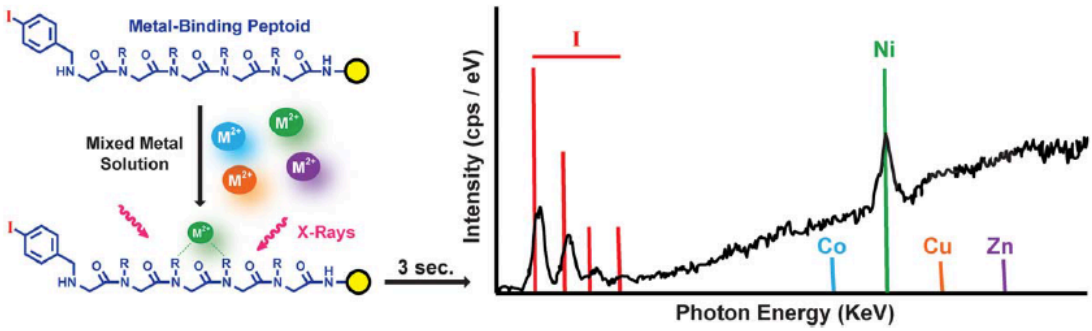

Figure 43. Schematic representation of screening OBOC peptoid libraries for metal binding using X-ray Fluorescence. Following incubation in a solution of mixed divalent metal species, library members are subjected to 3 seconds of X-ray irradiation, and spectra are acquired. The iodine signal confirms the presence of peptoid on resin, and binders are identified by the distinct atomic emission lines presented by each metal species. Here, the large nickel signal above the background indicates a nickel-binding interaction.

4.3 Results and Discussion

Design and Synthesis of the Peptoid Library:

We designed a family of peptoid sequences bearing side chain functional groups that would enable metal complexation. The peptoid sequences included *N*-substituted glycine monomers that emulate proteinogenic side chains such as histidine, glutamic acid, tryptophan, serine, and tyrosine. We also took advantage of the extensive chemical diversity offered by peptoid solid phase synthesis to include non-proteinogenic side chain groups, such as pyridylalanine (**Figure 44A)**. In addition, we evaluated a

negative control peptoid sequence, “ConC”, composed solely of alkyl side chains, and thus not anticipated to exhibit significant inherent metal-binding capabilities. Unmodified Tentagel resin beads, referred to as “ConTG”, were also subjected to analysis of metal binding.

To control for variations in the bead size and the amount of peptoid on single-bead samples, we incorporated a “reporter” monomer displaying an iodobenzyl group in the oligomer sequence designs at either the N- or C-terminus (**Figure 44A**). Iodine produces XRF emission lines similar in energy to those of metals of interest (Cu, Co, Ni, and Zn), but sufficiently distinct in the spectrum so as not to interfere with their emission lines (**See Appendix 2.1).** The presence and intensity of an iodine XRF signal could therefore be used to confirm the presence of the peptoid oligomers on resin and to enable ratiometric analysis of the metal to iodine signal. This ratio enables comparative evaluation of metal binding by different peptoid sequences.

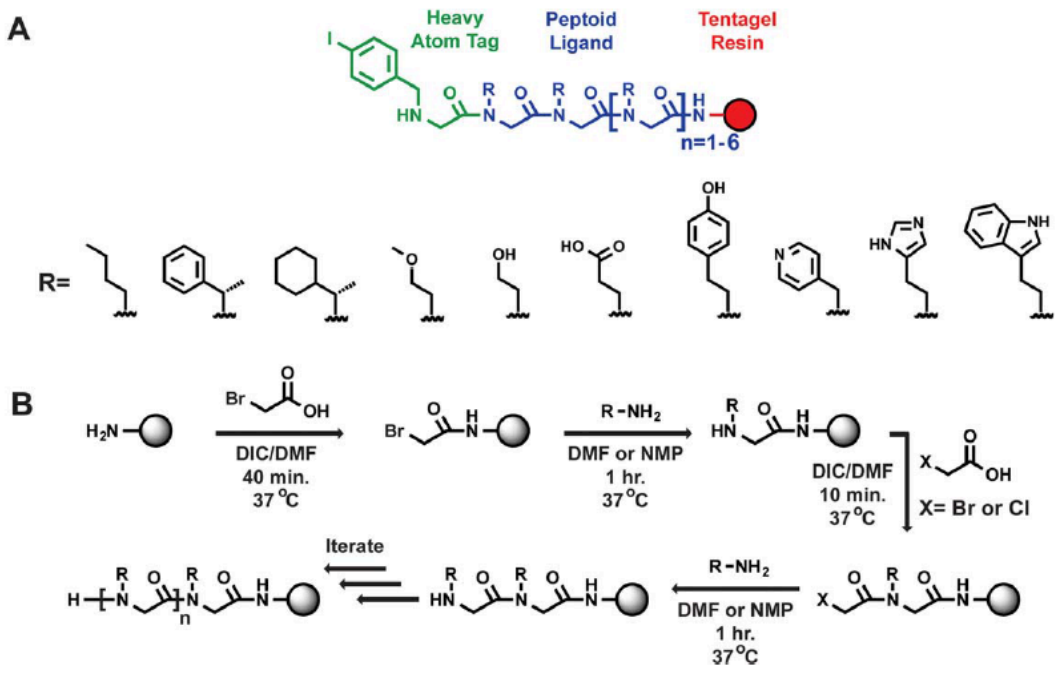

Figure 44. (A) Peptoid oligomer library member. The products include the Tentagel resin incorporating a PEG linker (red), the peptoid oligomer with diverse submonomers (blue), and a heavy atom tag, 4-iodobenzylamine, which was positioned at either the N or C terminus (green). The diversity of peptoid side chain groups incorporated into the library is shown below. (B) Synthesis of peptoid library on Tentagel resin. Iterated steps include either bromoacetylation or chloroacetylation using DIC as a coupling agent, followed by displacement with a primary amine. Grey spheres represent the Tentagel resin bead.

Following the design, a library of 35 peptoid sequences (**See Appendix 2.2**) was synthesized on NovaSyn TG amino resin HL according to a modified "submonomer" synthesis approach[69,70] at >80% purity (as determined by relative peak integration using RP-HPLC) (**Figure 44B, See Appendix 2.3)**. This synthesis protocol entails an iteration

of sequential haloacetylation and nucleophilic displacement by various primary amines. Suitably protected amine synthons were used to introduce potentially cross-reactive side chain functionalities. Oligomer synthesis on NovaSyn TG amino resin HL allowed for deprotection to liberate the side chain functional groups without cleavage of the oligomers from solid support.

XRF Analysis:

MXRF® analysis was conducted on library resin beads positioned within a 96 well plate. Resin-bound library members and controls were first affixed to XRpro® analytical array plate seals (XRpro Corp, Cambridge MA), using 96 well plate seals positioning four single-bead samples per well. Two replicate wells were tested for each peptoid sequence. Plate seals were adhered to standard 96 well plates containing a solution of four biologically relevant divalent metal species (Cu^{2+}, Co^{2+}, Ni^{2+}, Zn^{2+}) in aqueous buffer (pH 7) at a concentration of 500 μM/metal. The sealed 96 well plate was inverted so that the solution contacted the resin-bound library, and each peptoid oligomer was incubated separately in the metal mixture prior to MXRF analysis. Following incubation, 10 spectra were acquired for each resin bead using an XRpro® bench-top XRF instrument (XRpro Corp., Cambridge MA), providing 80 fluorescence spectra per sequence. XRF analysis was conducted through the thin plastic of the XRpro® analytical array plate seal without removing either the plate seal from the 96 well plate or the metal solution from the wells. Background readings were obtained from a position within each well that did not contain a peptoid sample bead, to enable background subtraction of the free metal solution present in each well (10 spectra per well) from the library spectra. This technique was particularly convenient, as it did not require removal of the beads

from solution or rinsing protocols. Notably, these 3,600 X-ray fluorescence readings were obtained and recorded in approximately three hours, an analysis rate of 28,800 readings/day. The experiments were conducted in triplicate against all library members to yield metal binding profiles for each of the oligomers.

Metal-binding peptoid sequences were identified by analyzing the XRF intensity from each of the metals against the signal of the iodine center incorporated within each peptoid oligomer (Metal:Iodine, M:I) (**See Appendix 2**). These ratios do not indicate precise stoichiometries, and thus, a 1:1 Metal:Iodine signal does not necessarily correspond to one metal atom bound per peptoid oligomer molecule. However, changes in the ratio for a specific metal can be quantitatively interpreted. For example, a 2:1 Cr:I ratio indicates a 2-fold higher amount of Cr bound to the peptoid than a 1:1 Cr:I ratio. Therefore, larger M:I ratios indicate better binders, relative to other sequences, and greater differences in the magnitude of M:I among different metals indicate enhanced selectivity for the given metal by the individual sequence. We observed some run-to-run variations in M:I fluorescence signal intensity, but overall binding patterns based on relative M:I values for different metal species could be interpreted (**See Appendix 2.4**).

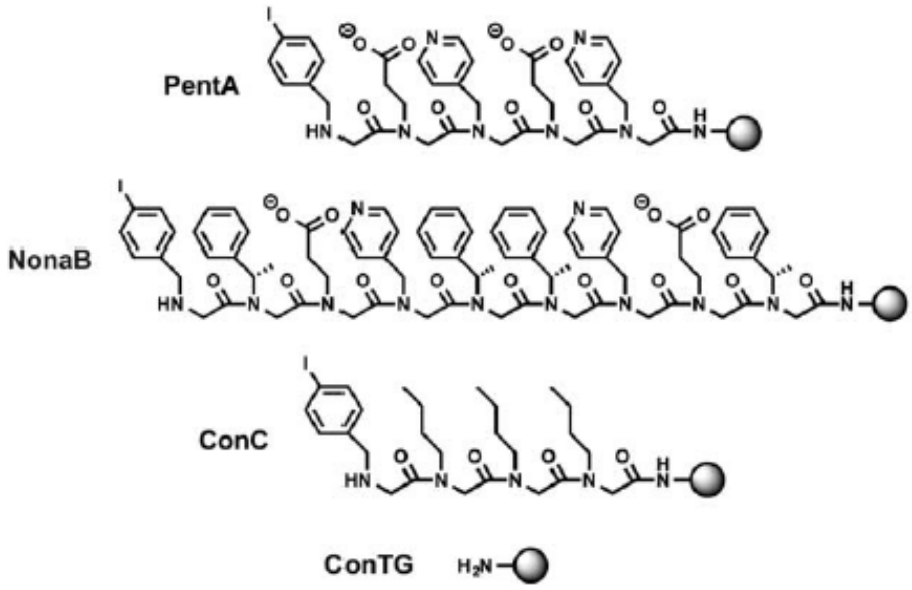

Figure 45. Chemical structures of peptoid hit compounds identified as nickel binders by Micro X-ray Fluorescence: **PentA** and **NonaB**. Controls used in the study: **ConC** and unmodified Tentagel Beads (**ConTG**).

A subset of peptoids from the library displayed binding capability for most of the metals present. Two peptoid sequences, a pentamer, **PentA**, and a nonamer, **NonaB**, (**Figure 45)** containing adjacently paired pyridine and carboxylic acid functionalities were found to preferentially bind nickel relative to the other three metals. (**Figure** 4**6, See *X-ray Fluorescence Screening of Peptoid Oligmers that Bind Copper, Zinc, and Nickel***) In contrast, the two controls (**ConC and ConTG)** presented negligible binding activity with all four metals. Notably, one sequence (**NonaD**), which similarly incorporated pyridine and carboxylic acid side chain groups within a different and non-adjacent sequence motif, did not exhibit the same strong selectivity for nickel or the large M:I values as observed for **PentA** and **NonaB. (See *X-ray Fluorescence Screening of***

Peptoid Oligmers that Bind Copper, Zinc, and Nickel) These results indicate that both monomer composition and sequence are important for establishing suitable metal binding environments, and also suggest that the proper positioning of multiple metal-complexing side chain types may be required to enable selective binding.

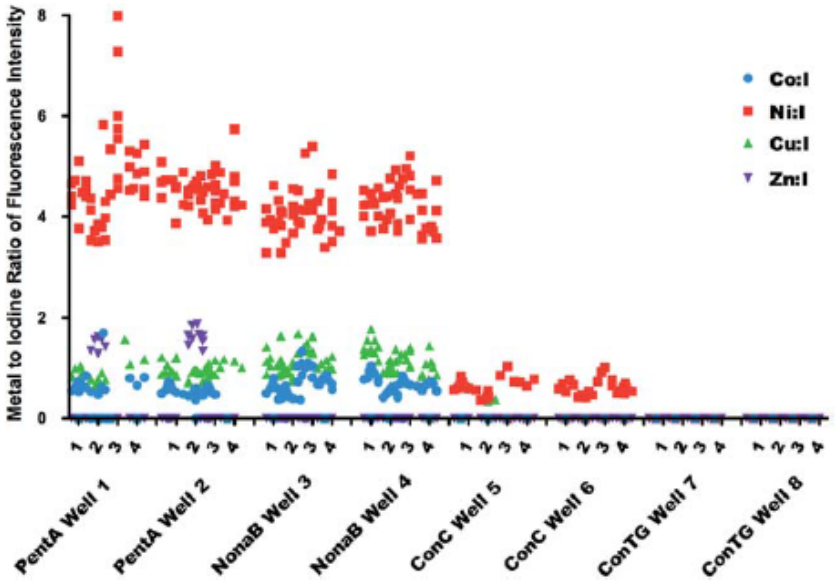

Figure 46. Results from the x-ray fluorescence metal-binding screen represented by Metal to Iodine Ratios (M:I) for peptoid sequences **PentA** and **NonaB** and for controls **ConC** and **ConTG** in the presence of four metal species of interest. To demonstrate reproducibility, the designation (1-4) following the sequence and well number denotes different beads bearing identical peptoid sequences. Each sequence was evaluated in wells in the multi-well plate. The pentamer **PentA** and the nonamer **NonaB** are shown to be capable of selectively complexing Ni.

Metal Complexation with Liberated Sequences:

Considering the strong response of resin-bound **PentA** and **NonaB** to Ni^{2+}, we anticipated that the liberated oligomers in free solution would participate in nickel complexation upon cleavage from resin. **PentA**, **NonaB**, and **ConC** were re-synthesized on Rink Amide resin, cleaved from solid support, and purified to >90% via RP-HPLC. The identity of the sequences was verified by ESI-MS (**See Appendix 2**). However, binding events between Ni^{2+} and **PentA** or **NonaB** could not be detected in solution (data not shown). Although the chemical composition of the resin-bound and liberated peptoid oligomers bearing C-terminal amides are distinct, the origin of variation in metal binding characteristics by immobilized versus free peptoids is a focus of continuing investigation.

4.2.3.4 Ni-Dimethylglyoxime Colorimetric Assay:

In order to validate the ability of resin-bound **PentA** and **NonaB** to bind Ni(II), a colorimetric on-resin assay with dimethylglyoxime, a competitive chelator for Ni(II), was performed.[45,59,] In this assay, Ni(II) binding is characterized by a color change to red within the bead matrix. As controls, **ConC** and unmodified Tentagel Beads (**ConTG**) were also analyzed. All resin beads were affixed to Tacky Dot™ slides and incubated in standard 96 well plates containing 3 mL of aqueous buffered 500 μM $Ni(NO_3)_2$ for three hours. Each individual sequence was plated in 12 separate wells. Prior to imaging, the beads were washed with buffer, then exposed to a 1% dimethylglyoxime solution. Relative to **ConC** and **ConTG**, which displayed no color change, **PentA** and **NonaB**

appeared bright red (**Figure 47**). These results confirm that **PentA** and **NonaB** bind Ni(II).

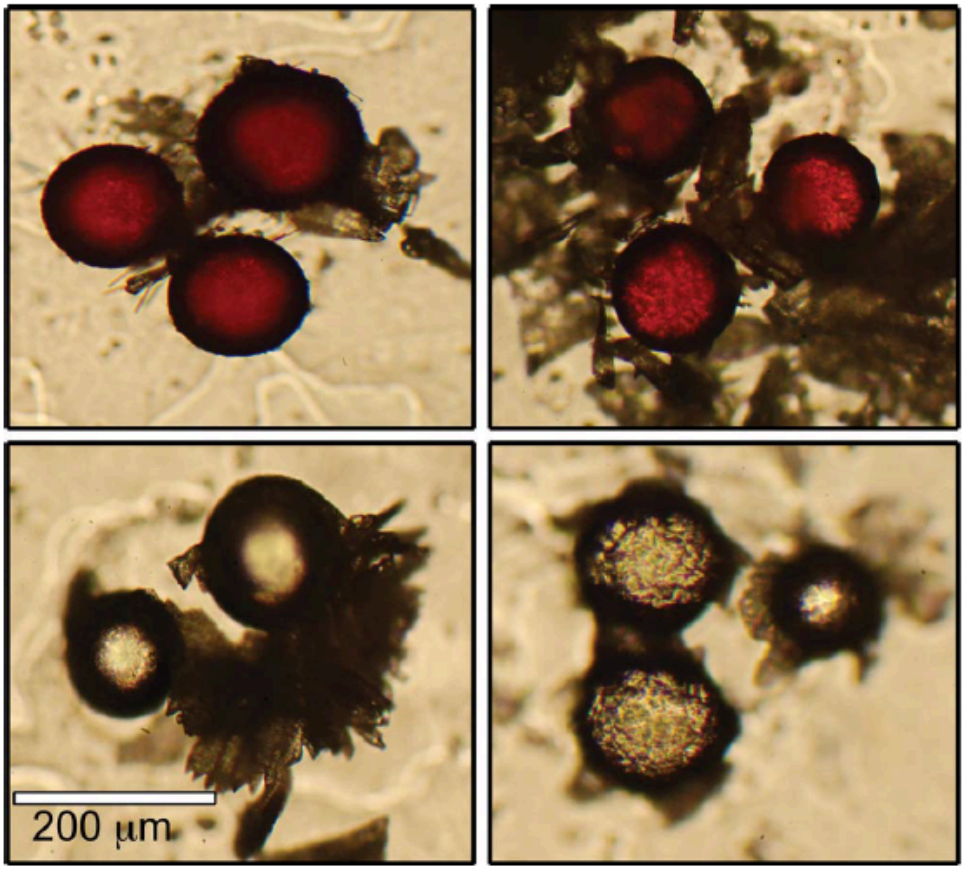

Figure 47. Microscope images of peptoids immobilized on TentaGel resin beads after incubation in nickel solution and exposure to 1% dimethylglyoxime solution. Clockwise from Left: **PentA**, **NonaB**, **ConTG**, **ConC**.

Nickel Depletion Assay:

Encouraged by the verification of nickel binding by colorimetric analysis, we sought to quantify the hit oligomers' ability to sequester Ni^{2+} from aqueous solution. Each of the resin-bound oligomers and controls was incubated in two different concentrations of buffered nickel solutions at pH 7. The solutions were then filtered and tested for nickel concentration, relative to the nickel stock solution.

When exposed to 10 mL of a nickel solution at an initial concentration of 24.1 μM ± 1.8 (0.241 μmol), both **PentA** or **NonaB** (1.95 μmol of each peptoid immobilized on resin, based on loading levels) achieved a dramatic reduction in the nickel concentration (**Figure 48**). Following incubation for 3 hours, the concentration of nickel remaining in solution was less than 0.97 μM ± 0.2, a value that was near the detection limit of the ICP-MS analysis. This corresponds to an average complexation of 96.0% of the initial Ni^{2+}, after incubation in the presence of **PentA.** Likewise, **NonaB** removed an average of 95.5% of the nickel, leaving 1.1 μM ± 0.3 of free Ni^{2+} in solution. In sharp contrast, neither **ConC** nor **ConTG** exhibited comparable capacity to deplete nickel from the same 24 μM starting solution, and their nickel depletion averaged 16.7% and 13.4%, respectively. This behavior is expected for control species lacking suitable functional groups to promote metal complexation. These findings are in agreement with those obtained from the MXRF experiments, indicating that the sequences' affinity for nickel follows the order: **PentA**, **NonaB**>>**ConC**>**ConTG**. An additional depletion assay conducted at ten times the initial concentration of nickel (222.5 μM ± 22.8) yielded similar affinity patterns. (**Figure 49**).

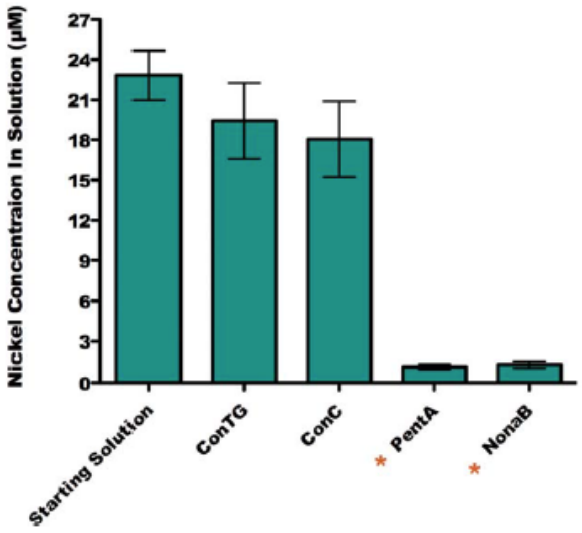

Figure 48. Chart of the nickel concentration in solution (μM) before and after exposure to resin beads. From Left: Ni concentration of the starting solution; Ni concentration after exposure to control, **ConTG**; control, **ConC**; pentamer, **PentA**; nonamer, **NonaB**. Error bars represent the standard deviation of the experimental results conducted in triplicate. ***** Indicates concentrations at the ICP-MS detection limit.

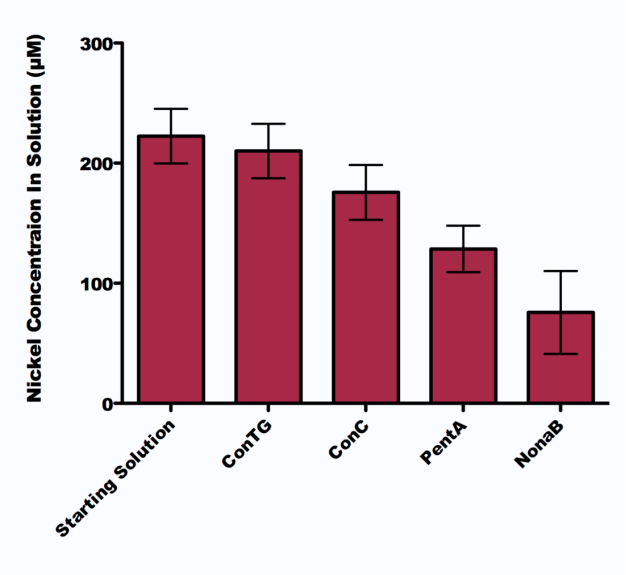

Figure 49. Chart of the nickel concentration in solution (μM) before and after exposure to resin beads (5 mg, 1.95 μmol). From Left: Ni^{2+} concentration of the starting solution before exposure to any beads; Ni^{2+} concentration after exposure to control, **ConTG**; control, **ConC**; MXRF® hit, **PentA**; MXRF® hit **NonaB**. Error bars represent the standard deviation of the experimental results conducted in triplicate.

X-ray Fluorescence Screening of Peptoid Oligmers that Bind Copper, Zinc, and Nickel

In addition to the proficient nickel binding peptoids, **PentA** and **NonaB**, which were identified by high throughput x-ray fluorescence analysis, results obtained for the other 33 sequences provide valuable information regarding unique peptoid sequences with affinity for different metal species as well as those that do not possess affinity for any of the metals present in the screen. Furthermore, analysis of sequences similar to **PentA** and **NonaB** offer insight into the presence and placement of the pyridyl and carboxylic acid side chain pairs that are critical for selective nickel binding.

The following discussion of the XRF results from the other library members offers further affirmation that XRF is a valid and useful screening tool and defines some properties that endow peptoids with a strong nickel-binding capability. While **PentA** and **NonaB** yielded the strongest and most selective response for any of the metals screened, many of the other peptoids in the library exhibited capability to bind at least one out of the four metal ions present in the assay. However, several peptoids (other than the negative control **ConC**) did not demonstrate any evidence for metal complexation. **Figure 50** depicts two sequences, **83B** and **85E**, with their respective M:I charts over three separate assays of the competitive metal binding study. Sequence **83B** is a pentamer and contains four side-chains capable of metal binding: three imidazole and one pyridyl side-chain. Two out of the three experiments indicate this peptoid is a zinc binder, typical of sequences with multiple imidazole residues,[71, 72] but in all cases, this sequence displays copper binding capability and is more selective for copper over nickel and cobalt (**Figure 50, top**). Additionally, in two out of the three experiments, the sequence is selective for copper over zinc, lending some support to the conclusion that this peptoid is a selective copper binder. Further experiments would be required to validate its affinity for copper over zinc.

In contrast to **83B**, **85E** yielded very low M:I ratios (less than 1) for all metals over all three trials of the screen (**Figure 50, bottom**). This is not surprising as this tetramer is functionalized with two ether and one phenolic side-chains, neither of which is known for its ability to tightly and effectively complex transition metal ions on its own, especially at a pH below the phenolic hydroxide's pka (pka ~9).[73] This sequence, and others

sequence in the library that yielded this type of binding behavior, were considered to be non-binding sequences".

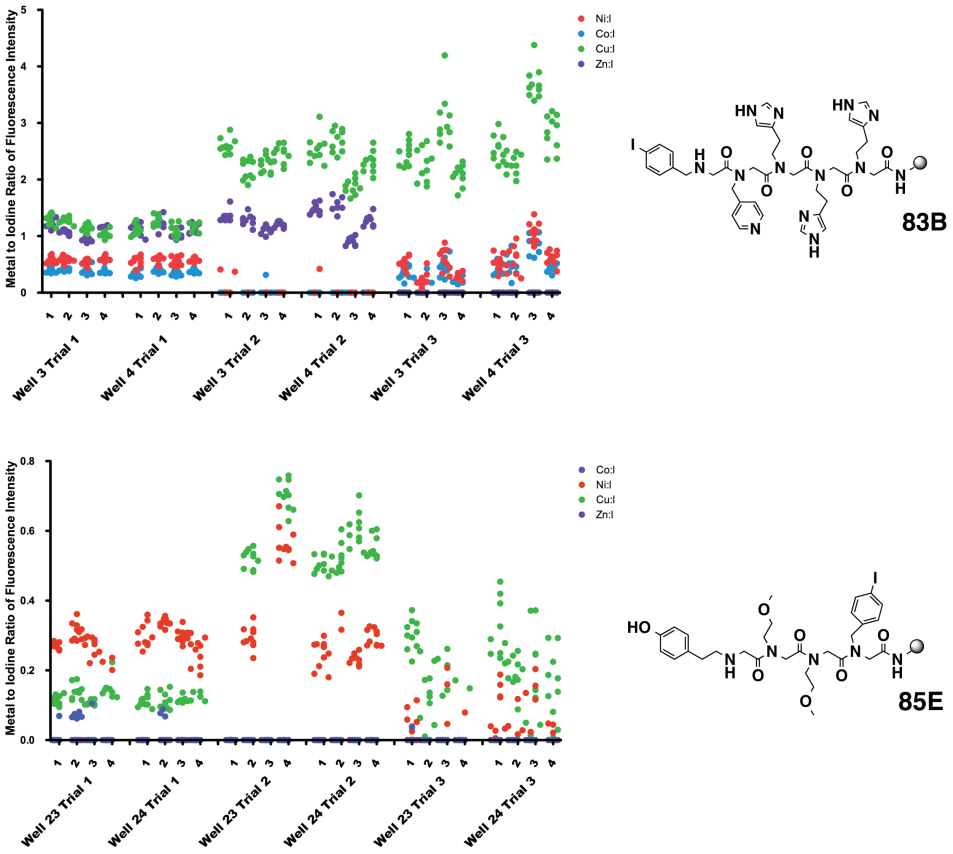

Figure 50. Representative MXRF® analysis of peptoid library members. Sequences corresponding to the analysis are depicted to the right of each graph. Each graph plots the metal to iodine ratio of fluorescence intensity (M:I) over three separate trials against the two wells that contained the sequence. Within each well, M:I are distinguished by separating the specific bead (1-4) that the M:I originated from. This figure depicts MXRF® analysis for a peptoid capable of copper binding, **83B** (top), compared to a non-binding sequence, **85E** (bottom).

Another sequence that presented metal binding capabilities was **91A** (**Figure 51, bottom**). This peptoid remarkably complexed three out of the four metals with high M:I

ratios, but seems to slightly prefer zinc with a low overall selectivity. Rich in imidazole and carboxylic acid electron donating ligands, this pentameric peptoid mimics natural zinc and copper binding peptides in sequence.[71 72]

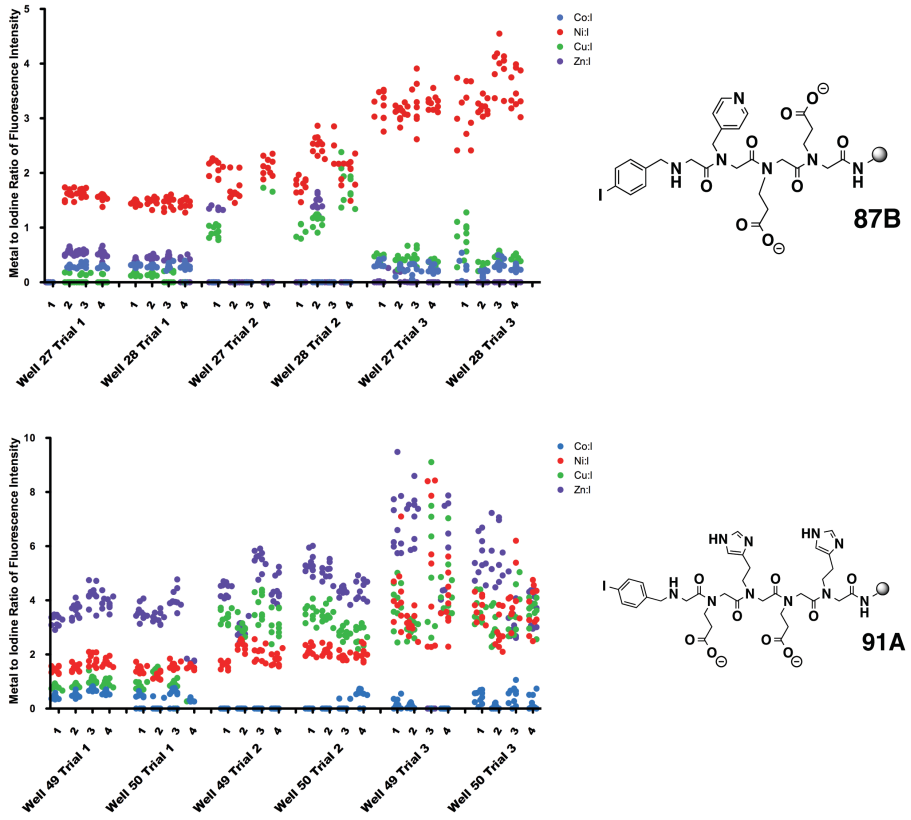

Figure 51. Representative library data from MXRF® analysis. Sequences corresponding to the analysis are depicted to the right of each graph. Each graph plots the metal to iodine ratio of fluorescence intensity (M:I) over three separate trials against the two wells that contained the sequence. Within each well, M:I are distinguished by separating the specific bead (1-4) that the M:I originated from. A nickel binding sequence, **87B** (top), is illustrated. Sequence **91A** (bottom), corresponds to a peptoid with binding capacity for all of the metals present, but exhibits moderate selectivity for zinc.

Given the high nickel affinity and selectivity observed in both **PentA** and **NonaB,** seemingly due to the two pairs of adjacent pyridyl and carboxylic acid side chains, other library members with similar, but not exact, binding motifs were compared to these two hit peptoids. Oligomer **87B** (**Figure 51, top**) emulates the sequence presented by **PentA**, with one pair adjacent pair of a carboxylic acid and pyridine sidechain, but leaves a second carboxylic acid without its pyridyl counterpart. As a result, the M:I intensity is diminished, and in one out of the three trials, the selectivity is curtailed as well. More experimentation would be required to confirm the decrease in selectivity, but it is clear from the data that this peptoid does not complex nickel as well as **PentA** (based on the magnitude of the M:I).

Figure 52 depicts two longer oligomers with some nickel binding capacity that can be compared to **NonaB** in terms of their length and spacing of the pyridine and carboxylic acid side chains. Sequence **NonaD** is a nonamer that contains only one of each of the nickel binding side chains, and separates them between two large, branched ring structures. While the oligomer maintains a scant preference for nickel, the overall selectivity is very low, as is the magnitude of the M:I ratios, not only for nickel, but for all metals present (**Figure 52**, **top**). The other sequence **103D**, is an octamer containing one adjacent pair of pyridine and carboxylic acid side chains, and one additional carboxylic acid residue, separated from the pair by one alpha-branched cyclohexyl side chain (**Figure 52**, **bottom**). Comparing this structure to **NonaD**, **103D** exhibits an enhanced selectivity for nickel, and a slightly higher Ni:I, similar to **87B.**

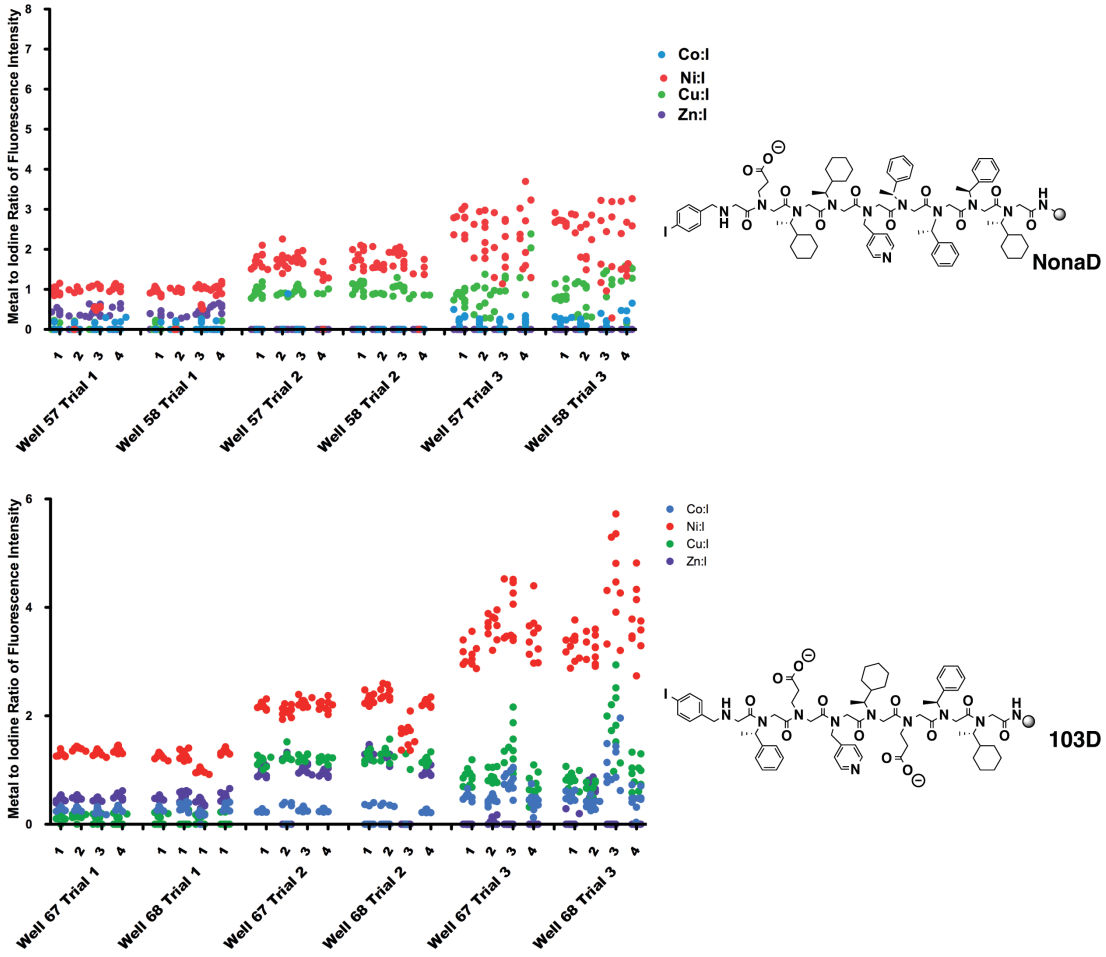

Figure 52. Representative MXRF® analysis of peptoid library members. Sequences corresponding to the analysis are depicted to the right of each graph. Each graph plots the metal to iodine ratio of fluorescence intensity (M:I) over three separate trials against the two wells that contained the sequence. Within each well, M:I are distinguished by separating the specific bead (1-4) that the M:I originated from. Both **NonaD** (top) and **103D** (bottom) exhibit nickel complexation. However, in contrast to both **PentA** and **NonaB**, for which the pyridyl and carboxylic acid functionalities are adjacent and equally paired, neither of these sequences completely fulfills those requirements. The Ni^{2+}

selectivity observed in both sequences presented above is diminished in comparison to either **PentA** or **NonaB**.

Analysis of these three oligomers in comparison to **PentA** and **NonaB** suggest that 2 pairs of adjacently positioned carboxylic acid and pyridine side chains are responsible for the high selectivity and M:I for nickel observed in the high throughput XRF analysis. Sequence **NonaD**, which separated the pyridine and carboxylate side chains, gave both low affinity and selectivity for nickel. Sequences **87D** and **103D**, both of which displayed one adjacent binding pair as well as one lone, unpaired carboxylic acid residue, demonstrated higher affinity and selectivity for nickel, but in both cases lower than that of **PentA** and **NonaB**. Oligomers containing additional pairs of these critical binding residues may exhibit enhanced selectivity and affinity for nickel complexation.

Solution Phase Binding Experiments of Hit Sequences

Once liberated from solid support and purified (**See Experimental and Appendix 2.4 Validation of Library Synthesis for experimental details**), we attempted to characterize **89A** and **101A**'s ability to complex nickel. Uv/vis, ^{1}H NMR, and MS spectroscopy as well as HPLC analysis were conducted as methods of verification of a binding event. The individual results of each of the experiments are detailed in **Appendix 2.4. Solution Phase Binding Experiments of Hits.** However, the conclusions reached from the collective analysis of the Uv/vis ^{1}H NMR, MS

spectroscopy, and HPLC analysis did not support the visualization of a binding event not only with **89A** and **101A** but also including **91A** and **83C**. Confounding aspects of these experiments included insolubility and precipitation of the metal and/or peptoid oligomers at a near neutral and buffered pH, solvent evaporation, and unreliable monitoring at wavelengths below 300 nm. Ultimately, ^{1}H NMR analysis did not clearly indicate response of peptoid oliogmers **89A** and **101A** to the presence of Ni^{2+}. We hypothesize that the multivalent presentation of the ligands while the peptoids are immobilized on tentagel resin may be required for the nickel binding events and strong XRF response, which justifies our inability to witness a binding event in solution.

4.4 Summary and Outlook

We demonstrate the use of high-throughput x-ray fluorescence to screen a library of peptoid oligomers for metal binding interactions in the presence of several, biologically relevant, competing metal ions. Two sequences display strong affinity for Ni(II) relative to the other metals present in solution out of 35 library members, while a handful of other sequences demonstrate binding capabilities for other metal species. Additional metal-binding assays, which include a qualitative colorimetric assay and a quantitative ICP-MS concentration depletion assay, demonstrate the viability of this technique. Using this small sample library as a model, it is reasonable to assume that, if the library were to be expanded to typical high throughput screening sizes, the potential exists for the discovery of many more peptoids with a set of diverse metal binding affinities.[46,49] Given the hundreds of available primary amines that can be incorporated

into the peptoid oligomer, there are innumerable sequence combinations to be made and tested for metal complexation. The application of this approach can be expanded to potentiate the discovery of new "metallopeptoid" sequences capable of performing additional functions. For example, peptoid sequences that preferentially bind specific metals could be elaborated into mimics of cosmeceutically active metallopeptides.

The scope of this screening protocol is not limited to the detection of metal-binding interactions.[74-77] The gain or loss of any atom with an atomic number larger than 12 can be monitored. Hence, the versatility, ease, and speed of this technique indicate that it will be a useful complement to previously established peptoid high-throughput screening methods and will enable the discovery of new families of functional oligomeric materials.[59,62,78,79]

4.5 Experimental Procedures

Materials:

Synthesis of the peptoid oligomers was initiated on either Rink Amide resin (Nova Biochem, 100-200 mesh, loading: 0.74 mmol/gram) or NovaSyn TG amino resin HL (Nova Biochem, 110 μm, loading: 0.39 mmol/gram). Bromoacetic acid (97%) was supplied by Sigma-Aldrich. Chloroacetic acid (99%), Trifluoroacetic Acid, TFA, (99%), N,N-Dimethylformamide, DMF, (anhydrous and amine free, 99.9%) and N,N' diisopropylcarbodiimide, DIC, (99%) were supplied by Alpha Aesar. Metal salts were obtained from the following sources: $Cu(NO_3)_2 \cdot 3H_2O$ (Acros Organics, 99%), $Co(NO_3)_2 \cdot 6H_2O$ (Alpha Aesar, 98-102%), $Ni(NO_3)_2 \cdot 6H_2O$ (98%, Alpha Aesar), $Zn(NO_3)_2 \cdot 6H_2O$ (Strem Chemicals, 98%). XRpro® analytical array plate seals were obtained from XRpro Corp, Cambridge MA . Other reagents and solvents were obtained from commercial sources and used without additional purification.

Submonomers: The introduction of specific peptoid side chain types was achieved through the use of the following primary amines as "submonomer" synthons (see below):

Non-proteinogenic: 2-methoxyethylamine (Sigma-Aldrich**,** 99%); **butylamine** (Sigma-Aldrich**,** 99.5%); (**S)-(+)-1-cyclohexylethylamine (**Alpha Aesar, 98%, 97% ee); **(S)-(-)-1-phenylethylamine** (TCI America**,** 98%); **benzylamine** (Alpha Aesar, 98%); **4-iodobenzylamine** (Alpha Aesar**,** 97%); **4-(aminomethyl) pyridine** (Sigma-Aldrich, 98%).

Proteinogenic: ethanolamine (Sigma-Aldrich, 99%); **histamine** (CalbioChem, Free base, 97%); **tyramine** (TCI America, 98%); **tryptamine** (Sigma-Aldrich, 98%); and **H-β-alanine-OtBu•HCl** (NovaBiochem).

Instrumentation:

Peptoid oligomers were analyzed by reverse-phase HPLC (analytical C_{18} column, Peeke Scientific, 5 mm, 120 Angstroms, 2.0x50 mm) on a Beckman Coulter Systems Gold 166 instrument. A linear gradient of 5-95% acetonitrile in water (0.1% TFA) over 10 min was used at a flow rate of 700 μL /min. Semi-preparative HPLC was performed using a Delta-Pak C_{18} column (Waters, 15mm, 100 Angstroms, 25x100mm). Peaks were eluted with a linear gradient of ACN/water (0.1% TFA) which depended on the sequence composition with a flow rate of 2.5 mL/min. Mass spectrometry was performed on an Agilent 1100 series LCMSD VL MS spectrometer. X-ray fluorescence measurements were performed using an XRpro® micro x-ray fluorescence system equipped with a 30 W Rh excitation source, silicon drift energy-resolving detector, and having a 100 μm nominal X-ray spot size. X-ray tube operating conditions were maintained at 35 kV and 600 mA. Single resin beads were analyzed using XRpro® analytical array plate seals (XRpro Corp., Cambridge MA) Each XRpro® plate seal (127.8 x 85.5 mm) was divided into 48 sections (2 wells/section on a standard 96 well plate). In each section identical sequences were immobilized, such that each sequence was positioned into two different, adjacent wells. All sequences in the library were immobilized in their own section, and sequences were not repeated in the same experiment. For the nickel dimethylglyoxime assay, the four sequences were

immobilized on an XRpro® analytical array plate seal (127.8 x 85.5 mm) such that was each sequence was positioned into 12 different wells. The beads were visualized using a Zeiss Axioscope 40 Microscope with a halogen lamp, and images were captured using a Nikon D80 camera with an exposure time of 1/40 sec. Quantitation of Nickel concentration was performed by inductively coupled plasma mass spectrometry (ICP-MS) at a contract facility.

Preparation of Peptoid Oligomers on Tentagel amino HL resin: Peptoid oligomers were synthesized according to a modified submonomer approach.[66, 70] The resin (10 mg, 0.0039 mmol reactive groups) was swelled for 1 hour in DMF before initiating the synthesis. Bromoacetylation was carried out by incubating the resin with a bromoacetic acid solution in DMF (1.2 M, 300 μL) and DIC (60 μL) for 40 minutes at 37°C and an agitation rate of 220 rpm. The resin was washed with 4x 1 mL DMF before displacement with the desired primary amine (1M in DMF or 2M in NMP for heterocyclic amines and 4-iodobenzylamine, 300 μL) for 1 hour at 37°C and an agitation rate of 220 rpm. The resin was washed with 5x 1mL DMF. For all steps subsequent to the addition of a heterocyclic amine, the iterative protocol was changed to acylation with chloroacetic acid solution in DMF (0.4M, 300 μL) with DIC (60 μL) for 10 minutes at 37°C and an agitation rate of 220 rpm. The washing and amine displacement steps were not modified. This two-step iterative process was repeated until the desired chain length and oligomer composition was achieved. Protecting groups were removed with a cocktail of 95% TFA, 2.5% TIPS, and 2.5% water (300 μL) at room temperature for 2

hrs. Resins were washed thoroughly with DCM, lyophilized, and stored under vacuum and desiccation until use.

Preparation of Peptoid Oligomers on Rink Amide resin: Peptoid oligomers were synthesized according to a modified submonomer approach.[66,70] Rink Amide Resin, 100 mg (0.074 mmol), was swelled in DMF for 30 minutes before initiating the synthesis. Bromoacetylation was carried out by incubating the resin with a bromoacetic acid solution in DMF (1.2M, 850 μL) and DIC (200 μL) for 20 minutes at room temperature and an agitation rate of 220 rpm. The resin was washed with 4x 1 mL DMF before displacement with the desired primary amine (1M in DMF or 2M in NMP for heterocyclic amines and 4-iodobenzylamine, 1 mL) for 30 minutes at room temperature and an agitation rate of 220 rpm. The resin was washed with 5x 1 mL DMF. For all steps subsequent to the addition of a heterocyclic amine, the iterative protocol was changed to acylation with chloroacetic acid solution in DMF (0.4M, 850 μL) with DIC (200 μL) at 37 ^{o}C for 10 minutes. Following a 4x 1 mL DMF wash, displacement with the primary amine (1M or 2M for heterocyclic amines, 1 mL) was conducted at 37^{o}C for 60 minutes. This two-step iterative process was repeated until the desired oligomer chain length and monomer sequence composition was achieved. The oligomers were cleaved from the resin using a cocktail containing 95% TFA, 2.5% TIPS, and 2.5% water (4 mL) at room temperature for 10 minutes. The solution was removed under reduced pressure, and the crude peptoid was re-suspended in acetonitrile/water, frozen, and lyophilized. Once thoroughly dried, crude peptoids were stored at 4^{o}C until characterization and purification.

Incubation of Sequences Synthesized on Tentagel resin with Metal Solution: Peptoid-functionalized Tentagel amino HL resin was immobilized on XRpro® analytical array plate seal as described above. The slide was affixed to a standard 96 well plate. Each well contained 3 mL of a 500 μM stock solution of each of the following metals in water: $Cu(NO_3)_2 \cdot 3H_2O$, $Co(NO_3)_2 \cdot 6H_2O$, $Ni(NO_3)_2 \cdot 6H_2O$, $Zn(NO_3)_2 \cdot 6H_2O$ (pH of metal stock was adjusted to 7-8 with 1M Tris buffer pH 8 prior to partitioning solution into the wells). The sealed 96 well plate was inverted so that the solution was able to make contact with the resin-bound library. The library was incubated for 18-24 hours in the metal solution prior to MXRF® analysis.

MXRF® Analysis

After incubation, XRF analysis was carried out under the instrument conditions described above without removing either the plate seal from the 96 well plate or the metal solution from the wells. Spectra were acquired through the thin plastic plate seal. Absorbances of emitted X-rays by the seal are consistent between samples and negligible at these photon energies.

Automated spectra acquisitions were performed for each bead in each well (4 beads per well) and the metal solution in each well (as a background reading), recording ten readings/sample (10 reading / bead; 80 readings/sequence; 10 background readings/well). Spectra were acquired for 3 live seconds and curve-fit using instrument

software to provide count rate output corresponding to the integrated area for emission peaks of elements of interest.

Calculation of Metal:I Ratios: First-pass analysis of MXRF® data was carried out to discard positions on analytical arrays that did not contain samples. A threshold for iodine signal was established using a method detection limit based on background measurements at well positions containing metal solutions but not sample beads (**Eq.1**). Data for sample positions that did not generate iodine signal in excess of this threshold were discarded as either vacant sample positions or resin bead samples lacking peptoid.

For Metal:I ratio calculations, MDL values were calculated for each element of interest. Signals below MDL values for a target element were considered to be 0. For elements with signals above MDL, Metal:I ratios were calculated from **Eq. 2**.

Eq. 1. $\mathbf{MDL_{element} = BG_{element} + 3\sigma_{element}}$

Where $\mathbf{MDL_{element}}$ is the method detection limit for the element of interest, $\mathbf{BG_{element}}$ is the average intensity of background readings for the element of interest, and $\boldsymbol{\sigma_{element}}$ is the standard deviation of intensities from background readings for the element of interest.

Eq. 2. $\mathbf{Metal{:}I = (Signal_{element} - BG_{element}) / (Signal_{Iodine} - BG_{Iodine})}$

Where **Metal:I** is the metal to iodine ratio, $\mathbf{Signal_{Element}}$ is the signal intensity for the element of interest, $\mathbf{BG_{Element}}$ is the average background for the element of interest, $\mathbf{Signal_{Iodine}}$ is the signal intensity for the element of interest, and $\mathbf{BG_{Iodine}}$ is the average background for iodine. Resulting data was processed and graphed for publication using Graphad Prism™.

Dimethylglyoxime Colorimetric Analysis: Tentagel amino HL resin functionalized with peptoids (**ConC, PentA, NonaB**) and unmodified Tentagel amino HL resin beads were immobilized on an XRpro® analytical array plate seal as described above. The slide was affixed to a generic 96 well plate. Each well contained 3 mL of a 500 μM solution of $Ni(NO_3)_2 \cdot 6H_2O$ in aqueous buffer (pH 7 adjusted with 0.5 M Tris buffer pH 8 prior to exposure to beads). The sealed 96 well plate was inverted so that the nickel solution was able to make contact with the resin-bound peptoids. Following a 3 hour incubation period in the nickel solution, the plate seal was removed, and the beads, which remained on the slide, were washed with 3 x 20 μL 0.5 M Tris buffer. The beads were quickly dried with a stream of nitrogen before exposure to a 1% dimethylglyoxime solution in methanol (100 μL). Once the methanol had evaporated, all beads were viewed under a microscope, and a representative color image of each sequence, on resin, was obtained.

Nickel Depletion Assay: Each peptoid sequence, immobilized on resin, was weighed (5 mg, 1.95 μmol) and incubated with agitation for 3 hours in either a 24.1 M ± 1.8

$Ni(NO_3)_2$ (0.241 μmol, 10 mL) or a 222.5 μM ± 22.8 $Ni(NO_3)_2$ (0.222.5 μmol, 1 mL) aqueous Tris-buffered solution (pH 7). The solutions were filtered to remove any resin beads and submitted for ICP-MS analysis of nickel concentration, along with samples of the starting nickel solutions.

MXRF Analysis

After washing and drying the slides, they were prepared for MXRF analysis. MXRF analysis was carried out under the instrument conditions described above. The Bruker M4 Tornado software was programmed to hit every bead in each well (4 beads per well) ten times over (10 readings/bead; 80 readings/sequence). The beads were analyzed with a live time exposure to X-ray radiation of 10 seconds.

4.6 References

1. Degtyarenko, K. In *Encyclopedia of Genetics, Genomics, Proteomics and Bioinformatics*; John Wiley & Sons, Ltd: Hoboken, NJ, 2004.
2. Finkelstein, J. *Nature.* **2009**, *460*, 813.
3. Trainer, J.; Roberts, V.; Getzoff, E. *Curr. Opin. Biotechnol.* **1991**, *2*, 582.
4. Liu, C.; Xu, H. *J. Inorg. Biochem*. **2002**, *88*, 77.
5. Frankel, A.; Berg, J.; Pabo, C. *Proc. Natl. Acad. Sci. USA*. **1987**, *84*, 4841.
6. Klug, A. *Annu. Rev. Biochem*. **2010**, *79*, 213
7. Nelson, D. L.; Cox, M. M. *Principles of Biochemisry*; W. H. Freeman, Ltd: United Kingdom,2008.
8. Radzicka, A.; Wolfenden, R. *Science.* **1995**, *267*, 90.
9. Lansdown, A.B.G; Mirastschijski, U.; Stubbs, N.; Scanlon, E.; Agren, M.S. *Wound Rep. Reg.* **2007**,*15*, 2–16.
10. Soo, C.; Shaw, W.W.; Zhang, X.; Longaker, M.T.; Howard, E.W.;Ting, K. *Plast. Reconstr. Surg*. **2000**, *105*, 638–647.
11. Ravanti, L. and Kahari V.M. Int. J. Mol. Med. **2000**, *6*,391–407.
12. *Protein Crosslinking: Nutritional and Medical Consequences, In: Advances in Experimental Medicine and Biology, vol. 86;* Friedman, M.; Ed.; Illustrated Springer Science & Business Media: New York, NY, 2013.
13. Juwarker, H.; Suk, J.-M.; Jeong, K.S. *Chem. Soc. Rev.* **2009**,*38*, 3316-3325.

14. *Metallofoldamers: Supramolecular Architectures from Helicates to Biomimetics.* Maayan, G. and Albrecht, M., Eds.;John Wiley & Sons, Chichester, UK, 2013.

15. Luo, T. and Kiick, K.L. *Bioconjugate Chem.* **2017**, *28*, 816−827.

16. Yu, S. M., Li, Y., & Kim, D. *Soft Matter*. **2011**,*7*, 7927–7938.

17. Kogan, G.; Šoltés, L.; Stern, R. *et al. Biotechnol. Lett.* **2007**, *29,*17-25.

18. Fraser, J.R.E.; Laurent, T.C.; Laurent, U.B.G. *J. Int. Med.* **1997**, *242*, 27-33.

19. Micklitsch, C.M.; Knerr, P.J.; Branco, M.C.; Nagarkar, R.; Pochan, D.J.; Schneider, J.P. Angew. Chem. **2011**,*123*, 1615 –1617.

20. Lemire, J.A.; Harrison, J.J.; Turner, R.J. *Nature Reviews Microbiology*. **2013**, *11,*371-384.

21. Scanlon, E. and Agren, M.S. *Wound Rep. Reg.* **2007**, *15*, 2–16.

22. Agren, M.S.; Soderberg, T.A.; Reuterving, C.O.; Hallmans, G.; Tengrup, I. *Eur. J. Surg.* **1991**, *157*, 97–101.

23. Akiyama, H.; Yamasaki, O.; Kanzaki, H.; Tada, J.; Arata, J. *J. Dermatol. Sci.***1998**, *17*, 67–74.

24. Podbielski, A.; Boeckh, C.; Haller, B. *J. Endod*. **2000**, *26*, 398–403.

25. Lansdown, A. B. G.; Mirastschijski, U.; Stubbs, N.; Scanlon, E.; Agren, M.S. *Wound Repair Regen.,* **2007**, *15*, 2-16.

26. Wiegand, C.; Heinze, T.; Hipler, U-C. *Wound Rep. Reg.* **2009**, *17,* 511–521.

27. Kim, J.; Kwon, S.; Ostler, E. *Journal of Biological Engineering.* **2009**,

3.

28. Purcel, B.P.; Lobb, D.; Charati, M.B.; Dorsey, S.M.; Wade, R.J.; Zellars, K.N.; Doviak, H.; Pettaway, S.; Logdon, C.B.; Shuman, J.A.; Freels, P.D.; Gorman, J.H.; Gorman, R.C.; Spinale, F.G.; Burdick. J.A. *Nature Materials.* **2014**, *13,* 653-661.
29. Drescher, W.H. Copper and Your Skin: Facelift in a Bottle [online publication], **2013**. Retrieved from: https://www.copper.org/publications/newsletters/innovations/2006/06/copper_your_skin.html
30. Pickart, L. and Shagan, S. *SOFWA-Journal* [online publication], **2015**. Retrieved from: [http://skinbiology.com/SOFW2015_CosmeceuticalTriPeptideGHK.pdf .
31. Gorouhi, F. and Maibach, H.I. *International Journal of Cosmetic Science*, **2009**, *31*, 327–345
32. Finkey, M.B.; Appa, Y. ; Bhandarkar, S. *Copper peptide and skin. In: Cosmeceuticals and Active Cosmetics*, 2nd edn; Elsner, P. and Maibach, H.I., Eds.; Marcel Dekker, New York, NY, 2005, pp. 549–564.
33. Abdulghani, A.A.; Sherr, A.; Shirin, S.; Solodkina, G.; Morales Tapia, E.; Wolf, B.; *et al*. *Dis. Manag. Clin. Outcomes.* **1998**, *1*, 136–141.
34. (a) Gellman, S.H. *Acc. Chem. Res*. **1998**, *31*,173–180. (b) Goodman, C.M.; Choi, S.; Shandler, S.; DeGrado, W.F. *Nat. Chem. Biol*. **2007**, *3,* 252–262.
35. DeGrado, W. F. *Chem. Rev.* **2001**, *101*, 3025.
36. Gellman, S. H. *Acc. Chem. Res*. **1998**, *31*, 173.
37. Knight, A.S.; Zhou, E. Y.; Francis, M.B.; Zuckermann, R.N. Adv. Mater.

2015, *38,* 5665–5691.

38. Kölmel, D.K.; Rudat, B.; Schepers, U.; and Bräse, S. *Eur. J. Org. Chem*. **2013**, 2761–2765.

39. Izzo I; Ianniello, G.; De Cola, C.; Nardone, B.; Erra, L.; Vaughan, G.; Tedesco, C.; DeRiccardis, F. *Org. Lett*. **2013**, *15*, 598-601.

40. Maayan, G.; Ward, M.; Kirshenbaum, K. *Chem. Commun*. **2009**, 56-58.

41. Lee, B.-C.; Chu, T.K.; Dill, K.A.; Zuckermann, R.N. *J. Am. Chem. Soc*. **2008**, *130*, 8847-8855.

42. Pirrung, M. C.; Park, K.; Tumey, L. N. *J. Comb. Chem*. **2002**, *4*, 329-344.

43. Maayan, G. and Lui, L-K. *Biolpolymers*. **2011**, *96*, 697-687.

44. Cola, D. C.; Fiorillo, G.; Meli, A.; Aime, S.; Gianolio, E.; Izzo, I; De Riccardis, F. *Org Biomol Chem*. **2014**, *12*, 424-431.

45. Knight, A.S.; Zhou, E.Y.; Pelton, J.G.; Francis, M.B. *J. Am. Chem. Soc*. **2013**, *135*, 17488–17493.

46. Fischer, A. E. O. and Naughton, D. P. J. *Inorg. Biochem*. **2004**, *98*, 343-346.

47. (a) Chen, C.L.; Qi, J.; Zuckermann, R.N.; DeYoreo, J.J. J. Am. Chem. *Soc*. **2011**, *133*, 5214-5217. (b) Li, R.; Smolyakova, A.; Maayan, G.; Rimer, J.D. *Chem. Mater.* **2017**, *29*, 9536–9546. (c) Tigger-Zaborov, H. and Maayan,G. *Journal of Colloid and Interface Science*. **2017**, *508*, 56–66. (d) Mohan, D.C.; Sadhukha, A.; Maayan,G. *Journal of Catalysis*. **2017**, *355*, 139–144. (e) Kaniraj, J.P. and Maayan, G. *Chem. Commun*. **2015***, 51*, 11096-11099.

48. Della Sala, G.; Nardone, B., De Riccardis, F.; Izzo, I. Org Biomol Chem

2013, *11*, 726-731.

49. (a) Knight, A.S., Zhou, E.Y., Francis, M. B. *Chem. Sci.* **2015**, *6,* 4042-4048. (b) Parker, B.F., Knight, A. S**.**, Vukovic, S., Arnold, J., Francis, M.B. *Ind. Eng. Chem. Res.* **2016**, *55*, 4187-4194. (c) Knight, A.S.; Kulkarni, R.U.; Zhou, E.Y.; Franke, J.M.; Miller, E.W.; Francis, M.B. *Chem. Commun.* **2017**, *53*, 3477-3480.

50. Zuckermann, R.N.; Martin. E.J.; Spellmeyer, D.C.; Stauber, G.B.; Shoemaker, K.R.; Kerr, J.M.; Figliozzi, G.M.; Goff, D.A.; Siani, M.A.; Simon, R.J.; Banville, S.C.; Brown, E.G.; Wang, L.; Richter, L.S.; Moos, W.H. *J. Med. Chem.***1994**, *37*, 2678-2685.

51. Zuckermann, R.N. *Biopolymers,* **2010**, *96*, 545-555.

52. Patch, J.A.; Kirshenbaum, K.; Seurynck, S.L.; Zuckermann, R.N.; Barron, A.E. *In Pseudo-peptides in Drug Discovery*; Nielsen, P.E., Ed.; Wiley-VCH: Weinheim, 2004, pp 1-31.

53. Huang, C.-Y.; Uno, T.; Murphy, J.E.; Lee, S.; Hamer, J.D.; Escobedo, J.A.; Cohen, F.E.; Radhakrishnan, R.; Dwarki, V.; Zuckermann, R.N. *Chem. Biol.* **1998***, 5*, 345-354.

54. Dohm. M.T.; Seurynck-Servoss, S.L.; Seo, J.; Zuckermann ,R.N.; Barron, A.E. *Biopolymers.* **2009**, *6,* 538-553.

55. Udugamasooriya D.G.; Dineen, S.P.; Brekken, R.A.; Kodadek, T. *J. Am. Chem. Soc.* **2008***,130*, 5744-5752

56. Paulick, M. G.; Hart, K. M.; Brinner, K. M.; Tjandra, M.; Charych, D. H.; Zuckermann, R. N. *J. Comb. Chem.* **2006***, 8*, 417-426.

57. Alluri, P.G.; Reddy, M.M.; Bachhawat-Sikder, K.; Olivos, H.J.; Kodadek,

T. *J. Am. Chem. Soc.* **2003**,*125*, 13995-14004.

58. Lam, K. S.; Salmon, S. E.; Hersh, E. M.; Hruby, V. J.; Kazmierski,W. M.; Knapp, R. J. *Nature.* **1991**, *354*, 82−84.

59. Knight, A.S.; Kulkarni, R.U.; Zhou, E.Y.; Franke, J.M.; Miller, E.W.; Francis, M.B. *Chem. Commun.* **2017**, *53*, 3477-3480

60. Francis, M. B.; Finney, N. S.; Jacobsen, E. N. *J. Am. Chem. Soc.***1996**, *118*, 8983-8984.

61. *X-Ray Data Booklet;* Thompson, Albert C., Ed.; 3rd ed. [Online]; Lawrence Berkeley National Laboratory, Berkeley, California, 2009. http://xdb.lbl.gov/xdb-new.pdf (accessed Apr 20, 2014).

62. Miller, T.C.; Mann, G.; Havrilla, G.J.; Wells, C.A.; Warner, B.P.; Baker, R.T. *J. Comb. Chem.* **2003**, *5*, 245-252.

63. Image Courtesy of the XRPro Corp.

64. Minogue, E.M.; Havrilla, G.J.; Taylor, T.P.; Warner, B.P.; Burrell, A.K. *New J. Chem.* **2006**, *30*, 1145-1148.

65. Image Courtesy of Horiba Scientific http://www.horiba.com

66. Culf, A.S. and Oulette, R.J. *Molecules*. **2010**, *15*, 5282-5335.

67. Miller, S.M.; Simon, R.J.; Ng, S.; Zuckermann, R.N.; Kerr, J.M.; Moos, W.H. *Drug Dev. Res.***1995**, *35,* 20-32.

68. Wetzer, M.; Kapoor, R.; Huang, W.; Barron, A.E. *Peptoid Oligomers: Peptidomimetics for Diverse Biomedical Applications; In Polymer Science: A Comprehensive Reference, vol. 10;* Elsevier B.V.: Amsterdam, The Netherlands, 2012, pp. 267-287.

69. Ganesh, S.D.; Saha, N.; Zandraa, O.; Zuckermann, R.N.; Sáha, P. *Polym. Bull*. **2017**, *74*, 3455–3466.

70. Burkoth,T.S.; Fafarman, A.T.; Charynch, D.H.; Connolly, M.D.; Zuckermann, R.N. *J. Am. Chem. Soc.* **2003**, *125*, 8841-8845.

71. Grasso, G.; Magrì, A.; Bellia, F.; Pietropaolo, A.; La Mendola, D.; Rizzarelli, E. *J. Inorg. Biochem*. **2014**, *130*, 92-100.

72. Fukasawa, K.M.; Hata, T.; Ono, Y.; Hirose, J. *Journal of Amino Acids*. **2011**, *2011*, 1-7.

73. Kiss, T. and Gergely, A. J. Chem. Soc. Dalton Trans. **1984**, 1951-1957.

74. Singer, D.M.; Zachara, J.M.; Brown, G.E.Jr. *Environ. Sci. Technol.* **2009***, 43,* 630- 6037.

75. Janssens, K; Vittiglio, G; Deraedt, I; et al. *X-ray Spectrom.* **2000***, 29,* 73-91.

76. Buleon, A.; Cotte, M.; Putaux, J.-L.; d'Hulst, C.; Susini, J. *Biochem. Biophys. Acta.* **2014**,*1840,* 113 - 119.

77. Grubman, A.; James, S.A.; James, J.; Duncan, C.; Volitakis, I.; Hickey, J.L. Crouch, P.J.; Donnelly, P.S.; Kanninen, K.M.; Liddell, J.R.; Cotman, S.L.; de Jonge, M.D.; White, A.R. *Chem. Sci.* **2014***, 5,* 2503-2516.

78. Sambasivan, R.; Zheng, W.; Burya, S.J.; Popp, B.V.; Turro, C.; Clementi, C.; Ball, Z.T. *Chem. Sci.* **2014***, 5*, 1401-1407.

79. Stanton, M.L. and Holcombe, J.A. *J. Comb. Chem.***2007***, 9*, 359-365.

Appendix 1

A Novel Transfection Modality for in vivo siRNA Delivery to Vocal Fold Fibroblasts

The contents of this appendix include a manuscript to which I contributed authorship, but did not provide experimental effort. These are the preliminary *in vitro* results across several cell lines using **Lipitoid** as a delivery vehicle, establishing optimal transfection conditions and cell toxicity data prior to our *in vivo* experiments.

A novel transfection modality for in vivo siRNA delivery to vocal fold fibroblasts
(Originally Published in Laryngoscope. Kraja, I.; Bing, R.; Hiwatashi, N.; Rousseau, B.; Nalband, D.M.; Kirshenbaum, K.; Branski, R.C. (2017), A novel transfection modality for in vivo siRNA delivery to vocal fold fibroblasts. Larynogscope, 127:E231–E237. DOI: 10.1002/lary.26432)

An obstacle to clinical use of RNA-based gene suppression is instability and inefficiency of current delivery modalities. Nanoparticle delivery likely holds great promise, but the kinetics and transfection conditions must be optimized prior to *in vivo* utility. We investigated a RNA nanoparticle complex incorporating a “lipitoid” transfection agent in comparison to a commercially-available reagent through the study of variables that influence transfection efficiency, *in vitro*. These variables included duration, dose, and number of administrations, as well as serum and media conditions. The target gene was Smad3, a signaling protein in the Transforming Growth Factor (TGF)-β cascade implicated in fibroplasia in the vocal folds and other tissues.

Results

Transfection Efficiency.

Two transfection methods were compared; one in which there was a single administration of reagents for 6 hours (standard transfection), and another in which there was extended period over the cells were exposed to prolonged transfection (continuous transfection). In our human vocal fold fibroblast cell line, standard transfection methods with Lipofectamine® significantly decreased Smad3 expression at 6, 24, 48 and 72 hours following transfection (**Figure 53;** p=0.0001, 0.0001, 0.0001,0.0092, respectively). With Lipitoid, Smad3 expression decreased significantly at 6, 24, 48 and 72 hours (p= 0.0001, 0.0001, 0.0001, and 0.0469, respectively). At 24 hours, Lipitoid yielded enhanced Smad3 suppression when compared to Lipofectamine® (p=0.0003).

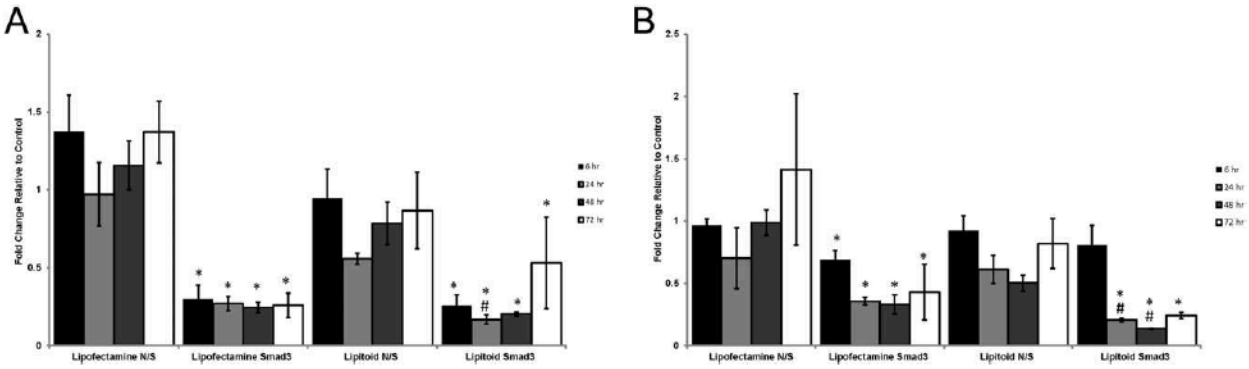

Figure 53. Smad3 expression as a function of standard transfection where cells were exposed to the transfection media for 6 hours (A) and continuous transfection where cells were exposed to the transfection media for the entire duration at the times indicated (B) methods in human vocal fold fibroblasts (N/S–random siRNA segments; *p<0.05 relative to control. #p<0.05 relative to Lipofectamine®/Lipitoid)

Under continuous transfection, Smad3 expression significantly decreased with Lipofectamine® at 6, 24, and 48 hours (p=0.0271, 0.0001, and 0.0001, respectively). Continuous transfection with Lipitoid decreased Smad3 expression at 24 and 48 hours (p<0.0001 for all; **Figure 53B)**. Similar to standard transfection conditions, Lipitoid outperformed Lipofectamine® at 24 and 48 hours (p=0.0003 and 0.0058 respectively) under continuous transfection.

Dose Response and Multiple Administrations.

siRNA concentration was kept constant, but concentrations of Lipofectamine® and Lipitoid were varied to determine optimal transfection conditions. Continuous transfection for 24 hours decreased Smad3 mRNA expression as a function of increasing concentration (**Figure 54A**). Lipofectamine® decreased Smad3 expression relative to control at 0.5, 1.0, 1.5, 2.0, and 2.5μg/mL (p<0.0001 for all). Continuous transfection with Lipitoid yielded decreased Smad3 expression relative to control at 1.0, 1.5, 2.0, and 2.5μg/mL (p<0.0001 for all).

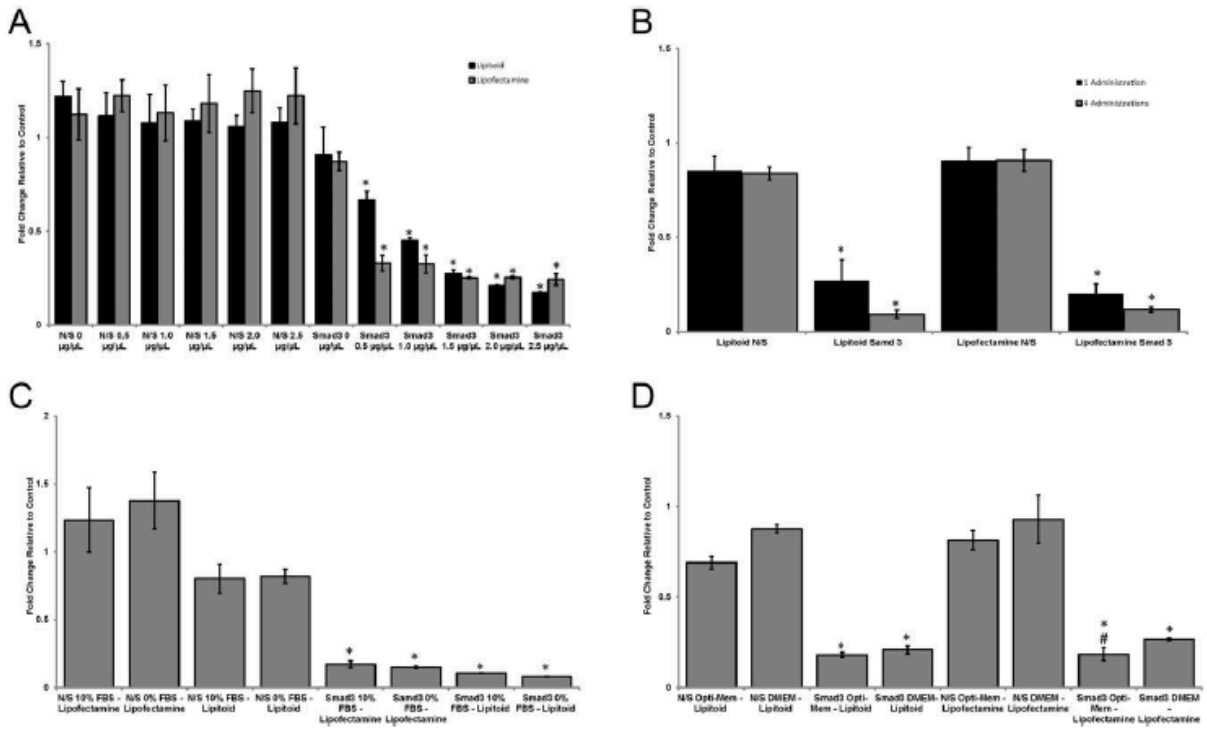

Figure 54. Smad3 expression under 24 hours continuous transfection as a function of lipid concentration (do of siRNA stays constant) (A), number of dose administrations, (B) presence of FBS (C) and media type (D)

(N/S–random siRNA oligonucleotide; *p<0.05 relative to control. #p<0.05 Opti-MEM relative to DMEM)

In order to observe the effects of multiple administrations of transfection reagents, HVOX were treated with 2.5μg/mL of Lipofectamine® or **Lipitoid** siRNA complex every 24 hours for 96 hours (**Figure 54B**) under continuous transfection. Multiple administrations yielded increased gene suppression across both reagents. At 96 hours, Smad3 expression decreased to 20% and 27% of control for Lipofectamine® and Lipitoid, respectively. In contrast, with repeated transfections every 24 hours, Smad3

expression decreased at 96 hours to 12% and 9% of control, respectively ($p<0.0001$ for all).

Optimal Transfection Conditions.

The effects of serum content (0% and 10% FBS) and media type (DMEM and Opti-MEM) were investigated with regard to transfection efficiency (**Figure 54C and D**). Under continuous transfection with Lipofectamine® for 24 hours in DMEM and Opti-MEM, Smad3 mRNA expression decreased to 18% and 27% control, respectively. For continuous transfection for 24 hours in DMEM with 10% FBS and 0% FBS, Smad3 mRNA expression decreased to 14% and 17% of control, respectively ($p<0.0001$ for all). In DMEM and Opti-MEM, Smad3 expression decreased to 18% and 21%, respectively, and with 10% FBS and 0% FBS, Smad3 expression decreased to 8% and 11%, respectively ($p<0.0001$ for all). No significant differences were observed when comparing Lipofectamine® with Lipitoid under these conditions. Lipofectamine with Opti-MEM performed significantly better than DMEM ($p=0.0081$). No differences were observed when comparing the media types with Lipitoid transfection.

Multiple Species Analysis.

In addition to experiments conducted in a human cell line, transfection efficiency was quantified in both rat and rabbit primary vocal fold fibroblasts. In rat VFF (**Figure 55 A)**, Smad3 mRNA decreased to 40% and 43% of control with Lipofectamine® and Lipitoid, respectively ($p=0.0003$, 0.0002, 0.0077, 0.0006 for Lipofectamine® at 6-72 hours, respectively; $p=0.0003$, 0.0043, 0.0076, 0.0009 for Lipitoid at 6-72 hours, respectively). Under continuous transfection (**Figure 55 B**), Smad3 expression decreased to 51% and

45% of control for Lipofectamine® and Lipitoid, respectively, at all time points (p=0.0001, 0.0267, 0.0014 for Lipofectamine® at 24-72 hours, respectively; p=0.0145, 0.0001, 0.0015, 0.0001 for Lipitoid at 6-72 hours, respectively). No differences were observed between Lipofectamine® and Lipitoid in rat VFF.

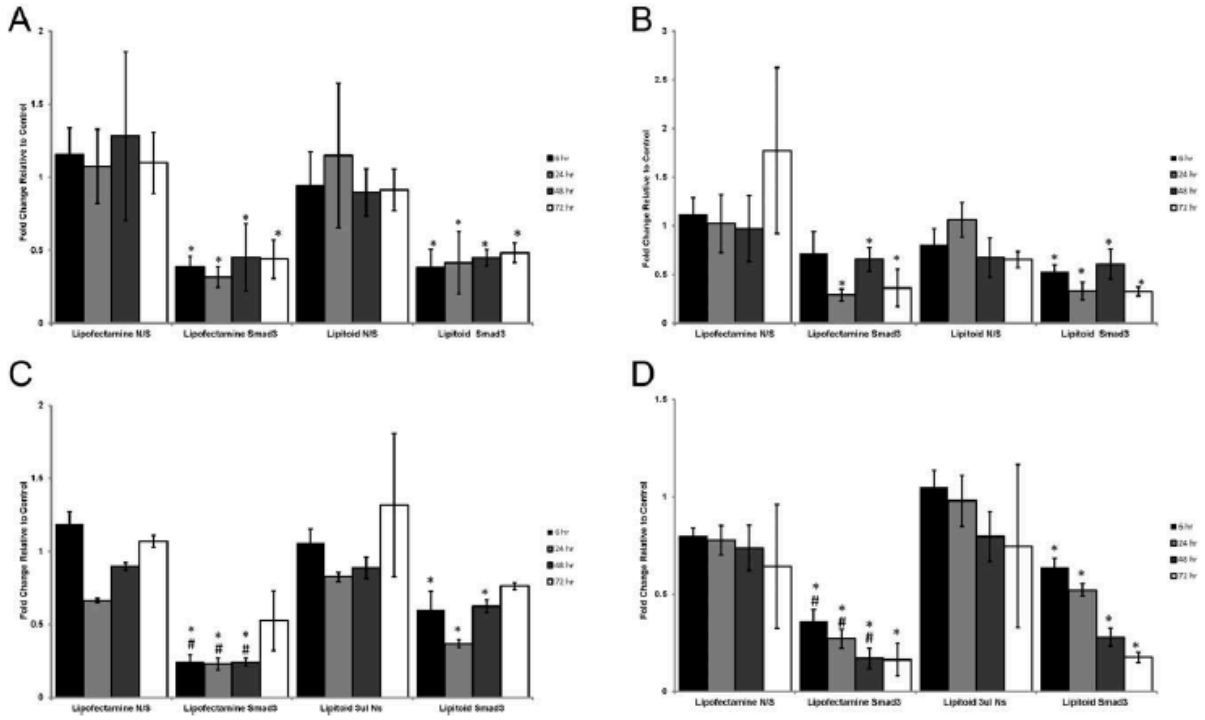

Figure 55. Smad3 expression following siRNA administration under standard (A) and continuous (B) transfection methods in rat Vocal Fold Fibroblasts (VFF) and standard (C) and continuous (D) transfection methods in rabbit VFF. (N/S–random siRNA segments; *p<0.05 relative to control. #p<0.05 relative to Lipofectamine®/Lipitoid)

In rabbit VFFs, Smad3 expression decreased with Lipofectamine® transfection to 31% and 24% of control under standard and continuous transfection, (**Figures 55 C and D**) respectively, at all time points (p=0.0001, 0.0001, 0.0001, 0.0082 under standard transfection at 6-72 hours respectively; p<0.0001 for all time points under

continuous transfection). With Lipitoid, Smad3 decreased to 40% and 24% for standard and continuous transfection, respectively ($p=0.0025$, 0.0001, 0.0001 for standard transfection at 6-48 hours respectively and $p<0.0001$ at all time points for continuous transfection). Similarly, Lipofectamine® yielded Smad3 suppression in rabbit VFFs under both standard ($p=0.0047$, 0.0025, 0.0001 for 6-48 hours, respectively) and continuous transfection ($p=0.0008$, 0.0003, and 0.0468 for 6-48 hours, respectively).

Discussion

Vocal fold injury and the complex reparative response often results in clinically-significant pathology. Current therapies for this tissue response are limited. Globally, we hypothesize that siRNA-based therapeutics hold significant promise in this regard. However, as outlined previously, issues of delivery remain problematic and warrant further investigation. Specifically, we hypothesize that lipid-compatible transfection reagents can facilitate highly-efficient siRNA therapeutics. Transfection reagents are likely to overcome limitations in delivery of uncomplexed siRNA in a therapeutic setting. However, current transfection reagents are not optimized for *in vivo* use and further investigation is needed to both develop novel reagents and optimize their efficiency in models of disease. To that end, we investigated the transfection efficiency of a peptidomimetic reagent, a lipitoid, in vocal fold fibroblasts across species to provide a foundation for future preclinical investigation.

We sought to quantify the efficiency of this lipitoid agent across transfection conditions, specifically, dose, time, and number of applications in both an immortalized human vocal fold fibroblast cell line as well as primary cultures from other commonly-

employed species utilized for *in vitro* vocal fold investigation. Two transfection protocols were employed. In the first, referred to as 'standard transfection', the transfection media was changed after six hours and replaced with standard cell culture media. In the second, termed 'continuous transfection', the transfection media was left throughout the duration of experimentation, in some cases, up to 96 hours. These two protocols were selected to observe the duration of gene suppression and to provide context for the potentially-fleeting nature of siRNA therapeutics *in vivo*. Under both standard and continuous transfection conditions, Smad3 expression decreased initially in the presence of either Lipitoid or Lipofectamine®. This effect, however, did not persist with standard transfection regardless of transfection reagent. Continuous transfection yielded persistent Smad3 suppression. These differences in gene expression relative to duration of transfection suggest that both reagents may be continuously active for at least 72 hours, at least in the contrived cell culture environment.

Variability was noted with regard to the Smad3 suppression across species. The mechanisms underlying these differences are unclear and were not specifically investigated, but may be related to varying metabolic environments across cell types. In rat vocal fold fibroblasts, transfection yielded significant knockdown of Smad3 at 6–24 hours consistent with standard knockdown potential of the two compounds. Interestingly, Smad3 suppression was enhanced in rabbit vocal fold fibroblasts compared to other species. Furthermore, in rabbit cells, Lipofectamine® was more effective at Smad3 knockdown; statistically-significant differences were noted between Lipofectamine® and Lipitoid. This effect was particularly pronounced during continuous transfection. In the

human and rat vocal fold fibroblasts, both Lipitoid and Lipofectamine® were equally effective at Smad3 knockdown.

The concentration of Lipofectamine® and Lipitoid in the context of constant siRNA concentrations, correlated with Smad3 suppression. As the relative concentration of transfection reagents was increased, Smad3 expression decreased. However, Lipitoid appeared more responsive to altered dose. These results were consistent with previous transfection studies in which cell viability and target gene suppression were observed to be dependent on the charge ratio between the applied cationic transfection reagent and the anion oligonucleotide; optimal results were obtained when this positive/negative charge ratio was maintained at about 3:1.[1] Prior work from the Kirshenbaum laboratory found increased cytotoxicity beyond the 3:1 positive/negative charge ratio suggesting that Smad3 suppression in this context may be related to cytotoxicity.[2]

Lipitoid was also more responsive to multiple administrations as a means to maintain an extended timecourse of Smad3 suppression. These differences may be indicative of differing kinetics between the two reagents, in addition to variable molecular mechanisms of siRNA delivery.[2] In order to facilitate the practical application of these compounds *in vivo,* media type and serum concentration were varied. Neither FBS nor media type altered Smad3 suppression. These data may suggest that conditions specific to the chosen cell culture environment are not required for effective transfection.

These data are encouraging with regard to the utility of Lipitoid as a means to effectively deliver siRNA, and suggest that under many conditions, Lipitoid can

outperform Lipofectamine® for *in vitro* siRNA transfection. However, optimal suppression of protein expression *in vivo* may necessitate extended exposure to the transfection reagent or repeated transfections, as performed in the current study. In both cases, limited toxicity as well as biocompatibility of the transfection reagent are critical. Although toxicity was not the focus of the current study, we have previously demonstrated minimal toxicity in cell culture in response to Lipitoid, in contrast to the observed toxicity of Lipofectamine®.[3-5] These data suggest that Lipitoid may be better suited for sustained dosing. Furthermore, the modular solid phase synthesis of chemically-diverse Lipitoid oligomer sequences facilitate the identification of particular sequence variants that enable optimized siRNA delivery to particular disease tissue types, including the vocal fold. Based on these findings, Lipitoid is likely to prove quite beneficial for siRNA delivery, particularly as the evolution to clinical applications will likely include more demanding protocols and a greater focus on both efficacy and safety at the cellular and organism level.

Summary and Outlook

Delivery of effective concentrations of siRNA to adequately treat pathological processes *in vivo* remains problematic. Transfection efficiency was quite high with Lipitoid as a function of transfection conditions and cell species. Cumulatively, these data are encouraging with regard to the potential utility of this nanoparticle for *in vivo* siRNA delivery. The modular oligomer sequence composition of lipitoids may facilitate variations in physicochemical properties of the transfection reagent to optimize pharmacological attributes and address critical challenges for introduction of siRNA mediated gene silencing to the clinical setting.

Experimental Procedures

Lipitoid Synthesis. Manual solid phase peptoid synthesis of Liptoid was conducted according to previously described procedures and purified by high performance liquid chromatography. [6]

Cell Lines. Several cell types were employed including an immortalized human vocal fold fibroblast cell line developed in our laboratory and referred to as HVOX.[7] Primary rat and rabbit vocal fold fibroblasts were also employed.

Standard Transfection. Cells were grown in 6-well plates to 80% confluency. siRNA and transfection reagent (Lipitoid or Lipofectamine®) were dissolved in 500µL Opti-MEM® (Life Technologies, Carlsbad CA); Opti-MEM is recommended for use with cationic lipid transfection reagents. For standard transfection, siRNA at a concentration of 5µM was combined with 1.00mg/mL Lipofectamine® or 1.07mg/mL Lipitoid. siRNA/lipid solution in reduced serum media (Opti-MEM®) was incubated at room temperature for 20 minutes and 500µL was added to each well containing 1.5mL of Dulbecco's Modified Eagle Medium (DMEM; Life Technologies, Carlsbad CA) with 10% Fetal Bovine Serum (FBS; Life Technologies, Carlsbad CA). The media was then changed to 10% FBS, 1% antibiotic DMEM after six hours. RNA was then harvested at the determined experimental endpoint.

Continuous Transfection. Cells and transfection reagents were prepared as described for Standard Transfection. Cells were then treated with transfection media through the duration of the experiment until the determined experimental endpoint (6, 24, 48, and 72 hours).

RNA Extraction and Quantification. At the appropriate experimental endpoint, RNA was extracted employing the Qiagen RNeasy Kit (Qiagen, Valencia CA). RNA was quantified using the NanoDrop 2000 UV-Vis Spectrophotometer (Thermo Scientific, Wilmington, DE) according to the manufacturer's protocol.

Quantitative Reverse Transcriptase-Polymerase Chain Reaction. The Taqman RNA-to-Ct 1-Step kit (Applied Biosystems, Grand Island, NY) was used to perform quantitative reverse transcriptase-polymerase chain reaction (RT-PCR). Sequences for Smad3 and glyceraldehyde-3-phosphate dehydrogenase (GAPDH) genes were obtained in the form of Taqman gene expression assays (Applied Biosystems). Quantitative RT-PCR (qRT-PCR) was run on the Applied Biosystems ViiA7 Real-Time PCR System, as recommended by the manufacturer. The ΔΔCt method was employed with GAPDH as the housekeeping gene.

Statistical Analyses. All experiments were performed in triplicate, at minimum. Data are presented descriptively as means +/- standard error of the mean (SEM). The dependent variable of interest was subjected to a one way analysis of variance. If the main effect was significant, post hoc comparisons were performed via the Scheffé method. Statistical significance was defined as $p < 0.05$ using StatView 5.0 (SAS Institute, Berkeley, CA).

Appendix 1 References

1. Masotti, A.; Mossa, G.; Cametti, C.; *et al. Colloids Surf. B. Biointerfaces*. **2009**, *68*,136–144.
2. Konca, Y.U.; Kirshenbaum, K.; Zuckermann, R.N. *Int. J. Nanomedicine*. **2014**, *10*, 2271–2285.
3. Utku, Y.; Dehan, E.; Ouerfelli, O.; *et al. Mol. Biosyst.* **2006**, *2*,312–317.
4. Uchida, E.; Mizuguchi, H.; Ishii-Watabe, A.; Hayakawa T. *Biol. Pharm. Bull.* **2002**, *25*,891–897.
5. Yamano, S.; Dai, J.; Moursi, A.M. *Mol. Biotechnol*. **2010**, *46*,287–300.
6. Murphy, J.E.; Uno, T.; Hamer, J.D.; Cohen, F.E.; Dwarki, V.; Zuckerman, R.N. *Proc. Natl. Acad. Sci. USA*. **1998**, *95*,1517– 1522.
7. Branski, R.C.; Barbieri, S.S.; Weksler, B.B.; *et al. Ann. Otol. Rhinol. Laryngol*. **2009**, *118*,218–226.

Appendix 2

Design, Synthesis, and Purification of Next Generation Lipitoid Variations

Introduction

Motivated by the *in vitro* and *in vivo* transfection success of the Lipitoid, we then sought to create variations of this design. **Lipitoid** was, in fact, just one of 22 of different sequences chosen during its initial development in the late 1990's.[1] **Lipitoid** was chosen as an optimal sequence with which to begin transfection experimentation because of its exceptional performance during *in vitro* trials concerning DNA transfection efficiency in HT1080 cells as well as its ability to protect the nucleic acid cargo from hydrolytic cleavage.[1] However, several other designs, which vary from **Lipitoid** in terms of the hydrophobic side chains presented and/or the lipid tail displayed at the N-terminus of the peptoid. **(Table 2)**

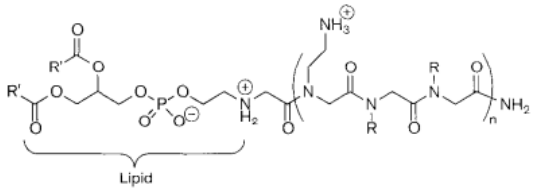

	Lipid*	R	n†	Designator‡	Molecular weight Calculated	Molecular weight found§
11	DMPE	2-Phenethyl	3	DMPE-$(NaeNpeNpe)_3$	1960.5	1959 .5
12	DMPE	(*S*)-1-phenylethyl	3	DMPE-$(NaeNspeNspe)_3$	1960.5	1959.6
13	DMPE	*p*-MeO-phenethyl	2	DMPE-$(NaeNmpeNmpe)_2$	1658.1	1658.0
14	DMPE	*p*-MeO-phenethyl	3	DMPE-$(NaeNmpeNmpe)_3$	2140.7	2139.7
15	DMPE	*p*-MeO-phenethyl	4	DMPE-$(NaeNmpeNmpe)_4$	2623.2	2622.0
16	DMPE	*p*-MeO-phenethyl	8	DMPE-$(NaeNmpeNmpe)_8$	4553.5	4551.3
17	DMPE	*p*-MeO-phenethyl	12	DMPE-$(NaeNmpeNmpe)_{12}$	6483.8	6480.8
18	DOPE	*p*-MeO-phenethyl	3	DOPE-$(NaeNmpeNmpe)_3$	2248.8	2248.0
19	DMPE	Pentyl	3	DMPE-$(NaeNpnNpn)_3$	1756.4	1755.4
20	DOPE	2-Methylbutyl	3	DOPE-$(NaeNmbNmb)_3$	1864.5	1864.4
21	DMPE	3-Methylbutyl	3	DMPE-$(NaeNiaNia)_3$	1756.4	1755.5
22	DOPE	3-Methylbutyl	3	DOPE-$(NaeNiaNia)_3$	1864.5	1864.3

Table 2. Lipitoid variations created by the Zuckermann Laboratory in 1998.[1] **Lipid abbreviations**: phosphatidylethanolamine; DOPE, dioleoyl phosphatidylethanolamine. phosphatidylethanolamine; DOPE, dioleoyl phosphatidylethanolamine. Note that the values of n also represent the number of formal positive charges on each lipitoid. **Submonomer abbreviations**: Nae, *N*-(2-aminoethyl)glycine; Nap, N-(3.amino-propyl)glycine; Npe, *N*-(2-phenylethyl)glycine; Nspe, *N*-[(S)-1 -phenylethyllglycine; Nmpe, *N*-[2-(4'.methoxylphenyl)ethylglycine; Npn, *N*-pentylglycine; Nmb, *N*-(2-methylbutyl)- glycine; Nia, *N*-(3-methylbutyl)glycine; § denotes analysis by electrospray mass spectrometry. ND, indicates the mass was not determined.

Four sequences, designed with the same pattern of cationic-hydrophobic-hydrophobic peptoid trimeric repeats, exhibit comparable and even superior transfection capabilities, incorporating pentyl and methylbutyl isomers and some substituting DMPE for the DOPE lipid moiety. Ultimately, Zuckermann *et. al.* concluded that aromatic, not

alkyl side chain peptoid functionalities, formed stronger complexes with the therapeutic nucleic acids and thereby protecting the cargo from degradation, presumably due to the large and planar aromatic rings intercalating between the base pairs and stabilizing the DNA polyplexes.

Note that since this last study progress has been made on the design and testing of a new generation of lipitoid sequences, and we hypothesize that lipitoids incorporating both alkyl and aromatic functionalities could potentially yield better transfection efficiency while forming stronger nanoparticle complexes with genetic cargo. Transfection has been shown to be sensitive to many experimental factors including, but not limited to: cell or tissue type, origin of cell type, and siRNA sequence.[1-4] Therefore, it is reasonable to postulate, that while **Lipitoid** has proven itself a general transfection workhorse, other sequences could be designed to tailor our transfection reagent to the specifications of the experiment.

Results and Discussion

With these details in mind, 9 variations of **Lipitoid,** lipitoids **1**-**8**, based off of the success of a few of the original Zuckermann library members from 1998 (**See Table 3** and **Figure 56**). **Lipitoids 1**-**6**, change the patterning and identity of some of the hydrophobic groups in the peptoid head portion, while **Lipitoids 7** and **8** swap 1,2-dimyristoyl-sn-glycero-3-phosphoethanolamine (DMPE) for 1-palmitoyl-2-oleoyl-sn-glycero-3-phosphoethanolamine (Pope) or 1,2-dipalmitoyl-sn-glycero-3-phosphoethanolamine (DPPE). With these 8 **Lipitoid** variations in hand, our goal is to test them for transfection efficiency of the SMAD3 siRNA in various cell types and origins. Promising sequences will go on to *in vivo* trials to potentially improve on our

initial successes with SMAD3 knockdown from localized delivery of SMAD3 siRNA to injured leporine vocal folds (See **Chapter 3.4**).

Lipitoid Sequence	Lipid	Trimer.1 (N-Term)	Trimer.2	Trimer.3 (C-term)
Lipitoid	DMPE	Cat-Mph-Mph	Cat-Mph-Mph	Cat-Mph-Mph
1	DMPE	Cat-*iPt*-Mph	Cat-*iPt*-Mph	Cat-*iPt*-Mph
2	DMPE	Cat-*iPt-iPt*	Cat-Mph-Mph	Cat-*iPt-iPt*
3	DMPE	Cat-Mph-Mph	Cat-*iPt-iPt*	Cat-Mph-Mph
4	DMPE	Cat-*Pen*-Mph	Cat-*Pen*-Mph	Cat-*Pen*-Mph
5	DMPE	Cat-*Pen-Pen*	Cat-Mph-Mph	Cat-*Pen-Pen*
6	DMPE	Cat-Mph-Mph	Cat-*Pen-Pen*	Cat-Mph-Mph
7	*POPE*	Cat-Mph-Mph	Cat-Mph-Mph	Cat-Mph-Mph
8	*DPPE*	Cat-Mph-Mph	Cat-Mph-Mph	Cat-Mph-Mph

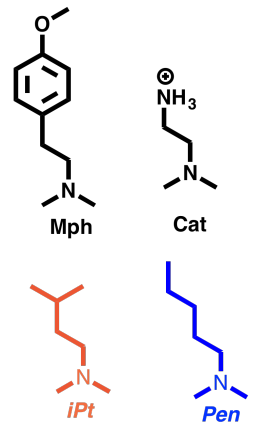

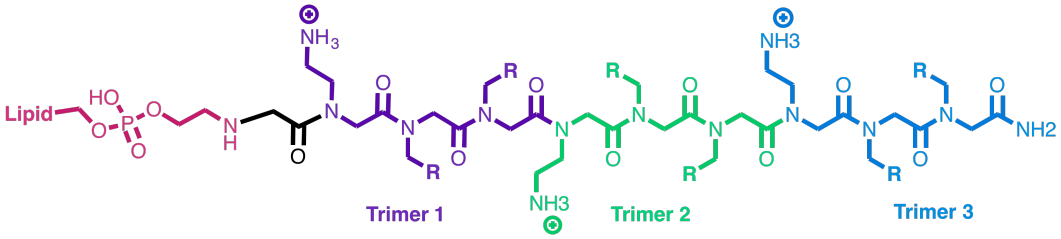

Table 3. Table of first generation **Lipitoid** and second generation sequence identities. (top).

Figure 56. Basic stucture of the **Lipitoid** variants, classified according according to their trimeric repearts by color. (bottom)

*Synthesis and Purification of **Lipitoids 1-8***

All **Lipitoids** were synthesized according to the same modified protocol as presented in **Section 3.3**. The protocol alteration of changing the reaction vessel from plastic syringe to glass scintillation vial when performing the lipid displacement (as described previously) was applied to the synthesis of this library as well. While the synthetic protocols for the variants were identical, the analytical HPLC methods and

purifications were unique to some of the sequences, probably due to the change in hydrophobicity of the peptoid head groups as well as the lipid tails, as witnessed by their extremely late HPLC retention times. Crude analytical traces, shown below, display varied levels of purity, and a few demonstrated the same high level of purity obtained from our crude **Lipitoid**. (**Figure 57**) It seems that varying the lipid group as well as altering the patterning and identity of the peptoid sequence directly affects the progress of the reaction to produce an HPLC spectrum consistent with a discrete product. Modifying the lipid groups, as executed in **Lipitoids 7-8** whose coupling efficiencies are sensitive to solvent conditions,[1] could be the source of impurities seen in the analytical spectra. Yet **Lipitoids 5** and **6**, bearing the same DMPE group as **Lipitoid** and **Lipitoid 2-4**, are visibly less pure. **Lipitoids 5** and **6** are designed with the two adjacent pentyl side chains and one amino propyl side chain in either one or two of the trimeric units contained in the peptoid portion of the sequence, flanking the termini, in the case of two repeats or sandwiched between two of the other units. Alkyl amines typically behave very well in peptoid synthesis,[5] so most likely the pentylamine, stored under ambient conditions, had begun to oxidize to the N-oxide derivatives.[6]

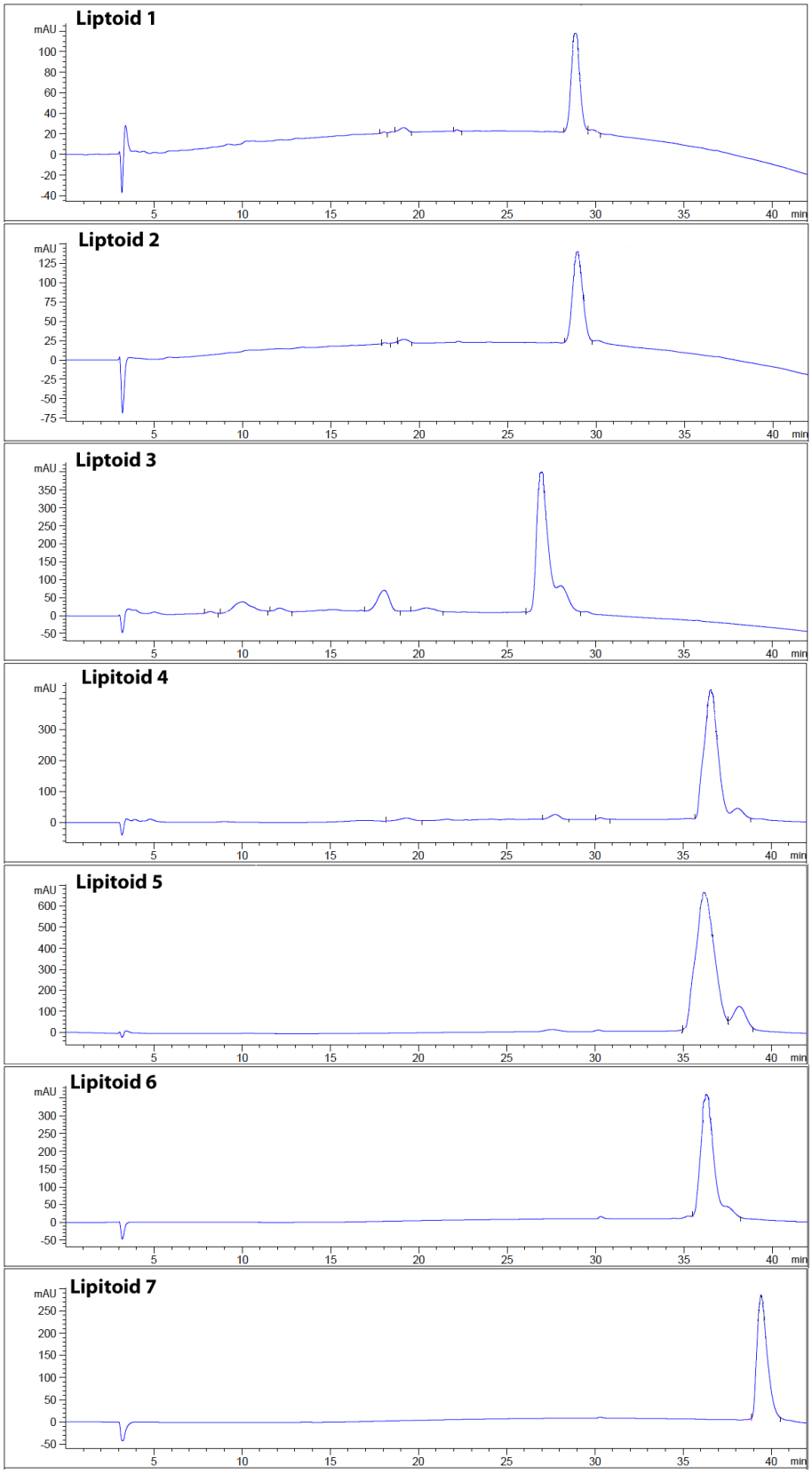

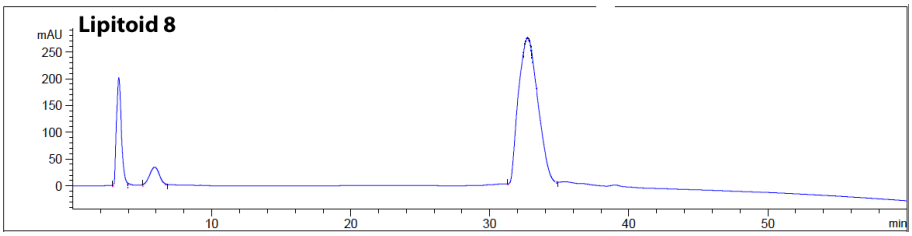

Figure 57. Crude RP-HPLC analytical spectra of **Lipitoid** sequences **1-8.** Lipitoids were analyzed with a linear gradient of acetonitrile in water (0.1% TFA) at a flow rate of 500 μL/min. Individual solvent gradients and analysis times varied depending on the sequence tested. See **Methods and Materials** for details.

In assays to affirm cell viability and Smad3 gene knockout using crude lipitoids, crude **Lipitoid** was tested in human fold fibroblasts against purified **Lipitoid** using an MTT assay and Smad3 RT-PCR. (**data not shown**) Establishing that crude compounds were practically as effective a transfection reagent as purified compounds, we bypassed the purification for **Lipitoids 1-4**,**8** which were generally of good purity immediately following cleavage from the resin. (**Figure 57**) Purification of the **Lipitoids** was a time-intensive effort, and we rationalized that by testing library members which contained relatively low amounts of impurities, we could perform a quick screen of their ability to obtain a simple yes/no readout on the transfection capability of these compounds. In the event that any of the sequences demonstrated a remarkable performance in comparison to **Lipitoid**, we would purify the sequence for further analysis and testing. Because **Lipitoids 5-7** exhibited excessively impure analytical traces, **Lipitoids 5-7** were purified using RP-HPLC to >95 % and the identity of each lipitoid variant was verified by MALDI-TOF/TOF spectrometry. (**Figures 58**) Sufficiently pure **Lipitoids 1-8** were given to the Branski Laboratory as lyophilized powders for *in vitro* testing.

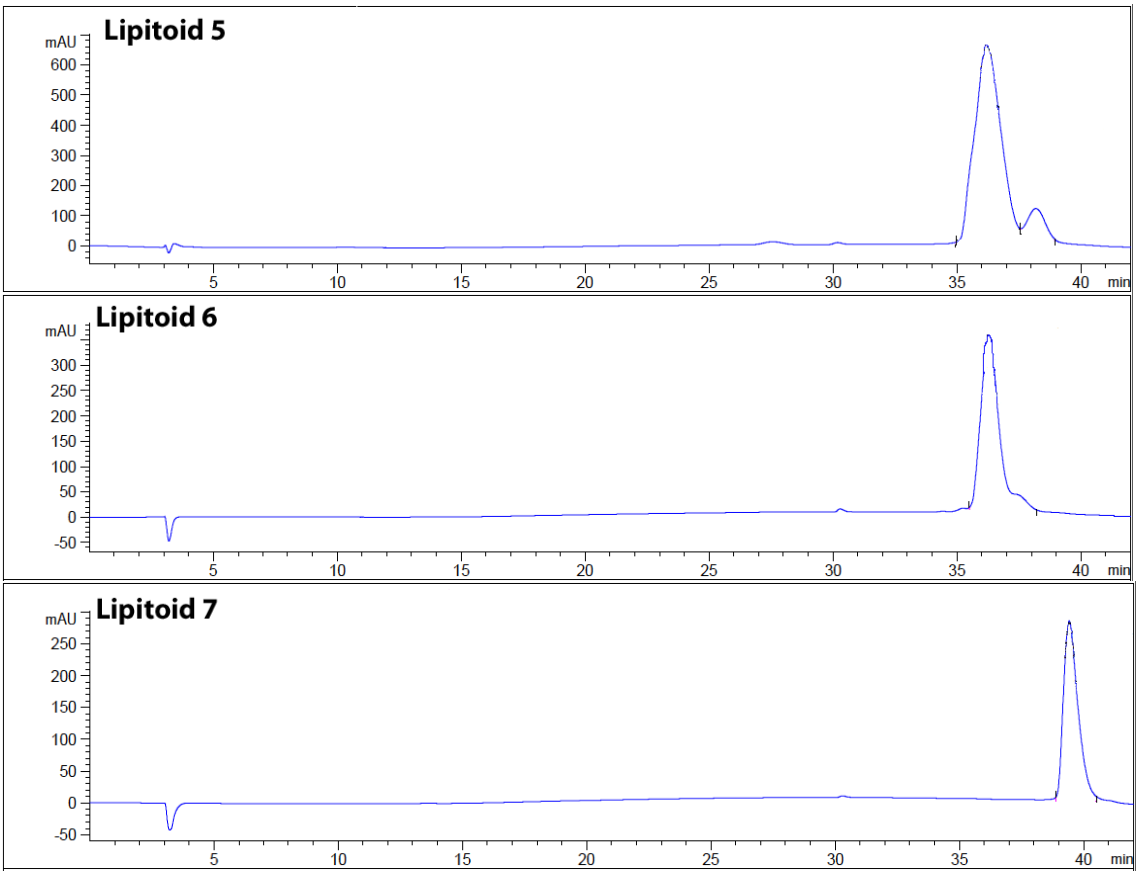

Figure 58. Purifed analytical HPLC traces of **Lipitoids 5-7**.

In some crude and purified samples, **Lipitoids 3-6** , a small, broad peak elutes immediately following the product peak. MALDI-MS analysis of these peaks show this to be the potassium complex of the desired lipitoid. This complex originates from the desalting procedure of the hydrochloride salt of the phosphotidylethanolamine prior to use in peptoid synthesis. 11 M KOH is employed to alter the pH of the phospholipid solution, removing the proton from the primary amine handle, rendering the primary amine active for nucleophilic attack and creating water as a byproduct. KCl**,** insoluble in 15% methanol in chlorobenzene, precipitates from solution, and evidently is difficult to remove the last traces of precipitate when working with volumes as small as 1 mL.

Experimental Procedures

Lipitoid Synthesis and Characterization

Materials:

Synthesis of the peptoid and peptide oligomers was initiated on Rink Amide resin (Nova Biochem, 100-200 mesh, loading: 0.74 mmol/gram). Bromoacetic acid (97%) was supplied by Sigma-Aldrich. Trifluoroacetic Acid, TFA, (99%), N,N-Dimethylformamide, DMF, (anhydrous and amine free, 99.9%) and N,N' diisopropylcarbodiimide, DIC, (99%) were supplied by Alpha Aesar. Pentylamine, 2-(4′-methoxyphenyl)ethylamine, isoamyl-amine, and ethylenediamine were purchased from Sigma Aldrich. Lipids were purchased from either Avanti Polar Lipids (Avanti Polar Lipids, Inc.) or Sigma Aldrich. Other reagents and solvents were obtained from commercial sources and used without additional purification.

Lipitoid Synthesis. Synthesis of the **Lipitoid** was conducted on solid phase according to previously described procedures according to a modified submonomer synthesis approach[62] and purified via high-performance liquid chromatography. Rink Amide Resin, 100 mg (0.074 mmol), was swelled in DMF for 30 minutes before initiating the synthesis. Bromoacetylation was carried out by incubating the resin with a bromoacetic acid solution in DMF (1.2M, 850 μL) and DIC (200 μL) for 20 minutes at room temperature and an agitation rate of 220 rpm. The resin was washed with 4x 1 mL DMF before displacement with the desired primary amine (1M in DMF) for 30 minutes at room temperature and an agitation rate of 220 rpm. The resin was washed with 5x 1 mL DMF. This two-step iterative process was repeated until the desired oligomer chain length and

monomer sequence composition was achieved before the addition of the lipophosphotidylethylamine. Prior to lipid addition, the peptoid sequence was bromoacetylated once more, and the resin washed and transferred to a glass scintillation vial. A 0.2M solution of **lipid** was prepared in 15% methanol/chlorobenzne and to it was added 0.95 eq. of 11M KOH. The solution was centrifuged, and the supernatant removed and to the scintillation vial containing the resin. Resins were exposed to the **lipid** solution for roughly 16 hours while shaking at 37°C. The resins were then washed copiously with 15% methanol/chorobenzene and after with 5 x 1mL DMF and 5 x 1mL DCM. The **Lipitoid** was cleaved from the resin using a cocktail containing 95% TFA, 2.5% TIPS, and 2.5% water (4 mL) at room temperature for 10 minutes. The solution was removed under reduced pressure, and the crude peptoid was re-suspended in acetonitrile/water, frozen, and lyophilized. Once thoroughly dried, crude **Lipitoid** was stored at 4°C until characterization and purification.

*Characterization and Purification of **Lipitoids 1-8**.* Lyophilized powders were suspeneded in a solution of aqueous acetonitrile then analyzed by MALDI-TOF/TOF and analytical RP-HPLC. **Lipitoids** were purified to >95% using a preparatory C_4 column. HPLC was on a Waters 2489 instrument using a Phenomenx Jupiter C_4 column (Phenomenex, 15 μm, 300 Angstroms, 10x250 mm). **Lipitoids** was detected at 220 nm during a linear gradient of 15-45% aqueous ACN with 0.1% TFA over 60 minutes at a flow rate of 5 mL/min. Fractions were consolidated, frozen, and lyophilized. Once dried, purified **Lipitoids** were stored at 4°C until analysis and *in vitro* and *in vivo* testing. Purity was assessed by reverse-phase HPLC (DeltaPak analytical C_4 column, Waters, 5 μm, 300 Angstroms, 3.9x150 mm) on an Agilent 1260 Infinity LC system. A linear

gradient of 20-80% acetonitrile in water (0.1% TFA) over 40 min. was used at a flow rate of 500 μL /min. Mass spectrometry was performed on an Agilent 1100 series LCMSD VL MS spectrometer or a Bruker Maldi-TOF TOF UltrafleXtreme MS Spectrophotomer using a saturated solution of α-Cyano-4-hydroxycinnamic acid prepared in 70% ACN(aq) with 0.1% TFA

Appendix 2 References

1. Huang, C.-Y.; Uno, T.; Murphy, J.E.; Lee, S.; Hamer, J.D.; Escobedo, J.A.; Cohen, F.E.; Radhakrishnan,R.; Dwarki, V.; Zuckermann, R.N. *Chemistry & Biology*. **1998**, *5,* 345–354.
2. Akhtar, S. and Benter, I.F. *The Journal of Clinical Investigation*. **2007**,*117*, 623-3632.
3. Murphy, J.E.; Uno, T.; Hamer, J.D.; Cohen, F.E.; Dwarki, V.; Zuckerman, R.N. Proc. Natl. Acad. Sci. USA, **1998**, *95*,1517– 1522.
4. Schiffmacher, A.T. and Keefer, C.L. *In Vitro Cell Dev. Biol. Anim*. **2012**, *48*, 403–406.
5. Culf, A.S. and Oulette, R.J. *Molecules*. **2010**,*15*, 5282-5335.
6. Aleksandrov, A.L. *Russ. Chem. Bull*. **1980**, *29*,1740.

Appendix 3

Additional Data and Experiments from Metal Binding Studies in Chapter 4: Rapid Identification of Nickel-binding Peptoid Oligomers by On-Resin X-ray Fluorescence Screening

Figure 59. Snapshot of a standard XRF spectrum from a resin-bound library member observed during MXRF® analysis. The X-axis denotes photon energy (keV), while the Y-axis represents Pulses / second / eV. The characteristic x-ray fluorescence energies for the atoms of interest (*Kα* and K_β lines for Co-Zn, and *L* emission line for I) are labeled in color. The large iodine signal at 3.94 keV, indicates the presence of peptoid on the bead.

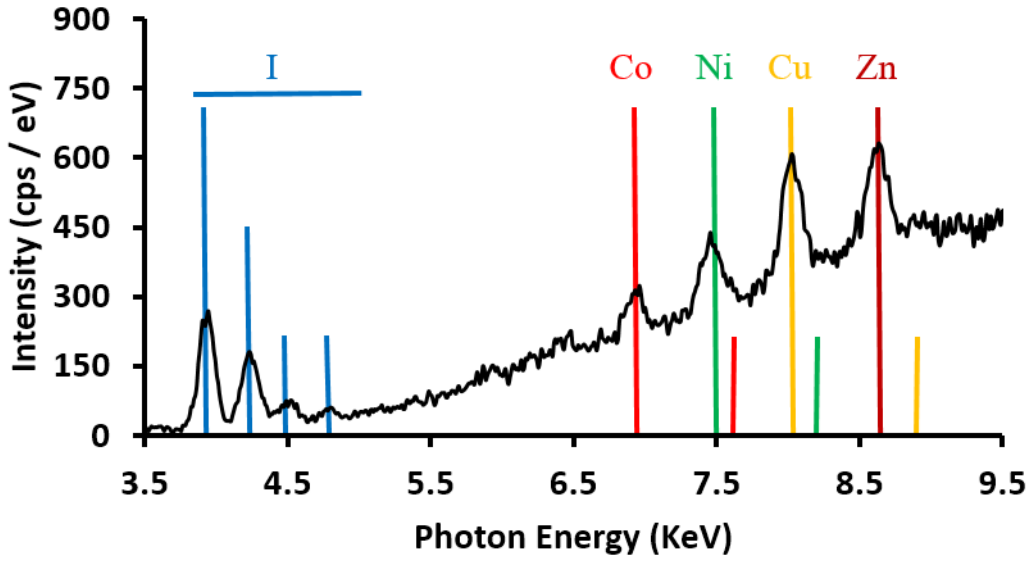

Figure 60. Depiction of the full 35-member peptoid oligomer library which was synthesized and used in the MXRF® screening. All library members are between 4-9 monomers in length. The 4-iodobenzyl sidechain, is included at either the C- or N-terminus of each peptoid oligomer for quantification purposes.

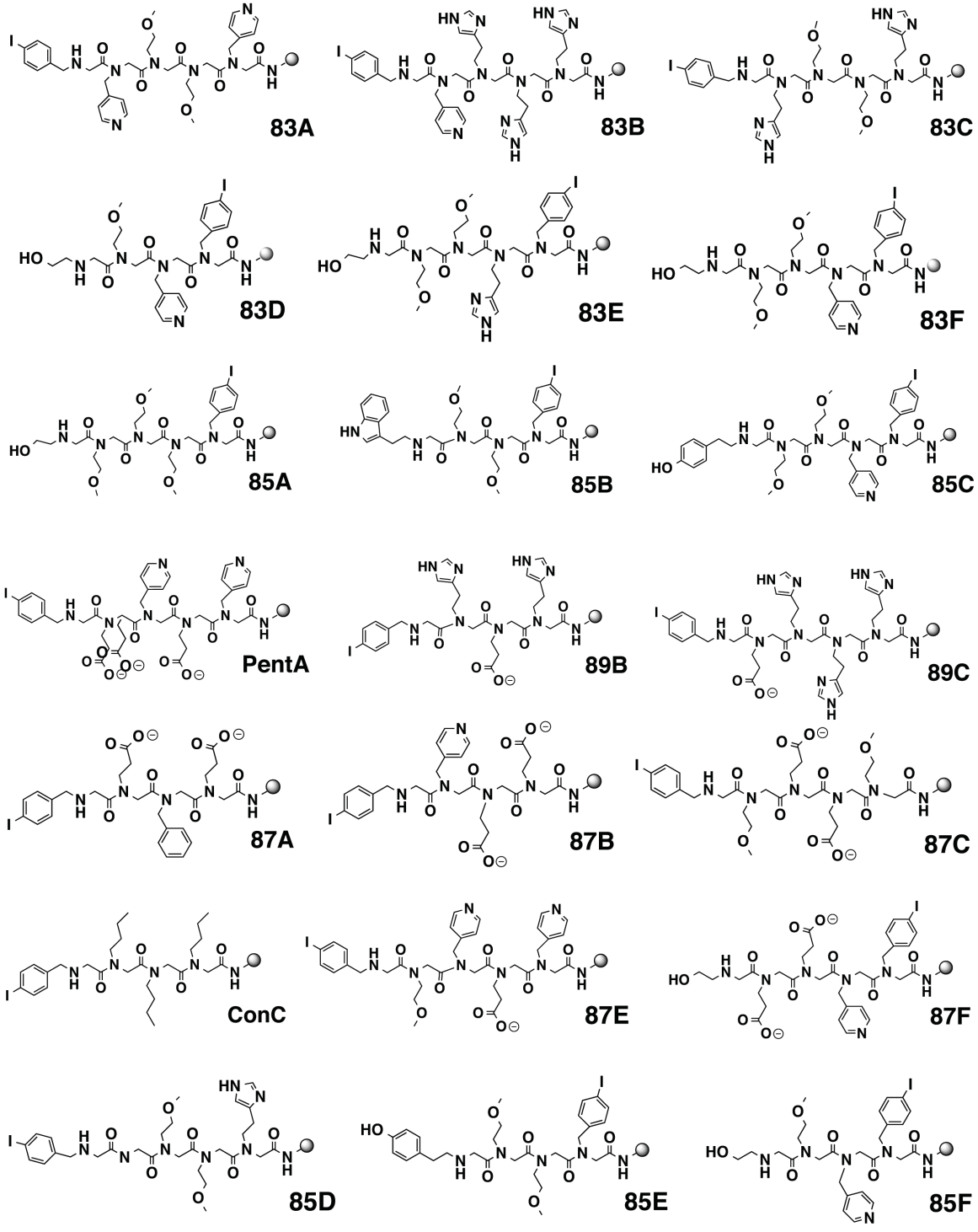

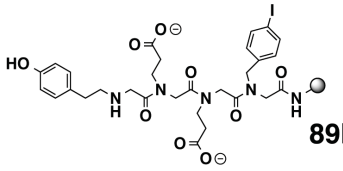

89D

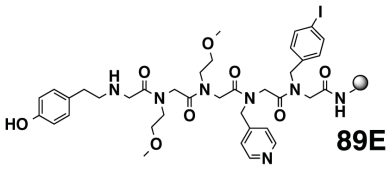

89E

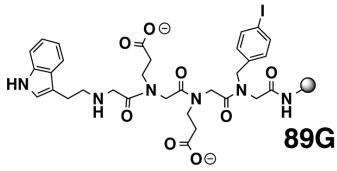

89G

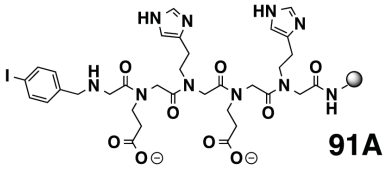

91A

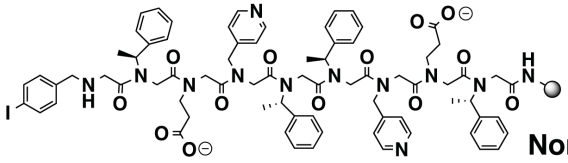

NonaB

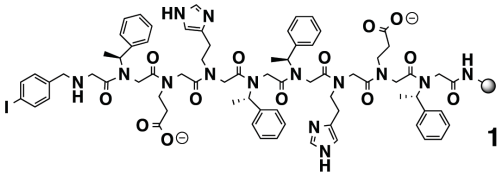

101B

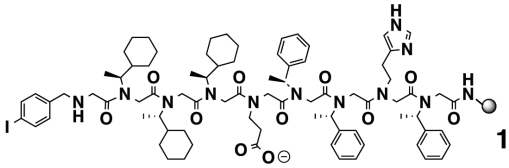

101C

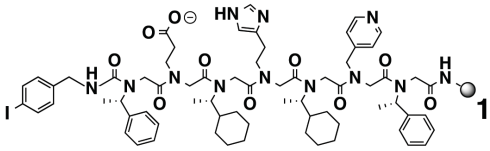

103C

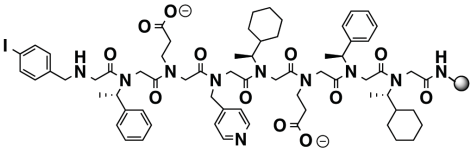

103D

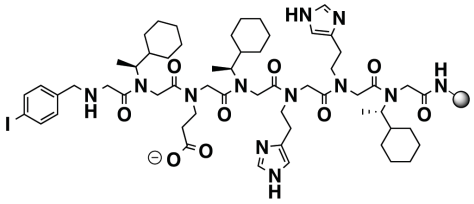

103A

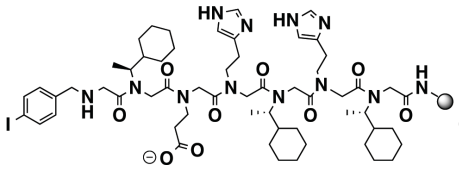

103B

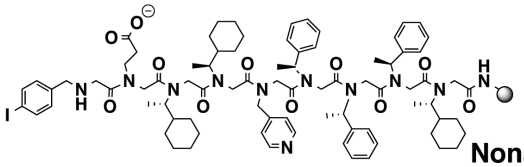

NonaD

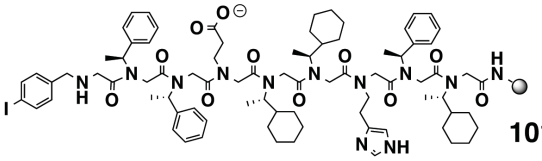

101E

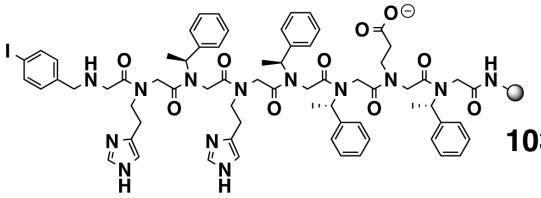

103E

Validation of Library Synthesis

Synthesis of library members was conducted using submonomers that have been previously validated for reproducible solid phase peptoid synthesis at high yield. Syntheses including these submonomers are typically obtained with purities ~90%.[1,2] Completion of each iterative synthetic step on Tentagel Resin was monitored via chloranil test[4], and the identity of the library members was validated by matched synthesis on Rink Amide resin, cleavage, and characterization by ESI-MS and RP-HPLC. Representative characterization data from crude library member **PentA**, is provided below (**Figure 61**).

Figure 61. RP-HPLC trace of crude **PentA** at 214 nm, shown to be >90% purity, with ESI-MS characterization data (inset).

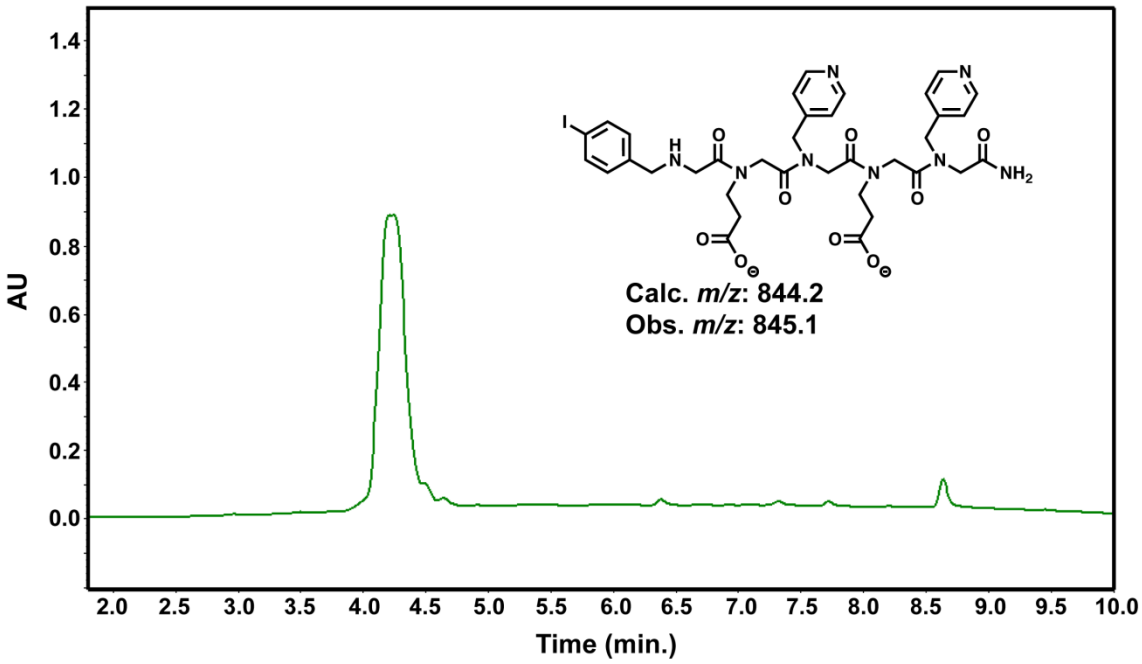

Figure 62. Data from two additional MXRF® analyses with sequences **PentA** and **NonaB** and controls **ConC** and **ConTG**. Each graph plots the metal to iodine ratio of fluorescence intensity (M:I) against the two wells that contained the sequence. Within each well, M:I are distinguished by separating the specific bead (1-4) that the M:I originated from. Some run-to-run variations in M:I fluorescence signal intensity were observed, but the overall pattern of relative M:I values for different metal species were consistent. These results identify **PentA** and **NonaB** as strong nickel binders, while controls **ConC** and **ConTG** do not demonstrate ability to complex any of the metal species tested.

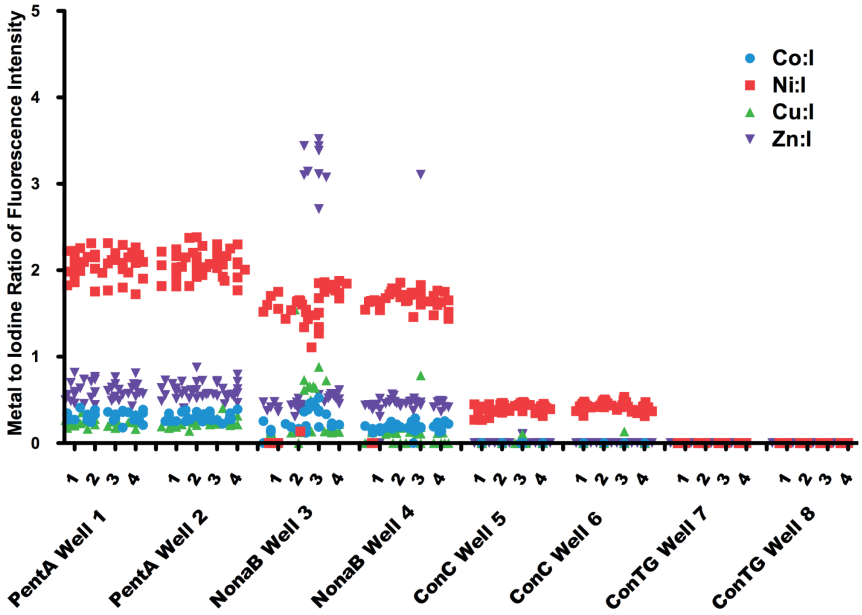

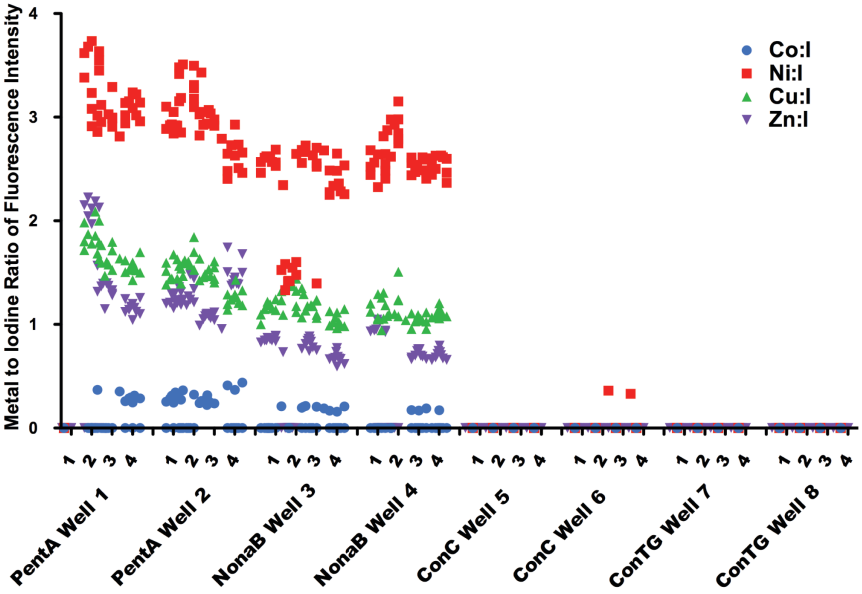

Solution Phase Binding Experiments

Once liberated from solid support and purified (**See Appendix A: Preparation of Peptoid Oligomers on Rink Amide resin for experimental details**), we attempted to characterize **89A** and **101A**'s ability to complex nickel. Uv/vis, ^{1}H NMR, and MS spectroscopy as well as HPLC analysis were conducted as methods of verification of a binding event.

First attempts at solution-phase binding were conducted in 100% HPLC grade water with sequence **89A** (108 uM) in a 1 cm path length quartz cuvette scanning from 190-800 nm. 1 equivalent (relative to the peptoid) of $Ni(NO_3)_2$ (Tris buffered to pH 8) was added and the solution was stirred to equilibrate. Spectra were taken every three minutes until no change was observed. This process was repeated for the 2nd and 3rd equivalent of metal. Upon addition of nickel, changes at 229 nm (appearance of a shoulder) 240 nm (disappearance) and 257 nm (decrease in magnitude) were observed, corresponding to the pyridyl and carboxylate functionalities. This was conducted for up to 4 full equivalents of nickel with potential saturation at 229 occurring at 3 equivalents (**Figure 63**).

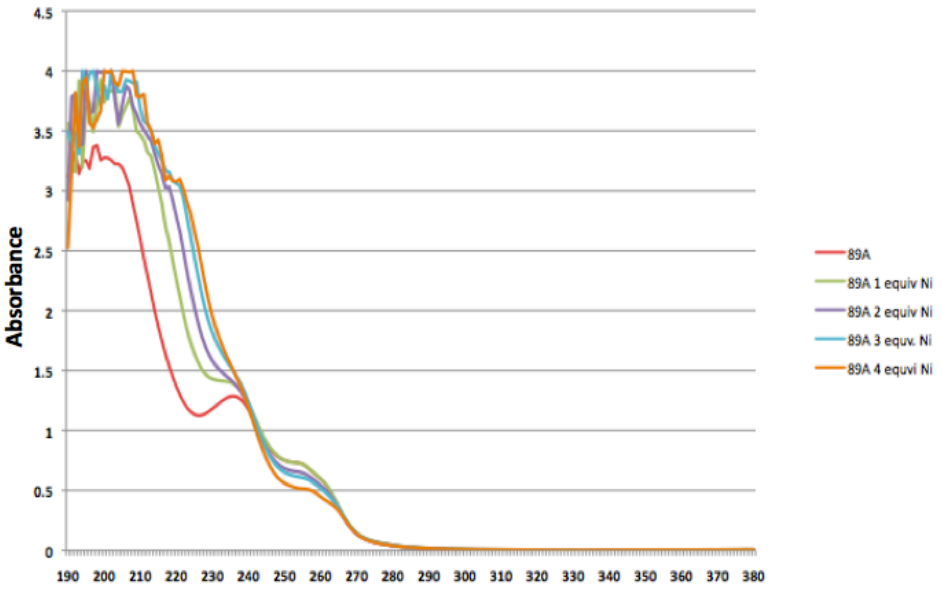

Figure 63. Uv/vis plot of the titration of Ni^{2+} into a 108 uM solution of **89A**.

Because sequence **101A** is not soluble in Tris buffer, the first binding attempts with this sequence were conducted in aqueous 30% acetonitrile at a concentration of 108.26 uM. The titration procedure outlined for sequence **89A** was repeated and similar spectral changes were observed. The change at 229 nm appeared to be a reliable monitoring wavelength, and the concentration for the next experiment was adjusted to 48 uM so that the detection limit would not be reached as quickly. The next experiment conducted the Nickel titration up to 13 equivalents, and this was compared to 13 equivalents of metal added to a 30% acetonitrile solution without any peptoid (**Figure 64**). Unfortunately, this experiment revealed a very large increase in the absorbance at 229 nm without any peptoid, so this wavelength was determined to be unfit for monitoring.

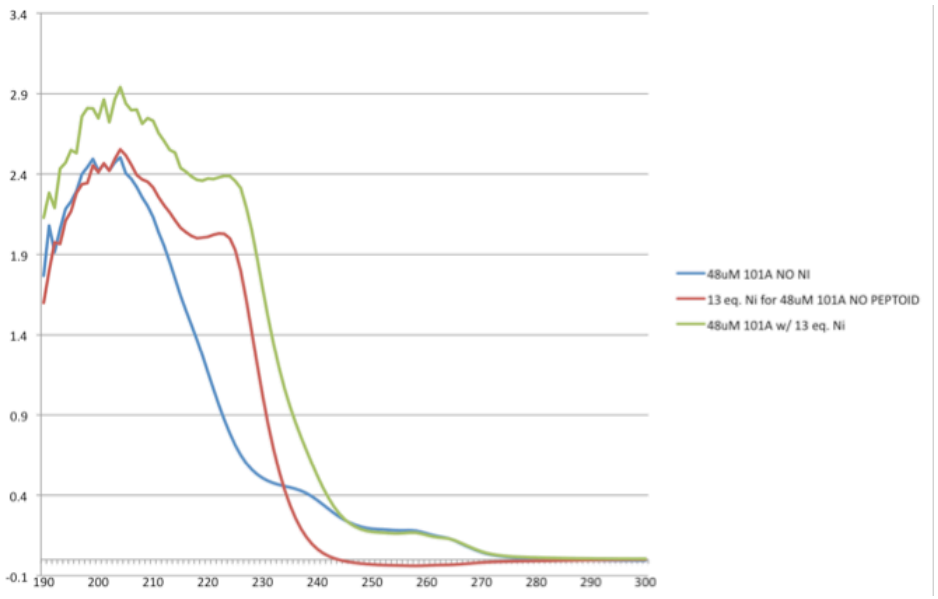

Figure 64. Uv/vis plot of the titration of Ni^{2+} into a 48 uM solution of **101A** showing without nickel (blue), with 13 equivalents of nickel relative to peptoid (green), and with 13 equivalents of nickel and without peptoid (red).

Instead, job plot analysis at 257 nm turned up something that looked to be either a 1:1 and/or a 1:~3 peptoid:metal stoichiometry (**Figure 65**). However, attempts to reproduce the data were unsuccessful, and we hypothesized that either evaporation of the solvent was occurring or that more control was needed over the pH.

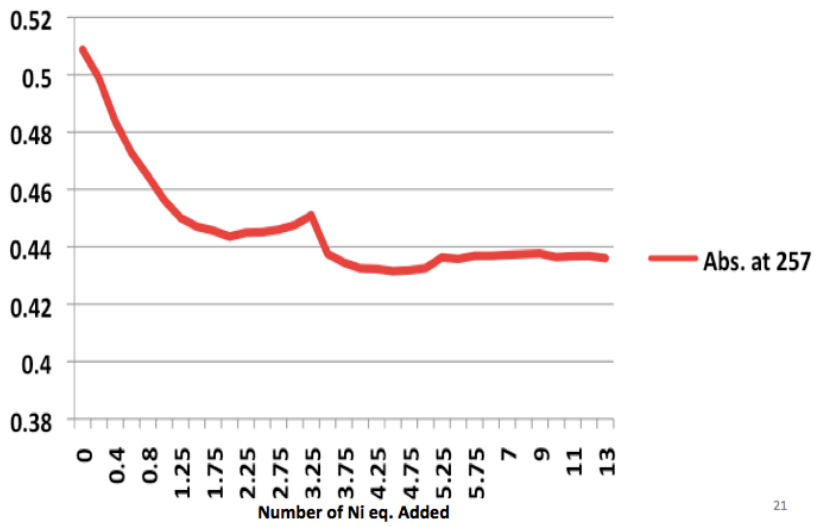

Figure 65 Job plot analysis of the Uv/vis titration at 257 nm of Ni^{2+} into a solution of **101A** in 30% aqueous acetonitrile. The data suggest a 1:1 and/or a 3:1 stoichometry.

Next, the solvent system for titration was changed to a 4:1 solution of methanol: water following previous metal binding work from our lab on a similar sequence.[5] **101A** was dissolved to a final concentration of 17 uM and the titration conducted up to 2 equivalents of metal, with a consistent increase at 257 nm (**Figure 66**.

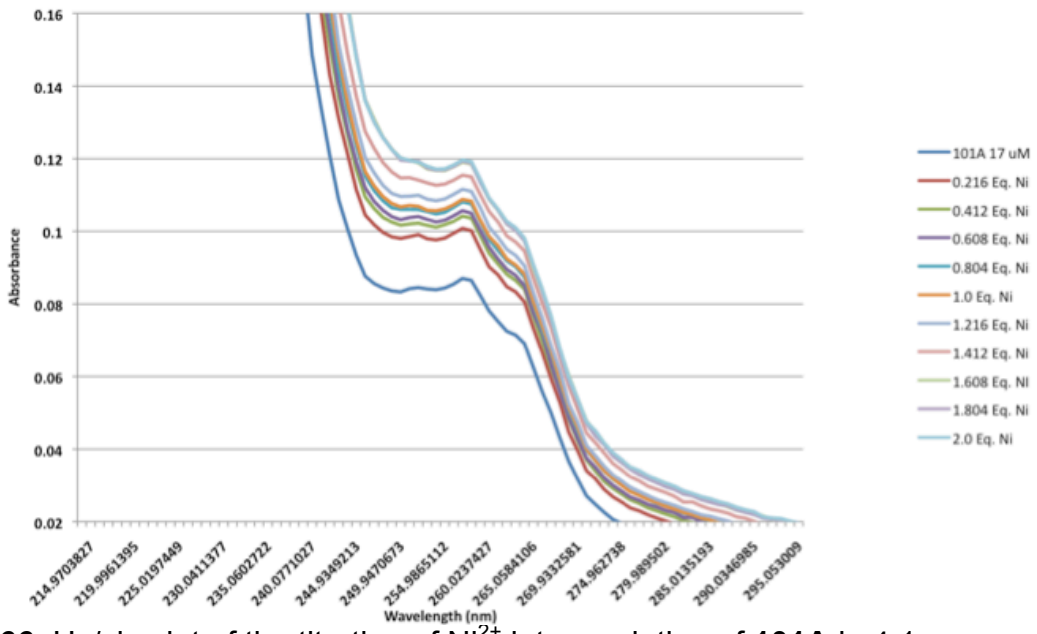

Figure 66. Uv/vis plot of the titration of Ni^{2+} into a solution of **101A** in 4:1 methanol:water. Here, the data shows an increase in absorbance at 257 nm, in contrast to the previous studies in 30% aqueous acetonitrile.

Yet, when the experiment was repeated the results were irreproducible, and an appreciable amount of solvent appeared to be vanishing as the titration progressed. Finally, to test the evaporation theory, 15 separate solutions of **101A** were prepared in 1 dram vials and each added a different amount of metal from 0-3 equivalents in 0.2 equivalent increments to represent the solution at the differing stages of titration. Each vial was sealed to prevent evaporation. Analysis of each of the vials was taken after 3 and 22 hours and compared on job plot analysis at 257 nm (**Figure 67)**. The two spectra show little deviation from each other, and the changes in the absorbance at 257 nm are noisy and slight. I concluded here that the previous increase at 257 nm was the

result of solvent evaporation, and that 257 was not a reliable wavelength to monitor at either.

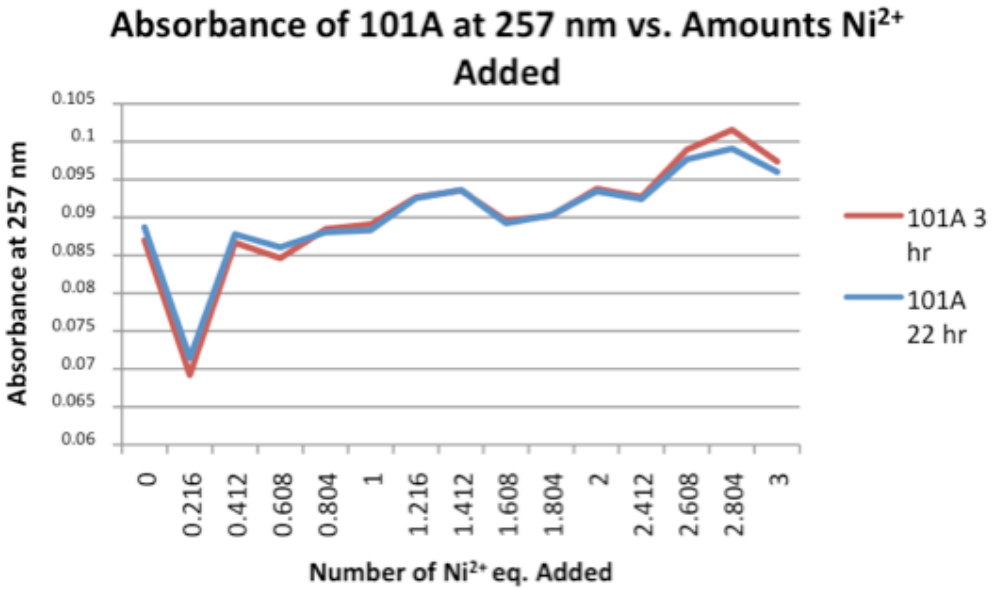

Figure 67. Job plot of the dram vial nickel binding experiment at 257nm between **101A** and Ni^{2+}. Each 0.2 equivalent of metal represents an experiment conducted in a separate, sealed dram vial with that corresponding amount of metal over the course of 22 hrs. The results are fairly reproducible over almost 24 hrs., indicating that the increase at 257 in the previous experiment was due to evaporation of the solvent.

Thinking that perhaps the pH instability was the culprit of a lack of binding readout, **101A** was then dissolved first in a minimal amount of 30% acetonitrile, then diluted into 50 mM N-ethyl morpholine buffer (pH 7) to afford a final peptoid concentration of 1mM. The titration protocol was modeled after Kritzer's work.[6] The titration was carried out in 0.1 molar equivalents (relative to peptoid) with a solution of $NiCl_2$. After each addition, the solution was allowed 3 minutes to equilibrate while

stirring, and then the spectrum was acquired while scanning wavelengths 190-800nm, with special attention paid from 300-600 nm to witness the Nickel d-d transitions at ~385 nm. However, after 0.1 equivalents of Ni was added a white, cloudy precipitate formed in the cuvette. This precipitate was isolated and MALDI and analytical HPLC analysis was conducted on it with the hope that this could be an insoluble metal:peptoid complex. However, MALDI analysis only revealed the sodiated peptoid, and HPLC traces matched those of the pure sequence (**Figure 68)**. The work was repeated by first dissolving **101A** in 50:50 isopropanol: water mixture to try and tune the solubility, but the precipitation occurred immediately upon metal exposure.

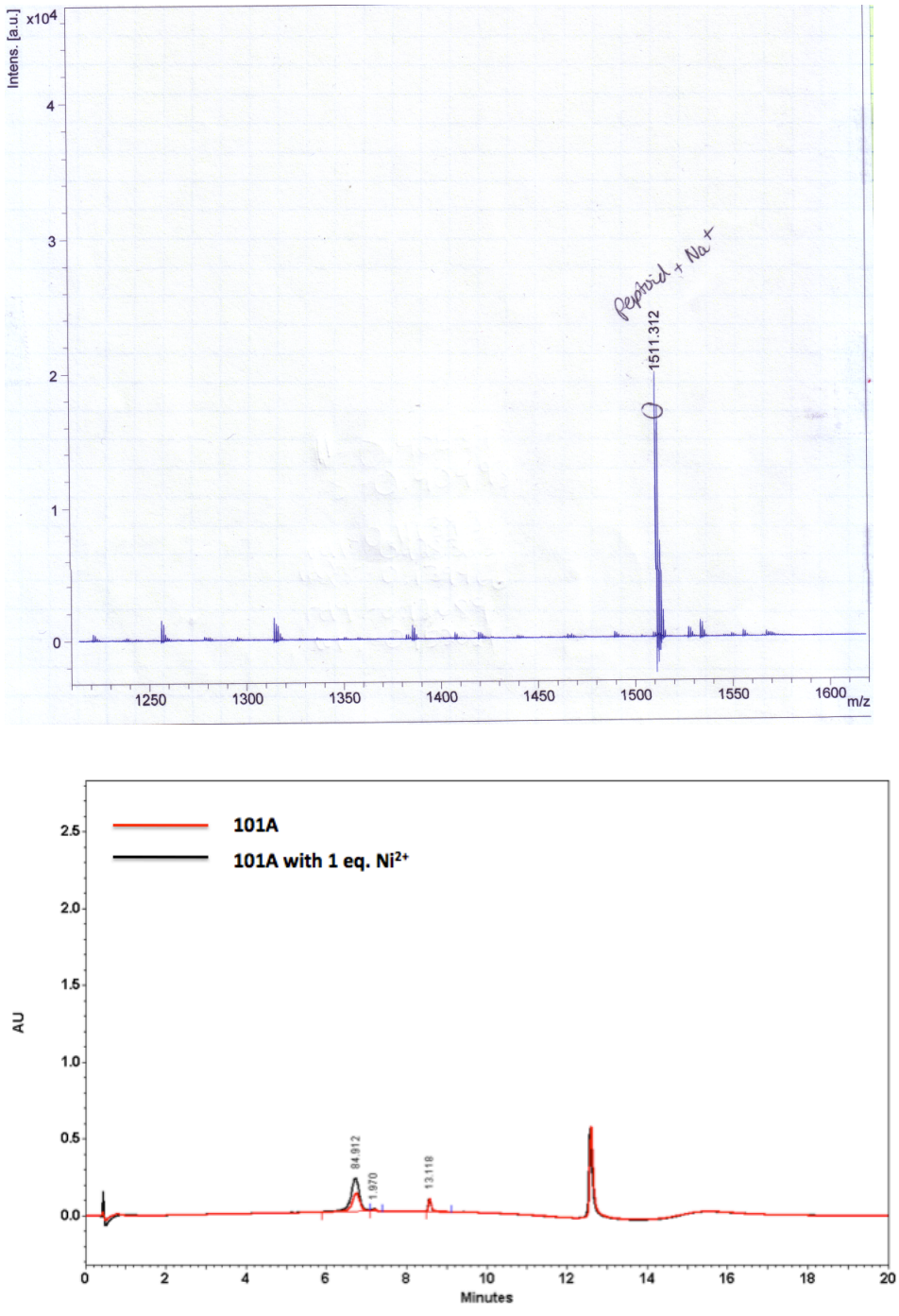

Figure 68. MALDI and analytical HPLC analysis of the isolated precipitate from the nickel binding experiments between **101A** and Ni^{2+} in aqueous buffered solution. The MALDI mass corresponds to the sodiated peptoid, while the HPLC trace (black)

aligns with that of the pure peptoid (red). These data prove that the precipitate formed was the insoluble peptoid.

In a final attempt to witness binding with **101A**, the sequence was dissolved in deuterated methanol to a concentration of 4.45mM and subjected to ^{1}H NMR. Spectrum was acquired before and after addition of 1 and 2 equivalents of $NiCl_2$ was added to the NMR tube. No change was observed after adding either 1 or 2 equivalents of Ni^{2+} to the peptoid solution (**Figure 69**). A binding event to Ni^{2+} should have been apparent with a **downfield** shift of the protons near the binding center as well as a coalescence of the signals due to Ni^{2+}'s paramagnetism if the coordination geometry around the Ni^{2+} is not square planar. The Kd of the complex must be greater the mM since we were not able to see any binding on the NMR timescale.[7]

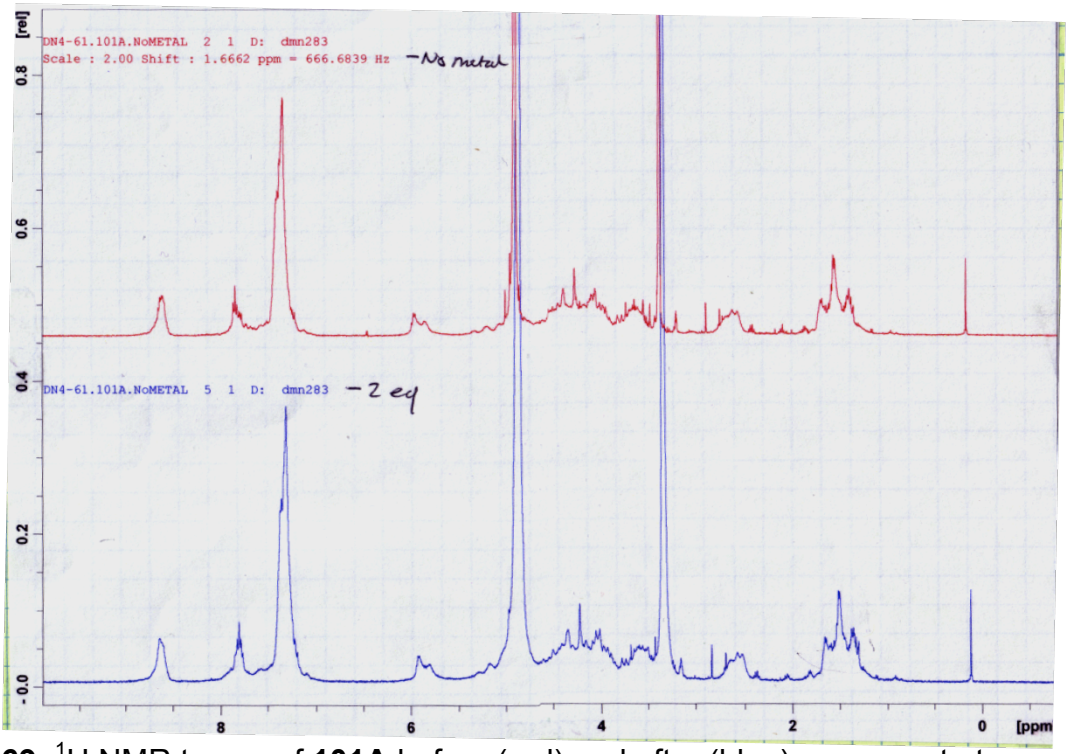

Figure 69. ^{1}H NMR traces of **101A** before (red) and after (blue) exposure to two equivalents (relative to peptoid) of $NiCl_2$. No apparent change in the spectrum was observed, especially in the aromatic region where the peptoid was believed to complex the pyridyl nitrogen, implying either a high Kd of binding, or no binding to Ni^{2+}.

Because sequence **89A** is completely water soluble, we surmised that the solubility issue of **101A** would not be a problem. The titration under Krizter's conditions was repeated until 2 full equivalents of $NiCl_2$ were added. No precipitation was observed, but a global increase over all absorbances was witnessed. A promising absorbance at 385 emerged, possibly indicating a nickel d-d transition, but saturation could not be reached. To test if this absorbance was due to the metal-peptoid interaction, a titration without peptoid was conducted into 50mM N-ethyl morphine buffer up to 6 equivalents, with the absorbance at 385 increasing linearly with each aliquot of metal (**Figure 70**).

Two more peptoid sequences identified as hits from the XRF analysis, **91A** and **83C** were then tested for binding to nickel and copper via the Kritzer method, with similar results as **89A**. (**Data not shown**)

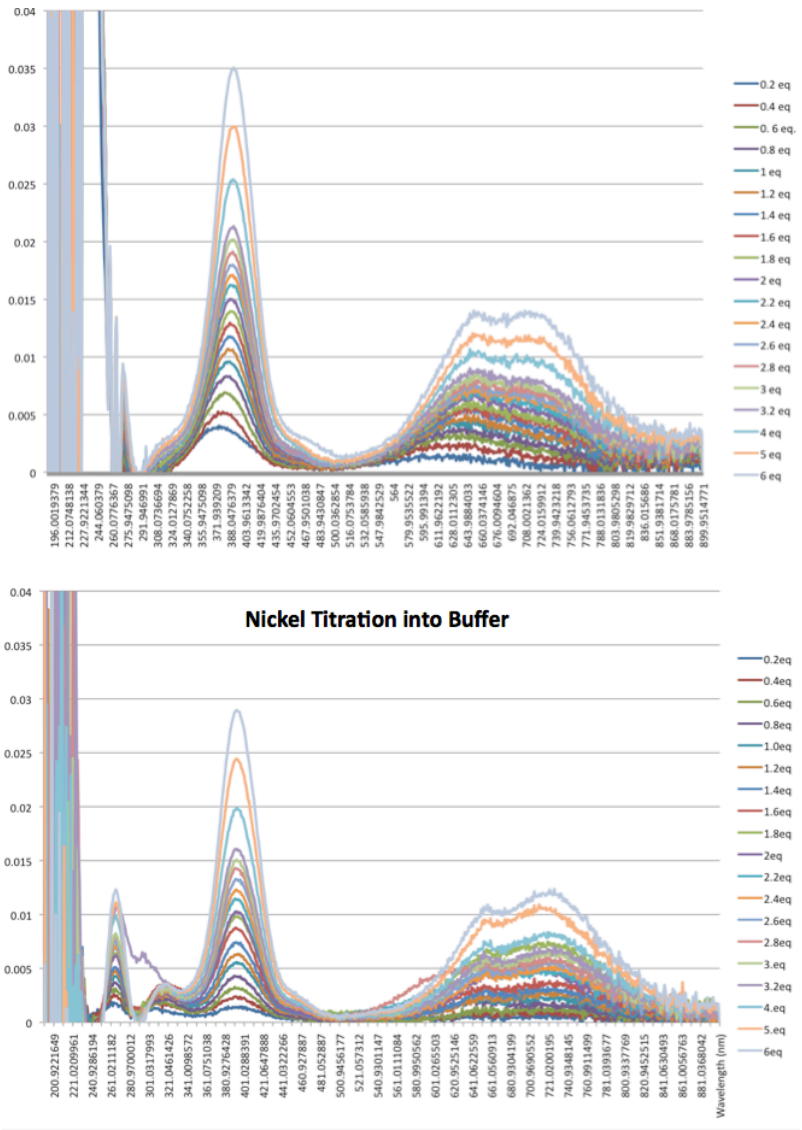

Figure 70. Uv/vis plot of the titration of Ni^{2+} into a 1 mM solution of **89A** showing a large, and increasing, absorbance at 385 nm. (Top). Uv/vis plot of the same titration experiment without peptoid (bottom) The same increasing absorbance at 385 nm is also

present in the experiment without peptoid, indicating that this absorbance does not correspond to a metal-peptoid interaction.

Designing Cyclic Metal-Binding Peptoids for Cu^{2+} Complexation

Computationally designing peptoids to display predictable structure and function is another active area of research in the Kirshenbaum lab, formed from a collaboration between our lab and the Bonneau lab. Once verified, this tool could be as invaluable as high throughput screening for the discovery of functional peptoid molecules. Two designs, based on the natural metalloenzyme active sites, were generated from the Bonneau lab using computational analysis to predict the side chain geometry of cyclic hexamer and octamer peptoid macrocycles (**Figure 71**). We hypothesized that the covalent constraints introduced by macrocyclization would provide a rigid and pre-organized binding environment to facilitate tight and selective metal complexation.

The cyclic hexamer, based on a nitrite reductase (**1AS6** from *Alcaligenes faecalis)* was synthesized using standard solid phase synthesis protocol on 2-chlorotrityl chloride resin and subject to head-to-tail macrocyclization with PYBOP and DIEA.[8] Once purified, the macrocycle was characterized by MS, MALDI, HPLC, and ^{1}H NMR (**Appendix 72**). The compound was dried and stored in a light- tight container under vacuum at -20^{o}C until use.

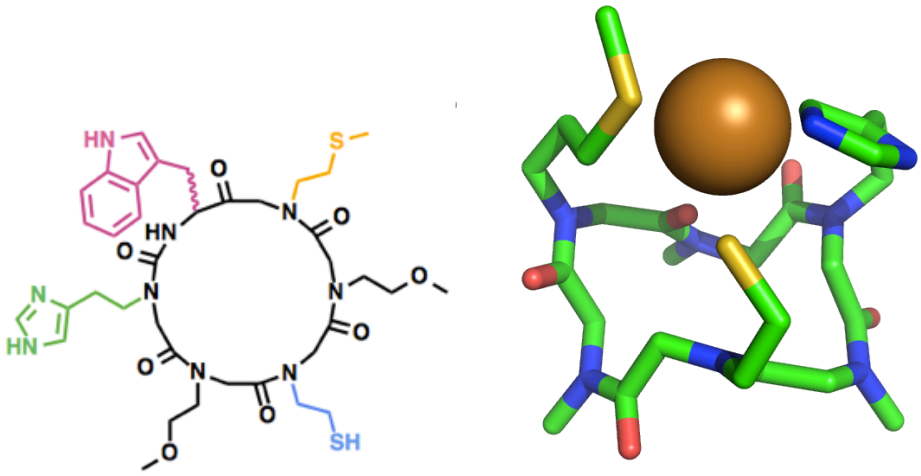

Figure 71 Bonneau Laboratory-designed cyclic peptoid macrocycle intended to bind metal (Right). The corresponding Chemdraw representation of the same macrocycle (Left).

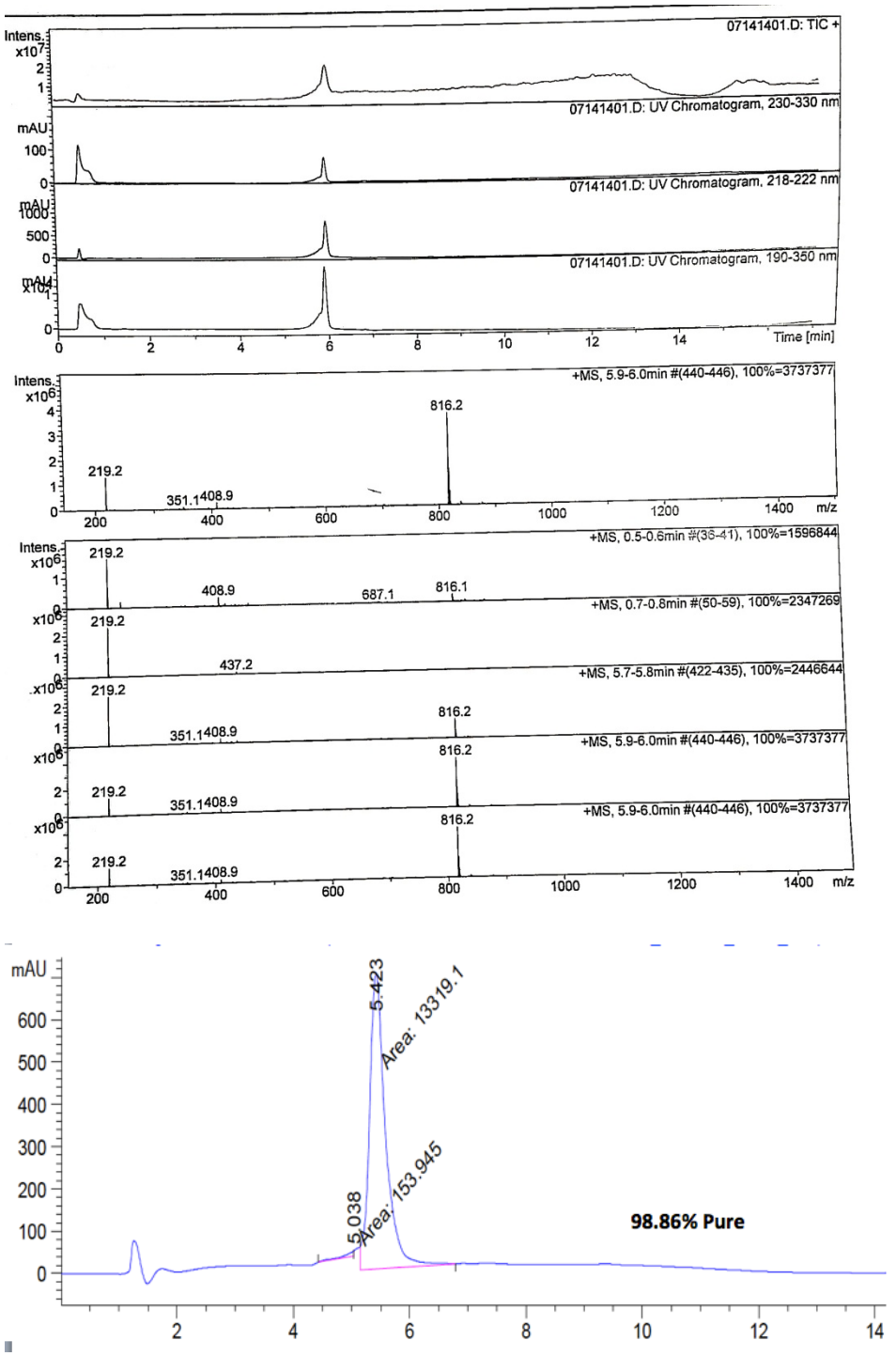

Figure 72. MS data and analytical HPLC trace of the cyclic metal-binding hexamer, validating the identity of the sequence and the high purity above 98%.

Uv/vis titrations were conducted under inert atmosphere at concentrations of 20.5 uM to 161.53 uM peptoid (concentration determined by Trp absorbance at 280 nm) in either 20mM MOPS buffer or 20mM N-ethyl morpholine buffer, with and without 100mM NaCl, and with and without sodium citrate as a Cu antioxidant.[9] Scanning wavelengths of 190-800, Uv/vis titrations of either increasing amounts of Cu^{2+}, Ni^{2}, Co^{2+}, or Zn^{2+} were conducted into the peptoid solution, but neither a reproducible binding curve nor a homogenous solution could be maintained. In all cases, a precipitate formed upon exposure to the metal solution, obscuring the absorbance readout. In the case of Cu^{2+} titrations, the precipitate was isolated and subjected to Maldi-TOF analysis. Under conditions of 20mM MOPS, without NaCl or citric acid, and without oxygen, many peaks corresponding to a copper complex as either a peptoid monomer or dimer can be witnessed (**Figure 73**). Additionally, the dimer, trimer, and tetramer assembly can be observed without metal as well.

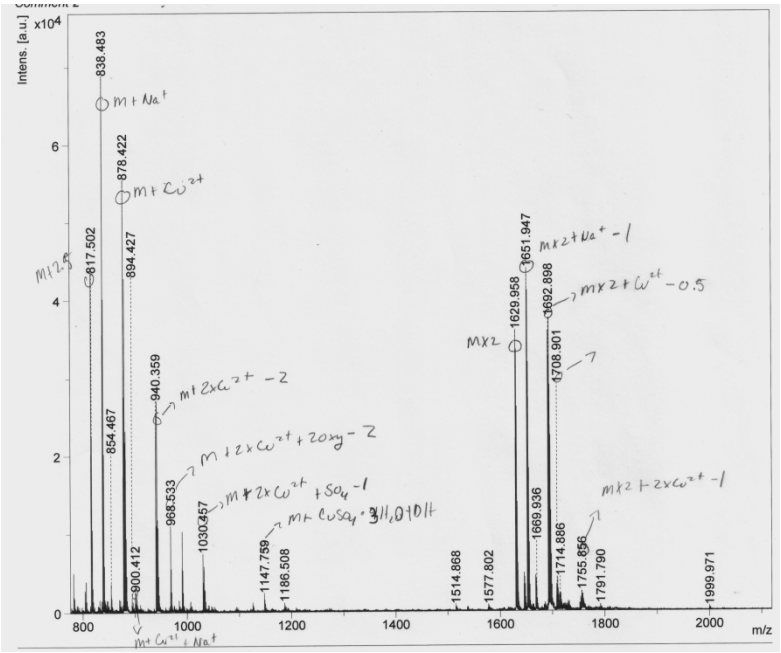

Figure 73. MALDI analysis of a solution of the cyclic hexamer titrated with 1 equivalent of Cu. Many masses corresponding to the Cu-peptoid complex can be observed as either as a monomer or a dimer, as well as a hetero or dinuclear metal center about the macrocycle. M^+: 816; M^+Na^+:838.4; M^++Cu^{2+}:878.4; M^++2xCu^{2+}:965.5; M^++2xCu^{2+}+ SO_4^{-1}:1030.45; M^++$CuSO_4$. $3H_2O$ + OH: 1147.75; 2xM: 1629.95; 2xM + Na^+-1: 1651.94; 2xM+Cu^{2+}-0.5: 1692.89; 2xM + 2xCu^{2+}-1: 1755.85.

We hypothesize that the metal is catalyzing the formation of a disulfide bridge between two or more macrocycles and causing aggregation of the peptoid, causing them to crash out of solution. This is supported by literature precedent concluding that Cu complexes in the presence of Trp and Cys are known Redox cycling molecules, and have been demonstrated to catalyze oxidation and reduction of cysteine thiol groups.[10]

Appendix 3 References

1. Culf, A.S. and Oulette, R.J. *Molecules*. **2010**, *15,* 5282-5335.

2. Burkoth,T.S.; Fafarman, A.T.; Charynch, D.H.; Connolly, M.D.; Zuckermann, R.N. *J. Am. Chem. Soc.* **2003**, *125*, 8841-8845.

3. *X-Ray Data Booklet*; Thompson, A.C., Ed.; 3rd ed. [Online]; Lawrence Berkeley National Laboratory, Berkeley, California, 2009. http://xdb.lbl.gov/xdb-new.pdf (accessed Apr 20, 2014).

4. *Fmoc Solid Phase Peptide Synthesis*; Chan, W.C. and White, P.D., Eds.; Oxford University Press: New York, 2004; pp 62.

5. Maayan, G.; Ward, M.; Kirshenbaum, K. *Proc. Natl. Acad. Sci. USA.* **2009**, *106*, 13679-13684.

6. Neupane, K. P.; Aldous, A. R.; Kritzer, J. A. *Inorg. Chem.* **2013**, *52*, 2729-2735.

7. Klewpatinond, M. and Viles, J. H. *Biochem. J.* **2007**, *404*, 393-402.

8. Yoo, B.; Shin, S. B. Y.; Huang, M. L.; Kirshenbaum, K. *Chem. Eur. J.* **2010**, *16*, 5528-5537.

9. Jackson, M. S. and Lee, J. C. *Inorg. Chem.* **2009**, *19*, 9303-9307.

10. (a) Sweeney, J. A.; Harmon, P. A.; Asher, S. A.; Hutnik, C. M.; Szabo, A. G. *J. Am. Chem. Soc.* **1991**, *113*, 7531-7537. (b) Lumb, I.; Singh, H.; Hundal, G. *Inorg. Chem.* **2014**, *53*, 7770-7779.

.